PHARMACEUTICAL APPROACHES ON NOVEL PHYTO DRUGS FOR THE TREATMENT OF HUMAN AILMENTS

Thesis Submitted

By

Rituparna Chaki

DOCTOR OF PHILOSOPHY (PHARMACY)

DEPARTMENT OF PHARMACEUTICAL TECHNOLOGY

FACULTY COUNCIL OF ENGINEERING & TECHNOLOGY

JADAVPUR UNIVERSITY

KOLKATA- 700 032, INDIA

2025

DEDICATED

TO MY

FAMILY

JADAVPUR UNIVERSITY

KOLKATA- 700 032, INDIA

Index No.: 274/18/Ph

1. Title of the Thesis: Pharmaceutical Approaches On Novel Phyto Drugs For The Treatment Of Human Ailments

2. Name, Designation & Institution of the Supervisor:

Name of the Supervisor: Prof. (Dr.) Subhash C Mandal

Designation: Professor

Institution: Pharmacognosy and Phytotherapy Research Laboratory,
Division of Pharmacognosy
Department Of Pharmaceutical Technology
Jadavpur University, Raja S.C. Mullick Road,
Kolkata–700032, India.

3. *List of Publications:*

(a) **Chaki R**, Basak S, Sharma A, Nasare VD, Ghosh N, Mandal SC. Biocompatible nanocarriers of bioactive flavonoid naringin: Design, formulation, and comprehensive characterization. J Appl Pharm Sci. 2025. http://doi.org/10.7324/JAPS.2025.222894.

List of Presentation in National/ International conferences:

a) **Chaki R**, Banerjee A, Ghosh B, Chakraborty P, Mandal SC. Formulation & evaluation of chitosan-based quercetin dihydrate nanoparticles for ocular drug delivery. In: Proceedings of the PSIT Conference; 2024 September 2-3; Kanpur, India. Abstract No: PSIT/PP01/0143.

b) **Chaki R**, Chakraborty P, Bera A, Panja J, Basak S, Ghosh N, Mandal SC. Exploring the anti-inflammatory and antimicrobial potential of copper nanoparticles loaded with

ellagic acid for ocular inflammation. In: Abstract Booklet of NATCON 2025; April 25-26; Durgapur, India. Abstract No: BCRCP-NATCON25-0019.

c) Chakraborty P, Bera A, Panja J, **Chaki R**. Gel based nanoparticles in drug delivery. In: Abstracts of BCRCP NATCON; 2024 Apr 5–6; Durgapur, India. Durgapur: Dr. B. C. Roy College of Pharmacy and Allied Health Sciences; 2024. Abstract No: BCR/NAT/24/P-055.

d) Panja J, Chakraborty P, Bera A, **Chaki R**. Fabrication of polycaprolactone based nanoparticles of naringin. In: Abstracts of BCRCP NATCON; 2024 Apr 5–6; Durgapur, India. Durgapur: Dr. B. C. Roy College of Pharmacy and Allied Health Sciences; 2024. Abstract No: BCR/NAT/24/P-073.

e) Shit S, Bera A, **Chaki R**. Enhanced drug loaded magic polymer polycaprolactone based nanocarriers of mangiferin. In: Abstracts of BCRCP NATCON; 2025 Apr 25–26; Durgapur, India. Durgapur: Dr. B. C. Roy College of Pharmacy and Allied Health Sciences; 2025. Abstract No: BCR/NATCON/25/I-46.

f) Bera A, Shit S, **Chaki R**. Mangiferin loaded grey metal nanoparticles: development and characterization. In: Abstracts of BCRCP NATCON; 2025 Apr 25–26; Durgapur, India. Durgapur: Dr. B. C. Roy College of Pharmacy and Allied Health Sciences; 2025. Abstract No: BCR/NATCON/25/I-50.

Book Chapters:

a) **Chaki R**, Ghosh N, Mandal SC. Phytopharmacology of herbal biomolecules. In: Mandal SC, Nayak AK, Dhara AK, editors. Herbal Biomolecules in Healthcare Applications. 1st ed. Academic Press; 2022. p. 101–19. ISBN: 9780323858526.

b) Ghosh N, **Chaki R**, Kundu A, Mandal SC. Herb and drug interaction. In: Mandal SC, Mandal V, Konishi T, editors. Natural Products and Drug Discovery. 1st ed. Elsevier; 2018. p. 467–90. ISBN: 9780081020814.

Statement of Originality

I, Rituparna Chaki registered on 01.06.2018 do hereby declare that this thesis entitled ***"Pharmaceutical Approaches On Novel Phyto Drugs For The Treatment Of Human Ailments"*** contains literature survey and original research work done by the undersigned candidate as part of Doctoral studies.

All information in this thesis have been obtained and presented in accordance with existing academic rules and ethical conduct. I declare that, as required by these rules and conduct, I have fully cited and referred all materials and results that are not original to this work.

I also declare that I have checked this thesis as per the "Policy on Anti Plagiarism, Jadavpur University, 2019", and the level of similarity as checked by iThenticate software is 5%.

Signature of Candidate:

Date :

Certified by Supervisor(s):

(Signature with date, seal)

CERTIFICATE FROM THE SUPERVISOR

This is to certify that the thesis entitled **"*Pharmaceutical Approaches on Novel Phyto Drugs for the Treatment of Human Ailments*"** submitted by Ms. Rituparna Chaki, who got her name registered on 01.06 2018 [Registration No. 1021813008 (Ref. No. 274/18/Ph)] for the award of Ph.D. (Pharmacy) degree of Jadavpur University, is absolutely based upon her own work under the supervision of **Prof. (Dr.) Subhash C. Mandal** and that neither her thesis nor any part of the thesis has been submitted for any degree/diploma or any other academic award anywhere before.

…….

Prof. (Dr.) Subhash C. Mandal (Supervisor)

Pharmacognosy and Phytotherapy Research Laboratory,
Division of Pharmacognosy
Department Of Pharmaceutical Technology
Jadavpur University, Raja S.C. Mullick Road,
Kolkata–700032, India.

ACKNOWLEDGEMENTS

One of the most fulfilling aspects of writing a thesis is the opportunity it provides to express gratitude to those who have contributed to its completion. Any accomplishment is the result of collective effort, and this work is no exception.

*At the very outset, I would like to express my heartfelt gratitude to my esteemed guide, Prof. (**Dr.) Subhash C. Mandal, Professor, Department of Pharmaceutical Technology, Jadavpur University**. His unwavering support, profound knowledge, and meticulous guidance have been instrumental in the successful completion of this project. I remain deeply indebted to him for his mentorship and professional excellence. It has been a great honor and privilege to work under his supervision—his inspirational leadership will remain with me as I continue my journey ahead. Truly, he has been a guide par excellence.*

*I extend my sincere thanks to **Prof. (Dr.) Samir Kumar Samanta, Principal, Dr. B.C. Roy College of Pharmacy and Allied Health Sciences**, as well as **Prof. (Dr.) Subhabrata Ray** and **Mr. Sagar Sengupta**, for their constant encouragement and invaluable support throughout the course of my research at Dr. B.C. Roy College of Pharmacy and AHS.*

*I am especially grateful to my husband, **Dr. Nilanjan Ghosh, Associate Professor, Department of Pharmaceutical Technology, Jadavpur University**, for his unwavering belief in me, his constant encouragement, and his countless sacrifices that enabled me to pursue and complete my research. His steadfast support has been my greatest strength.*

*I would also like to thank my colleague, **Prof. (Dr.) Souvik Basak**, for his continued support and assistance, and my dear students, whose enthusiasm and cooperation have consistently encouraged me along this journey.*

No words are enough to thank my parents, ***Mr. Biplab Chaki*** *and* ***Mrs. Rupa Chaki,*** *whose unconditional love and endless sacrifices have been the foundation of my achievements. I am equally thankful to my in-laws,* ***Shri Anjan Kr. Ghosh*** *and* ***Smt. Tanushree Ghosh****, for their blessings and constant encouragement.*

A special note of appreciation goes to my brother-in-law ***Dipanjan*** *and sister-in-law* ***Mousumi*** *for their unwavering moral support.*

Last but certainly not the least, my deepest love and gratitude for my daughter, ***Srestha Ghosh****, whose love, patience, and joyful presence have been my source of strength and rejuvenation throughout this journey.*

With utmost reverence, I bow my head before the ***Almighty, Maa Tarini****, for bestowing upon me the strength, courage, and perseverance to complete this thesis and for guiding me throughout my academic endeavors.*

Rituparna Chaki

Department of Pharmaceutical Technology,

Jadavpur University,

Kolkata -700 032

TABLE OF CONTENTS

LIST OF ABBREVIATIONS

AFM	Atomic Force Microscopy
AGN	Ellagic Acid-loaded Silver Nanoparticles
AgNPs	Silver Nanoparticles
AMPK	AMP-Activated Protein Kinase
ANOVA	Analysis of Variance
AuNPs	Gold Nanoparticles
BCS	Biopharmaceutics Classification System
BMR	Basal Metabolic Rate
CAT	Catalase
CCSEA	Committee for Control and Supervision of Experiments on Animals
CDs	Cyclodextrins
CGTase	Cyclodextrin Glucanotransferase
Cipro	Ciprofloxacin
CMC	Carboxymethyl Cellulose
COX	Cyclooxygenase
COX-2	Cyclooxygenase-2
CS	Chitosan
CuNPs	Copper Nanoparticles
DDAB	Didodecyl Dimethyl Ammonium Bromide
DEMC	Diethylmethyl Chitosan
DLS	Dynamic Light Scattering
DMEC	Dimethylethyl Chitosan
DMSO	Dimethyl Sulfoxide
DNA	Deoxyribonucleic Acid
Dorzo	Dorzolamide
DPPH	2,2-diphenyl-1-picrylhydrazyl
DSC	Differential Scanning Calorimetry
EA	Ellagic Acid
EAC	Ehrlich Ascites Carcinoma
EDX	Energy-Dispersive X-ray Spectroscopy
EE	Entrapment Efficiency
FBG	Fasting Blood Glucose
FQN	Quercetin-loaded Chitosan Nanoparticles
FTIR	Fourier-Transform Infrared Spectroscopy
GPx	Glutathione Peroxidase
HAp	Hydroxyapatite
HCT-116	Human colon cancer cell line
HDL	High-Density Lipoprotein
HEK 293	Human Embryonic Kidney 293 Cells
HET-CAM	Hen's Egg Test - Chorioallantoic Membrane
HMGB1	High Mobility Group Box 1
HO-1	Heme Oxygenase-1
HPC	Hydroxypropyl Cellulose
HPMC	Hydroxypropyl Methylcellulose
IAEC	Institutional Animal Ethical Committee
IC_{50}	Half-Maximal Inhibitory Concentration
ICCVAM	Interagency Coordinating Committee on the Validation of Alternative Methods
IL-12	Interleukin-12
IL-6	Interleukin-6
LC	Loading Capacity
LDL	Low-Density Lipoprotein
LPS	Lipopolysaccharide
MAPK	Mitogen-Activated Protein Kinase

MCF-7	Human breast cancer cell line
MDA	Malondialdehyde
MGF-g1	Glucosyl-α-(1→4)-mangiferin
MSN	Mangiferin-loaded Silver Nanoparticles
MTT	3-(4,5-Dimethylthiazol-2-yl)-2,5-diphenyl tetrazolium bromide
NAR	Naringenin
Naringin	A flavonoid, often used interchangeably with NAR
NaTPP	Sodium Tri-polyphosphate
NF-κB	Nuclear Factor kappa-light-chain-enhancer of activated B cells
NK cells	Natural Killer cells
NLC	Naringin-loaded Chitosan/TPP Nanoparticles
Nrf2	Nuclear factor erythroid 2-related factor 2
p53	Tumor suppressor protein p53
PAA	Polyacrylic Acid
PBS	Phosphate Buffered Saline
PC12	Pheochromocytoma cell line (rat adrenal medulla)
PCL	Polycaprolactone
PCLMP	Polycaprolactone-based Mangiferin Nanoparticles
PCLNP	Polycaprolactone-based Nanoparticles
PCs	Photon Correlation Spectroscopy
PDI	Polydispersity Index
PEG	Polyethylene Glycol
PEO	Polyethylene Oxide
PF68	Pluronic F68
PLGA	Poly(lactic-co-glycolic acid)
Prami	Pramipexole
PVC	Polyvinyl Chloride
PVP	Polyvinylpyrrolidone
RNA	Ribonucleic Acid
ROS	Reactive Oxygen Species
SA	Sodium Alginate
SEDDS	Self-Emulsifying Drug Delivery System
SEM	Scanning Electron Microscopy
SLN	Solid Lipid Nanoparticles
SNEDDS	Self-Nanoemulsifying Drug Delivery System
SOD	Superoxide Dismutase
SSG	Sodium Starch Glycolate
STZ	Streptozotocin
TC	Total Cholesterol
TEC	Triethyl Chitosan
TEM	Transmission Electron Microscopy
TG	Triglycerides
TGA	Thermogravimetric Analysis
TMC	Trimethyl Chitosan
TNF-α	Tumor Necrosis Factor-alpha
TPP	Tripolyphosphate
UV-Vis	Ultraviolet-Visible Spectroscopy
XRD	X-Ray Diffraction
ZP	Zeta Potential

LIST OF TABLES

LIST OF FIGURES

CHAPTER 1
INTRODUCTION

CONTENTS

1.1 Introduction to bioactive phytochemicals

Phytochemicals are chemical molecules isolated from plants, trees, or saplings one of the most important components of plants, with numerous therapeutic applications. They are that have a specific medicinal function with minimal unwanted effects. Since the inception of medicine, phytochemicals have played an important part in the field of pharmacy, as there were no distinct medicines in ancient times due to a lack of sophisticated machinery or technology to accomplish the operation. Only a few of the thousands of different chemical components that have shown promising therapeutic activity are used to treat medical conditions. Most phytochemicals are poorly understood due to a lack of knowledge; their physiochemical properties, dosage, toxicity, and adverse effects are unclear due to limited data collecting. With contemporary technology and knowledge of the physicochemical properties of any natural or synthetic substance, we can develop novel formulations based on natural ingredients (Harvey et al., 2008, Liu et al., 2004, Yuan et al., 2016, Liu et al., 2022, Kumar et al., 2013, Gurib-Fakim et al., 2006, Ekor et al., 2014).

Phytochemicals are being studied as prospective medication delivery systems for ailments such as cancer, diabetes, hypertension, and microbial infections. Researchers are looking into the compatibility of phytochemicals with a variety of delivery platforms, including liposomes, nanoparticles, niosomes, micelles, implant delivery systems, and nanotubes. These novel delivery systems aim to improve the bioavailability, stability, and therapeutic efficacy of phytochemicals, allowing for targeted medication delivery with fewer side effects (Wang et al., 2014, Yallapu et al., 2012).

1.2 Challenges to Delivery of Phytochemicals

This following section highlights various challenges and limitations associated with the formulation development of bioactive phytochemicals (Aqil et al., 2013).

1.2.1 Gastrointestinal Solubility:

The bioactivity of many phytochemical is limited because of low solubility. Furthermore, non-polar phytochemicals have a strong tendency to associate with each other and form a separate phase which is thermodynamically unfavourable. Sometimes phytochemicals can bind with other food components like as proteins or dietary fibres,

which reduces their bio accessibility in gastrointestinal fluids. (McClements, et al., 2015, Palafox-Carlos, et al., 2011, Bohn, et al., 2014, Saeidi, et al., 2021)

1.2.2 Gastrointestinal Absorption: Phytochemicals may be sometimes unable to reach the surfaces of the epithelium cells because they may become physically trapped within the mucus layer or may be too large to enter the mucus layer. Depending on the phytochemicals and their physiochemical properties, enterocytes or M-cells may absorb them through paracellular, transcellular, or endocytosis pathways. The transcellular pathway can be passive or active, depending on whether the phytochemicals simply diffuse via the necessary transporters or phospholipid bilayers. Phytochemicals can also be transferred out of cells via passive transport or efflux processes. Active transport and efflux processes are often dependent on the presence of protein transporters embedded in the outer membranes of epithelial cells.

To improve phytochemical uptake, a variety of techniques may be employed. Firstly, permeation enhancers can be added to a colloidal delivery system to increase epithelial cell membrane permeability or to open the tight junctions that separate nearby epithelium cells (increased paracellular transport). Second, efflux inhibitors can be used in a colloidal delivery method to inhibit any efflux transporters that may be present within the epithelial cell membranes. Third, phytochemicals can become trapped inside colloidal particles, which are absorbed by epithelial cells and eventually released into the systemic circulation. To attain this purpose, an effective colloidal delivery system design must include cellular absorption and efflux mechanisms, morphology, polarity, electrical characteristics, particle composition, and size. (Shimizu, et al., 2012, Yang, et al., 2020, Mu, et al., 2021, Rezhdo, et al., 2020, Kumar, et al., 2013)

1.2.3 Product Stability: Phytochemicals are frequently exposed to a variety of habitats, physical states, and environmental factors such as temperature, oxygen levels, light, and humidity, which can alter their physicochemical stability. Carotenoids, for example, breakdown chemically when exposed to high temperature, oxygen, light, or acidic environments. A phytochemical can be chemically stable under certain conditions, but it can also rapidly breakdown, resulting in loss of biological activity. The interaction

between food components and phytochemicals may potentially affect their stability and bioavailability. When carotenoids are integrated into dietary matrices containing milk proteins, they can breakdown in the presence of transition metals. It is therefore imperative to understand the precise nature of the local environment of a phytochemical in a particular delivery vehicle, as well as how this environment impacts its stability (Choe et al., 2006, Boon et al., 2010.)

In order to overcome the above limitations, processing processes and storage settings that minimize phytochemical loss can be attempted along with devising delivery vehicles for better phytochemical stability. For example, if the phytochemical degrades quickly under acidic or basic environments, these conditions can be avoided. Similarly, phytochemicals that are prone to photochemical destruction can be handled away from light. Furthermore, compounds such as antioxidants and chelating agents may be used to improve the chemical stability of phytochemicals.

1.2.4 Gastrointestinal Stability: Phytochemicals may potentially undergo biochemical changes in the gastrointestinal tract. For example, many polyphenols are processed by enzymes found throughout the GI tract. Phytochemicals can undergo Phase I or Phase II biotransformation in the liver or by microbes. As a result, in order to understand the primary parameters influencing the rate and degree of transformation during their passage through the GIT, alterations in the molecular structure of phytochemicals must be identified. (Manach et al., 2004, Selma et al., 2009, Crozier et al., 2010, Williams et al., 2004, D'Archivio et al., 2010)

1.3. Approaches to improve the therapeutic potential of phytochemicals:

While phytochemicals have tremendous therapeutic promise, many difficulties prevent them from being fully utilized as pharmacological agents such as low bioavailability, poor permeability, low water solubility, high toxicity, and instability. Nanotechnology has emerged as a viable answer to overcome restrictions, increasing phytochemical delivery. Nanocarriers including liposomes, nanoparticles, and micelles can increase phytochemical solubility, stability, and bioavailability, allowing for more focused administration and controlled release. Over the last decade, substantial research

has concentrated on replacing synthetic pharmaceuticals with natural phytochemicals in order to reduce the negative side effects associated with synthetic treatments. Nanotechnology not only addresses these issues, but it also opens up new paths for medications that were previously rejected owing to their limits. A complete synthetic and technical approach can lead to the creation of stable medicinal formulations made entirely of phytochemicals encapsulated in nanocarriers. Success in these initiatives offers better medical and pharmaceutical care with fewer side effects and lower costs while preserving maximal therapeutic efficacy (Wang, et al., 2014, Anselmo, et al., 2019, Yallapu, et al., 2012). The bioavailability of phytochemicals can be improved by any of the following methods.

1.3.1 Enhancement of dissolution or solubility: Drug dissolution or solubility can be increased by approaches such as nanonisation, molecular encapsulation using cyclodextrins, mixed micelles, solid dispersions.

- Nanonization is the process of reducing drug particles to nanometer sizes (usually between 100 and 500 nm), resulting in nanocrystals or nanosuspensions. This size decrease greatly boosts the surface area-to-volume ratio, which improves the drug's solubility in aqueous solutions. The increased surface area enhances the solubility and bioavailability of weakly water-soluble medicines. For example, one study found that nanonization of midazolam increased its solubility rate and bioavailability. The nanocrystals had a particle size of around 286.6 nm, resulting in a 2.72-fold improvement in bioavailability over the usual formulation. Additionally, nanocrystals can improve the pharmacokinetic aspects of phytochemicals. The same study found that the mean residence time of midazolam nanocrystals was substantially longer than that of the standard solution, indicating that the drug's effect was prolonged. Nanonization can improve the therapeutic efficacy of poorly soluble medicines by increasing dissolution rates and bioavailability(Da Silva, et al., 2020, Gao, et al., 2023, Singh, et al., 2021, Shegokar, et al., 2018, Kesisoglou, et al., 2019).

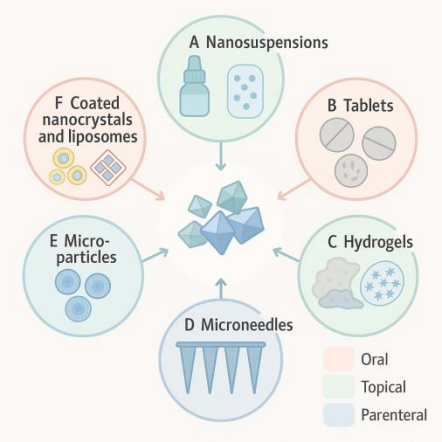

Figure 1: Nanocrystals and nanosuspensions used in various formulations (Rossier et al., 2024)

- Cyclodextrins (CDs) are cyclic oligosaccharides distinguished by their unique ability to form inclusion complexes with a variety of guest molecules via non-covalent interactions such as van der Waals forces and hydrophobic interactions. The hydrophobic interior cavity of CDs allows for the encapsulation of weakly water-soluble drugs and phytochemicals, increasing their solubility and stability. Because of their versatility, CDs serve as good delivery vehicles for nanoparticles, liposomes, microcapsules, and microspheres. CDs, by creating inclusion complexes, can increase the bioavailability, dissolution, and solubility of medicines that are poorly or insoluble. Furthermore, CDs aid in penetration across mucus and lipid layers by presenting the drug at the surface of biological barriers while preserving lipid structures. For example, studies have shown that administering insulin in a combination with CDs via the nasal route enhances its absorption. Sublingual drug administration is also a desirable route for CD-drug complexes because it avoids first-pass metabolism and allows direct entrance into systemic circulation via the mucosa. CDs are versatile and can be administered orally or intravenously. Orally, CDs increase the bioavailability of poorly soluble compounds, preserve them from degradation, aid in dispersion, and improve transport to the intestinal wall. CDs improve solubility when administered parenterally while retaining their pharmacokinetic features (Challa et al., 2005, Bilensoy et al., 2011, Davis et al., 2004, Hirayama et al., 1999, Loftsson et al., 2007, Stella et al., 1997)

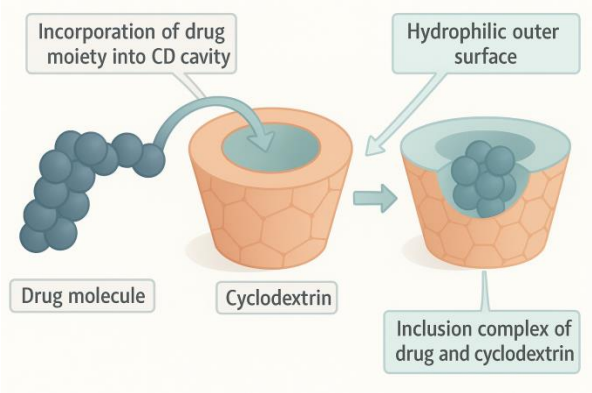

Figure 2: Role of cyclodextrin in drug solubilization (Yousaf et al., 2023)

- Mixed micelles: Nano-sized assemblies of amphiphilic di-block (hydrophilic-hydrophobic) or tri-block (hydrophilic-hydrophobic-hydrophilic) copolymers can be employed to create self-assembled polymer micelles of phytochemicals. The outer hydrophilic shell helps to stabilize the micelles in an aqueous environment, while the inner hydrophobic core serves as a drug reservoir. Ex-Pluronics® is comprised of PEO and PPO with variable HLB. These self-assemble polymeric amphiphiles create nanosized aggregates (mixed micelles) in aqueous solutions and have a distinct core-shell structure. Mixed micelles exhibit synergistic qualities, such as improved micelle stability and drug loading efficiency (Almgren et al., 2000, Torchilin et al., 2006, Kabanov et al., 2002, Jones et al., 2008, Batrakova et al., 2011).

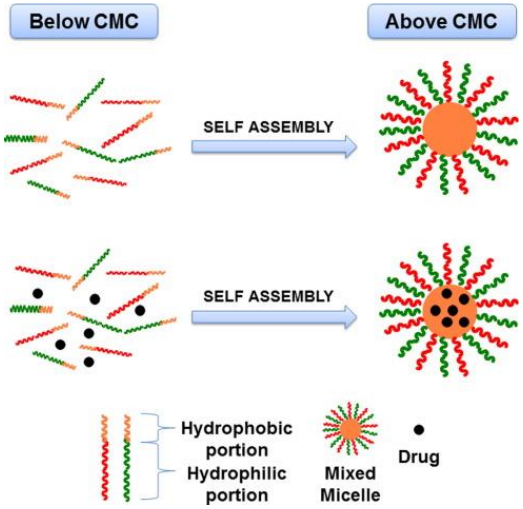

Figure 3: Schematic representation of formation of mixed micelles (Maximiliano et al., 2017)

- Solid dispersions: One or more active chemicals are dispersed in an inert carrier matrix in the solid state using the melting (fusion), solvent, or melting-solvent technique. The mechanisms underlying higher solubility and dissolution rate include drug particle size where solid solution is achieved, transition from crystalline to amorphous form, enhanced wettability of the drug by the carrier, and increased porosity of solid dispersion particles. Various hydrophilic carriers: PEG, PVP, HPC, HPMC, gums, sugar, mannitol, urea, HPMC phthalate, Eudragits,chitosan, hydrophilic swellable polymers like sodium CMC, SSG & pregelatinized starch (Patel et al., 2020, Jermain et al., 2018, Vasconcelos et al., 2016, Dhirendra et al., 2009, Savjani et al., 2012, Leuner et al., 2000, Serajuddin et al., 1999, Chiou et al., 1971, Craig et al., 2002).

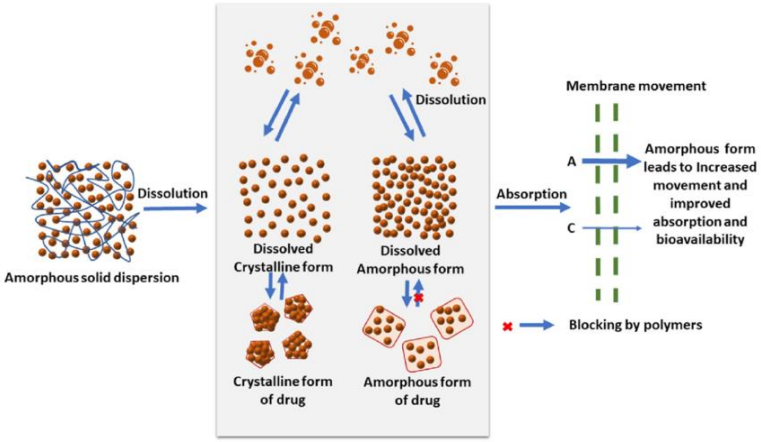

Figure 4: Representation of enhancement of solubility through solid dispersion technique (Nambiar et al., 2022)

1.3.2 Enhancement of permeability: Drug permeability can be improved by approaches such as mixed micelles, Self-emulsifying Drug Delivery Systems (SEDDS), Solid-lipid Nanoparticles (SLN) and vesicular carriers.

- SMEDDS and SNEDDS are pre-concentrate mixture of drug, oil, surfactant, co-surfactant, and, occasionally, co-solvent used to produce emulsions with droplet sizes ranging from a few nanometers to several microns. SMEDDS generate clear microemulsions with oil droplets ranging from 100 to 200 nm, whereas SNEDDS have droplet sizes lower than 100 nm. These delivery devices exhibit improved

solubilization of compounds, better release and absorption qualities due to dissolved drug in formulation and small droplet size which in turn increases membrane permeability due to surfactant presence and boosts lymphatic absorption. (Singh et al., 2009, Porter et al., 2007, Pouton et al., 2006, Date & Desai, 2016, Jaiswal et al., 2014).

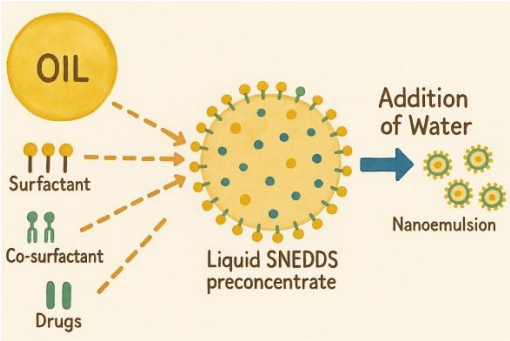

Figure 5: Schematic representation of SNEDDS (Sailor et al., 2021)

- SLNs are composed of a solid hydrophobic core with a monolayer of phospholipids coating; they are typically spherical, with an average diameter ranging from 10-1000 nm. The solid core holds the medication, which is dissolved or dispersed in the solid high melting fat matrix. The hydrophobic chains of phospholipids are embedded in the fat matrix and can transport lipophilic or hydrophilic medicines. Many biocompatible/biodegradable lipids solid at room temperature are utilized to manufacture SLNs such as triglycerides (e.g., Compritol 888 ATO and Dynasan 112), carnauba wax, beeswax, cetyl alcohol, emulsifying wax, cholesterol, and cholesterol butyrate. (Ramachandran & Thangarajan, 2016, Khan et al., 2006, Müller et al., 2000, Mehnert & Mäder, 2001, Pardeike et al., 2009).

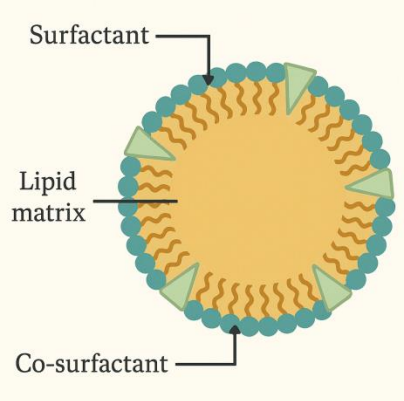

Figure 6: Schematic representation of SLN (Bayón-Cordero et al., 2019)

- Nanovesicles increase bioavailability of compounds by forming supramolecular adducts with precise stoichiometry. They also increase the rate and amount of solubilization in aqueous intestinal fluids and across biomembranes. Liposomes are made up of a flexible bilayer of phospholipids surrounded by an aqueous core, which improves stability and bioavailability. Niosomes prepared with non-ionic surfactants transport pharmaceuticals in a controlled/sustained way, addressing problems of insolubility, instability, low bioavailability, and rapid drug degradation; they entrap both hydrophilic and lipophilic compounds. Cholesterol gives the vesicle structure and rigidity, as well as membrane qualities such as permeability, elasticity, and mechanical strength.(Jacob et al., 2025, Riccardi et al., 2024, Moghassemi et al., 2023, Kazi et al., 2023, Moghassemi et al., 2023)

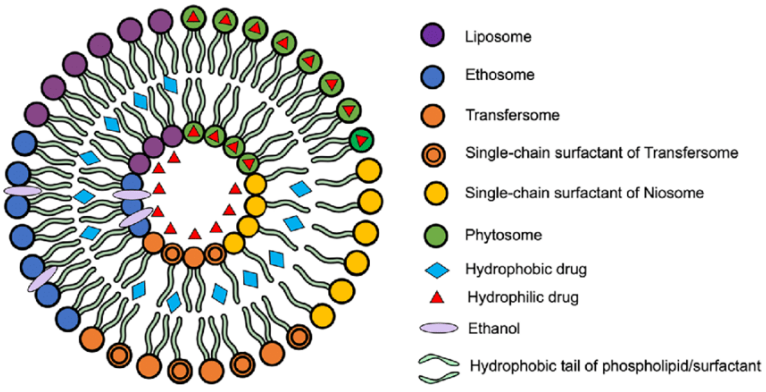

Figure 7: Schematic representation of Nanovesicles (Ramadon et al., 2022)

1.3.3 Enhancement of stability: Physicochemical stability of phytochemicals can be improved by several techniques such as molecular encapsulation using cyclodextrins, and bioadhesive delivery systems. Bio adhesion causes prolonged residence duration at the absorption site, allowing for increased interaction with the epithelial barrier; reduced drug delivery frequency; and effective drug concentration at the absorption site. Various mucoadhesive polymers used for the purpose are synthetic polymers such as Cellulose derivatives (Methylcellulose, Ethyl cellulose, Hydroxyl ethyl cellulose, Hydroxyl propyl cellulose, HPMC, Sodium CMC), PAA polymers (Carbomers, Polycarbophil), Poly hydroxyl ethyl methylacrylate, PEO, PVP, PVA (Tonnesen and Karlsen et al., 2002, Marttin et al., 1998).

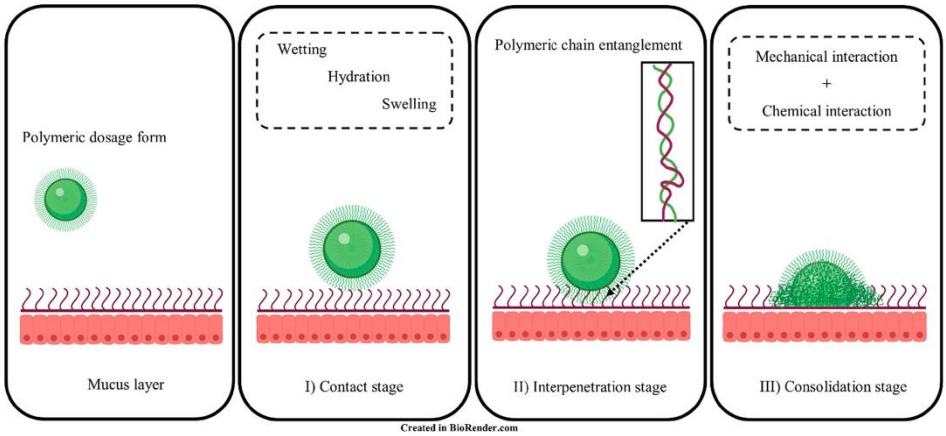

Figure 8: Schematic representation of stages of mucoadhesion (Yu et al., 2022)

1.4. Phytochemicals/Phytodrugs used in the present research

Phytochemicals, naturally occurring bioactive compounds found in plants, have garnered significant attention due to their potential health benefits and therapeutic applications. These compounds, including flavonoids, polyphenols, and xanthones, exhibit a wide range of pharmacological activities such as antioxidant, anti-inflammatory, antimicrobial, and neuroprotective effects. Among these bioactive compounds, naringin, ellagic acid, quercetin, and mangiferin are well-recognized for their medicinal properties.

Naringin, a naturally occurring flavonoid glycoside mainly found in citrus fruits such as grapefruits and oranges, has received substantial attention due to its broad spectrum of pharmacological actions. It has been widely reported to demonstrate powerful antioxidant, anti-inflammatory, antiviral, antibacterial, cardioprotective, and anticancer effects, making it a molecule of great therapeutic relevance (Garg et al., 2001; Alam et al., 2014; Salehi et al., 2019). These effects are mostly due to its ability to scavenge free radicals, regulate inflammatory pathways, and alter various cellular signaling systems. Despite its promising biological action, naringin's clinical use is limited due to its intrinsic low bioavailability. Several pharmacokinetic hurdles contribute to this issue, including poor solubility in aqueous solutions, low permeability across intestinal membranes, and significant first-pass metabolism, particularly in the liver and gut wall (Mulvihill and Huff, 2010). Following oral ingestion, naringin is rapidly hydrolyzed by intestinal enzymes and microbial flora, converting it to its aglycone form, naringenin, which is subsequently subjected to conjugation events such as glucuronidation and sulphation. These metabolic processes considerably lower its systemic availability, hence reducing its therapeutic use. To address these limitations, recent research has focused on enhanced drug delivery techniques to improve naringin's bioavailability and therapeutic efficacy. Nanoformulations with solid lipid nanoparticles and polymeric nanoparticles have shown increased stability, absorption, and sustained release. These delivery systems improve naringin's pharmacokinetic profile, making it more effective in treating oxidative stress disorders, metabolic diseases, and neurodegenerative problems (Jain et al., 2018; Ahmad et al., 2015).

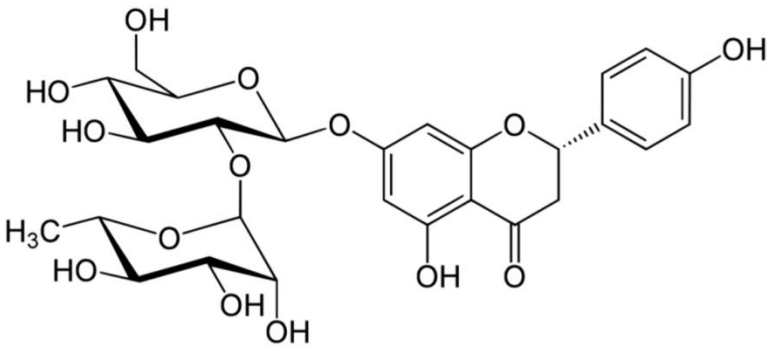

Figure 9: Molecular structure of naringin

Ellagic acid is a polyphenolic compound that exists naturally in a range of fruits, nuts, and vegetables. It belongs to the class of compounds known as ellagitannins, which are hydrolyzed in the body to release ellagic acid. This compound is known for its potent antioxidant properties and has been the subject of research for its potential health benefits. It has been proposed that ellagic acid function by reducing the oxidative stress occur inside body or by enhancing or inducing the enzymes associated with antioxidant. Many models are prepared to fully comprehend the antioxidant activity of ellagic acid, its cellular homeostasis and preventive mode of action. Ellagic acid has been reported to exhibit anticancer effect by altering the metabolism of systemic toxins and preventing the initial step of carcinogenesis enhanced by those chemicals. Narayanan et al. found out during their research that ellagic acid in gastric environment reduces GI arrest and causes tumour cell apoptosis by reducing overall cell growth. It also inhibits the cytogenetic damage caused by radiation therapy. Chen et al proposed that antitumor affectivity of ellagic acid could be used by modifying the protein kinase C which functions as marking receptor. This sudden alteration of cell membrane produces proton gradient which tamper with the natural order of proton pump present across the cell membrane. This mechanism of weak dissociation of targeted phenolics is the most important parameter for anti-microbial activity of ellagic acid (Shetty and Labbe 1998; Shetty and Wahlqvist 2004). Ellagic acid can also inhibit the growth of microorganism by prohibiting the metallic ion essential for cellular growth or by disrupting the normal mechanism of cell membrane and ion channels ultimately prohibiting the bacterial cellular growth. Rogerio et al. observed that paw edema of mouse is significantly decreased after injecting 1% solution. Possible involvement of cascade of inflammatory can be observed through COX pathway.

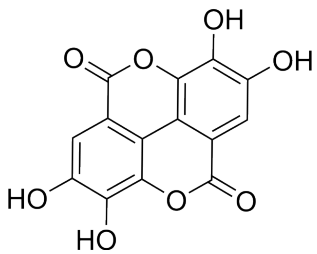

Figure 10: Molecular structure of ellagic acid

Quercetin is a naturally occurring flavonol found in many fruits, vegetables, and beverages, including onions, apples, berries, citrus fruits, red wine, and tea (Boots et al., 2008; Li et al., 2016). It is well-known for its powerful antioxidant, anti-inflammatory, antiviral, and anticancer properties, making it an attractive chemical for nutraceutical and pharmaceutical research. Among its many biological benefits, quercetin is well known for its involvement in ocular health, which includes the prevention of cataracts, age-related macular degeneration (AMD), and oxidative stress-induced retinal damage (Ishikawa et al., 2013). Quercetin has antioxidant properties by scavenging reactive oxygen species (ROS), reducing lipid peroxidation, and altering antioxidant defense pathways such the Nrf2 pathway (Boots et al., 2008). These actions in ocular tissues help protect sensitive components like the retina and lens from oxidative insults, which have been linked to a variety of vision-threatening disorders. Despite its therapeutic promise, quercetin's clinical applicability is severely constrained by its poor water solubility, low intestinal permeability, and significant first-pass metabolism, which results in limited oral bioavailability (Li et al., 2016; D'Andrea, 2015). To address these limitations, researchers have developed a variety of delivery technologies, including liposomes, solid lipid nanoparticles, polymeric micelles, and nanoemulsions, which increase solubility, stability, and targeted distribution. These improved formulations hold special promise for improving ocular delivery, assuring greater drug retention in ocular tissues, and decreasing systemic adverse effects.

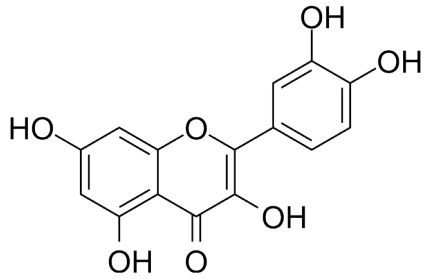

Figure 11: Structure of quercetin

Mangiferin, a naturally occurring xanthone glycoside found in mango leaves, bark, and peels, has been studied for its neuroprotective, anti-inflammatory, antioxidant, and antidiabetic properties (Chen et al., 2022; Saadati et al., 2024; González-Sarrías et al., 2022). It protects neurons by modulating oxidative stress pathways, suppressing pro-inflammatory cytokines, and inhibiting neuronal apoptosis, making it a promising treatment for neurodegenerative diseases like Alzheimer's and Parkinson's (Bhasin et al., 2021; Wang et al., 2023). Mangiferin reduces inflammation by downregulating NF-κB signaling and inhibiting the production of inflammatory mediators like TNF-α, IL-1β, and COX-2 (Sharma et al., 2023). Despite these advantageous qualities, its clinical application is limited due to poor water solubility, low intestinal permeability, and quick metabolism, all of which result in low oral bioavailability (Saha et al., 2023; Patel et al., 2022). These pharmacokinetic restrictions have prompted researchers to investigate innovative drug delivery systems such as nanocarriers, liposomes, solid lipid nanoparticles, and inclusion complexes with cyclodextrins in order to improve solubility, stability, and systemic absorption. Such approaches have showed promise in increasing the therapeutic efficacy of mangiferin for a variety of chronic inflammatory and neurological diseases. Ongoing research into formulation developments and tailored delivery systems is important for bringing mangiferin's preclinical potential to clinical use.

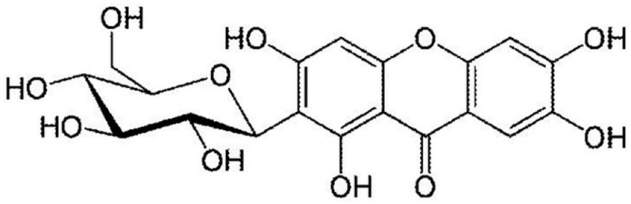

Figure 12: Structure of mangiferin

Table 1: Comparative analysis of phytochemicals used in the research

Parameter	*Naringin*	*Ellagic Acid*	*Quercetin*
Distribution	Flavonoid found in grapefruit & citrus-related species	Ellagic acid, a polyphenol abundant in various fruits and nuts. High concentrations are found in chestnuts, blackberries, etc.	a flavonoid with some of the richest sources as onions (especially red onions), apples, broccoli, grapes, berries tomatoes, and tea
Therapeutic Use	Anti-diabetic, Anti-inflammatory	Antioxidant, Antimicrobial	Anti-oxidant , Anti-inflammatory, Ocular Protection
Solubility	Poor in water	Poor in water	Poor in water
Bioavailability	Low	Low	Low
Challenges	Low Absorption, Rapid Metabolism	Low Absorption, Rapid Metabolism and elimination	Low Permeability, Limited Solubility

1.5. Types of Nanocarriers formulated in the present research

1.5.1 Natural polymer (chitosan) based nanocarriers

Chitosan is primarily derived from crab and shrimp cells, as well as fish scales, through deacetylation of chitin (a component of shell development). Chitosan can be extracted from arthropod shells using a 40% KOH solution heated to 90°C. Chitosan has been extensively explored in recent years due to its exceptional ability to operate as drug nanocarriers. They are inexpensive, can carry a wide range of drugs, and allow for long-term delivery. There are various chitosan nanoparticles available these days, however nanoparticles generated through ionic gelation are the most stable and can transport drugs for a longer period of time (Rinaudo et al., 2006, Dash al., 2011, Khor et al., 2003, Kean et al., 2010, Sreekumar et al., 2018, Bernkop-Schnürch et al., 2012, Reis et al., 2008)

The primary amine group in chitosan ($-NH_2$) has a great affinity for chemical interaction, providing a good reaction site for varied medicinal applications. The sulphur and phosphate groups improve physiochemical stability and trapping efficiency. When combined with chitosan, sodium tri-polyphosphate (NaTPP) works well as a crosslinking agent. They produce stable nanopockets that can transport drugs/phytochemicals to its

intended site of action while also prolonging its release. It is produced by heating a stoichiometric mixture of monosodium phosphate and disodium phosphate in a controlled environment (Bhumkar et al., 2006).

Chitosan treated with CH_3Cl and NaOH at 60^0°C produces N-trimethyl chitosan chloride (quaternized chitosan), which improves chitosan solubility in intestinal media. TMC-60 and TMC-40 are two different grades of N-trimethyl chitosan chloride that operate as bioenhancers for hydrophilic macromolecules. Chitosan is treated with thiol to produce thiolated chitosan for improved mucoadhesive properties (Bernkop-Schnürch et al., 2000, Kotzé et al., 1999)

Quaternization of chitosan opens up tight cell junctions and aids insulin absorption via CACO-2 cells with the help of numerous produced derivatives such as trimethyl (TMC), diethylmethyl (DEMC), dimethylethyl (DMEC), triethyl chitosan (TEC), and so on. When carboxylated chitosan is grafted with polymethyl methacrylate, pH-sensitive targeting becomes conceivable. The linkage of D,L-lactic acid with the -NH_2 groups in chitosan results in the development of a pH sensitive polymeric gel for delivering drugs to a specific region of the gastro intestinal tract via the mucus layer. Chitosan's versatility enables it to operate as a polymeric nanoparticle for a wide range of drug delivery applications (Sadeghi et al., 2008, Zhang et al., 2007, Berger et al., 2004)

Epigallocatechin and catechin are powerful antioxidants found in fresh green tea leaves. However, their applicability is limited due to breakdown in gastrointestinal fluid and a low absorption rate at the intestine wall. To address this issue, catechin and epigallocatechin have been encapsulated in polymeric chitosan nanoparticles, which not only dramatically lower degradation but also aids in the permeation (Dube et al., 2010, Dube et al., 2011, Liu et al., 2016). Tamoxifen, an anticancer medication, is slightly water soluble, and its total permeation rate across the intestinal epithelium cell lining is weak. It was observed that by producing tamoxifen-induced lecithin chitosan nanoparticles, the overall penetration rate of the medication was dramatically boosted (Barbieri et al., 2013, Barbieri et al., 2015) Similarly, Feng et al. formulated doxorubicin hydrochloride with carboxymethyl chitosan and chitosan. According to the findings, total absorption was significantly increased in the intestinal lining of the gastrointestinal lining (Feng et al., 2014). Sunitinib, a therapeutically active chemical for the treatment of

imatinib-resistant gastrointestinal stromal tumors and renal cell carcinoma, has a short biological half-life. The Chitosan nanoparticles encapsulating sunitinib displayed remarkable entrapment efficiency (98% entrapment) while enhancing the drug's sustainability over 72 hours (Gomathi et al., 2022).

Chitosan has high mucoadhesive qualities while remaining biodegradable and biocompatible, with low systemic toxicity. Chitosan not only adheres to the mucus wall but also aids in the opening of the tight junction, allowing the loaded drug to pass through. Chitosan nanoparticles treated with carboxymethyl have been a promising carrier for anti-epileptic drug, carbamazepine. Carboxymethyl chitosan nanoparticles increased the overall bioavailability of brain-targeted medicines when administered via nasal route. Studies demonstrate an incredible 150% increased exposure in the brain-plasma ratio (Liu et al., 2018).

The above examples thus prove that chitosan can be utilized in a variety of ways based on the application and the compatibility of the compound being loaded. This adaptability also enables for the creation of several types of nanoparticles. The following procedures are commonly used to create chitosan nanoparticles: microemulsion, ionic gelation, solvent evaporation (emulation-based evaporation technique), and solvent diffusion (emulsion-based). The major advantages of these approaches are that they can be prepared easily with reproducibility and high encapsulation efficiency. The degree of acetylation and the molecular weight are two main factors that determine the total size and surface charge of the produced nanoparticle. Hydrogen bonding, electrostatic interaction, and hydrophobic interactions are the fundamental chemical reactions that occur throughout the nanoparticle formation process.

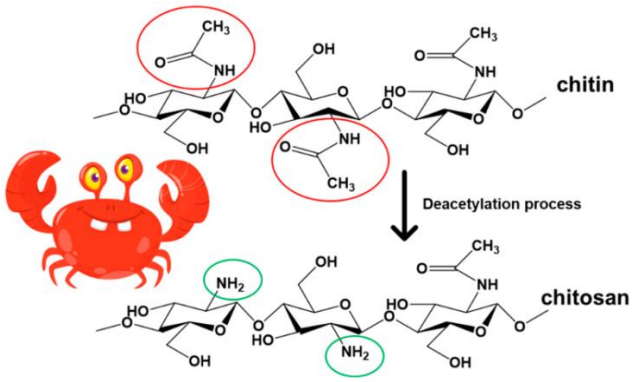

Figure 13: Structure of chitin and chitosan (Oyekunle et al., 2024)

1.5.2 Synthetic polymer (polycaprolactone) based nanocarriers

Synthetic polymeric nanocarriers have several advantages including controlled release, ability to protect physiologically active substances from the environment, and an improvement in bioavailability and therapeutic index. The nanocapsule is enclosed by a polymeric shell that regulates the drug's release profile from the oily core, in which the medication is typically dissolved. Because of the continuous polymeric network structure of nanospheres, drugs can be adsorbed onto their surfaces or retained within them. Polymer nanoparticles are classified into two types: matrix systems (nanospheres) and reservoir systems (nanocapsules).

Polycaprolactone (PCL) is synthetic biodegradable semi-crystalline, aliphatic polyester with a glass transition temperature of approximately -60 °C and a melting point of roughly 60°C and resists chemical hydrolysis appreciably. It is reported to lack toxicity with high drug permeability. It is extremely hydrophobic with a crystal polymer that breaks down extremely slowly without enzymes, both in vitro and in vivo. PCL is frequently added to resins to enhance their processing capabilities and final product attributes (such as impact resistance). PCL is a can be combined with starch to reduce costs and improve biodegradability, and can be added to polyvinyl chloride (PVC) as a polymeric plasticizer (Woodruff MA et al., 2010, Gajdosova V et al., 2022). PCL is typically produced by a polymerization technique that involves combining a monomer and an initiator at high temperatures while nitrogen is purged. The resultant polymer is then cooled, dissolved in an organic solvent, and washed to remove any unreacted particles. Following that, the polymer is freeze-dried and stored for later use, such as

scaffolding, microparticles, and nanoparticles. PCL can be used as a polymeric plasticizer in polyvinyl chloride (PVC) or combined with starch to improve biodegradability and minimize costs. It is compatible with many different materials (Bodaghifard et al., 2022, da Silva et al., 2011.)

PCL has multiple advantages, including biocompatibility, biodegradability, and ease of modification, making it ideal for a variety of applications, including tissue engineering. PCL can be functionalized to graft polymer chains, broadening its uses in biomedical science. Pure PCL lacks antibacterial activity, but treatment with various plant extracts have been shown to improve its antimicrobial capabilities (Kumari et al., 2021).

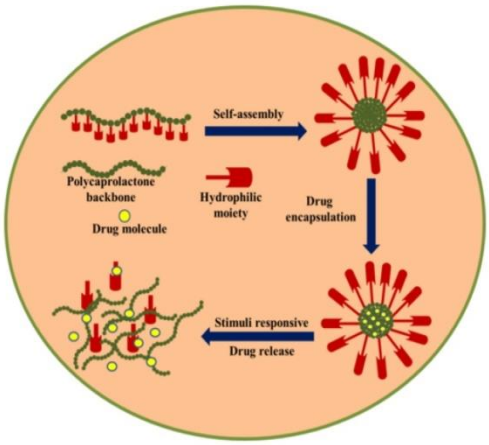

Figure 14: Representation of drug loaded PCL nanocarriers (Mandal et al., 2020)

5.2 Metal based nanocarriers

Metallic nanoparticles are a promising system with applications in drug delivery, optics, catalysis, electronics, and health sciences. Metallic nanoparticles often use chemical reducing agents such as sodium citrate, hydrazine, and sodium borohydride to reduce the appropriate precursor salts. The production of metallic nanoparticles for phytochemicals is a mostly unexplored field with enormous research potential. Tea, for example, is well-known for its antioxidant properties, which include phytocompounds such as polyphenols. Tea leaf extracts were recently employed in the green synthesis of AuNPs and AgNPs (Jang et al., 2010, Saha et al., 2010, Vivekanandhan et al., 2009, Philip et al., 2009, Kemp et al., 2009)

For centuries, researchers have explored the potential medical applications of colloidal gold. However, the synthesis and detailed evaluation of various gold nanoparticles (AuNPs) have gained significant momentum only in recent years. The ability to functionalize the surface of AuNPs with diverse targeting and therapeutic molecules has greatly expanded their biomedical utility—particularly in cancer treatment. Functionalized gold nanoparticles exhibit excellent biocompatibility and predictable biodistribution, making them promising candidates for the development of novel therapeutics. Gold nanoparticles have demonstrated great promise in oncology. Owing to their unique photophysical and optical properties, they are not only useful in cancer diagnostics but also in photothermal therapy (PTT). Unlike conventional therapies, gold nanoparticles are non-toxic and non-radioactive, reducing the risk of adverse effects. Their photothermal capabilities allow them to convert light into heat, effectively destroying surrounding cancerous tissue. This method has been employed in the treatment of soft tissue tumors, including those in the brain, cervix, prostate, and skin. Structurally, gold nanoparticles consist of clusters of gold atoms with diameters typically under 100 nm, enabling them to interact with visible light. Their colloidal solutions can range in color from deep red to black, depending on size and concentration—a property stemming from surface plasmon resonance (SPR). Furthermore, green synthesis approaches—particularly single-step methods—have proven effective for producing stable, non-toxic AuNPs and AgNPs suitable for therapeutic and diagnostic applications. The incorporation of phytochemicals from various plant species during synthesis enhances their anticancer potential and opens new avenues for designing tumor-specific nanomedicines (Ghosh et al., 2008, Hutchings et al., 2008, Dreaden et al., 2011, Jain et al., 2007, Huang et al., 2007, Daniel et al., 2004, Thakor et al., 2011).

Silver nanoparticles (*AgNP*s) are increasingly being utilized across a wide range of sectors, including clinical medicine, food processing, healthcare, consumer products, and industrial applications, due to their unique physical and chemical properties (Rai et al., 2009; Franci et al., 2015). These include optical, electrical, and thermal properties, high electrical conductivity, and significant biological activity (Morones et al., 2005; Ahamed et al., 2010). Because of these qualities, AgNPs have been used as antimicrobial agents in consumer and medical items, coatings for medical devices, optical sensors,

cosmetics, pharmaceutical formulations, diagnostics, orthopedics, and drug delivery systems (Marambio-Jones and Hoek, 2010; Chaloupka et al., 2010). Notably, AgNPs have shown promise as anticancer agents, increasing the efficacy of chemotherapy medicines (Gurunathan et al., 2013; Zhang et al., 2016). To accommodate the growing need for AgNPs, several synthesis methods have been developed. Traditional physical and chemical treatments, while effective, are frequently expensive and environmentally harmful (Iravani et al., 2014). Biological or green synthesis methods, on the other hand, provide a simple, quick, non-toxic, and environmentally friendly alternative, frequently producing nanoparticles with good solubility, stability, and bioactivity (Ahmed et al., 2016; Song and Kim, 2009). Surface chemistry, size, shape, morphology, structure, coating or capping agents, agglomeration behavior, and dissolution rate all have an impact on AgNPs' biological activity (McGillicuddy et al., 2017; Pal et al., 2007). Furthermore, the type of reducing agents used during synthesis has a significant impact on their cytotoxicity. The physicochemical features of AgNPs have a direct impact on cellular absorption, biodistribution, ability to traverse biological barriers, and therapeutic efficacy (Beer et al., 2012; Zaidan et al., 2018). Importantly, they can increase the bioavailability of active medicinal substances when given locally and systemically. As a result, the regulated synthesis of AgNPs with uniform size, shape, and surface functionality is critical for improving their performance in biological and clinical settings. AgNPs have several advantages, including large-scale production capacity, long-term stability, tailored drug delivery potential, minimal toxicity, and broad-spectrum antibacterial efficacy (Prabhu and Poulose, 2012; Kim et al., 2011).

Copper Based Nanoparticles (*CuNPs*) range in size from 1 to 100 nm and can be generated chemically or biologically (Usman et al., 2013; Borkow and Gabbay, 2005). Historically, these nanoparticles have been used as coloring agents as well as biological and antibacterial uses, making them quite intriguing (Ren et al., 2009). Their powerful antibacterial capabilities render them efficient against bacteria, fungi, and viruses (Cioffi et al., 2005; Azam et al., 2012). Copper nanoparticles are also being investigated for biological applications such as medication delivery, imaging, and therapy because of their capacity to selectively target certain cells or tissues, potentially leading to improved treatments for diseases such as cancer (Zhao et al., 2017; Vincent et al., 2016). Copper-

based nanoparticles are thus a flexible and promising nanomaterial class, with numerous applications in catalysis, antimicrobial coatings, and biomedicine (Ruparelia et al., 2008). When compared copper is less expensive and more readily available than silver or gold-based nanoparticles (Duncan and Richards, 2010). Copper nanoparticles have several advantages over traditional agents, including lower toxicity, cost-effectiveness, improved pharmacokinetics, and a sustained therapeutic effect (Gunawan et al., 2011). When used as antimicrobial agents, copper nanoparticles can help prevent antibiotic resistance and support more efficient drug delivery (Malhotra et al., 2020). Recent studies confirm their effectiveness in managing infectious diseases due to their strong antimicrobial properties.

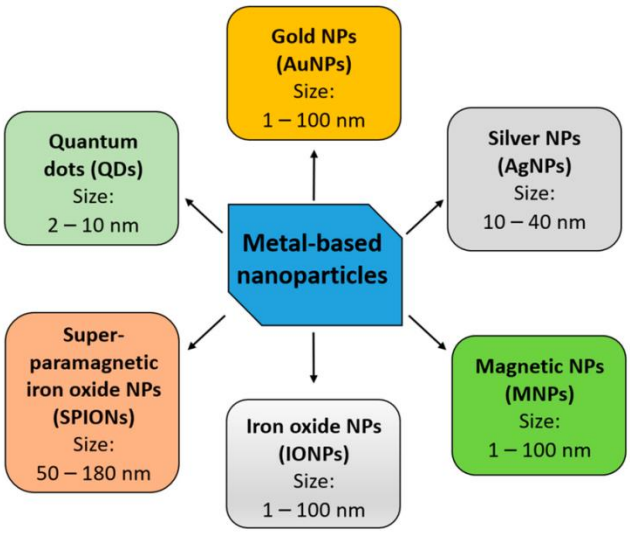

Figure 15: Representation of major types of metal nanoparticles (Gawel et al., 2022)

REFERENCES

- Ahamed M, AlSalhi MS, Siddiqui MK. Silver nanoparticle applications and human health. Clin Chim Acta. 2010;411(23–24):1841–8.
- Ahmad S, Sultana S, Alrobaian MM, Al-Khedhairy AA, Rahman A. Naringin ameliorates oxidative stress and inflammatory response in aluminum chloride induced neurotoxicity in rats. Life Sci. 2015;122:247–55.
- Ahmed S, Ahmad M, Swami BL, Ikram S. A review on plants extract mediated synthesis of silver nanoparticles for antimicrobial applications: a green expertise. J Adv Res. 2016; 7(1):17–28.
- Alam MA, Subhan N, Rahman MM, Uddin SJ, Reza HM, Sarker SD. Effect of citrus flavonoids, naringin and naringenin, on metabolic syndrome and their mechanisms of action. Adv Nutr. 2014;5(4):404–17.
- Almgren M. Mixed micelles and other structures in the solubilization of bilayer lipid membranes by surfactants. Biochim Biophys Acta. 2000;1508(1-2):146-63.
- Anselmo AC, Mitragotri S. Nanoparticles in the clinic: An update. Bioeng Transl Med. 2019;4(3):e10143.
- Aqil F, Munagala R, Jeyabalan J, Vadhanam MV. Bioavailability of phytochemicals and its enhancement by drug delivery systems. Cancer Lett. 2013 Jun 28;334(1):133–41.
- Azam A, Ahmed AS, Oves M, Khan MS, Habib SS, Memic A. Antimicrobial activity of metal oxide nanoparticles against Gram-positive and Gram-negative bacteria: a comparative study. Int J Nanomedicine. 2012;7:6003–9.
- Barbieri S, Buttini F, Rossi A, Bettini R, Colombo P, Ponchel G, et al. Ex vivo permeation of tamoxifen and its 4-OH metabolite through rat intestine from lecithin/chitosan nanoparticles. Int J Pharm. 2015;491(1-2):99–104.
- Barbieri S, Sonvico F, Como C, Colombo G, Zani F, Buttini F, et al. Lecithin/chitosan controlled release nanopreparations of tamoxifen citrate: Loading, enzyme-trigger release and cell uptake. J Control Release. 2013;167(3):276–283.

- Batrakova EV, Kabanov AV. Pluronic block copolymers: evolution of drug delivery concept from inert nanocarriers to biological response modifiers. J Control Release. 2008;130(2):98-106.
- Bayón-Cordero L, Alkorta I, Arana L. Application of solid lipid nanoparticles to improve the efficiency of anticancer drugs. Nanomaterials. 2019;9(3):474.
- Beer C, Foldbjerg R, Hayashi Y, Sutherland DS, Autrup H. Toxicity of silver nanoparticles—Nanoparticle or silver ion? Toxicol Lett. 2012;208(3):286–92.
- Berger J, Reist M, Mayer JM, Felt O, Peppas NA, Gurny R. Structure and interactions in covalently and ionically crosslinked chitosan hydrogels for biomedical applications. Eur J Pharm Biopharm. 2004;57(1):19-34.
- Bernkop-Schnürch A, Dünnhaupt S. Chitosan-based drug delivery systems. Eur J Pharm Biopharm. 2012;81(3):463-469.
- Bernkop-Schnürch A, Steininger S. Synthesis and characterisation of mucoadhesive thiolated polymers. Int J Pharm. 2000;194(2):239-247.
- Bhasin S, Maheshwari R, Kumar R, Khurana RK. Ellagic acid: Insights into its neuroprotective and anticancer properties. J Ethnopharmacol. 2021;273:113987.
- Bhasin S, Sharma R, Singh B. Emerging therapeutic potential of mangiferin in neurological disorders. Curr Neuropharmacol. 2021;19(6):857–67.
- Bhumkar DR, Pokharkar VB. Studies on effect of pH on cross-linking of chitosan with sodium tripolyphosphate: A technical note. AAPS PharmSciTech. 2006;7(2):E50.
- Bilensoy E. Cyclodextrins in pharmaceutics, cosmetics, and biomedicine: current and future industrial applications. Hoboken: John Wiley & Sons; 2011.
- Bodaghifard MA, Shabani I, Soleimani M, et al. Fabrication and examination of polyorganophosphazene/polycaprolactone nanofibrous scaffold for tissue engineering applications. Sci Rep. 2022;12(1):15049.
- Bohn T. Dietary factors affecting polyphenol bioavailability. Nutr Rev. 2014;72(7):429-52.
- Boon CS, McClements DJ, Weiss J, Decker EA. Factors influencing the chemical stability of carotenoids in foods. Crit Rev Food Sci Nutr. 2010;50(6):515-32.
- Boots AW, Haenen GR, Bast A. Health effects of quercetin: from antioxidant to

nutraceutical. Eur J Pharmacol. 2008;585(2-3):325–37.

- Borkow G, Gabbay J. Copper as a biocidal tool. Curr Med Chem. 2005;12(18):2163–75.
- Challa R, Ahuja A, Ali J, Khar RK. Cyclodextrins in drug delivery: an updated review. AAPS PharmSciTech. 2005;6(2):E329-57.
- Chaloupka K, Malam Y, Seifalian AM. Nanosilver as a new generation of nanoproduct in biomedical applications. Trends Biotechnol. 2010;28(11):580–8.
- Chen Y, Liu X, Jia J, Zhao M, Wang L. Pharmacokinetics, bioavailability, and metabolism of naringin: A comprehensive review. Pharmacol Res. 2022;181:106296.
- Chen Y, Zhang M, Liu X, Lin X. Neuroprotective effects of mangiferin: molecular mechanisms and therapeutic potential. J Ethnopharmacol. 2022;289:115003.
- Chiou WL, Riegelman S. Pharmaceutical applications of solid dispersion systems. J Pharm Sci. 1971;60(9):1281–302.
- Choe E, Min DB. Mechanisms and factors for edible oil oxidation. Compr Rev Food Sci Food Saf. 2006;5(4):169-86.
- Cioffi N, Torsi L, Ditaranto N, Tantillo G, Ghibelli L, Sabbatini L, et al. Copper nanoparticle/polymer composites with antifungal and bacteriostatic properties. Chem Mater. 2005;17(21):5255–62.
- Craig DQ. The mechanisms of drug release from solid dispersions in water-soluble polymers. Int J Pharm. 2002;231(2):131–44.Challa et al., 2005.
- Crozier A, Del Rio D, Clifford MN. Bioavailability of dietary flavonoids and phenolic compounds. Mol Aspects Med. 2010;31(6):446-67.
- D'Andrea G. Quercetin: a flavonol with multifaceted therapeutic applications? Fitoterapia. 2015;106:256–71.
- D'Archivio M, Filesi C, Varì R, Scazzocchio B, Masella R. Bioavailability of the polyphenols: status and controversies. Int J Mol Sci. 2010;11(4):1321-42.
- Da Silva CG, de Oliveira SA, de Sá Silva AC, et al. Poly(ε-caprolactone)-based 'green' plasticizers for poly(vinyl chloride). Polym Degrad Stab. 2011;96(10):183–188.

- Da Silva DC, do Pazo FV, de Andrade Ramos J, de Freitas LAP. Nanocrystals as a strategy to enhance drug delivery and bioavailability in pharmaceutical formulations. Int J Pharm. 2020;576:118960.
- Daniel MC, Astruc D. Gold nanoparticles: assembly, supramolecular chemistry, quantum-size-related properties, and applications toward biology, catalysis, and nanotechnology. Chem Rev. 2004;104(1):293–346.
- Dash M, Chiellini F, Ottenbrite RM, Chiellini E. Chitosan—A versatile semi-synthetic polymer in biomedical applications. Prog Polym Sci. 2011;36(8):981-1014.
- Date, AA, & Desai N. (2016). Dissolution enhancement of poorly water-soluble drugs via self-nanoemulsifying drug delivery systems (SNEDDS). In Drug Delivery Strategies for Poorly Water-Soluble Drugs (pp. 233-262). Springer, New York, NY.
- Davis ME, Brewster ME. Cyclodextrin-based pharmaceutics: past, present and future. Nat Rev Drug Discov. 2004;3(12):1023-35.
- Dhirendra K, Lewis S, Udupa N, Atin K. Solid dispersions: A review. Pak J Pharm Sci. 2009;22(2):234–46.
- Dreaden EC, Mackey MA, Huang X, Kang B, El-Sayed MA. Beating cancer in multiple ways using nanogold. Chem Soc Rev. 2011;40(7):3391–404.
- Dube A, Nicolazzo JA, Larson I. Chitosan nanoparticles enhance the intestinal absorption of the green tea catechins (+)-catechin and (−)-epigallocatechin gallate. Eur J Pharm Sci. 2010;41(2):219–225.
- Dube A, Nicolazzo JA, Larson I. Chitosan nanoparticles enhance the plasma exposure of (−)-epigallocatechin gallate in mice through an enhancement in intestinal stability. Eur J Pharm Sci. 2011;44(3):422–426.
- Duncan TV, Richards T. Nanotechnology and the future of food: a review. Trends Food Sci Technol. 2010;21(11):531–40.
- Ekor M. The growing use of herbal medicines: issues relating to adverse reactions and challenges in monitoring safety. Front Pharmacol. 2014 Jan 10;4:177.

- Feng C, Sun G, Wang Z, Cheng X, Park H, Cha D, Kong M, Chen X. Transport mechanism of doxorubicin loaded chitosan based nanogels across intestinal epithelium. Eur J Pharm Biopharm. 2014;87(3):390–400.
- Franci G, Falanga A, Galdiero S, Palomba L, Rai M, Morelli G, et al. Silver nanoparticles as potential antibacterial agents. Molecules. 2015;20(5):8856–74.
- Gajdosova V, Vik M, Ivankova O, et al. Biodegradable thermoplastic starch/polycaprolactone blends with co-continuous morphology suitable for local release of antibiotics. Int J Mol Sci. 2022;23(2):1045.
- Gao L, Liu G, Ma J, Wang X, Zhou L, Li X. Drug nanocrystals: In vivo performances. J Control Release. 2023;355:279-295.
- Garg A, Garg S, Zaneveld LJ, Singla AK. Chemistry and pharmacology of the citrus bioflavonoid naringin. Phytother Res. 2001;15(8):677–86.
- Gawel A, Singh R, Debinski W. Metal-based nanostructured therapeutic strategies for glioblastoma treatment—an update. Biomedicines. 2022;10:1598.
- Ghosh P, Han G, De M, Kim CK, Rotello VM. Gold nanoparticles in delivery applications. Adv Drug Deliv Rev. 2008;60(11):1307–15.
- Gomathi S, Balasubramanian S, Tamilselvan S, Selvamuthukumar S. Formulation and evaluation of chitosan nanoparticles loaded with sunitinib for improved oral bioavailability and sustained release. J Drug Deliv Sci Technol. 2022;74:103553.
- Gonzalez-Sarrias A, Espín JC, Tomás-Barberán FA. The potential of ellagic acid and its derivatives in cancer prevention and therapy. Mol Nutr Food Res. 2022;66(6):2100910.
- González-Sarrías A, Li L, Yuan T, Seeram NP. Role of mangiferin in prevention of inflammation and neurodegenerative diseases. Phytomedicine. 2022;104:154284.
- Gunawan C, Faiz M, Mann R, Ting KN, Marquis CP. Nanosilver's toxicity and potential for resistance: considerations for realistic risk assessment. Small. 2011;7(17):2431–40.
- Gurib-Fakim A. Medicinal plants: traditions of yesterday and drugs of tomorrow. Mol Aspects Med. 2006 Aug;27(1):1–93.

- Gurunathan S, Han JW, Eppakayala V, Jeyaraj M, Kim JH. Cytotoxicity of biologically synthesized silver nanoparticles in MDA-MB-231 human breast cancer cells. Biomed Res Int. 2013;2013:535796.
- Hajipour MJ, Fromm KM, Ashkarran AA, de Aberasturi DJ, de Larramendi IR, Rojo T, et al. Antibacterial properties of nanoparticles. Trends Biotechnol. 2012;30(10):499–511.
- Harvey AL. Natural products in drug discovery. Drug Discov Today. 2008 Oct;13(19-20):894–901.
- Hirayama F, Uekama K. Cyclodextrin-based controlled drug release system. Adv Drug Deliv Rev. 1999;36(1):125-41.
- Huang X, Jain PK, El-Sayed IH, El-Sayed MA. Gold nanoparticles: interesting optical properties and recent applications in cancer diagnostics and therapy. Nanomedicine. 2007;2(5):681–93.
- Hutchings GJ, Brust M, Schmidbaur H. Gold—An introductory perspective. Chem Soc Rev. 2008;37(9):1759–65.
- Iravani S, Korbekandi H, Mirmohammadi SV, Zolfaghari B. Synthesis of silver nanoparticles: chemical, physical and biological methods. Res Pharm Sci. 2014;9(6):385–406.
- Ishikawa Y, Kitamura M, Takahashi N, Nagasaka A, Natori A, Watanabe H, et al. Quercetin inhibits inflammatory mediators and modulates the Nrf2/HO-1 pathway in ARPE-19 cells. Invest Ophthalmol Vis Sci. 2013;54(10):6978–84.
- Jacob J, et al. Vesicular carriers for phytochemical delivery: a comprehensive review of techniques and applications. Pharmaceutics. 2025;17(4):464.
- Jain A, Garg NK, Tiwari A, Rathore K, Goyal AK, Vyas SP. Current understanding of the potential of naringin for targeting oxidative stress related neurodegenerative diseases. Curr Drug Targets. 2018;19(6):614–28.
- Jain PK, El-Sayed IH, El-Sayed MA. Au nanoparticles target cancer. Nano Today. 2007;2(1):18–29.
- Jaiswal, P., Aggarwal, G., Harikumar, S. L., & Singh, K. (2014). Self-emulsifying drug delivery system (SEDDS): A review. Journal of Drug Delivery and Therapeutics, 4(2), 25-33.

- Jang HD, Park SJ, Chang HK. Reduction of silver nanoparticles in the presence of natural polymers. J Mater Sci. 2010;45(5):1256–61.
- Jermain SV, Brough C, Williams RO 3rd. Amorphous solid dispersions and nanocrystal technologies for poorly water-soluble drug delivery – An update. Int J Pharm. 2018;535(1-2):379–92.
- Jones MC, Leroux JC. Polymeric micelles—a new generation of colloidal drug carriers. Eur J Pharm Biopharm. 1999;48(2):101-11.
- Kabanov AV, Batrakova EV, Alakhov VY. Pluronic block copolymers as novel polymer therapeutics for drug and gene delivery. J Control Release. 2002;82(2-3):189-212.
- Kazi KM. Niosomes: a promising approach for targeted drug delivery. GSC Biol Pharm Sci. 2023;27(1):199-210.
- Kean T, Thanou M. Biodegradation, biodistribution and toxicity of chitosan. Adv Drug Deliv Rev. 2010;62(1):3-11.
- Kemp MM, Kumar A, Mousa S, Dutta PK. Synthesis of gold nanoparticles using tea: A green approach. Langmuir. 2009;25(17):10283–90.
- Kesisoglou F, Panmai S, Wu Y. Nanosizing—Oral formulation development and biopharmaceutical evaluation. Adv Drug Deliv Rev. 2019;59(7):631-644.
- Khan, S., Baboota, S., Ali, J., Khan, F., & Kaur, S. (2006). Nanostructured lipid carriers: An emerging platform for improving oral bioavailability of lipophilic drugs. International Journal of Pharmaceutics, 323(1-2), 1-9.
- Khor E, Lim LY. Implantable applications of chitin and chitosan. Biomaterials. 2003;24(13):2339-2349.
- Kim SH, Lee HS, Ryu DS, Choi SJ, Lee DS. Antibacterial activity of silver-nanoparticles against Staphylococcus aureus and Escherichia coli. Korean J Microbiol Biotechnol. 2011;39(1):77–85.
- Kotzé AF, Thanou MM, Lueßen HL, de Boer AG, Verhoef JC, Junginger HE. Effect of the degree of quaternization of N-trimethyl chitosan chloride on the permeability of intestinal epithelial cells (Caco-2). Eur J Pharm Biopharm. 1999;47(3):269-274.

- Kumar S, Pandey AK. Chemistry and biological activities of flavonoids: an overview. ScientificWorldJournal. 2013 May 2;2013:162750.
- Kumar S, Pandey AK. Factors affecting absorption, metabolism, and bioactivity of dietary flavonoids in humans. Nutrients. 2013;5(11):4284-304.
- Kumari S, Panwar V, Yadav SK. Development of polycaprolactone nanofibers containing neem and lavender oils for antimicrobial applications. Membranes (Basel). 2021;11(10):712.
- Leuner C, Dressman J. Improving drug solubility for oral delivery using solid dispersions. Eur J Pharm Biopharm. 2000;50(1):47–60.
- Li Y, Yao J, Han C, Yang J, Chaudhry MT, Wang S, et al. Quercetin, inflammation and immunity. Nutrients. 2016;8(3):167.
- Liu F, Majeed H, Antoniou J, Li Y, Ma Y, Yokoyama W, et al. pH and temperature stability of (−)-epigallocatechin-3-gallate-beta-cyclodextrin inclusion complex-loaded chitosan nanoparticles. Carbohydr Polym. 2016;149:340–347.
- Liu RH. Health benefits of phytochemicals in functional foods. Nutr Rev. 2004 Nov;62(11):456–9.
- Liu S, Yang S, Ho PC. Intranasal administration of carbamazepine-loaded carboxymethyl chitosan nanoparticles for drug delivery to the brain. Asian J Pharm Sci. 2018;13(1):72–81.
- Liu Y, Sun M, Yao H. Phytochemicals and bioactive compounds in food. Front Nutr. 2022;9:820997.
- Loftsson T, Brewster ME. Pharmaceutical applications of cyclodextrins: basic science and product development. J Pharm Pharmacol. 2010;62(11):1607-21.
- Loftsson T, Duchêne D. Cyclodextrins and their pharmaceutical applications. Int J Pharm. 2007;329(1-2):1-11.Cai et al., 2012
- Malhotra B, Patel V, Patel A, Shah M. Copper nanoparticles: synthesis, characterization and their antimicrobial applications. Mater Today Proc. 2020;26:2513–7.
- Manach C, Scalbert A, Morand C, Rémésy C, Jiménez L. Polyphenols: food sources and bioavailability. Am J Clin Nutr. 2004;79(5):727-47.

- Mandal P, Shunmugam R. Polycaprolactone: a biodegradable polymer with its application in the field of self-assembly study. J Macromol Sci A. 2020;58(2):111–129.
- Marambio-Jones C, Hoek EM. A review of the antibacterial effects of silver nanomaterials and potential implications for human health and the environment. J Nanopart Res. 2010;12(5):1531–51.
- Marttin E, Verhoef JC, Merkus FW. Efficacy, safety and mechanism of cyclodextrins as absorption enhancers in nasal delivery of peptide and protein drugs. J Drug Target. 1998;6(1):17-36.
- Maximiliano Cagel, Tesan FC, Bernabeu E, Salgueiro MJ, Zubillaga MB, Moretton MA, Chiappetta DA. Polymeric mixed micelles as nanomedicines: Achievements and perspectives. Eur J Pharm Biopharm. 2017;113:211–228.
- McClements DJ, Li F, Xiao H. The nutraceutical bioavailability classification scheme: classifying nutraceuticals according to factors limiting their oral bioavailability. Annu Rev Food Sci Technol. 2015;6:299-327.
- McGillicuddy E, Murray I, Kavanagh S, Morrison L, Fogarty A, Cormican M, et al. Silver nanoparticles in the environment: sources, detection and ecotoxicology. Sci Total Environ. 2017;575:231–46.
- Mehnert, W., & Mäder, K. (2001). Solid lipid nanoparticles: Production, characterization, and applications. Advanced Drug Delivery Reviews, 47(2-3), 165-196.
- Moghassemi S, et al. Niosomes: composition, formulation techniques, and recent progress as delivery systems in cancer therapy. Pharmaceutics. 2023;16(2):223.
- Moghassemi S, et al. Niosomes: composition, formulation techniques, and recent advances in drug delivery and vaccine applications. Pharmaceutics. 2023;16(2):223.
- Morones JR, Elechiguerra JL, Camacho A, Holt K, Kouri JB, Ramirez JT, et al. The bactericidal effect of silver nanoparticles. Nanotechnology. 2005;16(10):2346–53.

- Mu C, Zhu W, Yang Y, Zheng Z, Li X, Zhang N, et al. Strategies to enhance oral bioavailability of flavonoids: a review. Food Res Int. 2021;141:110169.
- Müller RH, Mäder K, & Gohla S. (2000). Solid lipid nanoparticles (SLN) for controlled drug delivery – A review of the state of the art. European Journal of Pharmaceutics and Biopharmaceutics, 50(1), 161-177.
- Mulvihill EE, Huff MW. Naringenin metabolism in vitro and in humans: a focus on its potential to treat metabolic diseases. Adv Nutr. 2010;1(1):45–53.
- Nambiar A, Singh M, Mali AR, Serrano D, Kumar R, Healy A, Agrawal A, Kumar D. Continuous manufacturing and molecular modeling of pharmaceutical amorphous solid dispersions. AAPS PharmSciTech. 2022;23:10.
- Oyekunle DT, Nia MH, Wilson LD. Recent progress on the application of chitosan, starch and chitosan–starch composites for meat preservation—a mini review. J Compos Sci. 2024;8:302.
- Pal S, Tak YK, Song JM. Does the antibacterial activity of silver nanoparticles depend on the shape of the nanoparticle? A study of the gram-negative bacterium Escherichia coli. Appl Environ Microbiol. 2007;73(6):1712–20.
- Palafox-Carlos H, Ayala-Zavala JF, González-Aguilar GA. The role of dietary fiber in the bioaccessibility and bioavailability of fruit and vegetable antioxidants. J Food Sci. 2011;76(1):R6-R15.
- Pardeike, J., Hommoss, A., & Müller, R. H. (2009). Lipid nanoparticles (SLN, NLC) in cosmetic and pharmaceutical dermal products. International Journal of Pharmaceutics, 366(1-2), 170-184.
- Patel BP, Patel JK. A review on solid dispersion and carriers used therein for solubility enhancement of poorly water soluble drugs. Adv Pharm Bull. 2020;10(3):359–69.
- Patel DK, Kumar R, Prasad SK. Approaches to improve solubility and delivery of mangiferin: A review. J Drug Deliv Sci Technol. 2022;70:103153.
- Philip D. Green synthesis of gold and silver nanoparticles using Hibiscus rosa-sinensis. Physica E Low-dimens Syst Nanostruct. 2009;42(5):1417–24.

- Porter, C. J. H., Trevaskis, N. L., & Charman, W. N. (2007). Lipids and lipid-based formulations: Optimizing the oral delivery of lipophilic drugs. Nature Reviews Drug Discovery, 6(3), 231-248.
- Pouton, C. W. (2006). Formulation of self-emulsifying drug delivery systems. Advanced Drug Delivery Reviews, 58(7), 617-630.
- Prabhu S, Poulose EK. Silver nanoparticles: mechanism of antimicrobial action, synthesis, medical applications, and toxicity effects. Int Nano Lett. 2012;2(1):32.
- Rai M, Yadav A, Gade A. Silver nanoparticles as a new generation of antimicrobials. Biotechnol Adv. 2009;27(1):76–83.
- Ramachandran, R., & Thangarajan, S. (2016). Solid lipid nanoparticles: A review on recent perspectives and patents. Advanced Science, Engineering and Medicine, 8(8), 635-651.
- Ramadon D, McCrudden M, Courtenay A, Donnelly R. Enhancement strategies for transdermal drug delivery systems: current trends and applications. Drug Deliv Transl Res. 2022;12:758–791.
- Reis RL, Neves NM, Mano JF, Gomes ME, Marques AP, Azevedo HS. Natural-Based Polymers for Biomedical Applications. Elsevier; 2008.
- Ren G, Hu D, Cheng EW, Vargas-Reus MA, Reip P, Allaker RP. Characterisation of copper oxide nanoparticles for antimicrobial applications. Int J Antimicrob Agents. 2009;33(6):587–90.
- Rezhdo O, Specian A, Hall P, Miao J, Lunte S, Davies NM, et al. Passive and active transport of flavonoids: roles of bioavailability and bioefficacy. Pharm Res. 2020;37(7):129.
- Riccardi L, et al. Liposomes, transfersomes, and niosomes: production methods and their applications in the vaccinal field. J Transl Med. 2024;22:160.
- Rinaudo M. Chitin and chitosan: Properties and applications. Prog Polym Sci. 2006;31(7):603-632.
- Rossier, B., Jordan, O., Allémann, E. et al. Nanocrystals and nanosuspensions: an exploration from classic formulations to advanced drug delivery systems. Drug Deliv. and Transl. Res. 14, 3438–3451 (2024).

- Ruparelia JP, Chatterjee AK, Duttagupta SP, Mukherji S. Strain specificity in antimicrobial activity of silver and copper nanoparticles. Acta Biomater. 2008;4(3):707–16.
- Saadati S, Dadgar N, Rashidian A, Amini M, Vandamme T. Enhancement of naringin solubility and dissolution rate using solid dispersions in cellulose derivative matrices. Biointerface Res Appl Chem. 2024;14(5):183-195.
- Saadati S, Mohammadi R, Beheshti F. Mangiferin as a natural neuroprotective agent: a review on its pharmacological effects and mechanisms. Neurochem Res. 2024;49(2):123–32.
- Sadeghi AM, Dorkoosh FA, Avadi MR, Weinhold M, Bayat A, Delie F, et al. Permeation enhancer effect of chitosan and chitosan derivatives: Comparison of formulations as soluble polymers and nanoparticulate systems on insulin absorption in Caco-2 cells. Eur J Pharm Biopharm. 2008;70(1):270-278.
- Saeidi N, Sander MC, Koutsidis G, Fryer PJ. Structural and functional properties of phytochemicals in relation to bioavailability and bioefficacy: a review. Food Res Int. 2021;147:110449.
- Saha S, Mukherjee A, Chattopadhyay D. Bioavailability and pharmacokinetics of mangiferin: challenges and approaches. Drug Dev Res. 2023;84(2):167–76.
- Saha S, Pal A, Kundu S. Green synthesis of gold nanoparticles using tea: Size-controlled synthesis, stability and antimicrobial study. Colloids Surf B Biointerfaces. 2010;81(1):113–7.
- Sailor GU. Self-nanoemulsifying drug delivery systems (SNEDDS): An innovative approach to improve oral bioavailability. In: Shah N, editor. Nanocarriers: Drug Delivery System. Singapore: Springer; 2021. p. [Chapter 10].
- Salehi B, Fokou PVT, Sharifi-Rad M, Zucca P, Pezzani R, Martins N. The therapeutic potential of naringenin: a review of clinical trials. Pharmacol Res. 2019;139:264–75.
- Savjani KT, Gajjar AK, Savjani JK. Drug solubility: Importance and enhancement techniques. ISRN Pharm. 2012;2012:195727.
- Selma MV, Espín JC, Tomás-Barberán FA. Interaction between phenolics and gut microbiota: role in human health. J Agric Food Chem. 2009;57(15):6485-501.

- Serajuddin AT. Solid dispersion of poorly water-soluble drugs: Early promises, subsequent problems, and recent breakthroughs. J Pharm Sci. 1999;88(10):1058–66.
- Sharma A, Tomar RS, Kumar R. Anti-inflammatory and antioxidant activities of mangiferin in experimental models. Inflammopharmacology. 2023;31(1):15–24.
- Shegokar R, Müller RH. Nanocrystals: Industrially feasible multifunctional formulation technology for poorly soluble actives. Int J Pharm. 2018;549(1-2):193-206.
- Shimizu S. Structural and functional characteristics of intestinal absorption of flavonoids. Biosci Biotechnol Biochem. 2012;76(1):1-9.
- Singh S, Kumar R, Hemant K, Ram M, Shivakumar HN. Nanonization of poorly soluble drugs: a review. Eur J Pharm Biopharm. 2021;166:26-46.
- Singh, B., Bandopadhyay, S., Kapil, R., Singh, R., & Katare, O. P. (2009). Self-emulsifying drug delivery systems (SEDDS): Formulation development, characterization, and applications. Critical Reviews in Therapeutic Drug Carrier Systems, 26(5), 427-521.
- Song JY, Kim BS. Rapid biological synthesis of silver nanoparticles using Plantago asiatica leaf extract. Bioprocess Biosyst Eng. 2009;32(1):79–84.
- Sreekumar S, Goycoolea FM, Moerschbacher BM, Rivera-Rodriguez GR. Parameters influencing the size of chitosan-TPP nano- and microparticles. Sci Rep. 2018;8(1):4695.
- Stella VJ, Rajewski RA. Cyclodextrins: their future in drug formulation and delivery. Pharm Res. 1997;14(5):556-67.
- Thakor AS, Jokerst JV, Zavaleta CL, Massoud TF, Gambhir SS. Gold nanoparticles: a revival in precious metal administration to patients. Nano Lett. 2011;11(10):4029–36.
- Tonnesen HH, Karlsen J. Alginate in drug delivery systems. Drug Dev Ind Pharm. 2002;28(6):621-630.
- Torchilin VP. Micellar nanocarriers: pharmaceutical perspectives. Pharm Res. 2007;24(1):1-16.

- Usman MS, El Zowalaty ME, Shameli K, Zainuddin N, Salama M, Ibrahim NA. Synthesis, characterization, and antimicrobial properties of copper nanoparticles. Int J Nanomedicine. 2013;8:4467–79.
- Vasconcelos T, Marques S, das Neves J, Sarmento B. Amorphous solid dispersions: Rational selection of a manufacturing process. Adv Drug Deliv Rev. 2016;100:85–101.
- Vincent M, Duval RE, Hartemann P, Engels-Deutsch M. Contact killing and antimicrobial properties of copper. J Appl Microbiol. 2016;124(5):1032–46.
- Vivekanandhan S, Misra M, Mohanty AK. Green synthesis of silver nanoparticles using Solanum trilobatum leaf extract and their antimicrobial activity. Mater Lett. 2009;63(31):2603–5.
- Wang L, Zhao H, Guo C, Li W. Mangiferin-based nanoformulations for drug delivery in neurodegenerative diseases: recent trends. Int J Pharm. 2023;634:122645.
- Wang S, Su R, Nie S, Sun M, Zhang J, Wu D. Application of nanotechnology in improving bioavailability and bioactivity of diet-derived phytochemicals. J Nutr Biochem. 2014;25(4):363-376.
- Williams RJ, Spencer JP, Rice-Evans C. Flavonoids: antioxidants or signalling molecules? Free Radic Biol Med. 2004;36(7):838-49.
- Woodruff MA, Hutmacher DW. The return of a forgotten polymer—Polycaprolactone in the 21st century. Prog Polym Sci. 2010;35(10):1217–1256.
- Yallapu MM, Jaggi M, Chauhan SC. Curcumin nanoformulations: a future nanomedicine for cancer. Drug Discov Today. 2012;17(1-2):71-80.
- Yang C, Zhang C, Wang Z, Li Y. Intestinal transport and absorption mechanisms of flavonoids and their dietary implications. J Food Sci. 2020;85(6):1440-53.
- Yousaf R, Abdul Razzaq F, Asghar S, Irfan M, Ullah Khan I, Haroon Khalid S. Cyclodextrins: An Overview of Fundamentals, Types, and Applications. Cyclodextrins - Core Concepts and New Frontiers. IntechOpen; 2023.
- Yu L, Luo Z, Chen T, Ouyang Y, Xiao L, Liang S, et al. Bioadhesive nanoparticles for local drug delivery. Int J Mol Sci. 2022;23:2370.

- Yuan H, Ma Q, Ye L, Piao G. The traditional medicine and modern medicine from natural products. Molecules. 2016 May 13;21(5):559.
- Zaidan AL, Jalil MA, Mohd Yusof NA, Mohamad M, Abu Bakar F. The physicochemical characteristics of silver nanoparticles and their antimicrobial activity against food and waterborne pathogens. Int J Nanomedicine. 2018;13:759–70.
- Zhang N, Ping Q, Huang G, Xu W, Cheng Y, Han X. Preparation, characterization, and oral delivery of insulin-loaded carboxylated chitosan-grafted poly(methyl methacrylate) nanoparticles. Biomaterials. 2007;28(10):1882-1888.
- Zhang XF, Liu ZG, Shen W, Gurunathan S. Silver nanoparticles: synthesis, characterization, properties, applications, and therapeutic approaches. Int J Mol Sci. 2016;17(9):1534.
- Zhao Y, Tian Y, Cui Y, Liu W, Ma W, Jiang X. Small molecule-capped gold nanoparticles as potent antibacterial agents that target Gram-negative bacteria. J Am Chem Soc. 2010;132(35):12349–56.

CHAPTER 2
LITERATURE REVIEW

CONTENTS

2.1 Literature Review on Phytochemical Naringin

Elham et al., (2022) investigated naringin's anti-ulcer and anti-cancer potential while taking into account its limits in water solubility, permeability, and bioavailability. To address these challenges, Pluronic F68-based naringin micelles were developed and improved. The study evaluated in vitro release, storage stability, and cytotoxicity across many cell lines using an optimized micellar formulation. In addition, ethanol-induced gastric ulcers in rats and Ehrlich ascites carcinoma (EAC) models were employed to evaluate cytoprotective and anti-tumor activity. Micelles had a mean diameter of 74.80 ± 6.56 nm, narrow size distribution, and good entrapment effectiveness, resulting in sustained drug release of 48 hours compared to 10 hours with free naringin. The formulation showed good stability, with little fluctuations in drug entrapment and particle size over time. In vivo, the 1:50 naringin-PF68 micelles dramatically reduced gastric mucosal damage and the production of TNF-α, caspase-3, and IL-6, while boosting glutathione and superoxide dismutase levels at lower dosages than free naringin. The micelles showed increased anti-tumor action, as shown by decreased cell viability and tumor growth as compared to free naringin. The study concluded that 1:50 naringin-PF68 micelles are an effective delivery mechanism for anti-ulcer and anti-cancer treatments.

Abhisek et al., (2021) created polymeric nanoparticles (NAR-PLGA NPs) from biodegradable poly(lactic-co-glycolic acid) (PLGA) to increase naringenin (NAR) oral bioavailability and absorption. The work attempted to overcome the limits of NAR's poor solubility and limited bioavailability by incorporating it into PLGA-based nanoparticles, hence enhancing therapeutic efficacy when administered orally.

Wang et al., (2017) studied naringin's protective mechanisms against LPS-induced apoptosis in PC12 cells. Prior to LPS stimulation, PC12 cells were preconditioned with naringin for 18 hours to assess its influence on cell survival and protection. Naringin dramatically increased cell survival over time and at different concentrations. It also controlled the generation of reactive oxygen species (ROS), which reduced oxidative stress and restored antioxidant protein levels including nuclear factor and glutathione synthetase. This was the first study to show that naringin had anti-

inflammatory and antioxidant properties in PC12 cells, indicating that it could be used to treat neurodegenerative illnesses.

Minchan et al., (2016) studied the effects of naringin on LPS-induced TNF-α production and sepsis in a mouse model. The study discovered that naringin activates the AMP-activated protein kinase (AMPK), p38 MAPK, and NF-E2-related factor 2 (Nrf2) signaling pathways in peritoneal macrophages, upregulating heme oxygenase-1 (HO-1) expression. Naringin also inhibited HMGB1 expression in LPS-stimulated macrophages via HO-1-mediated pathways. Naringin-treated mice showed lower mortality and pulmonary damage in a sepsis model. These findings show that naringin has anti-inflammatory and antiseptic properties by altering critical molecular pathways, mainly through HO-1 induction.

Chtourou et al., (2015) investigated the efficacy of naringin in treating cisplatin-induced toxicity in Wistar rats. Cisplatin treatment significantly reduced glutathione and ascorbic acid levels while increasing catalase and superoxide dismutase (SOD) activity. Conversely, both membrane-bound ATPases and glutathione peroxidase activity decreased. Cisplatin also increased the mRNA expression of p53, NF-κB, and TNF-α. The cisplatin-treated group showed elevated levels of malondialdehyde (MDA), protein carbonyls, reactive oxygen species (ROS), and nitrite, indicating oxidative stress. Naringin at different doses improved tissue integrity and decreased MDA and TNF-α level. Naringin inhibited p53, NF-κB, and TNF-α pathway, reducing cisplatin-induced damage, inflammation, and apoptosis, according to histological study.

Ashraful Alam et al., (2014) investigated the effects of naringin on metabolic syndrome and demonstrated its potential as a therapeutic agent. Naringin, a flavonoid produced from citrus fruits, and its aglycone naringenin have considerable analgesic and anti-inflammatory activities. Numerous researches have demonstrated that naringin can help with obesity, diabetes, hypertension, and the general metabolic syndrome. This review largely investigated naringin's biological activities, with a focus on its function in lipid metabolism, oxidative stress, and obesity-related inflammation.

Ashraful Alam et al., (2014) found that naringin has strong anti-inflammatory and antioxidant properties. Several lines of evidence from the study indicate that naringin supplementation may be effective in the treatment of obesity, diabetes, hypertension, and metabolic syndrome. These effects are due to its capacity to regulate oxidative stress, lipid metabolism, and inflammatory responses.

2.2 Literature Review on Phytochemical Ellagic Acid

Zhang et al. (2023) created a multifunctional hydrogel dressing by adding ellagic acid (EA), a hydrophobic polyphenol with antioxidant and anti-inflammatory characteristics, into a thiol-ene photoclickable PEG hydrogel system. The addition of SH-β-cyclodextrin (SH-β-CD) improved EA loading efficiency, whereas DTT was utilized to adjust the hydrogel's mechanical stiffness. The resultant dressing was highly cytocompatible and had strong antibacterial, antioxidant, and anti-inflammatory properties. In vivo experiments with a rat wound model revealed a considerable reduction in wound area, efficient infection suppression, and stimulation of angiogenesis and collagen deposition. These findings highlight the EA-loaded PEG hydrogel's potential as a promising therapeutic technique for infected wound treatment as well as the creation of next-generation multifunctional wound dressings.

Sharifi-Rad et al. (2022) did a comprehensive evaluation of ellagic acid (EA), a naturally occurring polyphenolic chemical found primarily in pomegranates and other plant sources. The study stresses EA's antioxidant, anti-inflammatory, and antiproliferative characteristics, which are backed by data from various in vitro and in vivo models. The review also dives into the molecular pathways by which EA helps to prevent disease and improves overall human health, emphasizing its therapeutic potential in a variety of pathological diseases.

Harakeh et al. (2021) created biodegradable hollow zein nanoparticles to improve the oral administration of ellagic acid (EA), a polyphenol recognized for its powerful anti-inflammatory effects. The hollow-type zein nanoparticles (EA-HTZN) showed high drug loading capacity (326 mg/g), tiny particle size (~72 nm), and increased penetration effectiveness. In a mouse paw edema model, oral administration of EA-HTZN

dramatically reduced the production of pro-inflammatory cytokines, demonstrating considerable anti-inflammatory activity. Furthermore, EA-HTZN had a much higher bioavailability than EA solution, with a 3.6-fold increase and a 2.1-fold increase over solid EA nanoparticles. These findings indicate that hollow zein nanoparticles are a suitable platform for increasing the oral bioavailability and therapeutic efficacy of ellagic acid.

Hallan et al. (2020) conducted a preliminary study to investigate the topical application potential of ellagic acid (EA)-loaded nanostructured lipid carriers (NLCs), with the goal of increasing the bioavailability and therapeutic performance of EA, a polyphenolic compound known for its powerful antioxidant, anti-inflammatory, and anticancer properties. Owing to the poor solubility and limited skin penetration of EA, researchers created NLCs using a combination of solid lipid (Compritol® 888 ATO), liquid lipid (Miglyol® 812), and surfactants (Tween® 80), utilizing high-shear homogenization followed by ultrasonication to create a stable nanosystem. The optimized EA-NLCs had an average particle size of about 170 nm, a narrow size distribution, and a negative zeta potential, indicating good stability. The formulation demonstrated great entrapment efficiency (more than 85%), spherical morphology validated by transmission electron microscopy (TEM), and a prolonged release profile, extending EA's presence on the skin surface. Importantly, the DPPH experiment demonstrated that antioxidant activity was preserved after encapsulation. Ex vivo skin permeation tests on pig skin revealed considerably more penetration of EA from NLCs than free EA. Biocompatibility tests further proved the formulation's safety for topical usage. Overall, our study demonstrates that EA-loaded NLCs are a potential technique for increasing ellagic acid distribution and efficacy in dermatological and cosmetic applications, laying the groundwork for future research and product development in topical nanomedicine.

Lee et al. (2018) attempted to create functional beverage formulations including encapsulated epidermal growth agent (EA) and to assess the nanoparticles' physicochemical qualities both before and after encapsulation. Morphological and size distribution properties were analyzed with a particle size analyzer, and EA entrapment efficiency was determined using high-performance liquid chromatography (HPLC). The nanoparticles' sizes ranged from 100 to 200 nm, and their polydispersity index (PDI) was 0.3 to 0.4, indicating a consistent size distribution. The zeta potential of the EA-loaded nanoparticles was comparable to that of the control groups, indicating stable colloidal characteristics. An entrapment efficiency of almost 90% was obtained. These findings demonstrate the viability of EA-loaded nanoparticles as a technique for developing anti-inflammatory functional beverages.

Mady et al. (2017) studied methods for increasing the oral bioavailability of ellagic acid (EA), a bioactive molecule with promising anticancer properties. This study used poly(ε-caprolactone) (PCL) to create EA-loaded nanoparticles (EA-NPs) by emulsion-diffusion-evaporation method. The resultant nanoparticles have distinctive shape, as well as good drug loading and entrapment efficiencies. In vitro experiments on the Caco-2 and HCT-116 cell lines revealed that EA-NPs had more cytotoxicity and cellular uptake than free EA. Furthermore, in vivo pharmacokinetic experiments on New Zealand white rabbits indicated 3.6-fold increase in area under the curve for EA-NPs, indicating significantly increased oral bioavailability and bioactivity via PCL-based nanoparticle encapsulation.

Arulmozhi et al., (2013) emphasized the growing threat of cancer and the limits of traditional chemotherapeutics due to their significant side effects. They emphasized the importance of natural dietary components, particularly ellagic acid (EA), a naturally occurring phenolic antioxidant found in fruits and nuts such pomegranates, strawberries, and walnuts. EA has been proven to have a variety of biological actions, including anti-carcinogenic, antioxidant, anti-mutagenic, and antiviral properties, and it is effective against cancers such as lung, liver, skin, and colon cancer. However, EA's limited water solubility and poor membrane permeability limit its therapeutic potential. To address this, researchers devised a nanotechnology-based drug delivery strategy that employs

chitosan-based nanoparticles for targeted distribution. The ionic gelation process was utilized to create EA-loaded chitosan nanoparticles (EA-CS-TPP NPs) with a chitosan to TPP ratio of 4:1. These nanoparticles demonstrated great encapsulation efficiency and sustained drug release for 48 hours. UV-Vis spectroscopy, FTIR, SEM, EDX, zeta potential tests, and TGA were used to determine the morphology, stability, and interaction of EA and chitosan. The synthesised nanoparticles were spherical, with an average size of 176 nm. In vitro anticancer investigations on human oral cancer (KB) cell lines revealed considerable antiproliferative activity, establishing chitosan as a viable nanocarrier for increasing the therapeutic efficacy of ellagic acid.

Bala et al., (2004) investigated the problems of oral absorption of pharmaceutical solid dosage forms, highlighting the importance of drug disintegration, release from dosage form, and permeability across gastrointestinal membranes. These characteristics are important to the Biopharmaceutics Classification System (BCS), which classifies medications based on their water solubility and intestinal permeability, providing a scientific basis for predicting oral drug absorption. The study demonstrated the potential of nanoparticle-based drug delivery systems to improve the bioavailability of poorly water-soluble medicines, notably those in BCS Classes II, III, and IV. Nanoparticles improve absorption by allowing lymphatic transport, avoiding the hepatic first-pass impact, and providing prolonged or regulated release profiles. While BCS Class I medicines have great solubility and permeability, nanoparticle formulations can nevertheless give controlled release advantages. One specific example presented was ellagic acid (EA), a BCS Class IV phytochemical with strong anticarcinogenic and antioxidant effects. Despite its medicinal potential, EA has poor solubility, low permeability, and quick metabolism, limiting its oral bioavailability. To address these difficulties, the researchers investigated the encapsulation of EA in biodegradable PLGA nanoparticles, with PEG 400 serving as a co-solvent to increase solubility. The study emphasized the need of choosing appropriate encapsulation strategies based on the physicochemical features of both the medication and the carrier polymer.

2.3 Literature Review On Phytochemical Quercetin

Quercetin, a naturally occurring flavonoid found in fruits, vegetables, and grains, has received a lot of scientific attention due to its various pharmacological effects. Quercetin, one of the most renowned dietary antioxidants, is known for its powerful anti-inflammatory, anti-oxidative, anti-cancer, and antiviral properties. Several studies in vitro and in vivo demonstrate its ability to scavenge free radicals, alter important signaling pathways such as NF-κB and MAPK, and reduce lipid peroxidation.

Sadeghi-Ghadi et al. (2020) created hyaluronic acid-modified niosomes that encapsulated quercetin. The vesicular systems showed great entrapment efficiency (94.67%) and nanoscale particle size (~231 nm). The modified niosomes greatly increased quercetin's anti-inflammatory and antioxidant characteristics, indicating potential for treating inflammatory illnesses.

Sunoqrot et al. (2019) employed Eudragit S100 to manufacture pH-sensitive polymeric nanoparticles for colonic administration. The average size of the nanoparticles was 66.8 nm, with an entrapment effectiveness of 41.8%. These devices regulated the release of quercetin and boosted its delivery to colon cancer cells, significantly increasing its anticancer activity.

Li et al. (2016) investigated quercetin's cardioprotective properties against ischemia/reperfusion injury in rats. The study found that quercetin pretreatment significantly reduced the extent of myocardial infarctions and blood levels of cardiac enzymes such as creatine kinase-MB and lactate dehydrogenase. The findings indicate quercetin as a possible therapeutic drug for myocardial protection.

D'Andrea (2015) offered a comprehensive evaluation of quercetin's medicinal potential, including clinical implications. The review focused on quercetin's involvement in vascular health, metabolic syndrome, and inflammation-related illnesses. The publication summarizes clinical trials that found quercetin supplementation to be effective in lowering blood pressure, improving glycemic management, and reducing inflammation. However, the author mentioned constraints such as limited bioavailability and the need for better delivery mechanisms to increase therapeutic efficacy.

Mahfoudh-Boussaid et al. (2012) investigated the neuroprotective effects of quercetin on aluminum chloride-induced neurotoxicity in rats. Quercetin supplementation dramatically improved memory deficiencies and oxidative damage in brain tissue by increasing antioxidant enzyme levels of superoxide dismutase (SOD), catalase (CAT), and glutathione peroxidase (GPx). The study indicated that quercetin's antioxidant mechanism helps to reduce neurodegenerative alterations and may have therapeutic potential in situations such as Alzheimer's disease.

Kobori et al. (2011) investigated the anti-obesity effects of quercetin in mice fed a high-fat diet. The researchers found that quercetin administration lowered body weight gain, adipose tissue mass, and blood triglycerides. In adipose tissue, gene expression analysis demonstrated downregulation of adipogenic markers (PPARγ, C/EBPα) and inflammatory genes (TNF-α, IL-6). These findings show that quercetin may help manage obesity and related metabolic problems by regulating adipocyte differentiation and inflammation.

Boots et al. (2008) conducted a comprehensive assessment of quercetin's pharmacological properties, emphasizing its powerful antioxidant activity via direct radical scavenging and regulation of intracellular signaling pathways. They highlighted how quercetin regulates phase II detoxifying enzymes via the Nrf2 pathway and decreases pro-inflammatory cytokines by inhibiting NF-κB. Quercetin's dual role in oxidative stress and inflammation makes it a promising candidate for treating chronic disorders like cardiovascular disease and metabolic syndrome.

Kawai et al. (2008) investigated the bioavailability and metabolism of quercetin. The study found that dietary quercetin, which is mostly present as glycosides, is deglycosylated in the small intestine and then metabolized in the liver, resulting in conjugated forms such as quercetin glucuronides and sulfates. These metabolites retain biological activity and contribute to quercetin's overall effects. However, the study also highlighted the variety in absorption based on the dietary matrix and individual gut microbiota compositions.

Rivera et al. (2008) studied quercetin's antitumor efficacy in human breast cancer cells (MCF-7). Their findings revealed that quercetin suppressed cell proliferation in a dose-dependent manner by causing apoptosis and cell cycle arrest in the G1 phase. This impact was achieved by decreasing cyclin D1 and increasing p21 and p53 levels. Furthermore, quercetin reduced the expression of the anti-apoptotic protein Bcl-2, demonstrating its promise in breast cancer therapy.

2.4 LITERATURE REVIEW ON PHYTOCHEMICAL MANGIFERIN

According to Suya et al., (2023) mangiferin is a powerful antioxidant with a wide range of pharmacological activity, including antidiabetic, anticancer, cardioprotective, neuroprotective, anti-inflammatory, and antibacterial properties. Mangiferin is a bioactive chemical obtained mostly from the mango tree (*Mangifera indica*). Despite its extensive therapeutic potential, its clinical use is severely restricted due to poor solubility, low permeability, and low bioavailability. This review outlines the main pharmacological activities of mangiferin and underlines the need for both physical and chemical alterations to improve its therapeutic efficacy.

Yeon Lee et al. (2023) used cyclodextrin glucanotransferase (CGTase) from Thermoanaerobacter sp. to transglucosylate mangiferin, which dramatically improved its water solubility and antioxidant characteristics. The optimal settings (60 mU/mL CGTase, 25 mM mangiferin, 10% starch, 60°C, 10h) resulted in an 88.9% conversion rate to glucosyl-α-(1→4)-mangiferin (MGF-g1). MGF-g1 outperformed native mangiferin in terms of water solubility and antioxidant activity, including increased ferric reducing power, oxygen radical absorption capacity, and radical scavenging efficiency. MGF-g1 inhibited cyclooxygenase-2 (COX-2) with an IC_{50} value of 59.74 ± 2.8 μM, compared to 76.44 ± 11.7 μM for mangiferin, suggesting its possible use in the food and pharmaceutical industries.

Ji Yeon Lee et al. (2022) used cyclodextrin glycosyltransferase (CGTase) from Thermoanaerobacter sp. to transglucosylate mangiferin, which dramatically increased its solubility and antioxidant capacity. Under ideal conditions—25 mM mangiferin, 60 mU/mL CGTase, and 10% starch at 60°C for 10 hours—the conversion to mangiferin glucoside (MGF-g1) was 88.9%. NMR and MALDI-TOF validated the product as glucosyl-α-(1→4)-mangiferin. MGF-g1 showed a 5,093-fold improvement in water solubility over native mangiferin. Furthermore, it demonstrated increased antioxidant activity, including 1.6-fold higher DPPH radical scavenging activity, 1.24-fold higher oxygen radical absorption capacity, and 1.19-fold higher ferric reducing power. MGF-g1 inhibited cyclooxygenase-2 (COX-2) more effectively than mangiferin (IC_{50} = 76.44 μM), suggesting possible uses in pharmaceutical and food sectors.

According to *Kaurav et al., (2021)* mangiferin (2-C-β-D-glucopyranosyl-1,3,6,7-tetrahydroxyxanthen-9-one) is a bioactive chemical found in the mango plant's seeds, peel, and kernels. It has been widely investigated for its pharmacological qualities, which include antidiabetic, antioxidant, antibacterial, anticancer, immunomodulatory, and hypocholesterolemic effects. Mangiferin regulates transcriptional pathways and inhibits peroxisome proliferator-activated receptors (PPARs). These processes help to protect against a variety of cancers, including breast, lung, brain, and colon cancer. Furthermore, mangiferin suppresses lipid peroxidation, thereby shielding cells from oxidative injury.

According to *Suya et al. (2018),* mangiferin, a xanthonoid derived primarily from mango trees (*Mangifera indica*), has potent antioxidant activity as well as a variety of pharmacological effects such as antibacterial, anti-inflammatory, antitumor, antiviral, cardioprotective, neuroprotective, and immunomodulatory properties. Despite its significant therapeutic promise, mangiferin's clinical use is limited due to poor mucosal permeability, low aqueous solubility, and low bioavailability. To address these restrictions, a variety of physical and chemical modifications have been proposed. This detailed review outlines the key pharmacological activities of mangiferin and stresses its potency as a potentially therapeutic drug.

Shaoying et al. (2011) noted that mangiferin has minimal pharmacokinetic evidence, despite its importance in traditional Chinese medicine and various pharmacological effects. To close this gap, the scientists created a sensitive and selective HPLC-MS method for quantifying mangiferin in human plasma, with high accuracy and precision suited for clinical studies. This approach was used in a pharmacokinetic research with 21 healthy Chinese male volunteers who were given single oral dosages of 0.1, 0.3, and 0.9 g of mangiferin. Using a non-compartmental analytical model, the study found a peak plasma concentration (C_{max}) of 38.64 ± 6.75 ng/mL one hour after administration of the 0.9 g dose. The elimination half-life ($t_{1/2}$) was 7.85 ± 1.72 hours. Dose-dependent increases in absorption indicated nonlinear pharmacokinetics in humans.

2.5 Literature Review On Natural Polymer (Chitosan) Based Nanoparticles

AL-Nemrawi et al. (2018) created chitosan-based nanoparticles (CS NPs) utilizing the ionic gelation process using sodium tripolyphosphate (TPP) as a crosslinking agent. Chitosan, a biocompatible and biodegradable polymer, is commonly used in drug delivery and wound healing applications. The study looked at how several formulation parameters, such as chitosan molecular weight, degree of deacetylation, TPP concentration, stirring rate, and TPP addition rate, affected nanoparticle size, zeta potential, polydispersity, and stability. The results showed that increased TPP concentration reduced particle size, whereas higher stirring speeds and chitosan molecular weights promoted monodispersity and positive surface charge. Freeze-drying enhanced nanoparticle homogeneity and zeta potential. The study found that adjusting these parameters is vital for increasing the physicochemical and biological properties of CS NPs, which is required for furthering their clinical application in nanomedicine.

Leila et al. (2015) investigated the use of nanostructured delivery systems including chitosan (CS) nanoparticles to improve the therapeutic efficiency of Arrabidaea chica extract. Chitosan, a natural, biodegradable, and biocompatible polysaccharide, was combined with sodium tripolyphosphate (TPP) to create nanoparticles using the ionic gelation process. This approach involved electrostatic contact between cationic CS and anionic TPP, which resulted in stable, non-toxic nanoparticles that did not require chemical cross-linkers. The study sought to increase AcE's bioavailability, stability, and

antiulcerogenic effectiveness by using CS-based nanocarriers. Nanoparticles were created by changing TPP concentrations and introducing the cross-linker to a chitosan solution while vigorously stirring, followed by ultrasonication. The addition of AcE reduced particle size, indicating interactions between the extract and the polymer matrix. The CS-AcE nanoparticles were highly biocompatible in human fibroblast cultures and shown considerable antiulcer efficacy in albino rat models. These findings indicate that CS-TPP nanoparticles are a suitable platform for delivering plant-based medicines, particularly for gastrointestinal use.

Antoniou et al. (2014) used sodium tripolyphosphate (TPP) as a cross-linking agent to study the manufacture and use of chitosan nanoparticles (CSNPs) via ionotropic gelation. The protonated amino groups of chitosan, a biodegradable, biocompatible, and non-toxic polymer produced from chitin, electrostatically engage with multivalent TPP anions to generate nanoparticles. With encapsulation rates of up to 95% and nanoparticle sizes ranging from 50 to 300 nm, this gentle yet effective technique provides a potential delivery system for bioactive substances like medications, proteins, and essential oils. The study emphasizes how factors like chitosan molecular weight, CS:TPP mass ratio, pH, and salinity have a substantial impact on nanoparticle properties like size, shape, and dispersity. Furthermore, it was discovered that while extreme sonication resulted in structural deterioration, moderate ultrasonication improved nanoparticle homogeneity. When compared to bulk chitosan, these tailored CSNPs demonstrated improved antibacterial qualities, which qualified them for a range of culinary and medicinal uses.

Vimal et al., (2013) studied the usage of chitosan/tripolyphosphate (CS/TPP) nanoparticles as a non-viral gene delivery system to combat white spot syndrome virus (WSSV) in shrimp aquaculture. WSSV is a highly pathogenic DNA virus that causes quick death and substantial economic losses in the shrimp trade. Because of its wide host range and ferocity, managing the virus remains difficult. In the present investigation, chitosan, a biocompatible, biodegradable cationic polymer produced from crustacean shells, was employed to encapsulate plasmid DNA using TPP ionic gel. The CS/TPP nanoparticles were delivered orally to shrimp, allowing gene transfer to the intestinal epithelium and inducing strong antibody responses. The non-viral gene delivery

technology demonstrated promise in lowering the immunogenic and carcinogenic risks associated with viral vectors, making it a safer option for gene therapy. CS/TPP nanoparticles have also shown efficacy in transporting a variety of biomolecules, including siRNA, peptides, and proteins. Their mucoadhesive and membrane-permeabilizing abilities allow for deeper tissue penetration and higher delivery efficiency. This study emphasizes the potential of oral gene delivery in aquaculture using CS/TPP nanoparticles to treat viral infections such as WSSV.

Chitosan (CS), a linear copolymer of glucosamine and N-acetylglucosamine, was investigated by *Dong et al. (2013)* for the synthesis of nanoparticles (NPs) via ionic gelation, a straightforward and effective technique that uses tripolyphosphate (TPP) as the crosslinking agent. CS's unique features, including as biocompatibility, biodegradability, and cationic nature, make it a good material for medication, gene, and protein administration. The protonated amine groups of CS and the negatively charged TPP anions crosslink intramolecularly and intermolecularly during the ionic gelation process, creating submicron-sized nanoparticles. The size of the nanoparticles can be regulated by varying the volume ratios, pH, and CS and TPP concentrations. Using sodium alginate (SA) as a model, the study also looked at drug loading and demonstrated the ionic gelation-static mixing method's scalability and reproducibility for producing nanoparticles on a wide scale. The study showed how reliable this continuous synthesis method is, providing a viable strategy for industrial use.

Vimal et al. (2013) investigated the use of chitosan/tripolyphosphate (CS/TPP) nanoparticles for oral delivery of DNA vaccines against fish nodavirus, which causes viral nervous necrosis (VNN), a highly contagious disease affecting the nervous systems of marine fish species, particularly juveniles and larvae. The nodavirus genome is made up of two single-stranded RNA segments: RNA1 encodes RNA-dependent RNA polymerase, whereas RNA2 encodes the capsid protein. Effective immunization tactics are critical for managing VNN in aquaculture systems. In the present investigation, a DNA vaccine (pFNCPE42) targeting nodavirus was encapsulated within CS/TPP nanoparticles using the ionic gelation process, which is a popular methodology for creating chitosan-based nanogels. CS/TPP nanoparticles displayed the ability to infiltrate

tissues via capillaries and efficiently distribute plasmid DNA, siRNA, and proteins, indicating that they are excellent carriers for gene delivery. Oral injection of the CS/TPP-DNA vaccination to Asian sea bass resulted in effective gene expression in numerous tissues and provided considerable protection against nodavirus infection. The results suggest the promise of CS/TPP nanoparticles as a safe and effective non-viral delivery vehicle for DNA vaccines in aquaculture, improving disease resistance in commercially important fish species.

Suna et al. (2011) investigated the potential of chitosan-based nanoparticles (CS-NPs) for non-viral epidermal gene delivery. Chitosan's biocompatibility, biodegradability, and cationic nature allow it to successfully bind and preserve plasmid DNA (pDNA) against enzymatic degradation. In this study, CS-NPs were produced via ionic gelation with tripolyphosphate (TPP) and assessed for size, zeta potential, shape, encapsulation effectiveness, and stability against DNase I and serum. The nanoparticles have a positive surface charge and diameters less than 300 nm. The pSV-β-Gal reporter gene was used in in vitro release and gene transfection tests, which indicated successful transfection and sustained DNA release. The findings indicate that CS-NPs are a potential technology for topical gene delivery applications.

Qiongming et al. (2011) investigated the use of chitosan/tripolyphosphate (CS/TPP) nanoparticles as an interleukin-12 (IL-12) delivery method in the treatment of colorectal cancer (CRC) with liver metastases, which accounts for a considerable proportion of CRC-related mortality. While surgical resection and biological therapies are presently employed to treat liver metastases, combined chemotherapy is frequently just palliative and causes severe systemic damage. Furthermore, some research suggests that surgery may, paradoxically, promote metastatic progression. IL-12, a multifunctional cytokine, has a high potential for eliciting antitumor immunity by activating T helper 1 cells, natural killer (NK) cells, and cytotoxic T lymphocytes. However, the clinical use of IL-12 has been restricted due to its systemic toxicity when taken intravenously. Chitosan, as a nonviral vector, is biocompatible, mucoadhesive, and capable of encapsulating macromolecules, making it a suitable choice for IL-12 delivery. In this study, CS/TPP nanoparticles were designed to encapsulate IL-12 in order to enable liver-

specific delivery while minimizing systemic damage. The nanoparticles were engineered to be taken up by Kupffer cells, the liver's resident macrophages, and breakdown under lysosomal conditions, releasing IL-12 straight into the hepatic milieu. The delivery system efficiently boosted local immune responses, as seen by enhanced infiltration of NK cells and T lymphocytes in the liver, which inhibited CRC hepatic metastases. These findings imply that CS/TPP-based IL-12 nanocarriers could be a more tailored and safer cytokine therapy option for colorectal cancer hepatic metastases, with the ability to stimulate liver-resident antitumor immunity while avoiding systemic side effects.

The use of chitosan nanoparticles as a delivery mechanism for vitamin C was examined by *Alishahi et al. (2011)* in order to improve its stability and bioavailability, especially in aquaculture applications. An important antioxidant, vitamin C is unstable in the presence of heat, light, and oxygen, which makes it difficult to preserve during feed preparation. Sodium tripolyphosphate (TPP) was utilized as a crosslinker in the ionic gelation process to encapsulate vitamin C in chitosan, a biocompatible, biodegradable, and mucoadhesive polysaccharide. The resultant chitosan–TPP–vitamin C nanoparticles allowed for regulated release and offered defense against gastrointestinal deterioration. Rainbow trout (Oncorhynchus mykiss) were used to test the stability and in vivo effectiveness of the nanoparticles. When compared to control groups, fish fed chitosan nanoparticles enriched with vitamin C exhibited noticeably improved immunological markers, including serum lysozyme and complement activity. The results demonstrate chitosan's dual function as an immunological stimulant and protective carrier, suggesting that it may enhance aquaculture's nutrient delivery and immunomodulation.

Anitha et al. (2010) explored into the use of chitosan (CS) nanoparticles (NPs) as a polymeric drug delivery system to improve the oral bioavailability of hydrophilic chemicals like catechin, a polyphenolic antioxidant. Low permeability, enzymatic degradation, and significant first-pass metabolism all limit the oral administration of these medicines. Chitosan, a cationic, biocompatible, and mucoadhesive polysaccharide, has the ability to temporarily open tight junctions in epithelial cells, improving drug absorption. To maximize particle size and drug entrapment, CS NPs were produced utilizing a modified ionic gelation process using tripolyphosphate (TPP) under different

pH settings. Catechin was added to CS NPs using magnetic stirring, and the resulting formulations were evaluated for size, zeta potential, entrapment efficiency, and in vitro release. The FTIR measurement indicated ionic crosslinking and hydrogen bonding between catechin and CS. The optimized nanoparticles showed sustained release, with 32% catechin release after 24 hours and around 60% enzymatic breakdown. The findings indicate CS NPs as a promising carrier system for increasing the oral distribution and bioavailability of catechin because of their mucoadhesive qualities and regulated release behaviour.

For possible biological uses, *Anitha et al. (2009)* investigated the synthesis and characterisation of chitosan (CS) and its derivatives, O-carboxymethyl chitosan (O-CMC) and N,O-carboxymethyl chitosan (N,O-CMC). Deacetylation of chitin, a linear polysaccharide mostly obtained from crustacean shell waste, yields chitosan, which has advantageous qualities such low toxicity, biodegradability, and biocompatibility. Because of these characteristics, chitosan and its nanoparticles can be used as vaccine carriers, in tissue engineering, and in the delivery of drugs and genes. CS, O-CMC, and N,O-CMC nanoparticles were created by ionic cross-linking calcium chloride ($CaCl_2$) and sodium tripolyphosphate (TPP). FT-IR, AFM, SEM, and DLS were used to characterize the particles. All formulations showed negligible toxicity in cytotoxicity tests conducted on breast cancer cell lines using the MTT assay. Antibacterial efficacy rose with concentration, according to MIC assays used to measure antibacterial activity against the ATCC strain of Staphylococcus aureus. N,O-CMC had the strongest antibacterial activity among the studied nanoparticles, followed by O-CMC, while CS nanoparticles had the weakest. These findings highlight the potential of modified chitosan derivatives as biocompatible and powerful antibacterial nanocarriers.

Sofia et al (2008) investigated use of chitosan (CS) nanoparticles as carriers for regulated administration of dorzolamide (Dorzo) and pramipexole (Prami). Ionic gelation was used to create CS nanoparticles, with tripolyphosphate (TPP) serving as crosslinking agent. Nanoparticle production was optimal at CS/TPP ratios between 4:1 and 6:1, resulting in particles ranging from 200 nm to 1 µm. Dorzo, a glaucoma medication, was encased in CS nanoparticles for ocular administration. The goal of this

strategy was to improve medication retention on ocular surface while also increasing bioavailability. Prami, a dopamine agonist to treat Parkinson's disease, was loaded with CS nanoparticles for oral delivery, for sustained drug release and reducing dose frequency. Nanoparticle characterization indicated mucoadhesive characteristics and regulated medication release profiles. FT-IR and DSC investigations revealed that Dorzo remained solid, but Prami produced molecular dispersion within nanoparticle matrix. In vitro release investigations confirmed drugs are released slowly in relevant biological media indicating CS nanoparticles are efficient carriers for both ocular and oral controlled drug delivery systems.

In order to treat Alzheimer's disease (AD), *Wang et al. (2008)* investigated the possibility of using chitosan as a nasal delivery mechanism for estradiol (E2). They emphasized that the aging population is contributing to an increase in AD, a neurological disease. Because of its biocompatibility and biodegradability, chitosan, a cationic polysaccharide produced from chitin, finds extensive application in a variety of sectors, including medicines. The authors stressed that the nasal route of medication delivery presents a viable substitute for avoiding the blood-brain barrier and directly reaching the brain through the olfactory system. Chitosan is the perfect carrier for hydrophilic medications like estradiol because it can improve mucosal adhesion and alter paracellular transport by causing tight junctions to open in nasal epithelial cells. Chitosan's dual properties of bioadhesion and transport augmentation make it a useful tool for enhancing the bioavailability of nasal medication formulations used to treat AD.

Tran et al. (2007) investigated the use of chitosan nanoparticles as a delivery system for antisense oligonucleotides in oral illness therapy. Chitosan, a biocompatible and mucoadhesive polymer, was utilized to create nanoparticles by ionic gelation with sodium tripolyphosphate (TPP). Oligonucleotides were added before or after crosslinking, and the resulting formulations were tested for release kinetics with spectrophotometry and capillary zone electrophoresis. The researchers discovered that pH and the oligonucleotide loading method had a substantial impact on the release profile. The nanoparticles allowed for prolonged release, ensuring oligonucleotide stability in a simulated salivary environment for up to 12 hours. These results support the

use of low molecular weight chitosan nanoparticles as excellent carriers for regulated oligonucleotide delivery in oral medicinal applications.

Yan et al. (2005) examined chitosan-based nanoparticles as viable oral medication delivery technology for ammonium glycyrrhizinate. Chitosan, biocompatible and biodegradable cationic polysaccharide, has mucoadhesive characteristics, increases permeability, and promotes gastrointestinal stability. Nanoparticles were created using ionic gelation process with sodium tripolyphosphate (TPP) and modified with polyethylene glycol (PEG) to increase their transport properties. These nanoparticles showed high drug loading efficiency, regulated release behavior with early burst effect followed by sustained release, and good retention of ammonium glycyrrhizinate. The study emphasizes efficacy of chitosan nanoparticles as oral delivery platform for poorly absorbed medicines.

2.6 Literature Review on Synthetic Polymer (Polycaprolactone) Based Nanoparticles

The important function of poly-ε-caprolactone (PCL) in drug delivery and biological applications is discussed by *Aminu and Audu (2023).* The remarkable mechanical qualities, high encapsulation effectiveness, low toxicity, and biodegradability of PCL make it stand out. Due to these characteristics, PCL has been a popular option for drug delivery systems and other biomedical applications. Over the past 50 years, its significance has increased, especially in the creation of nanomedicines for cutting-edge therapeutic applications.

The objective of *Badran et al. (2023)* was to create chitosan-coated poly-ε-caprolactone (PCL) nanoparticles (NPs) loaded with bromocriptine mesylate (BM) for nasal administration to the brain. To optimize the PCL NPs, they used a Box–Behnken factorial design and a response surface technique. In order to optimize the nanoparticle properties for improved distribution, the study examined three independent formulation parameters: sonication duration (C), D-α-tocopherol polyethylene glycol 1000 sulfate (TPGS) concentration (B), and PCL payload (A).

Bio-polymeric nanoparticles (NPs) produced by the phase inversion composition (PIC) approach utilizing polycaprolactone (PCL) and its copolymer with poly(ethylene glycol) (PCL-b-PEG) were studied by *Łukasiewicz et al. (2021).* Their endocytosis, immunological response, and effect on cell survival in murine macrophages were the main topics of the investigation. Initial in vitro tests of both kinds of NPs as possible drug nanocarriers were successful. Notably, the clathrin-mediated route demonstrated higher uptake of non-pegylated PCL NPs. Crucially, neither kind of nanoparticle significantly increased the production of nitric oxide (NO) or pro-inflammatory cytokines, nor did it impair cell survival. These findings imply that the produced NPs are viable options for applications involving the delivery of pharmaceuticals.

El-Habashy et al. (2020) used a 2^3-factorial design and wet chemical precipitation to create hybrid hydroxyapatite/polycaprolactone (HAp/PCL) nanoparticles (NPs). In addition to having good Ca/P ratios and mesoporosity, these nanoparticles preserved HAp crystallinity. The HAp/PCL NPs, which were created via emulsification-solvent evaporation, demonstrated improved osteogenic potential by encouraging osteodifferentiation, mesenchymal cell proliferation, and decreased cytotoxicity. They showed modest expression of Runx-2 and osteopontin and enhanced expression of bone sialoprotein after 10 days, suggesting that they have the capacity to regenerate bone.

The potential of polycaprolactone (PCL) in pharmacological and biological applications, specifically in cancer nanomedicine, was reviewed by *Espinoza et al. (2019).* A ubiquitous polymer found in scaffolds and microparticles, PCL is biodegradable, biocompatible, and bioresorbable. The review highlights its growing significance in nanomedicine by stressing its qualities and adaptability in drug delivery systems for the treatment of cancer.

The application of polycaprolactone (PCL) nanoparticles in medication delivery was reviewed by *Ibrahim, et al. (2018).* Because of its tunable qualities, PCL, biodegradable polyester, is frequently utilized as a carrier in biomedical applications. The review emphasizes the effectiveness of nanoprecipitation in the synthesis of PCL nanoparticles, which improve the bioavailability and therapeutic potential of medications and bioactive substances. The study highlights the function of PCL nanoparticles in

controlled drug delivery systems and demonstrates how they can be used in a range of therapeutic settings.

Khan et al. (2017) used a nanoprecipitation technique that was adjusted for a number of process parameters to create drug-loaded polycaprolactone (PCL)-based nanoparticles. The nanoparticles had charges of -16.8 mV and -11.2 mV, respectively, and were about 200 nm in size (blank) and 216 nm (drug-loaded). Their potential for targeted drug administration in biomedical applications was demonstrated by the study's exploration of their antifouling qualities and in vitro drug release.

Fijan et al. (2012) optimized a number of process parameters to create drug-loaded polycaprolactone (PCL) nanoparticles via a nano-precipitation technique. The antifouling qualities and in vitro drug release of the resultant nanoparticles were assessed. With an average size of 216 nm for drug-loaded particles and 200 nm for blank nanoparticles, the study described the surface properties and shape of the nanoparticles, indicating their potential for use in biomedical applications.

The degradation characteristics of polycaprolactone (PCL) and poly(lactide-co-glycolide) (PLGA) were compared by *Nair and Laurencin (2007).* They investigated the use of PCL-OX microspheres loaded with paclitaxel in vivo while keeping the drug's plasma content steady at 6–9 µg/ml for 28 days. Within two months of implantation, the body eliminated the PCL and PLGA microspheres. Additionally, the study discovered that in the rats' subcutaneous layer, PCL-OX microspheres showed tissue compatibility on par with PLGA microspheres.

Gunatillake and Adhikari (2003) emphasized the special physicochemical characteristics, mechanical strength, and viscoelasticity of polycaprolactone (PCL), underscoring its applicability in tissue engineering. These characteristics make PCL a very versatile material for biomedical applications since they enable it to be sculpted into different forms and degradation durations based on the particular biodegradation kinetics.

2.7 Literature Review on Metal Based Nanoparticles

Using sonication and the thin-film hydration technique, *Jayachandran et al. (2023)* created liposomes filled with silver nanoparticles (AgNP) for cancer treatment. According to DLS, FESEM, and FTIR analysis, the liposomes had a particle size of 172.1 nm, a high encapsulation efficiency of 82.25%, and a zeta potential of -21.5 mV. Studies on drug release in vitro revealed diffusion-controlled release, with a notable release around pH 5.5, suggested the possibility of tailored cancer treatment. The release kinetics confirmed controlled release qualities by adhering to the Higuchi and Korsmeyer–Peppas models.

Using ciprofloxacin (Cipro) as a model drug, *Hussein-Al-Ali et al (2022)* studied the use of silver nanoparticles (AgNPs) for drug delivery. AgNPs were created using alginate as a coating agent and silver nitrate, which produced a crystalline Cipro-AgNPs nanocomposite. Spherical particles with a needle-clustered shape, a positive zeta potential of 6.5 mV, and an average size of 96 nm were discovered by characterization procedures. With a 98% release at 750 minutes, the drug release followed a gradual, regulated procedure that matched the Hixson-Crowell model. According to toxicity evaluation, Cipro-AgNPs can be used for controlled, long-term drug delivery.

Because of their special qualities, *Burdusel et al. (2021)* emphasized the silver nanoparticles' (AgNPs') remarkable potential in a range of biomedical applications. AgNPs have shown useful in the development of advanced therapeutic approaches, antibacterial agents, drug delivery systems, medicinal coatings, tissue regeneration materials, and diagnostic platforms. AgNPs' biological interactions, intrinsic antibacterial and anti-inflammatory qualities, and possible toxicity are the main topics of the review, which also summarizes the most recent findings on their medicinal uses and biofunctional traits.

A review of the various uses of copper nanoparticles (CuNPs) in agriculture and medical was conducted by *Crisan et al. (2021).* Strong antibacterial, antifungal, antiviral, and anticancer effects are displayed by CuNPs, which are produced using a variety of techniques. CuNPs are positioned as prospective substitutes in the fight against infections and illnesses, as the review discusses their production, methods of action, and possible toxicity while highlighting their efficacy against bacteria that are resistant to many drugs.

The strong antibacterial capabilities of silver nanoparticles (AgNPs) against both Gram-positive and Gram-negative bacteria, including those that are resistant to multiple drugs, were emphasized by *Bruna et al. (2020).* When paired with antibiotics, AgNPs' many modes of action and synergistic effect increase antibacterial efficacy while lowering dosages and adverse effects. In addition to analyzing the variables affecting AgNPs' cytotoxicity and antibacterial qualities, the review highlights the potential of AgNPs in healthcare applications for infection treatment and prevention.

In their study, *Shanmuganathan et al. (2019)* examined the medical uses of silver nanoparticles (AgNPs), paying special attention to their antibacterial capabilities. The study emphasized the benefits of biologically synthesizing AgNPs, which is less expensive and more ecologically benign than conventional techniques. The review discussed a number of uses, such as nanogels, silver-based dressings, and coatings for medical devices. The study highlighted the increased interest in AgNPs as therapeutic agents for a variety of disorders, but it also underlined the need for safer production techniques because of possible safety concerns, despite their widespread use.

The effects of drug formulations based on metal nanoparticles in the treatment of complex disorders were covered by *Rizvi and Saleh (2018).* Nanoparticles, which range in size from 100 to 500 nm, were designed to release drugs in a targeted and controlled manner while combining imaging, therapeutic, and stealth capabilities. These systems allowed targeted medication administration to particular tissues by modifying their size, surface properties, and material composition, which enhances patient compliance and lowers toxicity. The potential of nanotechnology to improve diagnostic testing and treat

diseases like cancer and AIDS was highlighted as a significant advancement in medical science.

The importance of silver nanoparticles (AgNPs) in biological applications, specifically in the diagnosis and treatment of cancer, was investigated by *Zhang et al. (2016).* AgNPs' many bioactive qualities, such as their anti-inflammatory, antibacterial, antifungal, and anti-cancer actions, are highlighted in the review. The processes underlying AgNPs' anti-cancer action are also covered, and therapeutic approaches to current problems are presented. In addition to predicting future advancements in their study within nanomedicine, the article highlights the critical role that AgNPs play in improving nanotechnology and nanoscience for disease diagnosis, treatment, and prevention.

The impact of silver nitrate ($AgNO_3$) and silver nanoparticles (AgNPs) on the oxygen consumption and basal metabolic rate (BMR) of Eurasian perches was examined by *Bilberg et al. (2009).* AgNP exposure dramatically raised BMR, with the largest rise occurring at 300 μg/L. On the other hand, BMR was unaffected by silver nitrate at 386 μg/L. The work highlighted the environmental hazards connected to the disposal of nanosilver in aquatic environments by showing that exposure to AgNPs may reduce fish hypoxia tolerance, possibly through effects on gill function.

Dawadi et al. (2005) emphasized the revolutionary influence of nanomaterials, especially silver nanoparticles (AgNPs), across a variety of scientific domains. AgNPs are known to have antibacterial properties that improve medication efficacy and allow for targeted drug delivery. Because of their surface plasmon resonance, they also show promise in wearable and biosensors. Although AgNPs can be produced using both biological and physicochemical processes, their cytotoxicity and environmental effects necessitate cautious handling. AgNPs' synthesis, characterisation, usage, and hazards are the main topics of the review.

The antibacterial capabilities of silver nanoparticles (AgNPs) against Escherichia coli and other Gram-negative bacteria were examined by *Sondi and Salopek-Sondi (2004).* According to the study, AgNPs seriously damaged the bacterial cell walls, increasing permeability and causing cell death. They found pits in the bacterial membranes and other structural damage using scanning electron microscopy (SEM) and transmission electron microscopy (TEM). The study emphasizes AgNPs' potential as safe, effective, and reasonably priced antibacterial medicines.

2.8 REFERENCES

- Alam MA, Subhan N, Hossain H, Hossain M, Reza HM, Rahman MM, et al. Effect of naringin on metabolic syndrome: A review. Pharmacol Res. 2014;94:71–81.
- Alishahi A, Mirvaghefi AR, Tehrani MR, Farahmand H, Koshio S, Dorkoosh FA, et al. Chitosan nanoparticle to carry vitamin C through the gastrointestinal tract and its absorption by rainbow trout (Oncorhynchus mykiss): Preparation, characterization and in vivo investigation. Iran J Pharm Res. 2011;10(4):811–820.
- Al-Nemrawi NK, Alshraiedeh NH, Zayed GM, Altamimi MA. Effect of formulation variables on the characteristics of chitosan nanoparticles using ionic gelation method. Tropical Journal of Pharmaceutical Research. 2018;17(3):463–70.
- Aminu N, Audu MM. Poly-ε-caprolactone (PCL): A versatile polymer for drug delivery and biomedical applications. J Biomed Mater Res. 2023;58(6):119-130.
- Anitha A, Divya Rani VV, Krishna R, Sreeja V, Selvamurugan N, Nair SV, Tamura H, Jayakumar R. Synthesis, characterization, cytotoxicity and antibacterial studies of chitosan, O-carboxymethyl and N,O-carboxymethyl chitosan nanoparticles. Carbohydr Polym. 2009;78(4):672–7.
- Antoniou J, Liu F, Majeed H, Qi J, Yokoyama W, Zhong F. Physicochemical and morphological properties of size-controlled chitosan–tripolyphosphate nanoparticles. Colloids Surf A Physicochem Eng Asp. 2015;465:137–46.
- Arulmozhi V, Pandian K, Mirunalini S. Ellagic acid encapsulated chitosan nanoparticles as a novel drug delivery system. Int J Biol Macromol. 2013;62:93–7.
- Badran MM, Alanazi AE, Ibrahim MA, Alshora DH, Taha E, Alomrani HA. Optimization of Bromocriptine-Mesylate-Loaded Polycaprolactone Nanoparticles Coated with Chitosan for Nose-to-Brain Delivery: In Vitro and In Vivo Studies. Polymers (Basel). 2023 Sep 26;15(19):3890.
- Bala I, Hariharan S, Kumar MN. PLGA nanoparticles in drug delivery: the state of the art. Crit Rev Ther Drug Carrier Syst. 2004;21(5):387–422.
- Bilberg, K., Mortensen, A. S., Jensen, F., et al. (2009). Effects of silver nanoparticles on oxygen consumption in the Eurasian perch (Perca fluviatilis). Environmental Toxicology and Chemistry, 28(2), 408-415.

- Boots AW, Haenen GR, Bast A. Health effects of quercetin: from antioxidant to nutraceutical. Eur J Pharmacol. 2008;585(2-3):325–337.
- Bruna, S., Gonzalez, M., & Rodríguez, M. (2020). Silver nanoparticles as potent antibacterial agents: A review. International Journal of Antimicrobial Agents, 55(4), 105-112.
- Burdusel M, Gherasim O, Mocan T, et al. Silver nanoparticles in biomedical applications: the state of the art. Nanomaterials. 2021;11(4):858.
- Chtourou Y, Aouey B, Kebieche M, Fetoui H. Protective role of naringin against cisplatin-induced oxidative stress, inflammatory response and apoptosis in rat striatum via suppressing ROS-mediated NF-κB and p53 signaling pathways. Chem Biol Interact. 2015;239:76–86.
- Crisan D, et al. (2021). Copper nanoparticles in medicine and agriculture: Synthesis, mechanisms of action, and potential applications. Nanomedicine: Nanotechnology, Biology, and Medicine, 32, 102-110.
- D'Andrea G. Quercetin: a flavonol with multifaceted therapeutic applications? Fitoterapia. 2015;106:256–271.
- Dawadi S. Silver nanoparticles: Synthesis, characterization, and applications. J Nanomater. 2005;11(3):223-231.
- Dong Y, Liu F, Zhang Z, Zhang L, Zhao X, Li J, et al. Ionic gelation-based synthesis of chitosan nanoparticles for drug delivery applications. J Nanopart Res. 2013;15(9):1-13.
- Du S, Wang M, Liu Z, Jia Y, Wang C, Wang T, et al. Research progress on the pharmacological effects and new dosage forms of mangiferin. Front Pharmacol. 2023;14:1125767.
- Du S, Zhang Y, Nie Y, Tao J, Xu H, Chen Z, et al. Pharmacological effects of mangiferin and its potential application in the prevention and treatment of disease. Front Pharmacol. 2018;9:1354.
- Dudhania AR, Gupta RK. Chitosan–tripolyphosphate nanoparticles as potential carriers for catechin. Int J Biol Macromol. 2010;47(2):248–54.

- Dung TH, Sugimoto Y, Inoue Y, Ikezaki H, Yoshino H. Preparation of antisense oligonucleotide-loaded chitosan nanoparticles and their release characteristics. International Journal of Pharmaceutics. 2007;343(1-2):26–33.
- El-Habashy SE, et al. Hydroxyapatite/polycaprolactone nanoparticles for bone regeneration: Synthesis, characterization, and osteogenic potential. J Biomed Mater Res A. 2020;108(5):1113-1124.
- Espinoza SM, et al. Poly-Ɛ-caprolactone as a promising polymer in cancer nanomedicine. Nanomedicine. 2019;14(4):23-35.
- Fijan S, Turk SS, et al. Drug-loaded polycaprolactone (PCL)-based nanoparticles: optimization of process parameters in a nano-precipitation approach for antifouling and in vitro drug release applications. J Nanoparticle Res. 2012;14(8):1-9.
- Gil M, Kim YK, Hong SB, Lee SH, Kim YH, Jeon SH, et al. Naringin decreases TNF-α and HMGB1 release from LPS-stimulated macrophages and improves survival in a CLP-induced sepsis mouse model. Front Pharmacol. 2016;7:389.
- Gunatillake PA, Adhikari R. Biodegradable synthetic polymers for tissue engineering. Eur Cells Mater. 2003;5(1):1-16.
- Hallan SS, Sguizzato M, Pavoni G, Baldisserotto A, Drechsler M, Mariani P, et al. Ellagic acid-loaded nanostructured lipid carriers for topical application: a preliminary study. Molecules. 2020;25(6):1449.
- Harakeh S, Abu-Alhail S, Diab-Assaf M, Kansara I, Dhingra K, Akhtar N, et al. Ellagic acid-loaded biodegradable hollow zein nanoparticles for oral delivery: Enhanced bioavailability and anti-inflammatory effects. Int J Pharm. 2021
- Hou S, Zhu X, Wei X, Chen G, Liu H, Lu W, et al. Pharmacokinetics and bioavailability study of mangiferin in humans using a newly developed high-performance liquid chromatography–mass spectrometry method. J Pharm Biomed Anal. 2011
- Hussein-Al-Ali, H., Alhamadani, M. A., Al-Sulaiman, H., et al. (2022). Silver nanoparticles (AgNPs) for ciprofloxacin delivery: Synthesis, characterization, and drug release studies. Materials Science and Engineering: C, 135, 112741.

- Ibrahim KE, Bakhiet AO, et al. Drug delivery methods based on polycaprolactone nanoparticles: Synthesis, drug composition, and applications. J Drug Deliv Sci Technol. 2018;47:246-254.
- Jayachandran R, Ramachandran S, et al. Silver nanoparticles-loaded liposomes for cancer management: synthesis, characterization, and in vitro release studies. Mater Sci Eng C. 2023;144:112136.
- Kaurav M, Sharma R, Patel DK, Sagar N, Kumar S. Mangiferin: a natural xanthonoid with multipotent pharmacological activities. Phytochemistry Reviews. 2021;20(2):491–512.
- Kawai Y, Nishikawa T, Shiba Y, Saito S, Murota K, Terao J. Macrophage as a target of quercetin glucuronides in human atherosclerotic arteries: implication in the anti-atherosclerotic mechanism of dietary flavonoids. J Biol Chem. 2008;283(14):9424–9434.
- Khan HA, Baig FK, et al. Drug-loaded polycaprolactone-based nanoparticles: Optimization, antifouling capacity, and in vitro drug release applications. J Nanomater. 2017;2017:1-9.
- Kobori M, Masumoto S, Akimoto Y, Oike H. Chronic high intake of quercetin reduces oxidative stress and promotes expression of antioxidant and longevity genes in mice. Nutr Res. 2011;31(8):561–567.
- Lee H, Yoon Y, Yoon IS, Lee JY, Yu J, Kim DD, et al. Development of a functional beverage using epidermal growth factor-loaded nanoparticles: Physicochemical characterization and potential application. Food Sci Biotechnol. 2018;27(1):155–62.
- Lee JY, Lee Y, Jin Y, Shin KS, Yun JW, Lee YR, et al. Improved water solubility and antioxidant properties of mangiferin by enzymatic glucosylation using CGTase from Thermoanaerobacter sp. LWT - Food Science and Technology. 2022;181:115278.
- Li Y, Yao J, Han C, Yang J, Chaudhry MT, Wang S, Liu H, Yin Y. Quercetin, inflammation and immunity. Nutrients. 2016;8(3):167.
- Łukasiewicz S, et al. Bio-polymeric nanoparticles for endocytosis, immunological response, and cell survival in murine macrophages. J Biomed Mater Res B Appl Biomater. 2021;109(5):800-809.

- Mady FM, Essa H, El-Ammawi TS, El-Say KM, Abdelkader DH. Enhancing the oral bioavailability and cytotoxicity of ellagic acid using poly(ε-caprolactone) nanoparticles. Int J Nanomedicine. 2017;12:7405-7417.
- Mahfoudh-Boussaid A, Zaouali MA, Hadj-Ayed K, Miled AH, Saidane-Mosbahi D, Ghoul-Mazgar S. Protective effect of quercetin on aluminum chloride-induced oxidative stress in rat cerebral cortex. Brain Res Bull. 2012;88(6):586–592.
- Mohamed EA, El-Gizawy SA, Hassen SZ, ElMeshad AN, Ghoneim MM, Alqahtani FY, et al. Antiulcer and anticancer effects of naringin-loaded Pluronic F68 mixed micelles: formulation, characterization, and evaluation in ethanol-induced ulcer and Ehrlich ascites carcinoma models. Pharmaceutics. 2022;14(4):813.
- Nair LS, Laurencin CT. Polymeric nanofibers and scaffolds for tissue engineering. In: Biomaterials Science: An Introduction to Materials in Medicine. 2nd ed. Academic Press; 2007. p. 103-122.
- Özbaş-Turan S, Akbuğa J, Aral C. Controlled release of plasmid DNA from alginate–chitosan beads: effect of chitosan and calcium concentration on DNA release. Pharmazie. 2011;66(11):836–42.
- Pal A, Sharma T, Aditya A, Ghosh B, Majumdar S. Development and evaluation of naringenin-loaded polymeric nanoparticles for the treatment of metabolic syndrome: Pharmacokinetic and pharmacodynamic studies. Pharm Res. 2021;38(7):1259–75.
- Papadimitriou S, Bikiaris D, Avgoustakis K, Karavas E, Georgarakis E. Chitosan nanoparticles loaded with dorzolamide and pramipexole. Carbohydr Polym. 2008;73(1):44–54.
- Rivera L, Morón R, Sánchez M, Zarzuelo A, Galisteo M. Quercetin ameliorates metabolic syndrome and improves the inflammatory status in obese Zucker rats. Obesity (Silver Spring). 2008;16(9):2081–2087.
- Rizvi SA, Saleh AM. Applications of nanoparticle systems in drug delivery and cancer therapy. Nanomaterials (Basel). 2018 Feb 26;8(1):51.
- Sadeghi-Ghadi Z, Gholami L, Ghasemiyeh P, Mohammadi-Samani S. Hyaluronic acid-modified niosomes for targeted delivery of quercetin: Preparation, characterization, and anti-inflammatory and antioxidant effects. Drug Dev Ind Pharm. 2020;46(9):1410–9.

- Servat-Medina L, de Souza CM, de Oliveira JR, Amorim MIF, Saldanha-Araujo F, Gelfuso GM, et al. Chitosan-based nanoparticles for the oral delivery of Arrabidaea chica standardized extract: Development, characterization, and in vivo evaluation of antiulcer activity. Int J Nanomedicine. 2015;10:3895–3906.
- Shanmuganathan, R., Choi, J. S., Park, Y. J., et al. (2019). Silver nanoparticles: Synthesis, characterization, and biomedical applications. Journal of Nanoscience and Nanotechnology, 19(3), 1740-1753.
- Sharifi-Rad J, Quispe C, Durazzo A, Lucarini M, Souto EB, Santini A, et al. Ellagic acid as a potential therapeutic agent for human diseases: A mechanistic review. Food Chem. 2022;370:130978.
- Sondi I, Salopek-Sondi B. Silver nanoparticles as antimicrobial agents: A case study against Escherichia coli. J Colloid Interface Sci. 2004;275(1):177-182.
- Sunoqrot S, Bardaweel SK, Abukhalil MH, Alqudah DA, Tarawneh AH, Al-Mahallawi AM. Development of pH-sensitive polymeric nanoparticles for colon-targeted delivery of quercetin: Formulation, characterization and cytotoxicity studies. J Drug Deliv Sci Technol. 2019;52:257–64.
- Vimal S, Taju G, Gopikrishna G, Raj NS, Madan N, Sood N, et al. Chitosan tripolyphosphate (CS/TPP) nanoparticles: a potential delivery system for oral administration of plasmid DNA in shrimp. Aquaculture. 2013;404–405:124–30.
- Vimal S, Taju G, Gopikrishna G, Raj NS, Madan N, Sood N, et al. Oral administration of DNA vaccine using chitosan nanoparticles against fish nodavirus in Asian seabass. Fish Shellfish Immunol. 2013;35(5):1516–23.
- Wang H, Xu YS, Wang ML, Cheng C, Bian R, Yuan H, et al. Protective effect of naringin against the LPS-induced apoptosis of PC12 cells: Implications for the treatment of neurodegenerative disorders. Int J Mol Med. 2017;39(4):819–30.
- Wang X, Li X, Zhang Y, Chen Z, Song X, Liu Z, et al. Chitosan as a potential delivery system for estradiol via the nasal route for Alzheimer's disease treatment. Int J Pharm. 2008;360(1-2):138-145.
- Wu Y, Yang W, Wang C, Hu J, Fu S. Chitosan nanoparticles as a novel delivery system for ammonium glycyrrhizinate. Int J Pharm. 2005;295(1-2):235–45.

- Xu Q, Tanaka Y, Ikegami Y, Tokunaga Y, Ochiya T, Kosaka N, et al. Intravenous delivery of interleukin-12 gene using chitosan nanoparticles for liver metastasis of colorectal cancer. Cancer Sci. 2011;102(12):2061–7.
- Zhang W, Lu Z, Li H, Zhang X, Liu Y, Zhai G. A thiol–ene photoclickable PEG hydrogel incorporating ellagic acid for enhanced antibacterial and anti-inflammatory wound healing. Int J Biol Macromol. 2023;236:124096.
- Zhang, Y., Wang, Y., Wang, H., et al. (2016). Biomedical applications of silver nanoparticles in cancer diagnosis and treatment. Nanomedicine: Nanotechnology, Biology, and Medicine, 12(1), 215-227.

CHAPTER 3

AIM AND OBJECTIVE

.

3.1. Aim

- To prepare and compare various pharmaceutical carriers based on Natural polymer (Chitosan), Synthetic polymer (Polycaprolactone) and Metal-based (Silver & Copper) nanoparticles.
- To load phyto drugs naringin, ellagic acid, quercetin and mangiferin into the various nanocarriers.
- Evaluate the various characteristics for the developed nanoparticulate carriers.
- Evaluation of the biological activities of the prepared nanocarriers.

3.2. Objectives

3.2.1 To select and justify the use of phyto-compounds—naringin, ellagic acid, quercetin, and mangiferin—based on their known pharmacological activities and limitations related to solubility, bioavailability, or stability.

3.2.2 To formulate and optimize pharmaceutical nanocarriers using three different categories of materials:

- Natural polymers: Chitosan based nanoparticle systems for their controlled release characteristics.
- Synthetic polymers: Polycaprolactone (PCL)-based nanoparticles for sustained release and improved stability.
- Metal-based systems: Silver (Ag) and Copper (Cu) nanoparticles for synergistic antimicrobial or antioxidant properties.

3.2.3 To incorporate the selected phyto-drugs into each type of nanocarrier system, ensuring optimal encapsulation efficiency, stability, and drug loading capacity.

3.2.4 To optimize critical formulation variables such as polymer/metal concentration, drug-to-carrier ratio, stirring speed, solvent system, etc.

3.2.5 To characterize the developed nanocarriers in terms of:

- Particle size and distribution
- Surface charge (Zeta potential)
- Morphology (using SEM and/or TEM)
- Crystallinity and chemical interactions (via XRD, FTIR, DSC, TGA)

3.2.6 To perform in vitro drug release studies for each formulation under simulated physiological conditions and evaluate the release kinetics to understand the drug release mechanism.

3.2.7 To evaluate the biological efficacy of each formulation, including:

- Antioxidant activity (e.g., DPPH radical scavenging assay)
- Anti-inflammatory potential (e.g., Carrageenan-induced paw edema model in rats)
- Anti-diabetic activity (e.g., Streptozotocin-induced diabetes model in rats)
- Antimicrobial activity (particularly for Ag and Cu-based formulations)
- Transcorneal permeation studies (for evaluating ocular drug delivery and anti-inflammatory potential)
- HET-CAM test (Hen's Egg Test on Chorioallantoic Membrane to evaluate ocular irritancy)

3.2.8 To compare the performance of chitosan-based, PCL-based, and Ag/Cu-based nanocarriers in terms of:

- Drug loading and release profile
- Stability and size distribution
- Enhancement of bioactivity over pure drugs

3.2.9 Summarize the results and comprehensively analyze and summarize the findings from all formulations, characterizations, and evaluations.

4. Plan of Work in Various Phases

4.1 Phase I: Selection, Procurement, and Preformulation Studies

Activities:

- Literature review on pharmacological activities and formulation challenges of naringin, ellagic acid, quercetin, and mangiferin.
- Evaluation of physicochemical properties of the drugs (solubility, melting point, UV/IR spectra).
- Selection and procurement of polymers (chitosan, polycaprolactone) and metal salts ($AgNO_3$, $CuSO_4$) for nanocarrier synthesis.
- Preliminary compatibility studies (e.g., FTIR) between drugs and excipients.
- Finalization of model ailments/indications for biological activity (e.g., inflammation, diabetes, antimicrobial therapy, ocular delivery).

4.2 Phase II: Formulation Development and Optimization:

- Preparation of:

✓ Chitosan-based nanoparticles

✓ PCL-based nanoparticles

✓ Silver and Copper metal nanoparticles.

- Optimization of formulation parameters.
- Preliminary encapsulation efficiency and drug loading studies.
- Selection of best formulations based on optimization results.

4.3 Phase III: Characterization and In Vitro Evaluations

Activities:

- Physicochemical characterization:
- ✓ Particle size and zeta potential
- ✓ Morphological analysis (SEM/TEM)
- ✓ FTIR, DSC, DTA, TGA, and XRD studies
- In vitro drug release studies and modeling of release kinetics.
- Antioxidant activity assessment (DPPH assay) for specific formulations.
- Antimicrobial activity testing (zone of inhibition/MIC determination) for relevant formulations.
- Transcorneal permeation and HET-CAM test for ocular formulations.

4.4 Phase IV: In Vivo Studies, Data Analysis, and Report Compilation

Activities:

- In vivo anti-inflammatory study (Carrageenan-induced paw edema).
- In vivo anti-diabetic study (Streptozotocin-induced diabetes model).
- Comparative evaluation of all formulations.
- Compilation of data, statistical analysis, and interpretation of results.

CHAPTER 4

MATERIALS & METHODS

CONTENTS

Section A: Natural Polymer (Chitosan) Based Nanocarriers

4.1 Naringin Loaded Chitosan Nanoparticles

Table 2: List of materials required for the preparation of Naringin Loaded Chitosan Nanoparticles

Name	*Rationality*	*Source*
Naringin	Phytochemical	Sigma Aldrich
Chitosan	(≥75% deacetylated)	Sigma Aldrich
Glacial Acetic Acid	For activation of chitosan	HiMedia Laboratories
Sodium Tripolyphosphate	Crosslinking agent for chitosan	HiMedia Laboratories
Dialysis membrane MW cut off, 12400	For drug release study	Sigma Aldrich.

4.1.1 Physicochemical and Pharmacological Profile of Naringin

Naringin is a flavonoid glycoside composed of glycone naringenin and disaccharide neohesperidose attached to the hydroxyl group at the C-7 position. It gives many citrus fruits their bitter flavor and can be found in tomatoes, grapefruits, and other citrus fruits (Saini et al., 2023) and exhibits a broad pharmacological profile encompassing antioxidant, anti-inflammatory, anti-apoptotic, cardioprotective, neuroprotective, and anti-cancer activities (Garg et al., 2023). Its antioxidant activity is mediated through free radical scavenging and upregulation of endogenous antioxidant enzymes, while its anti-inflammatory effects are attributed to the inhibition of pro-inflammatory cytokines and NF-κB signaling (Sharma et al., 2021).

Table 3: Physicochemical Properties of Naringin

Property	*Value*	*Notes*	*Reference*
Molecular Formula	$C_{27}H_{32}O_{14}$	Flavonoid glycoside	Gattuso et al., 2007
Molecular Weight	580.53 g/mol	Includes aglycone naringenin + disaccharide neohesperidose	Gattuso et al., 2007
Appearance	White to off-white crystalline powder		Sigma-Aldrich Product Data Sheet
Solubility in Water	~475 mg/L	Poor aqueous solubility due to hydrophobic nature	Bai et al., 2020
Melting Point	166°C		PubChem (CID: 442428)
Oral Bioavailability	Low	Due to poor solubility and extensive first-pass metabolism	Bai et al., 2020

4.1.2 Preformulation studies

Determination of absorption maxima and Preparation of Calibration Curve of Naringin: A 100 mL volumetric flask was filled with precisely weighed 100 mg of the medication. Ten milliliters of ethanol were added to this in order to fully dissolve the naringin. Demineralized (DM) water was then added to bring the volume up to 100 mL, yielding a stock solution containing 1000 µg/mL. To create a working solution of 100µg/mL, suitable dilutions were made from this stock using DM water. The sample solution was scanned with a double-beam UV-Visible spectrophotometer in the 200–800 nm wavelength range (Beckett et al., 2005).

The calibration curve was plotted by measuring absorbance across various concentration ranges of naringin solutions between 2-20µg/ml using UV-Visible Spectrophotometer at the absorbance maxima.

Solubility Studies: An excess naringin was added to different solvents and agitated constantly at room temperature until equilibrium was reached in order to assess saturation solubility. After filtering, the filtrates were suitably diluted. At 285 nm, a UV-Visible spectrophotometer was used to measure concentration in each solution.

Melting Point Determination: The open capillary method was used to determine naringin's melting point. A capillary tube holding a modest amount of the phytochemical was put in a Theil's tube with liquid glycerol. The melting point was determined by gently heating the tube until the medication started to melt.

4.1.3 Method of preparation of Naringin Loaded Chitosan (NLC) nanocarriers

NLC nanocarriers were created via the ionic gelation technique. Acetic acid 1% (v/v) was used to prepare chitosan solution. The chitosan solution was continuously mixed as naringin was added dropwise. Over the course of two hours, while stirring continuously, the chitosan solution was gradually combined with the sodium tripolyphosphate (TPP) solution, which was kept at 4°C. Chitosan was used at different concentrations (0.5–2 mg/ml). Drug was incorporated into the NLC nanocarriers at a concentration of 0.25 mg/ml. Amount of TPP used was optimized at 0.5 mg/ml which

was fixed for all formulations. To find the best formulation, a range of TPP volumes, drug concentrations, and polymer concentrations were tested using different stirring speed. (Hoang et. al, 2022, Kumar et al., 2012)

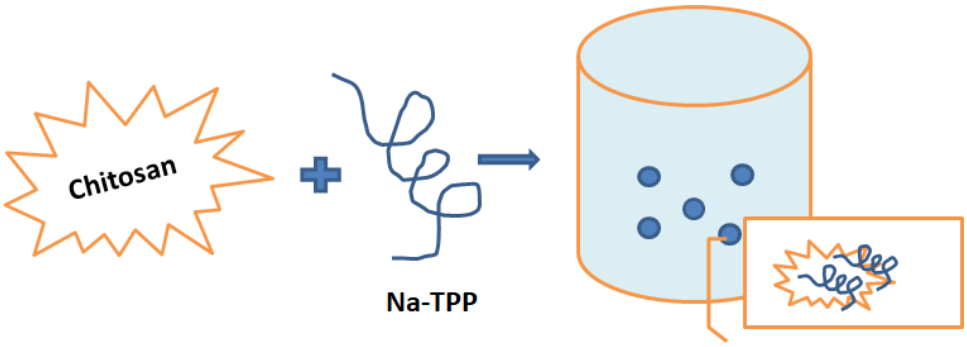

Figure 16: Schematic representation of Chitosan nanocarriers

4.1.4 Characterizations of NLC Nanocarriers

4.1.4.1 FTIR spectrum analysis: FTIR studies were carried out for naringin, chitosan and the NLC carriers under identical conditions to detect any possible interactions between the components that may lead to precipitation of the drug. It was carried out by mixing the sample with potassium bromide (KBr) to form a pellet and scanning the sample over a wavelength from 4000 to 400 cm^{-1}.

4.1.4.2 X-ray crystallography analysis: The X-ray crystallography of naringin, blank NLC carriers, and NLC carriers containing naringin was performed by Cu Kα radiation, at a voltage of 40 kV and 30 mA. The angle of scanning was adjusted from 5° to 70°, and the scanning rate was 4°/min.

4.1.4.3 Entrapment efficiency: After ultra-centrifuging NLC samples, the sediment and supernatant fluids were gathered. Absorbance was then measured with a UV spectrophotometer in the supernatant for the unentrapped drug concentration (Joshi et al., 2014). Entrapment efficiency (EE) and drug loading capacity (LC) was determined using the equation:

EE= (Amount of naringin encapsulated into formulation)/ (Amount of the total naringin added) x100

LC= (Weight of naringin in formulation)/(Total weight of the formulation) x100

4.1.4.4 Physical characterization: Using a particle size analyser, dimension of the prepared NLCs was determined. A suitable concentration of NLC was agitated at 100 rpm and maintained at 37°C in distilled water. After being allowed to dry at ambient temperature, the NLC nanocarriers' structure was examined using a scanning electron microscope (SEM) to study their surface properties. For TEM, a drop of diluted NLC suspension was deposited on a film-coated copper grid, stained with one drop of 2% (w/v) aqueous solution of phosphotungstic acid, and then allowed to dry for contrast enhancement.

4.1.5 In vitro release study: Naringin, equivalent to 5 mg, was filled into a dialysis bag and placed in phosphate buffer solution (PBS, pH 7.4, 50 mL). The beaker was magnetically stirred at 100 rpm while being kept at 37 ± 0.5^{0}C. UV spectrophotometry was used to measure the absorbance after 5 ml samples were taken out and replaced with fresh buffer solution at predefined intervals (Joshi et al., 2014, Shadab Md et al., 2019).

4.1.6 Cytotoxicity study: Human derived embryonic kidney HEK 293 cells were procured from The National Collection of Cell Sciences (NCCS), Pune. The cells were kept in modified Eagle's medium (MEM) supplemented with 2 mM glutamine, 10% fetal bovine serum that has been heat-inactivated, 1% penicillin-streptomycin solution, and 5% CO_2 at 37°C in a humidified atmosphere. The MTT (3(4,5-dimethlythiazol-eyl) 2,5-diphenly-tetrazoliumbromide) technique was employed to assess the vitality of cells in vitro. In 96-well plates, 8000 HEK 293 cells were planted each well and allowed to attach for full day. The following day, the used media was removed and replaced with new glutamine medium containing varying concentrations of naringin (6.25 µM, 12.25 µM, 25 µM, 50 µM, and 100 µM) for 24 hours. After the target time point was reached, 20 µL of MTT dye (5 mg/ml) dissolved in phosphate buffer saline was added to each well, and the incubator was left in dark for 4 hours at 37°C. After carefully extracting media containing MTT dye, 100 µL of DMSO was given to each well to dissolve the formazan crystal. The wells were then left for 10 minutes at room temperature in the dark. Each well's absorbance was calculated using a micro-plate reader at 570 nm. (Hussain et al., 1993)

$$\text{Cell viability (\%)} = (A_{\text{treatment}} - A_{\text{blank}}) / (A_{\text{control}} - A_{\text{blank}}) \times 100$$

4.1.7. Anti-inflammatory Activity:

Male and female Wistar rats weighing between 100 and 150 g were employed to assess the formulation's anti-inflammatory properties. Before the trials began, the rats were given a balanced food and unlimited access to water for approximately two weeks while they adjusted to the laboratory environment. Every animal was housed at 24±2ºC with a relative humidity of 60±5% and exposed to a 12/12 hour light/dark cycle by the appropriate institutional review body. Animal experiments in the present study and the study protocol was reviewed and approved by Institutional Animal Ethical Committee (IAEC) of Dr B C Roy College of Pharmacy and AHS (Reference No: BCRCP/IAEC/2/2019). The paw edema model induced by the phlogistic agent, carrageenan, was employed to evaluate the anti-inflammatory activity of prepared NLC carriers. Rats were divided into five groups (n = 6), and were given one of the following treatments: Group 1: distilled water + carrageenan; Group 2: blank formulation + carrageenan; Group 3: free naringin (50 mg/kg, p.o) + carrageenan; Group 4: NLC (50 mg/kg, p.o) + carrageenan, and Group 5; diclofenac (10 mg/kg, p.o.) + carrageenan. Thereafter, 0.1 mL of carrageenan (1% w/v in saline) was injected into the sub-plantar tissue of the right hind paw one hour after the various treatments were administered in order to cause edema. After administering carrageenan, paw volume was measured plethysmographically at 0th, 1st, 2nd, 3rd, 4th, and 6th hours (Mandal et al., 2000, Mandal et al., 2003). The % of inhibition was calculated using the following formula:

$$\% \text{ Inhibition} = (\text{Increase in paw edema}_{control} - \text{Increase in paw edema}_{treated}) / \text{Increase in paw edema}_{control}) \times 100$$

The results are expressed as mean ± SEM. Analysis of results was performed by one-way ANOVA followed by Dunnets test. Values of $p < 0.05$ were considered to be statistically significant.

4.2 Chitosan- Based Quercetin Dihydrate Nanoparticles

4.2.1 Materials Required Quercetin Loaded Chitosan Nanoparticles

Table 4: List of materials required

Name	Rationality	Source
Quercetin	Phytochemical	Sigma Aldrich
Chitosan	(≥75% deacetylated)	Sigma Aldrich
Glacial Acetic Acid	For activation of chitosan	HiMedia Laboratories
Sodium Tripolyphosphate	Crosslinking agent for chitosan	HiMedia Laboratories
Dialysis membrane MW cut off, 12400	For drug release study	Sigma Aldrich

4.2.2 Physicochemical & pharmacological profile of quercetin

Quercetin is a naturally occurring flavonol, a subclass of flavonoids. Five hydroxyl (-OH) groups are located at positions 3, 5, 7, 3′, and 4′, and a three-ring system (a chromone backbone with an extra phenyl group at position 2) makes up its structure. These hydroxyl groups facilitate metal ion chelation and free radical scavenging, which add to its potent antioxidant qualities. The anti-inflammatory, antiviral, anticancer, cardioprotective, and neuroprotective properties of quercetin are enhanced by its conjugated and planar structure, which facilitates effective interaction with biomolecules. Its pharmacological potential is further supported by its capacity to alter signaling pathways such as PI3K/Akt, MAPK, and NF-κB. (Boots et al., 2008, Li et al., 2016, Kumar et al., 2013)

Table 5: Physicochemical Properties of Quercetin

Property	*Value / Description*	*Reference*
Molecular Formula	$C_{15}H_{10}O_7$	Kumar *et al.*, 2013
Molecular Weight	302.24 g/mol	Kumar *et al.*, 2013
Melting Point	316–317°C	Boots *et al.*, 2008
Solubility in Water	Poor (<2 mg/L)	Li *et al.*, 2016
Log P (Partition Coefficient)	~1.8–2.1	Boots *et al.*, 2008
Appearance	Yellow crystalline powder	Sigma-Aldrich, 2025

4.2.3 Method of preparation of Quercetin Loaded Chitosan (FQN) nanocarriers

FQN nanocarriers were created via the ionic gelation technique. Acetic acid 1% (v/v) was used to prepare chitosan solution. The chitosan solution was continuously mixed as quercetin was added dropwise. Over the course of two hours, while stirring continuously, the chitosan solution was gradually combined with the sodium tripolyphosphate solution, which was kept at 4°C. Chitosan was used at different concentrations (0.5–2 mg/ml). Quercetin was incorporated into the FQN nanocarriers at a concentration of 0.25 mg/ml. Amount of TPP used was optimized at 0.5 mg/ml which was fixed for all formulations. To find the best formulation, a range of TPP volumes, drug concentrations, and polymer concentrations were tested. (Hoang et al., 2022, Kumar et al., 2012).

4.2.4 Characterizations of FQN Nanocarriers

4.2.4.1 Entrapment efficiency: After ultra-centrifuging FQN samples, the sediment and supernatant fluids were gathered. Absorbance was then measured with a UV spectrophotometer in the supernatant for unentrapped drug concentration (Joshi et al., 2014). Entrapment efficiency (EE) and drug loading capacity (LC) was determined using the equation:

EE= (Amount of quercetin encapsulated into formulation)/ (Amount of the total quercetin added) x100

LC= (Weight of quercetin in formulation)/ (Total weight of the formulation) x100

4.2.4.2 Physical characterization: Using a particle size analyzer, dimension of the prepared FQNs was determined. A suitable concentration of FQN was agitated at 100 rpm and maintained at 37°C in distilled water. After being allowed to dry at ambient temperature, the FQN nanocarriers structure was examined using a scanning electron microscope (SEM) to study their surface properties. For TEM, a drop of diluted FQN suspension was deposited on a film-coated copper grid, stained with one drop of 2% (w/v) aqueous solution of phosphotungstic acid, and then allowed to dry for contrast enhancement.

4.2.5 In vitro release study:

Quercetin, equivalent to 5 mg, was filled into a dialysis bag and placed in phosphate buffer solution (PBS, pH 7.4, 50 mL). The beaker was magnetically stirred at 100 rpm while being kept at 37±0.5^{0}C. UV spectrophotometry was used to measure the absorbance after 5 ml samples were taken out and replaced with fresh buffer solution at predefined intervals (Joshi et al., 2014, Shadab Md et al., 2019).

4.2.6 Ocular Eye Irritancy Test: HET- CAM Test

The Hen's Egg Test on the Chorioallantoic Membrane (HET-CAM) is an alternative in vitro method used to evaluate the irritancy potential of chemicals or formulations, particularly for ocular applications. For nine days, fertilized hen eggs are kept at 37–38°C with a humidity of about 60%. The eggs are taken out of the incubator for examination on the ninth day of embryonic development. To determine whether an embryo is viable, eggs are candled. For the test, only viable eggs are chosen. The eggshell is precisely cut to reveal the chorioallantoic membrane (CAM) through a rectangular or circular window. After carefully removing the inner membrane, 2-3 mL of 0.9% saline is added to the CAM to wet it. The CAM surface is directly coated with a predetermined volume of the test material. For five minutes, the CAM is continuously monitored for indications of Hemorrhage (bleeding), Vascular lysis (vessel disintegration), Coagulation (protein denaturation/clotting). At one and five minutes after application, reactions are graded. The reaction's severity of hemorrhage, lysis, and coagulation is assessed and noted. This examination serves as a substitute for the Draize rabbit eye test. Because it preserves biological relevance while avoiding the use of live animals, it is valued for its ethical benefits. (Luepke, 1985, Spielmann et al., 1997, Borenfreund et al., 1988, Worth et al., 2002, ICCVAM, 2010)

4.2.7 Permeation Study across Excised Goat's Cornea

The corneal permeation potential of quercetin nanoparticle formulations (FQN1–FQN4) was assessed in vitro using a Franz diffusion cell in contrast to a simple quercetin suspension. A local slaughterhouse provided the fresh goat eyes, which were then properly cleaned with saline solution. The corneas served as the experiment's biological membrane after being carefully removed to preserve their structural integrity. With the endothelium side in touch with the receptor fluid and the epithelial side facing the donor compartment, each cornea was positioned between the donor and receptor compartments of the Franz diffusion cell. To replicate the ocular surface temperature, the receptor compartment was filled with phosphate-buffered saline (PBS, pH 7.4), kept at 34 ± 0.5°C, and constantly mixed with a magnetic stirrer (Gaudana et al., 2010, Saettone et al., 1995). A fixed volume of the test formulation (quercetin suspension/nanoparticle formulations) was placed in the donor compartment. To maintain sink conditions, samples were taken out of the receptor compartment and replaced with new PBS at prearranged intervals. The amount of quercetin that permeated the cornea was measured using UV-visible spectrophotometry. (Maurice et al., 1984)

Figure 17: Isolation of Goat's cornea for permeation study across Franz Diffusion cell (Dave et al., 2014)

Three important parameters enhancement ratio (ER), flux (J), and cumulative permeation were assessed from the study. The entire amount of drug that diffused over the cornea over the course of six hours is known as cumulative permeation, and it is measured in µg/cm². The slope of the linear part of the cumulative permeation versus time plot is used to determine flux, which is the steady-state rate of drug penetration and is expressed in µg/cm²/h. The enhancement ratio, which shows the relative improvement in drug penetration, is calculated by dividing the flux of the test formulation by that of the reference suspension (Tiwari et al., 2011; Koehl et al., 2000).

4.2.8 Antioxidant Activity Study for Quercetin-Loaded Nanoparticles: DPPH Assay

The 2,2-diphenyl-1-picrylhydrazyl (DPPH) free radical scavenging assay, a popular and well-established technique for evaluating the free radical scavenging activity, was used to assess the antioxidant potential of quercetin-loaded nanoparticles (FQN1–FQN6) (Blois et al., 1958).

Before being used, a 0.1 mM DPPH solution was made in methanol and kept at room temperature in the dark. Different concentrations of quercetin-loaded formulations and free quercetin (5, 10, 20, and 40 µg/mL) were prepared in methanol for the study.

1 mL of the test sample (free quercetin/nanoparticle formulation) was added to each 2 mL aliquot of DPPH solution. The mixture was then vortexed and allowed to sit at room temperature for 30 minutes in the dark.

Methanol was used to create a control sample. A UV-Visible spectrophotometer was used to detect the solution's absorbance at 517 nm following incubation. Every measurement was carried out in triplicate, and the mean ± standard deviation was used to express the findings (Brand-Williams et al., 1995; Kumari et al., 2021). The following formula was used to determine the DPPH radical's % inhibition: *Inhibition (%) =* $(A_0 - A_1/A_0) \times 100$

Where $A_{0\ is}$ *the absorbance of the control (DPPH + methanol) and* A_1 *is the absorbance of the sample (DPPH + test compound).*

4.2.9 Anti-inflammatory Activity:

Male and female Wistar rats weighing between 100 and 150 g were employed to assess the formulation's anti-inflammatory properties. Before the trials began, the rats were given a balanced food and unlimited access to water for approximately two weeks while they adjusted to the laboratory environment. Every animal was housed at 24±2ºC with a relative humidity of 60±5% and exposed to a 12/12 hour light/dark cycle by the appropriate institutional review body. Animal experiments in the present study and the study protocol was reviewed and approved by Institutional Animal Ethical Committee (IAEC) of Dr B C Roy College of Pharmacy and AHS (Reference No: BCRCP/IAEC/2/2019).

The paw edema model induced by the phlogistic agent, carrageenan, was employed to evaluate the anti-inflammatory activity of prepared FQN carriers. Rats were divided into five groups (n = 6), and were given one of the following treatments: Group 1: distilled water + carrageenan; Group 2: blank formulation + carrageenan; Group 3: free quercetin (50 mg/kg, p.o) + carrageenan; Group 4: FQN (50 mg/kg, p.o)+ carrageenan , and Group 5; diclofenac (10 mg/kg, p.o.) + carrageenan. A single hour following the administration of the various agents, the right hind paw's sub-plantar tissue was injected with 0.1 mL carrageenan (1% w/v in saline) to induce edema.

After administering carrageenan, paw volume was measured plethysmographically at 0th, 1st, 2nd, 3rd, 4th, and 6th hours (Mandal et al., 2000, Mandal et al., 2003). The % of inhibition was calculated using the following formula: $\%\ Inhibition = (Increase\ in\ paw\ edema_{control} - Increase\ in\ paw\ edema_{treated}) / Increase\ in\ paw\ edema_{control}) \times 100$

The results are expressed as mean ± SEM. Analysis of results was performed by one-way ANOVA followed by Dunnets test. Values of $p < 0.05$ were considered to be statistically significant.

SECTION B: Synthetic Polymer (Polycaprolactone) Based Nanocarriers

4.3. Polycaprolactone (PCL) Based Nanocarriers of Naringin

Table 6: List of materials required for Naringin Loaded Polycaprolactone Nanoparticles

Name	*Rationality*	*Source*
Naringin	Experimental Phytochemical	Sigma-Aldrich Chemicals Private Limited
Polycaprolactone (MW 14, 000 g/mol)	Polymer	Sigma-Aldrich Chemicals Private Limited
Sodium hydroxide	Maintain pH	Sigma-Aldrich Chemicals Private Limited
Tween-80	Surfactant	Sigma-Aldrich Chemicals Private Limited
HCl	Stabilizing agent	LabChem, India.

4.3.1 Preparation of PCL nanoparticles (PCLNP)

Polycaprolactone based nanoparticles were prepared using the nanoprecipitation method. To make an organic solution, 50 mg of polycaprolactone was dissolved in acetone, and then 50 mg of drug solution was added. The pH was maintained at 7.4, and it was further stabilized by acidifying with 0.1M HCl. To make an aqueous solution, Tween-80 was added to 100 mL of water and agitated for 5 minutes. The organic solution was then added dropwise to the aqueous solution, and the combination was agitated for an hour at 300 rpm at first, then 900 rpm to evaporate the solvent. Following that, the mixture was centrifuged for 20 minutes at 4°C/13,000 rpm. The pellet was freeze-dried after being washed twice with deionized water to produce naringin-loaded PCL nanoparticles (Fessi et al., 1989, Miladi et al., 2016).

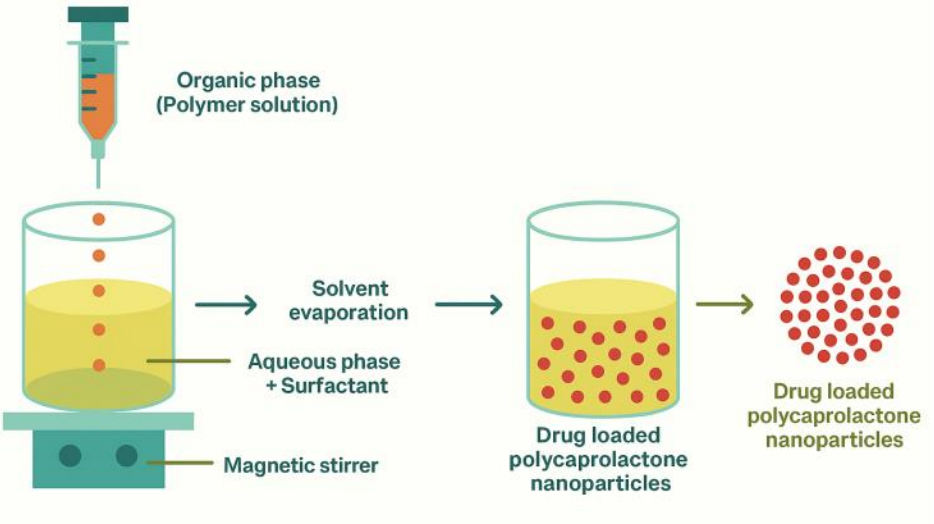

Figure 18: Schematic representation of preparation of polycaprolactone based nanocarriers (Ramanujam et al., 2018)

4.3.2 Drug Encapsulation Efficiency and Drug Loading:

To determine the drug encapsulation, the encapsulated naringin was separated from the nanoparticle by centrifugation at 10,000 rpm for 30 minutes. The amount of naringin encapsulated and loaded into PCL nanoparticles was determined using an ultraviolet spectrophotometer, UV-1800 Shimadzu, Japan (Bagheri et al., 2022, Shafiq etal., 2017). The following formulas were utilized to determine the drug loading and encapsulation efficiency: *Encapsulation efficiency (%) = Amount of encapsulated drug/Initial amount of drug used/ 100*

Drug loading (%) =Added drug −Free (Unentrapped drug)/Polymer amount x 100

4.3.3 Particles Morphology and Surface Characteristics:

Scanning Electron Microscopy (SEM) was used for the synthesized PCL nanoparticles to analyze their surface morphology, shape, and appearance at a voltage of 10 kV.

4.3.4 Drug polymer interaction study:

Thermogravimetric analysis (TGA) and differential scanning calorimetry (DSC) are methods used to investigate thermal characteristics. As a function of temperature, it calculates the heat flow related to chemical and physical changes. An empty reference pan and a tiny quantity of sample are put in a sample pan. The difference in heat flow between the reference and sample pans is determined when both pans are heated or cooled under controlled conditions. To show significant thermal events including melting, crystallization, glass transitions, and reactions, this data is plotted against temperature (Skoog etal., 2017). Thermal analysis, DSC and TGA tests were performed to establish the physical state and interaction of naringin with polymer. Analytical samples utilized in the investigation included pure naringin and PCL nanoparticles with and without naringin. The test instrument was a Differential Scanning Calorimeter Q200 (TA Instruments, USA). All measurements were carried out at a nitrogen purge rate of 50 mL/min within 20–500°C, at 10°C per minute.

4.3.5 Infrared Spectroscopy (IR):

IR spectroscopy involves the measurement of the absorption, transmission, or reflection of infrared light by a sample. The IR spectroscopic analysis of Polycaprolactone nanoparticles assisted in identifying the functional groups present. Pure naringin and PCL nanoparticles, both with and without naringin, were thoroughly dried and compacted into pellets before being employed as analytical samples.

4.3.6 Particle size analysis & zeta potential:

Dynamic light scattering (Zetasizer -Nano ZS, Malvern Instruments Limited, UK) was used at 25^0C to assess the size and zeta potential of produced nanoparticles, which impacts their stability and uptake into cells. Distilled water was used as the dispersant.

4.3.7 In-vitro drug release study:

The release characteristics of naringin from the nanoparticles were determined using a dialysis membrane. 20 milligrams of formulation was administered to the dialysis bag, along with 5ml of distilled water. The dialysis bag was then tied and immersed in 450 mL of release medium at 37°C, stirred with a magnetic stirrer at 50 rpm (Gao et al., 2012, Vasir et al., 2007, Murthy et al., 1993, Dash et al., 2012)

4.3.8 In vivo anti-diabetic study:

The anti-diabetic study was conducted on Wistar rats (male and female) which were purchased from M/s Chakraborty Enterprise, Kolkata, India. The rats weighed approximately between 125 and 150 g. Standard animal care guidelines according to Committee for Control and Supervision of Experiments on Animals (CCSEA) were followed for the acclimatization of rats. The animals were housed at temperature of 23±2ºC, humidity of 50-60% along with a light and dark cycle of 12 hours. Rats were fed with standard pellet diet and water ad libitum. The experimental studies carried out in the present study are in accordance with CCSEA guidelines and were permitted by the institutional animal ethical committee of Dr B C Roy College of Pharmacy and AHS (Approval No: BCRCP/IAEC/12/2018).

In the current investigation, diabetes was induced in experimental rats by a single intraperitoneal injection of streptozotocin (STZ). STZ was dissolved in 0.1M citrate buffer (pH 4.5) and was administered at a dose of 60 mg/kg, b.w. Following STZ administration in the rats, 5% dextrose solution was given by oral gavage, to prevent the onset of hypoglycemic shock. A fasting plasma glucose level of 250 mg/dL was chosen as a cut-off for diabetes induction, and rats with blood glucose levels above 250 mg/dL after 72 hours of STZ injection were incorporated in the study (Ying et al., 2022, Mukhopadhyay et al., 2016). Rats were randomly allocated in six groups, with 6 rats in each group (n=6). The six groups were as follows: Group 1; Normal control rats; Group II; Diabetic control rats; Group III; Standard control group; diabetic rats treated with Glipizide (5 mg/kg b.w); Group IV; Blank control group; diabetic rats treated with blank nanoparticles; Group V; Naringin only group; diabetic rats treated with free Naringin (50 mg/kg b.w); Group VI; PCLNP group; diabetic rats treated with naringin loaded

nanoparticles (50 mg/kg b.w). The treatment duration for all the groups was of 28 days and the treatments administered in respective groups were by oral route after overnight fasting. Blood was collected from the tail vein in fasting state and blood glucose levels were estimated using a glucometer. Blood glucose levels were measured on day 0, day 7, day 14 and day 28. The data was analyzed using Prism 5.0. The results are expressed as mean ± SEM. Analysis of results was performed by one-way ANOVA followed by Dunnet test. Values of $p < 0.05$ were considered to be statistically significant.

4.4. Polycaprolactone Based Nanocarriers of Mangiferin

Table 7: List of materials required for Mangiferin Loaded Polycaprolactone Nanoparticles

Name	*Rationality*	*Source*
Mangiferin	Experimental Phytochemical	Sigma-Aldrich Chemicals Private Limited
Polycaprolactone (MW 14, 000 g/mol)	Polymer	Sigma-Aldrich Chemicals Private Limited
Sodium hydroxide	Maintain pH	Sigma-Aldrich Chemicals Private Limited
Tween-80	Surfactant	Sigma-Aldrich Chemicals Private Limited
HCl	Stabilizing agent	LabChem, India.

4.4.1 Physicochemical & pharmacological profile of mangiferin

Mangiferin is a naturally occurring C-glucosyl xanthone, structurally defined as 1,3,6,7-tetrahydroxyxanthone-C2-β-D-glucoside. It has a C-linked β-D-glucose unit and a xanthone nucleus that has been replaced with hydroxyl groups, which add to its remarkable pharmacokinetic and antioxidant qualities. In terms of pharmacology, mangiferin demonstrates a wide spectrum of bioactivities, such as neuroprotective, anti-inflammatory, antidiabetic, anticancer, and antioxidant properties. Its polyphenolic structure gives it the ability to effectively scavenge reactive oxygen species, which contributes to its antioxidant potential (Leiro et al., 2004). By affecting the AMPK and GLUT4 signaling pathways, it improves insulin sensitivity and regulates glucose uptake in metabolic diseases including diabetes (Saha and Das, 2019). According to Sánchez et al. (2006), it has anti-inflammatory and neuroprotective properties because it inhibits NF-κB activation and lowers pro-inflammatory cytokines. Furthermore, by activating apoptosis and preventing tumor growth through the modification of pathways such PI3K/Akt and MAPK, mangiferin exhibits anticancer potential (Imran et al., 2017).

Table 8: Physicochemical Properties of Mangiferin

Property	*Value*	*Reference*
Molecular Weight	422.34 g/mol	Sánchez et al., 2006
Melting Point	272–274°C (decomposes)	Imran et al., 2017
Solubility in Water	Moderate (~50–100 mg/L at 25°C)	Leiro et al., 2004
Solubility in Organic Solvents	Soluble in ethanol, DMSO, methanol	Leiro et al., 2004
Log P (octanol/water)	~−0.26	Saha and Das, 2019
pKa Values	~5.7, 8.5 (phenolic OH groups)	Afzal et al., 2019
Appearance	Yellow crystalline powder	Sánchez et al., 2006

4.4.2 Preformulation studies

Determination of λmax by U.V. Spectrophotometer: A 100 mL volumetric flask was filled with precisely weighed 100 mg of the mangiferin. Ten milliliters of ethanol were added to this in order to fully dissolve the mangiferin. Demineralized (DM) water was then added to bring the volume up to 100 mL, yielding a stock solution containing 1000 µg/mL. To create a working solution of 100µg/mL, suitable dilutions were made from this stock using DM water. The sample solution was scanned with a double-beam UV-Visible spectrophotometer in the 200–800 nm wavelength range (Beckett et al., 2005)

Preparation of Calibration Curve of Mangiferin: The calibration curve was plotted by measuring absorbance across various concentration ranges of mangiferin solutions between 2-20µg/ml using UV-Visible Spectrophotometer at the absorbance maxima.

Solubility Studies: An excess mangiferin was introduced to different solvents and agitated constantly at room temperature until equilibrium was reached in order to assess saturation solubility. After filtering, the filtrates were suitably diluted and analyzed using UV-Visible spectrophotometer to measure concentration in each solution.

Melting Point Determination: The open capillary method was used to find mangiferin's melting point. A capillary tube holding a modest amount of the phytochemical was put in a Theil's tube with liquid glycerol. The melting point was determined by gently heating the tube until the medication started to melt (Cooper et al., 1986)

4.4.3 Preparation of PCL nanoparticles

Polycaprolactone based nanoparticles were prepared using the nanoprecipitation method. To make an organic solution, 50 mg of polycaprolactone was dissolved in acetone, and then 50 mg of drug solution was added. The pH was maintained at 7.4, and it was further stabilized by acidifying with 0.1M HCl. To make an aqueous solution, Tween-80 was added to 100 mL of water and agitated for 5 minutes. The organic solution was then added dropwise to the aqueous solution, and the combination was agitated for an hour at 300 rpm at first, then 900 rpm to evaporate the solvent. Following that, the mixture was centrifuged for 20 minutes at 4°C/13,000 rpm. The pellet was freeze-dried after being washed twice with deionized water to produce mangiferin-loaded PCL nanoparticles (Fessi et al., 1989, Miladi et al., 2016)

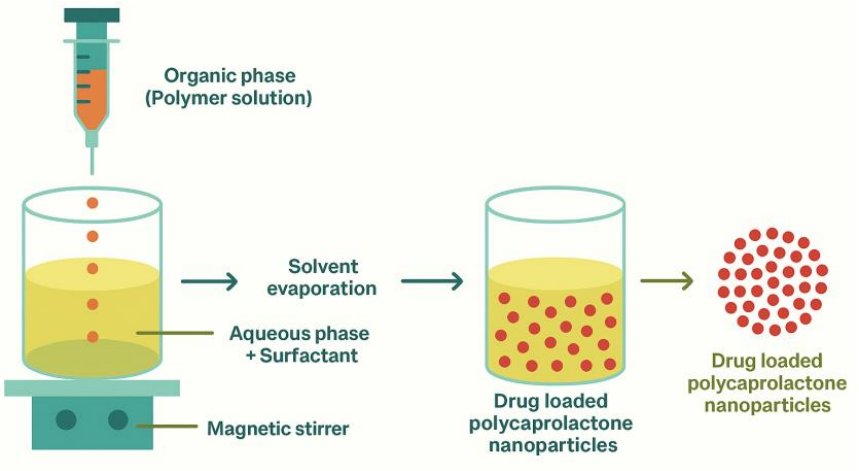

Figure 18: Schematic representation of preparation of polycaprolactone based nanocarriers (Ramanujam et al., 2018)

4.4.4 Characterizations of Nanocarriers

4.4.4.1 FTIR spectrum analysis: The FTIR studies were carried out for mangiferin and nanocarriers with and without mangiferin under identical conditions to detect any possible interactions between the components that may lead to precipitation of the drug. It was carried out by mixing the sample with potassium bromide (KBr) to form a pellet and scanning the sample over a wavelength from 4000 to 400 cm^{-1}.

4.4.4.2 X-ray crystallography analysis: The X-ray crystallography of mangiferin and nanocarriers with and without mangiferin was performed by Cu Kα radiation, at a voltage of 40 kV and 30 mA. The angle of scanning was adjusted from 5° to 70°, and the scanned rate was 4°/min.

4.4.4.3 Drug Encapsulation Efficiency and Drug Loading: The encapsulated mangiferin was separated from the nanoparticle by centrifugation at 10,000 rpm for 30 minutes. The amount of mangiferin encapsulated and loaded into PCL nanoparticles was determined using an ultraviolet spectrophotometer, UV-1800 Shimadzu, Japan (Bagheri et al., 2022, Shafiq et al., 2017) . The following formulas were utilized to determine the drug loading and encapsulation efficiency:

Encapsulation efficiency (%) = Amount of encapsulated drug/Initial amount of drug used/ 100

Drug loading (%) =[Added drug −Free (Unentrapped drug)]/Polymer amount x 100

4.4.4.4 Particles Morphology and Surface Characteristics: Scanning Electron Microscopy (SEM) was used for the synthesized PCL nanoparticles to analyze their surface morphology, shape, and appearance at a voltage of 10 kV.

4.4.4.5 Drug polymer interaction study (Thermal analysis): Thermogravimetric analysis (TGA) and differential scanning calorimetry (DSC) are methods used to investigate a substance's thermal characteristics. As a function of temperature, it calculates the heat flow related to chemical and physical changes. An empty reference pan and a tiny quantity of sample are put in a sample pan. The difference in heat flow between the reference and sample pans is determined when both pans are heated or cooled under controlled conditions. To show significant thermal events including melting, crystallization, glass transitions, and reactions, this data is plotted against temperature (Skoog etal., 2017). Thermal analysis, DSC, and TGA tests were performed to establish the physical state and interaction of naringin with polymer. Analytical samples utilized in the investigation included pure mangiferin and PCL nanoparticles with and without mangiferin. The test instrument was a Differential Scanning Calorimeter Q200 (TA Instruments, USA). All measurements were carried out at a nitrogen purge rate of 50 mL/min within 20–500°C, at 10°C per minute.

4.4.4.6 Particle size analysis & zeta potential:

Dynamic light scattering (Zetasizer -Nano ZS, Malvern Instruments Limited, UK) was used at 250C to assess the size and zeta potential of produced nanoparticles, which impacts their stability and uptake into cells. Distilled water was used as the dispersant.

4.4.5 In-vitro drug release study:

Mangiferin was released from produced nanoparticles via a dialysis membrane. 20 milligrams of formulation was administered to the dialysis bag, along with 5ml of distilled water. The dialysis bag was then tied and immersed in 450 mL of release medium at 37°C, stirred with a magnetic stirrer at 50 rpm (Gao et al., 2012, Vasir et al., 2007, Murthy et al., 1993, Dash et al., 2012).

4.4.6 In vivo Antidiabetic and hypolipidemia study:

The antidiabetic and hypolipidemia study was conducted on Wistar rats (male and female) which were purchased from M/s Chakraborty Enterprise, Kolkata, India. The rats weighed approximately between 125 and 150 g. Standard animal care guidelines according to Committee for Control and Supervision of Experiments on Animals (CCSEA) were followed for the acclimatization of rats. The animals were housed at temperature of 23±2ºC, humidity of 50-60% along with a light and dark cycle of 12 hours. Rats were fed with standard pellet diet and water ad libitum. The experimental studies carried out in the present study are in accordance with CCSEA guidelines and were permitted by the institutional animal ethical committee of Dr B C Roy College of Pharmacy and AHS (Approval No: BCRCP/IAEC/12/2018).

In the current investigation, diabetes was induced in experimental rats by a single intraperitoneal injection of streptozotocin (STZ). STZ was dissolved in 0.1M citrate buffer (pH 4.5) and was administered at a dose of 60 mg/kg, b.w. Following STZ administration in the rats, 5% dextrose solution was given by oral gavage, to prevent the onset of hypoglycemic shock. A fasting plasma glucose level of 250 mg/dL was chosen as a cut-off for diabetes induction, and rats with blood glucose levels above 250 mg/dL after 72 hours of STZ injection were incorporated in the study (Ying et al., 2022, Mukhopadhyay et al., 2016).

Rats were randomly allocated in six groups, with 6 rats in each group (n=6). The six groups were as follows: Group 1; Normal control rats; Group II; Diabetic control rats; Group III; Standard control group; diabetic rats treated with Glipizide (5 mg/kg b.w); Group IV; Blank control group; diabetic rats treated with blank nanoparticles; Group V; Naringin only group; diabetic rats treated with free Naringin (50 mg/kg b.w); Group VI; PCLNP group; diabetic rats treated with naringin loaded nanoparticles (50 mg/kg b.w). The treatment duration for all the groups was of 28 days and the treatments administered in respective groups were by oral route after overnight fasting. Blood was collected from the tail vein in fasting state and blood glucose levels were estimated using a glucometer. Blood glucose levels were measured on day 0, day 7, day 14 and day 28.

Serum was separated from collected blood after 28 days and used for estimating the serum lipid profile such as total cholesterol (TC), triglyceride (TG), high-density lipoprotein (HDL) and cholesterol which are also the lipid markers for atherosclerosis.

The data was analyzed using Prism 5.0. The results are expressed as mean±SEM. Analysis of results was performed by one-way ANOVA followed by Dunnets test. Values of $p < 0.05$ were considered to be statistically significant.

SECTION C: Metal Based Nanocarriers

4.5. Formulation and Characterization of Ellagic Acid Loaded Silver Nanoparticles

Table 9 Materials required for Silver nanoparticles of ellagic acid

Chemicals name	*Rationality*	*Source*
Ellagic Acid	Experimental Phytochemical	Sigma Aldrich
Silver Nitrate	Polymer	Sigma Aldrich
Ascorbic Acid	Reducing Agent	Sigma Aldrich
Ethanol	Solvent	Sigma Aldrich
Didoceyl Dimethyl Ammonium Bromide	Stabilizing Agent	Sigma Aldrich
Diyalysis Membrane -110	In-Vitro Drug Release	HIMEDIA
DMSO	Drug Solubility	Sigma Aldrich

4.5.1 Phytochemical & Pharmacological Profile of Ellagic Acid:

A naturally occurring polyphenolic molecule with a dilactone structure, ellagic acid is frequently found in fruits and vegetables such almonds, pomegranates, and berries. In terms of chemistry, it is made up of two lactone rings and four hydroxyl groups grouped on a biphenyl structure that is produced by the oxidative coupling of two gallic acid units. The molecule, which has the chemical formula $C_{14}H_6O_8$, is known for its anti-inflammatory, anti-cancer, and antioxidant qualities. Its capacity to bind metal ions and scavenge free radicals is facilitated by its planar aromatic structure (Clifford et al., 2000; Landete et al., 2011)

Ellagic acid mainly functions as a polyphenolic substance, influencing many processes. Scavenging free radicals and boosting natural antioxidant defenses are the sources of its antioxidative qualities. Ellagic acid also affects angiogenesis, apoptosis, and cell cycle progression by modifying cellular signaling pathways and reducing inflammation. It also exhibits promise in DNA repair and epigenetic regulation, underscoring its complex function in maintaining cellular homeostasis and preventing illness (Seeram et al., 2004; García-Niño et al., 2014).

Table 10: Physicochemical characteristics of Ellagic Acid

Parameter	*Description*	*Reference*
Chemical Name	2,3,7,8-Tetrahydroxy[1]benzopyrano[5,4,3-cde][1]benzopyran-5,10-dione	Teel et al., 1988
Molecular Weight	302.19 g/mol	Teel et al., 1988
Appearance	Pale yellow to light brown crystalline powder	Landete et al., 2011
Solubility	Poorly soluble in water; soluble in DMSO, ethanol, and methanol	Landete et al., 2011
Melting Point	~350 °C	Clifford et al., 2000
pKa Values	~6.45 and 7.45 (phenolic hydroxyl groups)	García-Niño et al., 2014
Log P (octanol/water)	~1.04 (low lipophilicity)	Seeram et al., 2004
Bioavailability	Low oral bioavailability due to poor water solubility and metabolism	Seeram et al., 2004

4.5.2 Preformulation studies

Determination of λmax by U.V. Spectrophotometer: Using a UV-Visible spectrophotometer, the absorbance maxima of ellagic acid were determined. After being precisely weighed, 50 mg of ellagic acid was added to a 100 mL beaker. Five milliliters of ethanol were added to the mixture, and it was agitated until the chemical was completely dissolved. Appropriate dilution was made and the resultant solution was scanned in the UV spectrophotometer (Shimadzu 1800, Japan) in the 200–400 nm wavelength range. Ellagic acid's highest absorbance was recorded at about 360 nm, which is in line with its distinctive UV absorption because of the conjugated aromatic structure.

Preparation of Calibration Curve of Ellagic Acid: Using a UV Spectrophotometer (Shimadzu 1800, Japan), various dilution from 2 to 20 µg/ml were scanned at λmax (360 nm), and varying absorbance was noted.

Solubility Studies: Saturated solubility evaluations were carried out by shaking an excess amount of pure drug, in various solvents at room temperature. Then samples were filtered, suitably diluted, and analyzed for the drug using UV-Visible spectrophotometer at 360nm.

Melting Point Determination: The melting point of Ellagic acid was determined using the open capillary method. The drug was filled into a capillary and placed in a Theil's tube filled with liquid glycerol. The tube was heated and the temperature at which the drug melted was noted.

FTIR-Spectroscopy Study: Fourier Transform Infrared spectroscopy is a valuable technique for characterizing nanoparticles. It identifies functional groups and molecular interactions by measuring the absorption of infrared light at various wavelengths. This information is crucial for understanding the chemical composition and surface modifications of nanoparticles. The prepared silver nanoparticles were checked for any interaction with ellagic acid and the results were also compared with blank nanoparticles of silver without drug loading.

4.5.3 Method of Preparation of Silver Nanoparticles:

Silver nanoparticles (AGN) were synthesized using ellagic acid with ascorbic acid serving as an reducing agent. First, a 0.5 M ascorbic acid solution was prepared in deionized water. Different molar quantities of silver nitrate (0.1 M, 0.25 M, 0.5 M, 1 M, and 2 M) were made separately in deionized water. Using dimethyl sulfoxide (DMSO) as a solvent, a 25 mg solution of ellagic acid was made and gradually added to the silver nitrate solution while being continuously stirred. After agitating the mixture for half an hour at room temperature, the ascorbic acid solution was gradually added while stirring. This reaction was maintained under ambient conditions for another 30 minutes. The pH of the solution was adjusted to 7.4 using 0.1 M sodium hydroxide. The development of silver nanoparticles was demonstrated by a noticeable shift in color to dark brown. Didodecyl dimethyl ammonium bromide (DDAB) solution in deionized water (0.1 M and 0.2 M) was added to the reaction mixture in order to stabilize the nanoparticles. To ensure full precipitation, the solution was further agitated for three to four hours. In order to improve the yield of nanoparticles, it was then refrigerated for the entire overnight. To obtain the nanoparticles, the resultant dispersion was centrifuged at 11,000 rpm and 0–4 °C. To get rid of the stabilizers and unreacted chemical compounds, the precipitate was extensively cleaned with deionized water. Following cleaning, the nanoparticles were dried at 40°C in a hot air oven and kept for further evaluation (Sharma et al., 2009).

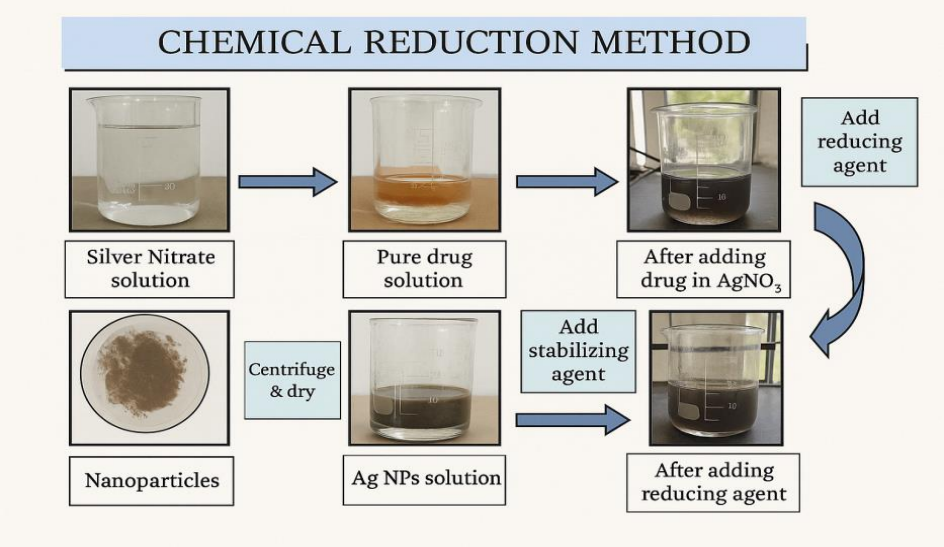

Figure 19: Preparation of silver nanoparticles using chemical reduction method

4.5.4 Characterization of silver nanoparticles

4.5.4.1 Drug Excipient Interaction Study: (Thermal analysis): Differential thermal analysis and Thermogravimetric analysis was used to compare the thermal profiles of drug-loaded silver nanoparticle (AGN) formulations, blank silver nanoparticles, and pure ellagic acid in order to study drug–excipient interaction. A Shimadzu-DSC50 Differential Scanning Calorimeter was used for the analysis. The scan's temperature range was set between 100°C and 1000°C, with heating rate of 10°C per minute. Standard aluminum pans were used for entire examination, carried out in a nitrogen atmosphere to prevent oxidative degradation (Skoog et al., 2007).

4.5.4.2 Particle Size Analysis: Nanoparticles' pharmacokinetics, biodistribution, toxicity, and stability are all greatly influenced by their size and zeta potential. Aggregation of nanoparticles, elevated cytotoxicity, and decreased targeting efficacy might result from improper zeta potential. The formulation of nanoparticles with a restricted size distribution and consistent shape is crucial for achieving the best in vivo performance. Using Zetasizer Nano ZS (Malvern Instruments, UK) at 25 °C, the study's mean particle size and size distribution were ascertained. The polydispersity index (PDI), which measures the homogeneity of the nanoparticles, was used to express the particle size distribution. The zeta potential of the nanoparticles was measured in order to determine the surface charge (Danaei et al., 2018).

4.5.4.3 Determination of Drug Entrapment Efficiency: The amount of free (unentrapped) drug in the supernatant following centrifugation was used to calculate the drug entrapment efficiency (EE) of the nanoparticles. The suspension was centrifuged after the formulation was prepared, and the clear supernatant was gathered. For spectrophotometric analysis, a 2 mL aliquot of the supernatant was diluted with 2 mL of ethanol to guarantee adequate solubilization and clarity. A UV-Visible spectrophotometer was then used to measure the diluted sample's absorbance at the drug's predefined absorption maxima. This method allows for the estimation of the actual amount of drug entrapped within the nanoparticles (Sharma et al., 2015). A standard calibration curve was used to determine the amount of drug present in the supernatant, and the following formula was used to determine the entrapment efficiency: (%)=$Actual\ drug\ content\ in\ Nanoparticles/Total\ drug\ used\ in\ Formulation\times 100$

4.5.4.4 Surface Morphology Studies: A potent analytical method for examining the size, shape, and structural properties of silver nanoparticles is scanning electron microscopy (SEM). SEM produces comprehensive topographical and compositional information by moving a concentrated electron beam across the sample surface to produce high-resolution pictures. Because it allows for accurate nanoparticle characterization, SEM is a crucial tool in nanotechnology (Goldstein et al., 2017). This is made possible by in-depth visualization at the nanoscale.

4.5.5 In-Vitro Drug Release Studies and Drug release kinetics for AGN nanoparticles: The in-vitro drug release profile of AGN nanoparticles was evaluated using a dialysis membrane diffusion technique in phosphate buffer saline (PBS, pH 7.4) as the dissolution medium. Following being recovered by centrifugation, the nanoparticles carrying the entrapped medication were resuspended and put in a dialysis bag (Himedia; molecular weight cut-off 12,000–14,000 Da) that had been pre-activated according to usual procedure. After carefully loading the nanoparticle suspension into one end of the dialysis bag and sealing the other end to stop leaks, the bag was sealed. Using a magnetic stirrer, the dialysis bag was constantly stirred at 100 rpm while submerged in 450 mL of

PBS that was kept at 37 ± 2 °C. To maintain sink conditions, aliquots (5 mL) of the medium were taken out at predetermined intervals and replaced with an equivalent volume of fresh buffer. A UV-Visible spectrophotometer was used to perform spectrophotometric analysis on the samples.

The cumulative drug release data were fitted to a number of mathematical models, such as zero-order, first-order, Higuchi, and Korsmeyer-Peppas models, in order to assess the drug release kinetics. The mechanisms of drug release from the nanoparticles, such as diffusion-controlled, erosion-controlled, or a mix of both processes, were identified with the aid of these models (Dash et al., 2010).

4.5.6 Anti-oxidant activity of ellagic acid loaded silver nanoparticles: The 2,2-diphenyl-1-picrylhydrazyl (DPPH) free radical scavenging assay, a popular and well-established technique for evaluating the free radical scavenging activity, was used to assess the antioxidant potential of ellagic-loaded silver nanoparticles (AGN1–AGN6) (Blois et al., 1958). Before being used, a 0.1 mM DPPH solution was made in methanol and kept at room temperature in the dark. Different concentrations of ellagic acid-loaded formulations and free ellagic acid (5, 10, 20, and 40 µg/mL) were prepared in methanol for the study.

1 mL of the test sample (free ellagic acid/nanoparticle formulation) was added to each 2 mL aliquot of DPPH solution. The mixture was then vortexed and allowed to sit at room temperature for 30 minutes in the dark. Methanol was used to create a control sample. A UV-Visible spectrophotometer was used to detect the solution's absorbance at 517 nm following incubation. Every measurement was carried out in triplicate, and the mean ± standard deviation was used to express the findings (Brand-Williams et al., 1995; Kumari et al., 2021). The following formula was used to determine the DPPH radical's % inhibition: $Inhibition\ (\%) = (A_0\text{-}A_1/A_0) \times 100$

Where A_0 is the absorbance of the control (DPPH + methanol) and A_1 is the absorbance of the sample (DPPH + test compound).

4.6. Formulation and Characterization of Mangiferin Loaded Silver Nanoparticles

Table 11 Materials required for mangiferin loaded silver nanoparticles

Chemicals name	*Rationality*	*Source*
Mangiferin	Experimental Phytochemical	Sigma Aldrich
Silver Nitrate	Polymer	Sigma Aldrich
Ascorbic Acid	Reducing Agent	Sigma Aldrich
Ethanol	Solvent	Sigma Aldrich
Didoceyl Dimethyl Ammonium Bromide	Stabilizing Agent	Sigma Aldrich
Dialysis Membrane -110	In-Vitro Drug Release	HIMEDIA
DMSO	Drug Solubility	Sigma Aldrich

4.6.1 Method of Preparation of Silver Nanoparticles:

Silver nanoparticles (MSN) were synthesized using mangiferin with ascorbic acid serving as reducing agent. First, a 0.5 M ascorbic acid solution was prepared in deionized water. Different molar quantities of silver nitrate (0.1 M, 0.25 M, 0.5 M, 1 M, and 2 M) were made separately in deionized water. Using dimethyl sulfoxide (DMSO) as a solvent, a 25 mg solution of mangiferin was made and gradually added to the silver nitrate solution while being continuously stirred. After agitating the mixture for half an hour at room temperature, the ascorbic acid solution was gradually added while stirring. This reaction was maintained under ambient conditions for another 30 minutes. The pH of the solution was adjusted to 7.4 using 0.1 M sodium hydroxide. The development of silver nanoparticles was demonstrated by a noticeable shift in color to dark brown. Didodecyl dimethyl ammonium bromide (DDAB) solution in deionized water (0.1 M and 0.2 M) was added to the reaction mixture in order to stabilize the nanoparticles. To ensure full precipitation, the solution was further agitated for three to four hours. In order to improve the yield of nanoparticles, it was then refrigerated for the entire overnight. To obtain the nanoparticles, the resultant dispersion was centrifuged at 11,000 rpm and 0–4 °C. To get rid of the stabilizers and unreacted chemical compounds, the precipitate was extensively cleaned with deionized water. Following cleaning, the nanoparticles were dried at 40°C in a hot air oven and kept for further evaluation (Sharma et al., 2009).

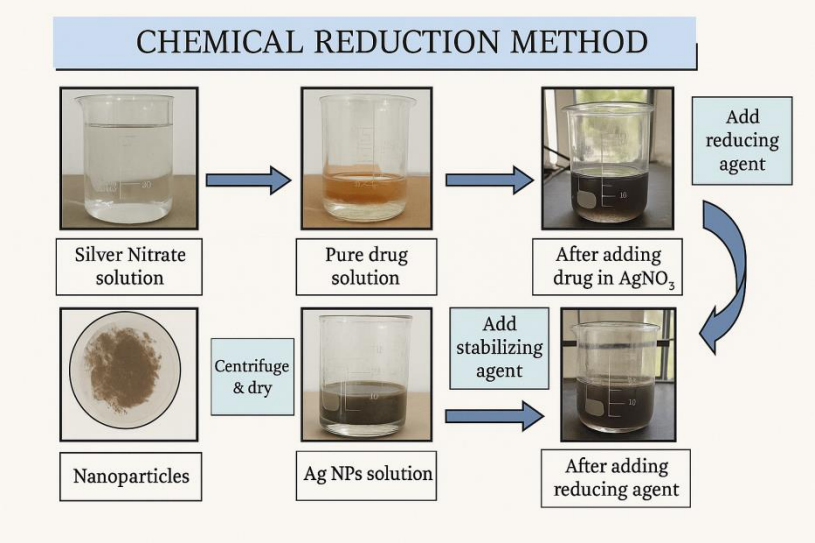

Figure 20: Preparation of silver nanoparticles for mangiferin

4.6.2 Characterization of silver nanoparticles

4.6.2.1 Drug Excipient Interaction Study: Thermal analysis

Differential Scanning Calorimetry (DTA) and thermogravimetric analysis (TGA) was used to compare the thermal profiles of drug-loaded silver nanoparticle (MSN) formulations, blank silver nanoparticles, and pure mangiferin in order to study drug–excipient interaction. A Shimadzu-DSC50 Differential Scanning Calorimeter was used for the analysis. Additionally, the device was utilized to create computer-based displays of the DSC thermograms. The scan's temperature range was set between 100°C and 1000°C, with a heating rate of 10°C per minute. Standard aluminum pans were used for the entire examination, which was carried out in a nitrogen atmosphere to prevent oxidative degradation (Skoog et al., 2007).

4.6.2.2 Particle Size Analysis: Nanoparticles' pharmacokinetics, biodistribution, toxicity, and stability are all greatly influenced by their size and zeta potential. Aggregation of nanoparticles, elevated cytotoxicity, and decreased targeting efficacy might result from improper zeta potential. The formulation of nanoparticles with a restricted size distribution and consistent shape is crucial for achieving the best in vivo performance. Using Zetasizer Nano ZS (Malvern Instruments, UK) and photon correlation spectroscopy (PCS) at 25 °C, the study's mean particle size and size

distribution were ascertained. The polydispersity index (PDI), which measures the homogeneity of the nanoparticles, was used to express the particle size distribution. The zeta potential of the nanoparticles was measured in order to determine the surface charge (Danaei et al., 2018).

4.6.2.3 Determination of Drug Entrapment Efficiency: The amount of free (unentrapped) drug in the supernatant following centrifugation was used to calculate the drug entrapment efficiency (EE) of the nanoparticles. The suspension was centrifuged after the formulation was prepared, and the clear supernatant was gathered. For spectrophotometric analysis, a 2 mL aliquot of the supernatant was diluted with 2 mL of ethanol to guarantee adequate solubilization and clarity. A UV-Visible spectrophotometer was then used to measure the diluted sample's absorbance at the drug's predefined absorption maxima. This method allows for the estimation of the actual amount of drug entrapped within the nanoparticles (Sharma et al., 2015). A standard calibration curve was used to determine the amount of drug present in the supernatant, and the following formula was used to determine the entrapment efficiency: $(\%) = Actual\ drug\ content\ in\ Nanoparticles / Total\ drug\ used\ in\ Formulation \times 100$

4.6.2.4 Surface Morphology Studies: A potent analytical method for examining the size, shape, and structural properties of silver nanoparticles is scanning electron microscopy (SEM). SEM produces comprehensive topographical and compositional information by moving a concentrated electron beam across the sample surface to produce high-resolution pictures. Because it allows for accurate nanoparticle characterization, SEM is a crucial tool in nanotechnology. Understanding the physicochemical characteristics and behavior of nanoparticles is essential for their development and use in industries such as materials science, electronics, and medicine (Goldstein et al., 2017).

4.6.3 In-Vitro Drug Release Studies and Drug release kinetics:

The in-vitro drug release profile of mangiferin from the nanoparticles was evaluated using a dialysis membrane diffusion technique in phosphate buffer saline (PBS, pH 7.4) as the dissolution medium. Following being recovered by centrifugation, the nanoparticles carrying the entrapped medication were resuspended and put in a dialysis bag (Himedia; molecular weight cut-off 12,000–14,000 Da) that had been pre-activated according to usual procedure. After carefully loading the nanoparticle suspension into one end of the dialysis bag and sealing the other end to stop leaks, the bag was sealed. Using a magnetic stirrer, the dialysis bag was constantly stirred at 100 rpm while submerged in 450 mL of PBS that was kept at 37 ± 2 °C. To maintain sink conditions, aliquots (5 mL) of the medium were taken out at predetermined intervals and replaced with an equivalent volume of fresh buffer. A UV-Visible spectrophotometer was used to perform spectrophotometric analysis on the samples.

The cumulative drug release data were fitted to a number of mathematical models, such as zero-order, first-order, Higuchi, and Korsmeyer-Peppas models, in order to assess the drug release kinetics. The mechanisms of drug release from the nanoparticles, such as diffusion-controlled, erosion-controlled, or a mix of both processes, were identified with the aid of these models (Dash et al., 2010).

4.6.4 Evaluation of antibacterial efficacy of mangiferin loaded silver nanoparticles

Using the agar well diffusion method, the antibacterial activity of the silver nanoparticle loaded with mangiferin was assessed against strains of *Escherichia coli* (Gram-negative) and *Staphylococcus aureus* (Gram-positive). For comparison, four distinct test samples were used: (1) pure mangiferin (25 µg/ml), (2) standard ciprofloxacin (10 µg/ml) and, (3) blank silver nanoparticle (no drug), and (4) mangiferin-loaded silver nanoparticle formulation. 100 µL of the samples were added to each well, and the plates were then incubated for 24 hours at 37 °C. Zones of inhibition were measured in millimeters. Efficiency of inhibition was assessed by comparing with the reference standard using dose calculations (Rajendran et al., 2016).

4.7 Formulation and Characterization of Ellagic Acid Loaded Copper Nanoparticles

Table 12 Materials required for Copper nanoparticles of ellagic acid

Chemicals name	*Rationality*
Ellagic Acid	Experimental Phytochemical
Dimethyl sulfoxide	Solvent system for Ellagic Acid
Copper sulfate pentahydrate	Metallic compound
Ascorbic acid	Antioxidant for colloidal copper nanoparticles
De-ionized Water	Solvent
Sodium hydroxide	pH adjuster
Ethanol	Solvent system for reducing agent
Sodium borohydride	Reducing Agent
Carbopol 934	Gelling Agent

4.7.1 Method of Preparation of copper Nanoparticles: There have two steps to prepare the Gel based Nanoparticles.

- Preparation of copper Nanoparticles:
- Preparation of gel from the prepared nanoparticles.

Preparation of Copper nanoparticles (CuNPs):

Chemical reduction was used to yield copper nanoparticles loaded with ellagic acid. After making a 0.02 M solution of ascorbic acid in deionized water, a 0.01 M solution of copper sulfate pentahydrate was prepared. After mixing the two solutions with magnetic stirring, a sodium hydroxide solution was used to lower the pH to 7.0. The mixture was stirred continuously for 30 minutes at room temperature prior to ellagic acid, which had been dissolved in dimethyl sulfoxide (DMSO), was added. A 1M sodium borohydride solution in ethanol was then added dropwise while being continuously stirred. In ambient conditions, the reaction mixture was agitated for two to three hours. The development of copper nanoparticles was indicated by a shift in color from blue to blackish-green. For better precipitation, the suspension was refrigerated for the whole night. Following centrifugation, the generated nanoparticles were collected, cleaned of stabilizers and unreacted components using deionized water, and then dried (Patil et al., 2021).

Preparation of Gel Containing Ellagic Acid-Loaded Copper Nanoparticles (EGCN): To formulate the gel, Carbopol 934 was dispersed in deionized water and allowed to hydrate completely under gentle stirring to form a uniform gelling base. The previously synthesized copper nanoparticles infused with ellagic acid were gradually added to the Carbopol gel base while being constantly stirred to ensure even dispersion after the gelling solution was ready. A homogenous, smooth gel was produced with copper nanoparticles loaded with ellagic acid that could be used topically and evaluated further (Kumar et al., 2020).

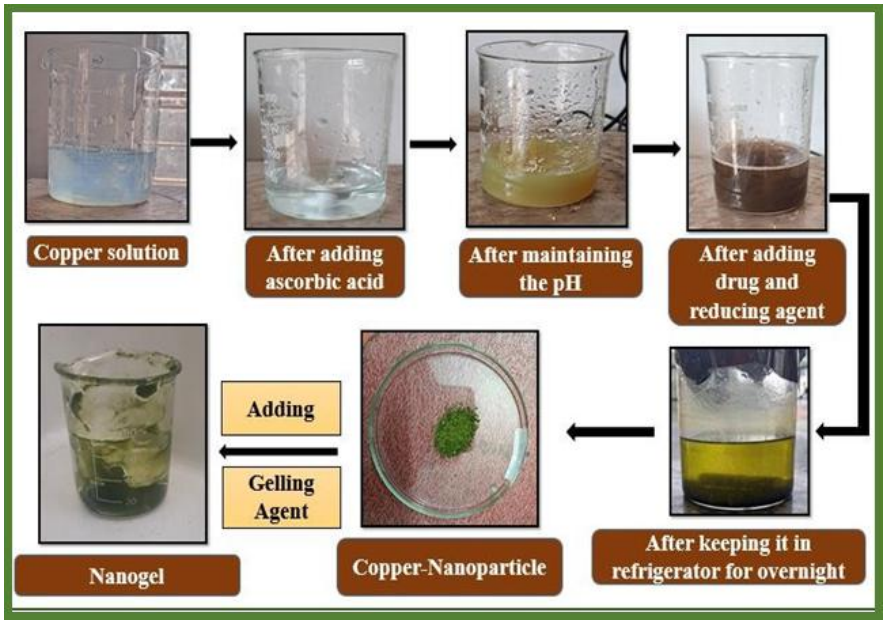

Figure 21: Preparation of Gel based Ellagic Acid loaded Copper Nanoparticle using chemical reduction method

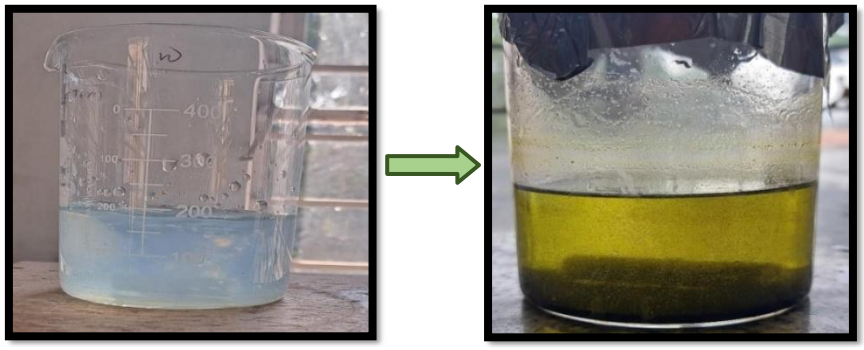

Figure 22: Colloidal solution of copper nanoparticles, initial blue colour turned blackish green

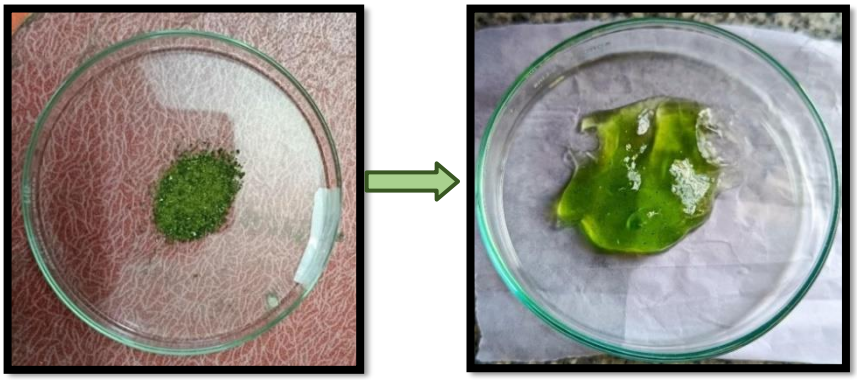

Figure 23: Preparation of Gel Containing Ellagic Acid-Loaded Copper Nanoparticles

4.7.2 Drug Excipient Interaction Study: (Thermal analysis)

Thermal analysis such as DSC, TGA was used to compare the thermal profiles of ellagic loaded nanoparticle (CuNPs) formulations, blank copper nanoparticles, and pure mangiferin in order to study drug–excipient interaction. A Shimadzu-DSC50 Differential Scanning Calorimeter was used for the analysis. Additionally, the device was utilized to create computer-based displays of the DSC thermograms. The scan's temperature range was set between 100°C and 1000°C, with a heating rate of 10°C per minute. Standard aluminum pans were used for the entire examination, which was carried out in a nitrogen atmosphere to prevent oxidative degradation (Skoog et al., 2007).

4.7.3 Particle Size Analysis:

The formulation of nanoparticles with a restricted size distribution and consistent shape is crucial for achieving the best in vivo performance. Using Zetasizer Nano ZS (Malvern Instruments, UK) and photon correlation spectroscopy (PCS) at 25 °C, the study's mean particle size and size distribution were ascertained. The polydispersity index (PDI), which measures the homogeneity of the nanoparticles, was used to express the particle size distribution. Using the Zetasizer Nano ZS via laser Doppler anemometry, the zeta potential of the copper nanoparticles was measured in order to determine the surface charge (Danaei et al., 2018).

4.7.4 Determination of Drug Entrapment Efficiency:

The amount of free (unentrapped) ellagic acid in the supernatant following centrifugation was used to calculate the drug entrapment efficiency (EE) of the nanoparticles. The suspension was centrifuged after the formulation was prepared, and the clear supernatant was gathered. For spectrophotometric analysis, a 2 mL aliquot of the supernatant was diluted with 2 mL of ethanol to guarantee adequate solubilization and clarity. A UV-Visible spectrophotometer was then used to measure the diluted sample's absorbance at the drug's predefined λ_{max}. This method allows for the estimation of the actual amount of ellagic acid entrapped within the nanoparticles (Sharma et al., 2015). The amount of drug present in the supernatant was determined and the following formula was used to determine the entrapment efficiency:

$$(\%)=Actual\ \ drug\ \ content\ \ in\ \ Nanoparticles/Total\ \ drug\ \ used\ \ in\ \ Formulation\times 100$$

4.7.5 Surface Morphology Studies: SEM produces comprehensive topographical and compositional information by moving a concentrated electron beam across the sample surface to produce high-resolution pictures. Because it allows for accurate nanoparticle characterization, SEM is a crucial tool in nanotechnology (Goldstein et al., 2017). This is made possible by in-depth visualization at the nanoscale. The shape, size, and dispersion of the copper nanoparticles loaded with ellagic acid that were integrated into the gel were investigated using Transmission Electron Microscopy (TEM). To scatter the nanoparticles, a tiny amount of the gel formulation was first diluted with deionized water. To guarantee even distribution and avoid aggregation, the diluted sample was quickly sonicated. A drop of this dispersion was applied on a copper TEM grid coated with carbon and let to dry naturally. The grid was placed into the TEM chamber for imaging once it had dried. A high-resolution transmission electron microscope running at a 200 kV accelerating voltage was used for the analysis. The shape, size distribution, and surface properties of the nanoparticles were observed by taking pictures at different magnifications. TEM provided critical insight into the nanoscale structure of the copper particles and confirmed the spherical morphology and size uniformity essential for biomedical applications (Bibi et al., 2016).

4.7.6 In-vitro Drug Release Analysis:

The in-vitro drug release profile of AGN nanoparticles was evaluated using a dialysis membrane diffusion technique in phosphate buffer saline (PBS, pH 7.4) as the dissolution medium. Following being recovered by centrifugation, the nanoparticles carrying the entrapped medication were resuspended and put in a dialysis bag (Himedia; molecular weight cut-off 12,000–14,000 Da) that had been pre-activated according to usual procedure. After carefully loading the nanoparticle suspension into one end of the dialysis bag and sealing the other end to stop leaks, the bag was sealed. Using a magnetic stirrer, the dialysis bag was constantly stirred at 150 rpm while submerged in 450 mL of PBS that was kept at 37 ± 2 °C. To maintain sink conditions, aliquots (5 mL) of the medium were taken out at predetermined intervals and replaced with an equivalent volume of fresh buffer.

The cumulative drug release data were fitted to a number of mathematical models, such as zero-order, first-order, Higuchi, and Korsmeyer-Peppas models, in order to assess the drug release kinetics. The mechanisms of drug release from the nanoparticles, such as diffusion-controlled, erosion-controlled, or a mix of both processes, were identified with the aid of these models (Dash et al., 2010).

4.7.7 Optimization & Evaluation of Gel based Nanoparticles

4.4.7.1 Viscosity study:

The viscosity of gel-based nanoparticle formulations is a key parameter that significantly influences their stability, drug release profile, and overall therapeutic performance. Due to its ability to provide controlled release of the encapsulated medication and ease of administration, this characteristic is particularly advantageous for biomedical applications. The concentration, size, and physicochemical makeup of gel matrix are some of the variables that affect the viscosity of nanoparticle gels. Therefore, in order to guarantee stability, therapeutic efficacy, and reproducibility, precise viscosity measurement is essential throughout formulation development (El-Sherbiny et al., 2015).

To assess copper nanoparticle gel loaded with ellagic acid's flow characteristics, and suitability for topical delivery, viscosity was assessed using Brookfield digital viscometer (Model DV-II+ Pro, Brookfield Engineering Labs, USA) equipped with spindle number 64 with rpm 10–100 rpm to find the shear-rate-dependent viscosity at 25 ± 1°C and at variety (Pandey et al., 2020).

4.4.7.2 Spreadability coefficient of prepared Gel based Nanoparticles

Since spreadability influences both patient compliance and therapeutic efficacy, it is an essential property of gel-based nanoparticle formulations, particularly in topical drug delivery systems. Parallel plate approach was used to assess spreadability of ellagic acid-loaded copper nanoparticle gel. In this method, a fixed amount of gel (approximately 1 g) was placed between two glass slides, and a known weight (500 g) was applied on the upper slide for 5 minutes. The diameter to which the gel spreads was recorded, and the spreadability coefficient (S) was calculated using the formula: $S = (M \times L) / T$; where M is the weight applied (g), L is the length moved by the slide (cm), and T is the time taken (s).

4.4.7.3 *In-vitro* Drug Permeation Study: To evaluate the release behavior of ellagic acid-loaded copper nanoparticle gel, in vitro drug release experiments were conducted employing a Franz diffusion cell. The study's objectives were to assess controlled release properties and simulate transdermal medication delivery. The donor and receptor compartments were separated by dialysis membrane, MWCO 12,000–14,000 Da. Phosphate buffer saline (PBS, pH 7.4) was added to the receptor chamber, kept at 37 ± 0.5°C and constantly stirred with a magnetic bead to ensure uniformity. The donor chamber was filled with suitable quantity of the gel coated with nanoparticles (1–2 g), and apparatus was sealed to prevent evaporation. At specified intervals (e.g., 0.5, 1, 2, 4, 6, 8, 12, and 24 hours), aliquots were taken from receptor chamber and replaced by fresh buffer. UV-Visible spectrophotometry was used to evaluate samples in order to calculate the total amount of drugs released. Given the gel matrix and copper nanoparticle encapsulation, the formulation demonstrated sustained drug release, indicating its potential for topical medicinal applications (Desai et al., 2020).

4.4.7.4 Evaluation of antibacterial efficacy of Ellagic acid loaded copper nanoparticles gel: Using the agar well diffusion method, the antibacterial activity of the copper nanoparticle (EGCN) gel loaded with ellagic acid was assessed against strains of *Escherichia coli* (Gram-negative) and *Staphylococcus aureus* (Gram-positive). For comparison, four distinct test samples were used: (1) pure ellagic acid (25 µg/ml), (2) standards streptomycin (10 µg/ml) and ciprofloxacin, (3) blank copper nanoparticle gel (no drug), and (4) drug-loaded copper nanoparticle gel formulation. 100 µL of the samples were added to each well, and the plates were then incubated for 24 hours at 37 °C. Zones of inhibition were measured in millimeters. Efficiency of inhibition was assessed by comparing with the reference standard using dose calculations (Rajendran et al., 2016).

4.8 REFERENCES

- Afzal M, Safer AM, Afzal O, et al. Mangiferin: A review of its pharmacological and pharmacokinetic properties. World J Pharm Pharm Sci. 2019;8(8):121–134.
- Allain CC, Poon LS, Chan CS, Richmond W, Fu PC. Enzymatic determination of total serum cholesterol. Clin Chem. 1974 Apr;20(4):470-5. PMID: 4818200.
- Bagheri M, Bayat F, Rezazadeh M, et al. Doxorubicin-loaded polycaprolactone nanoparticles: synthesis, characterization, and release study. BMC Chem. 2022;16(1):22.
- Bai Y, Chen X, Zhong Q, Guo Y, Zhang Y. Pharmacokinetics and metabolism of naringin and naringenin following oral and intravenous administration in humans. Front Pharmacol. 2020;11:481984.
- Beckett AH, Stenlake JB. Practical Pharmaceutical Chemistry. 4th ed. New Delhi: CBS Publishers & Distributors; 2005. p. 275–300.
- Bibi I, Nazar N, Iqbal M, Kamal S, Sultan M, Nouren S, et al. Green synthesis of copper oxide nanoparticles using Salvadora persica root extract and their characterization and antibacterial activity. Arab J Chem. 2016;12(8):4333–4344.
- Borenfreund E, Babich H, Martin-Alguacil N. In vitro cytotoxicity of surfactants used in cosmetics and ophthalmics on murine and human cells. Toxicol In Vitro. 1988;2(3):183-192.
- Brand-Williams W, Cuvelier ME, Berset C. Use of a free radical method to evaluate antioxidant activity. LWT-Food Sci Technol. 1995;28(1):25–30.
- Clifford MN, Scalbert A. Ellagic acid and other hydrolyzable tannins – chemistry and occurrence. J Sci Food Agric. 2000;80(7):1118–1127.
- Cooper J, Gunn C. Cooper and Gunn's Tutorial Pharmacy. 6th ed. New Delhi: CBS Publishers & Distributors; 1986. p. 276–278.
- Danaei M, Dehghankhold M, Ataei S, Hasanzadeh Davarani F, Javanmard R, Dokhani A, et al. Impact of particle size and polydispersity index on the clinical applications of lipidic nanocarrier systems. *Pharmaceutics*. 2018;10(2):57.
- Dash TK, Konkimalla VB. Poly-ε-caprolactone based formulations for drug delivery and tissue engineering: A review. J Control Release. 2012 Feb 10;158(1):15-33.
- Dave V, Paliwal S. A novel approach to formulation factor of aceclofenac eye drops

efficiency evaluation based on physicochemical characteristics of in vitro and in vivo permeation. Saudi Pharm J. 2014;22(3):240–5.

- Den Hartogh DJ, Tsiani E. Antidiabetic properties of naringenin: a citrus flavonoid. Biochim Biophys Acta Gen Subj. 2019;1863(1):130–139.
- Desai PR, Jain R, Mohanraj VJ. Topical delivery of therapeutic agents from nanocarriers: basic mechanisms and strategies for drug release. Curr Drug Deliv. 2020;17(7):615–630.
- El-Sherbiny IM, El-Baz NM, Yacoub MH. Hydrogel nanoparticles in nanomedicine: challenges and applications. Biomater Sci. 2015;3(5):962–972.
- Fessi H, Puisieux F, Devissaguet JP, Ammoury N, Benita S. Nanocapsule formation by interfacial polymer deposition following solvent displacement. Int J Pharm. 1989;55:R1–4
- Fossati P, Prencipe L. Serum triglycerides determined colorimetrically with an enzyme that produces hydrogen peroxide. Clin Chem. 1982 Oct;28(10):2077-80. PMID: 6812986.
- Gao W, Zhang L. Co-delivery of paclitaxel and DNA from cationic lipid-based nanoparticles for cancer therapy. Biomaterials. 2012 Jul;33(30):8707-15.
- García-Niño WR, Zazueta C. Ellagic acid: Pharmacological activities and molecular mechanisms involved in liver protection. Pharmacol Res. 2015;97:84–103.
- Garg A, Kumar A, Singh S. Pharmacological properties and therapeutic potential of naringin: A comprehensive review. Phytother Res. 2023;37(1):45–59.
- Gattuso G, Barreca D, Gargiulli C, Leuzzi U, Caristi C. Flavonoid composition of citrus juices. Molecules. 2007;12(8):1641–73. doi:10.3390/12081641
- Gaudana R, Ananthula HK, Parenky A, Mitra AK. Ocular drug delivery. AAPS J. 2010;12(3):348-60.
- Goldstein JI, Newbury DE, Michael JR, Ritchie NWM, Scott JHJ, Joy DC. Scanning Electron Microscopy and X-ray Microanalysis. 4th ed. New York: Springer; 2017.
- Heim KE, Tagliaferro AR, Bobilya DJ. Flavonoid antioxidants: chemistry, metabolism and structure-activity relationships. J Nutr Biochem. 2002;13(10):572-584.
- Hoang NH, Le Thanh T, Sangpueak R, Treekoon J, Saengchan C, Thepbandit W, et al. Chitosan nanoparticles-based ionic gelation method: A promising candidate for plant disease management. Polymers (Basel). 2022; 14(4):662.
- Hussain RF, Nouri AME, Oliver RTD. A new approach for measurement of cytotoxicity using colorimetric assay. J Immunol Methods. 1993; 160:89–96.

- Imran M, Arshad MS, Butt MS, Kwon JH, Arshad MU, Sultan MT. Mangiferin: a natural miracle bioactive compound against lifestyle related disorders. Lipids Health Dis. 2017;16(1):84.
- Interagency Coordinating Committee on the Validation of Alternative Methods (ICCVAM). ICCVAM Test Method Evaluation Report: In Vitro Ocular Toxicity Test Methods for Identifying Severe Irritants and Corrosives. NIH Publication No. 10-7553. Research Triangle Park, NC: National Institute of Environmental Health Sciences; 2010.
- Joshi G, Kumar A, Sawant K. Enhanced bioavailability and intestinal uptake of gemcitabine HCl loaded PLGA nanoparticles after oral delivery. *Eur J Pharm Sci*. 2014; 60:80–89.
- Kim JH, Park SH, Lee JW, Cho YJ, Kim KS. Evaluation of the accuracy and consistency of six glucometers for blood glucose measurement. Diabetes Metab J. 2015 Feb;39(1):61–5.
- Koehl NJ, Menei P, Chariau B, Benoit JP. Evaluation of corneal permeation of model drugs from water-in-oil microemulsions. Int J Pharm. 2000;206(1-2):73-82.
- Kumar L, Verma S, Singh A, Chauhan R. Formulation and evaluation of herbal gel containing green synthesized copper nanoparticles for antimicrobial activity. J Drug Deliv Ther. 2020;10(4):142–147.
- Kumar S, Dilbaghi N, Saharan R, et al. Nanotechnology as emerging tool for enhancing solubility of poorly water-soluble drugs. BioNanoSci. 2012; 2:227–250.
- Kumar S, Pandey AK. Chemistry and biological activities of flavonoids: an overview. ScientificWorldJournal. 2013;2013:162750. doi:10.1155/2013/162750
- Kumari A, Yadav SK, Yadav SC. Biodegradable polymeric nanoparticles based drug delivery systems. Colloids Surf B Biointerfaces. 2021;75(1):1–18.
- Landete JM. Ellagic acid: foods, intestinal metabolism and health effects. Food Res Int. 2011;44(5):1150–1160.
- Leiro J, Arranz JA, Yáñez M, Ubeira FM, Sanmartín ML, Orallo F. Expression profiles of genes involved in the immune response in human leukocytes treated with mangiferin. Int Immunopharmacol. 2004;4(6):763-774.
- Lenzen S. The mechanisms of alloxan- and streptozotocin-induced diabetes. Diabetologia. 2008 Feb;51(2):216–26.
- Li Y, Yao J, Han C, Yang J, Chaudhry MT, Wang S, et al. Quercetin, inflammation and immunity. Nutrients. 2016;8(3):167. doi:10.3390/nu8030167

- Luepke NP. Hen's egg chorioallantoic membrane test for irritation potential. Food Chem Toxicol. 1985;23(2):287-291.
- Mandal SC, Lakshmi SM, Kumar CK, Sur TK, Boominathan R. Evaluation of anti-inflammatory potential of Pavetta indica Linn. leaf extract (family: Rubiaceae) in rats. Phytother Res. 2003; 17(8):817–820. Boots AW, Haenen GRMM, Bast A. Health effects of quercetin: from antioxidant to nutraceutical. Eur J Pharmacol. 2008;585(2-3):325–37. doi:10.1016/j.ejphar.2008.03.008
- Mandal SC, Maity TK, Das J, Saba BP, Pal M. Anti-inflammatory evaluation of Ficus racemosa Linn. leaf extract. J Ethnopharmacol. 2000; 72:87–92.
- Maurice DM, Mishima S. Ocular pharmacokinetics. In: Sears ML, editor. Pharmacology of the Eye. Berlin: Springer; 1984. p. 19-116.
- Md S, Alhakamy NA, Aldawsari HM, Asfour HZ. Neuroprotective and antioxidant effect of naringenin-loaded nanoparticles for nose-to-brain delivery. Brain Sci. 2019; 9(11):275.
- Miladi K, Sfar S, Fessi H, Elaissari A. Nanoprecipitation process: from particle preparation to in vivo applications. Polymer Nanoparticles for Nanomedicines 2016. p. 17–53.
- Mukhopadhyay P, Maity S, Chakraborty S, Rudra R, Ghodadara H, Solanki M, Chakraborti AS, Prajapati A, Kundu P. Oral Delivery of Quercetin to Diabetic Animals Using Novel pH Responsive Carboxypropionylated Chitosan/Alginate microparticles. RSC Adv. 2016; 6:73210–73221.
- Murthy RSR, Dorle AK, Jagtap AG, Joshi NV. Poly(ε-caprolactone) microspheres for controlled release of anti-inflammatory drugs. J Microencapsul. 1993 Jan-Mar;10(1):21-9.
- Pandey A, Singh M, Shukla R, Mishra A. Formulation and evaluation of copper nanoparticle-loaded gel for topical delivery. Int J Appl Pharm. 2020;12(6):96–101.
- Parasuraman S, Raveendran R, Kesavan R. Blood sample collection in small laboratory animals. J Pharmacol Pharmacother. 2010 Jul;1(2):87–93.
- Rajendran NK, Kumar SS, Houreld NN, Abrahamse H. A review on nanoparticle based treatment for wound healing. J Drug Deliv Sci Technol. 2016;35:66–72.
- Ramanujam R, Sundaram B, Janarthanan G, Devendran E, Venkadasalam M, Milton MCJ. Biodegradable polycaprolactone nanoparticles based drug delivery systems: a short review. Biosci Biotech Res Asia. 2018;15(3):635–43.

- Ravikumar P, Selvamuthukumar S, Ranjithkumar R. Nanostructured topical drug delivery: a review on current status. J Pharm Sci Res. 2011;3(6):1227–1231.
- Reddy SS, Shaik A, Trinath J, Reddy CS. Antihyperglycemic activity of glipizide in STZ-induced diabetic rats. J Basic Clin Pharm. 2012 Sep;3(3):311-5.
- Rotimi SO, Rotimi OA, Duru CU, Ebebeinwe OO, Abiodun AO, Oyeniyi BO. Naringin enhances reverse cholesterol transport in high-fat/low-cholesterol diet-fed rats. J Food Biochem. 2018;42(5):e12573.
- Saettone MF, Salminen L. Ocular inserts for topical delivery. Adv Drug Deliv Rev. 1995;16(1):95-106.
- Saha S, Das S. Regulation of NF-κB and associated pathways in mangiferin-mediated protection against oxidative stress and inflammation. Eur J Pharmacol. 2019;844:199-210.
- Saini A, Sharma A, Kaur H, Arora S. Naringin: A citrus flavonoid with diverse therapeutic potentials. J Appl Pharm Sci. 2023;13(2):10–20.
- Sánchez GM, Re L, Giuliani A, Núñez-Sellés AJ, Davison GP, León-Fernández OS. Protective effects of mangiferin on oxidative stress induced by indomethacin in rat duodenal mucosa. Planta Med. 2006;72(5):421-426.
- Seeram NP, Adams LS, Henning SM, Niu Y, Zhang Y, Nair MG, et al. In vitro antiproliferative, apoptotic and antioxidant activities of punicalagin, ellagic acid and a total pomegranate tannin extract are enhanced in combination with other polyphenols as found in pomegranate juice. J Nutr Biochem. 2005;16(6):360–367.
- Shafiq S, Shakeel F, Talegaonkar S, et al. Polycaprolactone and chitosan nanoparticles as carriers for enoxaparin: preparation, characterization, and in vitro release. J Drug Deliv.;2017:4925495.
- Sharma R, Singh H, Gupta A. Anti-inflammatory mechanisms of naringin: Insights from recent studies. Inflammopharmacology. 2021;29(3):897–910.
- Sharma VK, Yngard RA, Lin Y. Silver nanoparticles: Green synthesis and their antimicrobial activities. Adv Colloid Interface Sci. 2009;145(1–2):83–96.
- Skoog DA, Holler FJ, Crouch SR. Principles of instrumental analysis. 7th ed. Boston: Cengage Learning; 2017.

- Spielmann H, Gerner I, Kalweit S, et al. The ECVAM prevalidation study on the HET-CAM test: assessment of ocular irritation properties of chemicals. Altern Lab Anim. 1997;25(2):191-203.
- Teel RW, Martin RM. Disposition of the plant phenol ellagic acid in the mouse following oral administration by gavage. Xenobiotica. 1988;18(4):397–405.
- Tiwari R, Pathak K. Nanostructured ophthalmic drug delivery system of levofloxacin: in vitro and in vivo evaluation. Nanomedicine. 2011;7(4):627-33.
- Vasir JK, Labhasetwar V. Biodegradable nanoparticles for sustained drug delivery in cancer therapy. Nanomedicine: Nanotechnology, Biology and Medicine. 2007;2(2):147-57.
- Worth AP, Balls M. Alternative (non-animal) methods for chemicals testing: current status and future prospects. ATLA. 2002;30 Suppl 1:1-125.
- Ying Wang, Tanushree Karmakar, Nilanjan Ghosh, Souvik Basak, Nanda Gopal Sahoo. Targeting mangiferin loaded N-succinyl chitosan-alginate grafted nanoparticles against atherosclerosis - A case study against diabetes mediated hyperlipidemia in rat. Food Chem. 2022 Feb 15:370:131376

CHAPTER 5

RESULTS & DISCUSSION

CONTENTS

Section A: Natural Polymer (Chitosan) Based Nanocarriers

5.1 Naringin Loaded Chitosan/TPP Nanoparticles (NLC)

5.1.1 Synthesis of NLC nanocarriers:

Naringin loading into chitosan is facilitated by electrostatic attraction, hydrogen bonding, and hydrophobic interactions. Chitosan, a hydrophilic organic polymer, has a positive charge due to protonation in an acidic environment. Naringin, with hydroxyl and glycoside groups, can create hydrogen bonds with chitosan's amino groups, keeping it stable inside the matrix. Hydrophobic pockets in chitosan can capture lipophilic naringin molecules and load them into the chitosan network. Stabilization of naringin within the chitosan matrix may be due to weak van der Waals forces, which facilitate non-covalent interactions over short distances. Chitosan's gel-like network in aqueous environments allows it to form complexes with drug molecules such as naringin. When chitosan is dissolved in an acidic solution, it swells and turns cationic. When naringin is added to the chitosan solution, it interacts with the chitosan through hydrogen bonding and electrostatic interactions leading to the formation of nanoparticles (Agnihotri et al., 2004, Sajjan et al., 2016, Yadav et al., 2018).

5.1.2 Preformulation studies

Naringin exhibited absorption maxima at 285 nm which was similar to the reported value. The calibration curve plotted by measuring absorbance across various concentration ranges of naringin solutions between 2-20µg/ml using UV-Visible Spectrophotometer at the absorbance maxima 285 nm exhibited good linearity (r^2) which satisfied Beer-Lambert's law in the given concentration range. The result is presented below in Table 13.

Table 13: Calibration curve data for naringin

Concentration (µg/mL)	Mean Absorbance ± SE
2	0.100 ± 0.0012
4	0.199 ± 0.0017
6	0.308 ± 0.0020
8	0.404 ± 0.0018
10	0.509 ± 0.0018
12	0.615 ± 0.0017
14	0.714 ± 0.0018
16	0.816 ± 0.0020
18	0.890 ± 0.0012
20	0.975 ± 0.0017

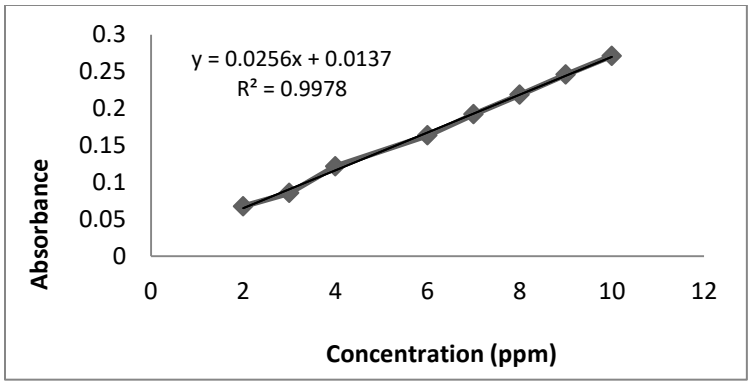

Figure 24: Calibration curve of naringin

Solubility Studies: The measured aqueous solubility of naringin was found to be 28.5 ± 1.2 µg/mL. This low solubility highlights the hydrophobic nature of naringin and indicates a potential challenge in achieving sufficient bioavailability through conventional aqueous formulations.

Melting Point Determination: The observed melting point of naringin was approximately 250–252°C, which aligns well with reported literature values. The sharp melting point range indicates the purity of the compound and confirms the crystalline nature of the isolated phytochemical.

FTIR spectral analysis: FTIR spectra of naringin revealed two prominent peaks corresponding to the wavenumber of the hydroxyl group at wave number regions 1664.02 cm^{-1} and 3330.14 cm^{-1}. The compound's structure and the outcome of the IR spectrum assessment for naringin matched, confirming the result. The IR spectra of chitosan show several absorption bands corresponding to its functional groups. A broad peak around 3431.78 cm^{-1} is observed due to the stretching vibrations of hydroxyl (O-H) groups, often associated with hydrogen bonding. The N-H stretching of primary amine groups is also present, overlapping with the O-H band. The C-H stretching vibrations of the chitosan polymer backbone appear at 2925.98 & 2881.09 cm^{-1}. The most prominent peaks are the amide I band at 1642.03 cm^{-1}, which corresponds to the stretching of carbonyl bonds from residual N-acetyl groups in partially deacetylated chitosan. The C-N stretching of amine groups shows characteristic peaks around 1381.03 & 1320.80 cm^{-1}. The FTIR spectra of the chitosan nanoparticle verified the presence of the chitosan's important peak. The tip of the peak in chitosan nanoparticles has shifted to 3427.85 cm^{-1}, indicating an increase in hydrogen bonding; in TPP. The FTIR spectrum of a chitosan nanoparticle

loaded with naringin revealed a characteristic peak change from 1664.02 cm^{-1} to 1642.09 cm^{-1}, indicating that naringin had been incorporated into the chitosan nanoparticle without any possible interaction that may lead to precipitation of the drug (Figure 25).

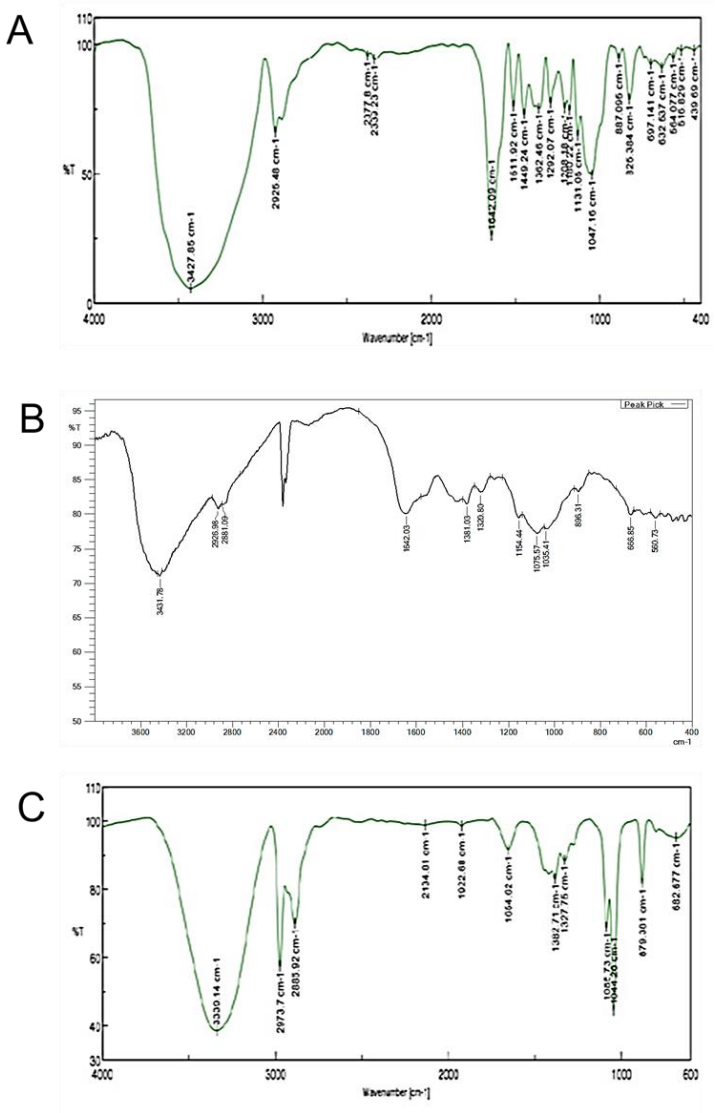

Figure 25 (A) FTIR spectra of Naringin (B) FTIR spectra of Chitosan (C) FTIR spectra of NLC formulation

XRD Study: The naringin-polymer (Chitosan) characterization has further been done with the help of X Ray Diffraction (XRD) spectra of the compound together with the polymer (Chitosan). The drug diffractogram (Figure 26 A) shows that most of the peaks are sharp and crisp indicating that the drug bears mostly crystalline nature in its form. However, the chitosan peaks (Figure 26B) revealed suppressed and interspersed peaks suggesting its

amorphous nature. Diffractogram of NLC formulation (Figure 26 C) reveal high resemblance with the polymer suggesting that the polymer has been in the outer core of the formulation while the drug has been entrapped inside the polymeric core. Moreover, the height of the peaks of the formulation at specific 2θ values are found to be quite different from that of the polymer as well as naringin suggesting that there have been change of crystallinity or arrangement of atoms in specific planes of the formulation. This could be a plausible inference that the change of crystallinity or atomic arrangement (marked by the change of intensity of peaks) might be due to the naringin-polymer interaction that has incurred to the value addition of the complex.

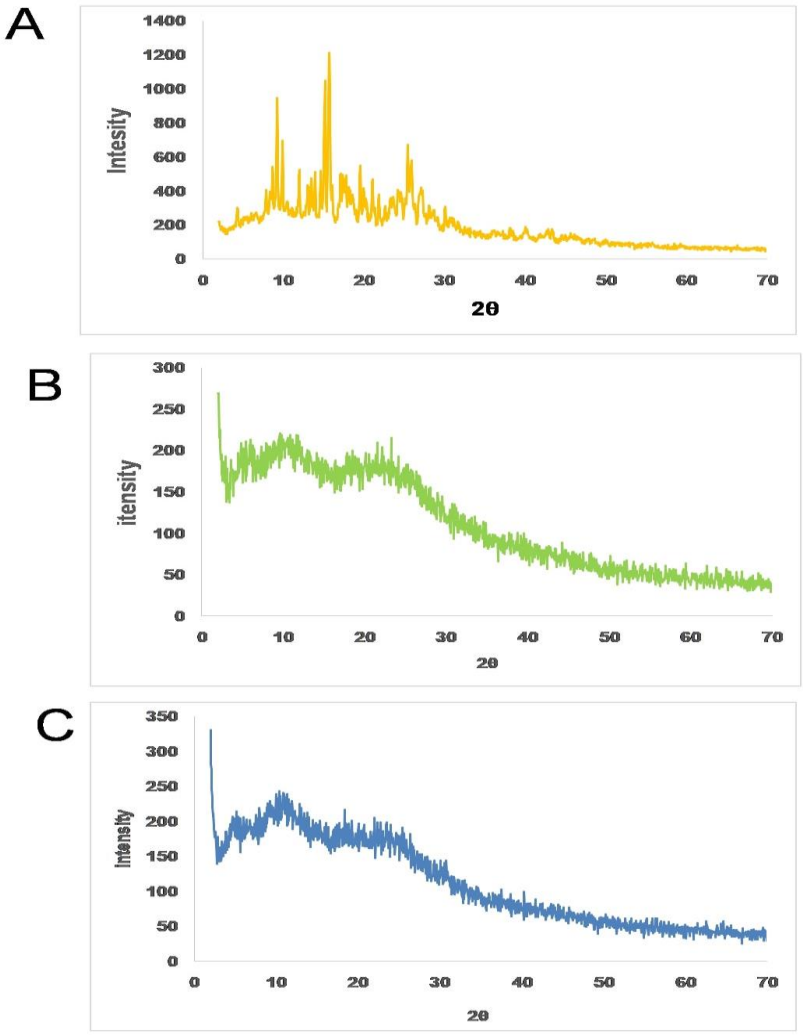

Figure 26 (A) XRD spectra of Naringin (B) XRD spectra of Chitosan (C) XRD spectra of NLC formulation

5.1.3 Characterization and optimization of NLC nanocarriers

In order to produce NLC nanocarriers with the desired size range, the formulation process variables were optimized. The zeta potential (ZP), particle size, entrapment efficiency, and polydispersity index (PDI) were all significantly impacted by each of these process variables. Table 14 illustrates how increasing the chitosan concentration affects ZP, PDI, and average particle size. Particle size average, PDI, and ZP all grew progressively with rise in the level of chitosan. The particle size of the prepared nanoparticles ranged from 91.92-250.5 nm which suggested that the size of the nanoparticles increased as the concentration of chitosan increased from 0.5 to 2 mg/ml. The zeta potential of the nanoparticles varied around +30mV which indicated a good stability for the prepared nanoparticles. Figure 27 depicts the particle size of one of the optimized formulations. Furthermore, increasing the chitosan content from 0.5 to 1 mg/ml resulted in a noticeable improvement in the nanoparticles' encapsulation efficiency. However, an increase in concentration beyond 1.5 mg/ml further showed a decrease in the drug entrapment, possibly because of inconsistent interaction of chitosan with tripolyphosphate. At higher chitosan concentrations, this could be explained by the formation of more chitosan chains per volume.

Table 14: Optimization parameters for the prepared batches

Formulation	Chitosan (mg/ml)	Avg. Particle Size (nm)	Zeta Potential (mV)	Loading Capacity (%LC)	Entrapment efficiency (%EE)
NLC1	0.5	91.92	25.6	25.4	75.25
NLC2	1	101.3	28.1	16.67	82.41
NLC3	1.5	115.21	32.2	12.5	87.5
NLC4	2	170.5	36.6	10.2	90.8
NLC5	5	205.1	38.5	8.01	55.2
NLC6	10	250.1	45.3	5.26	35.2

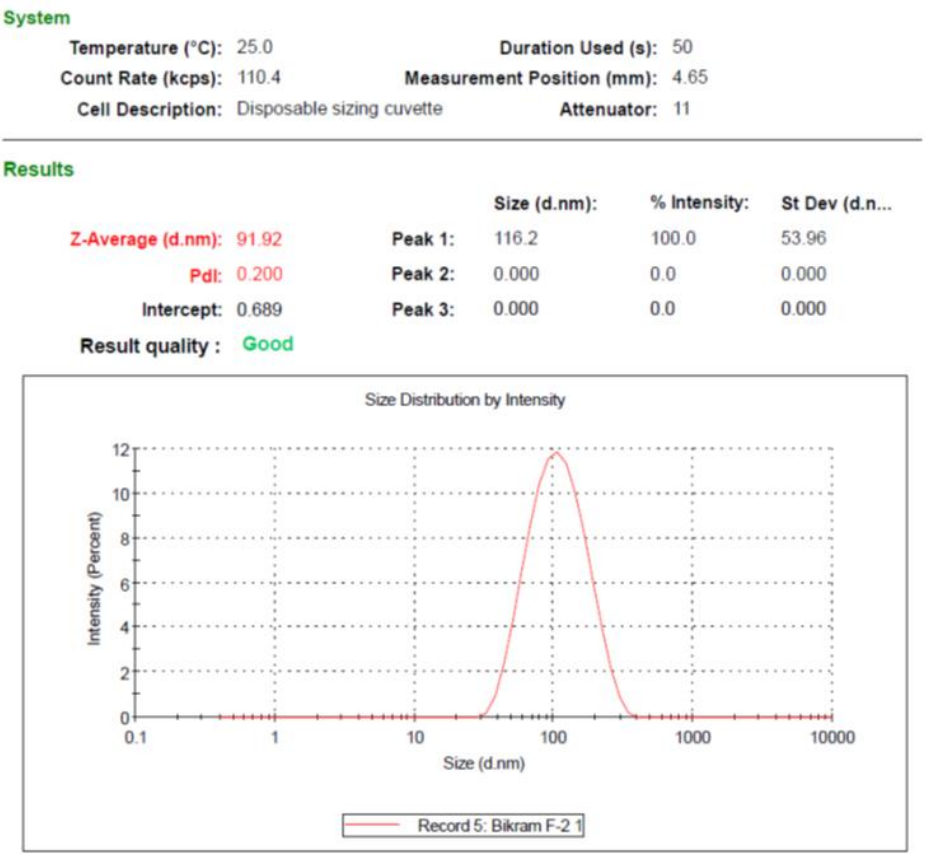

Figure 27: Particle size distribution of optimized formulation

The NLC nanocarriers were spherical, well-separated, uniformly distributed, and had a rough surface and morphology, according to morphology studies. Figure 28 exhibits well dispersed nanocarriers of chitosan through TEM (Figure 28 (b)) under a magnification of 200X which corroborates with the results obtained by SEM (Figure 28 (a)).

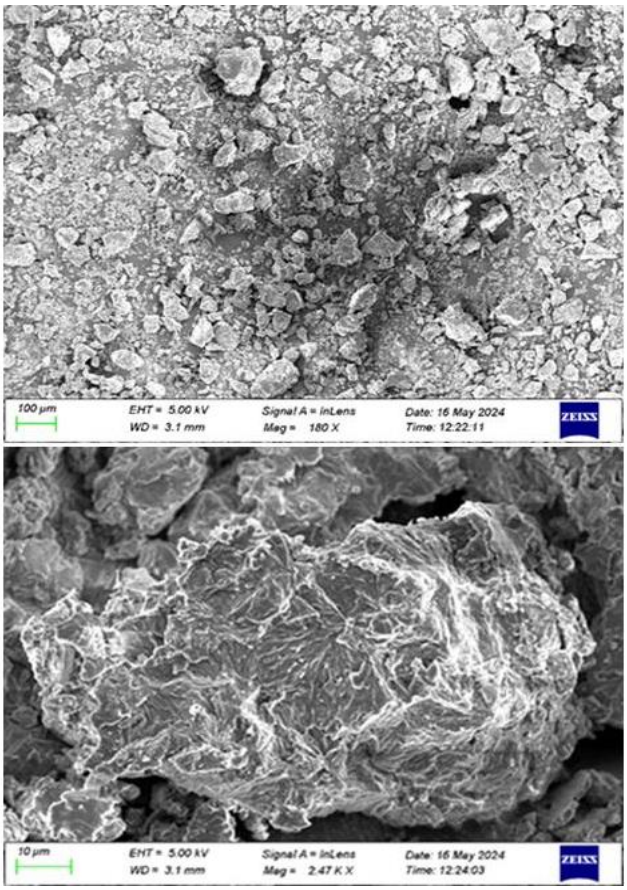

Figure 28(a): SEM Image of Drug loaded nanoparticles

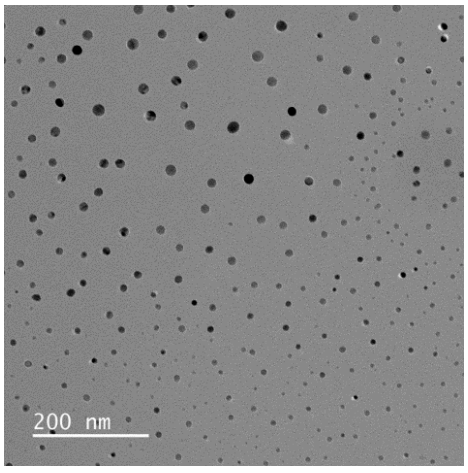

Figure 28 (b): TEM Image of Drug loaded nanoparticles

5.1.4 In Vitro Release Studies:

Drug release studies indicated that a controlled release of approximately 65% of the drug could be achieved over six hours. All of the formulations, however, displayed a 15% burst release within the first hour. It is possible that the surface of the nanocarriers contained drug molecules, which would account for the initial fast release. The drug embedded in the matrix was the cause of the consistent and slow release of naringin from NPs. Results clearly suggests that with an increase in chitosan concentration there is a reduction in the rate of drug release from the nanocarriers (Figure 29) (Herdiana et al., 2021).

In order to know the mechanism of drug release from the formulations, the release data were treated according to zero-order, first-order, Higuchi, Hixson-Crowell and Korsmeyer Peppas model. None of the formulations followed complete zero order release pattern. The release profiles could be best expressed by Higuchi's plot as it exhibited high linearity (R^2>0.98). Thus, the mechanism of drug release from nanocarriers can be described by diffusion controlled mechanism with a burst release. The release exponent n was found to be less than 0.45 in the Korsmeyer-Peppas model for all formulations, which indicates Fickian diffusion, meaning drug release is controlled primarily by a diffusion mechanism without significant polymer relaxation or swelling. Since the Higuchi model also describes diffusion-driven release, the high linearity observed in the Higuchi plot ($R^2 > 0.98$) aligns well with the Fickian diffusion mechanism. This confirms that the drug release from the formulation follows a diffusion-controlled process without significant contributions from polymer erosion or swelling (Figure 30).

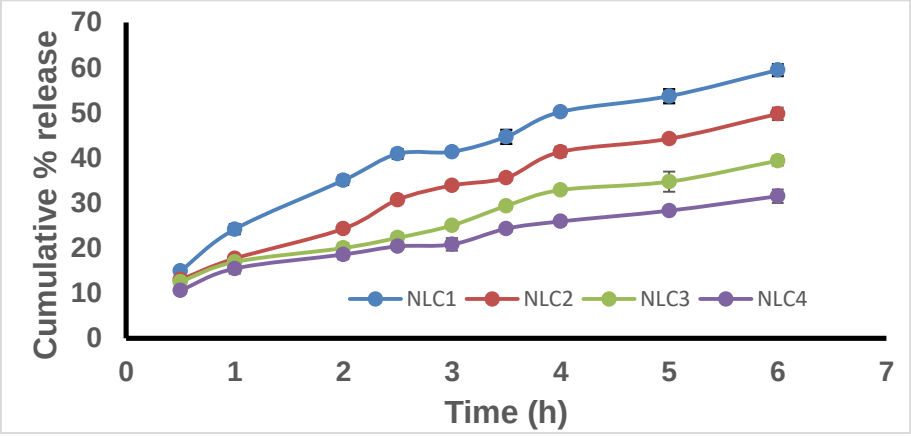

Figure 29: Release profile of NLC formulations

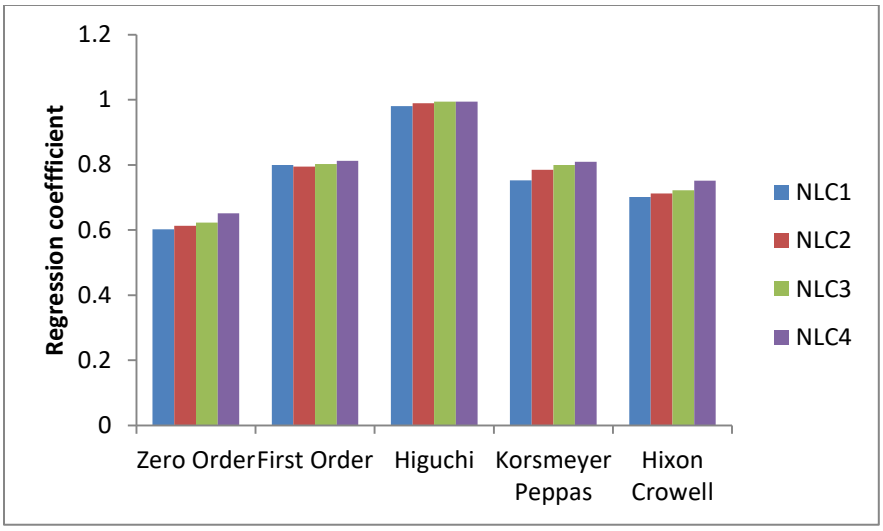

Figure 30: Release kinetics of NLC formulations

5.1.5 MTT assay for assessing cytotoxicity:

MTT test showed that the NLC formulations were non-toxic to the cells. The absorbance values increased at naringin doses in certain concentrations of NLC, but were non-significant as compared to untreated cells ($p>0.05$). Figure 31 represents cell viability analysis. For viability, HEK 293 cells were treated with the indicated concentrations (0-100 μM) of naringin (NLC) for 24 hours and MTT assay was performed to check cell viability. The data are presented as means of triplicate samples for each treatment and values given as Mean±SEM. Statistical analysis was performed by Students t-test; Bars = SE; n.s=non-significant. The cells exhibited optimal viability at the highest concentration of NLC (100 μM) and 0.5% chitosan, it was concluded that the cells were healthy safe at these concentrations which are nontoxic to the normal cell's growth and viability. Additionally, we saw no morphological alterations in the HEK 293 cells following the medication treatment as in comparison with the untreated group. Figure 32 represents images of morphological changes of untreated control and NLC-treated HEK 293 cells observed under an inverted light microscope (20×magnification) and no morphological changes are observed (Ramezani et al., 2014).

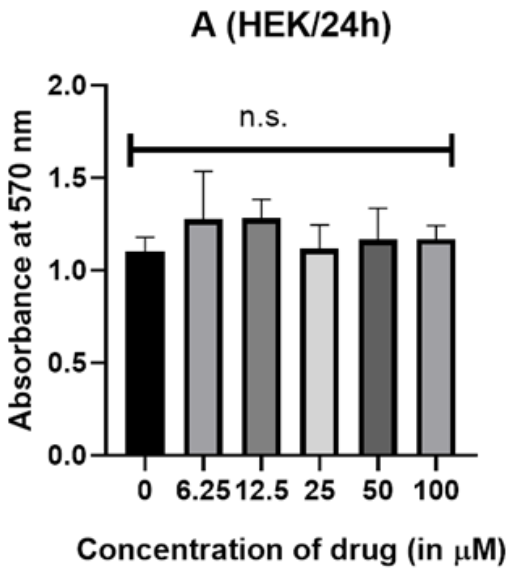

Figure 31: Graph showing MTT assay for cytotoxicity analysis on HEK cells at different drug concentrations against control

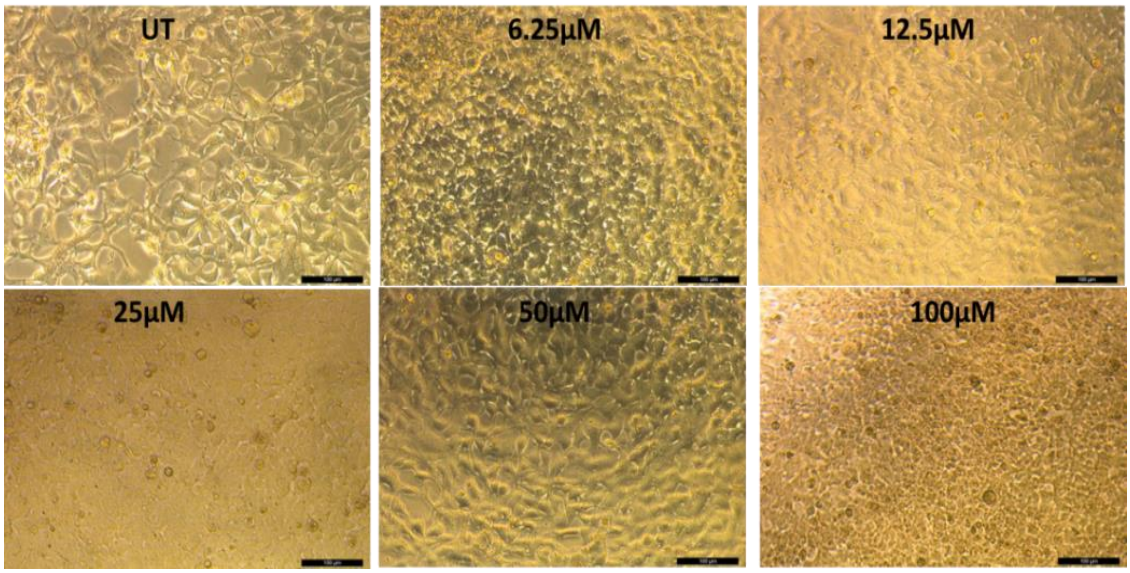

Figure 32: HEK cells at different drug concentrations of NLC

5.1.6 Anti-inflammatory activity:

The acute anti-inflammatory efficacy of NLC has been assessed using pleurisy caused by carrageenan. Carrageenan is utilized in the screening process for anti-inflammatory compounds because it is a phlogistic agent and creates a severe inflammatory response when injected locally into a rat's paw. Carrageenan-induced inflammation occurs in three distinct phases: the first is characterized by the release of serotonin and histamine; the second is brought about by kinin production, bradykinin being the most prominent; and the third is regulated by prostaglandins. NLC inhibited the development of rat paw edema considerably during the middle phase of carrageenan induced inflammation, and this effect was more pronounced during the third phase. This suggests that the anti-inflammatory properties of NLC may be mediated by reduction of prostaglandin activity in conjunction with the effects of vasoactive molecules (histamine, serotonin, and kinins). (Ismail et al., 2011, Bamgbose et al., 1981, Lo et al., 1982, Wang et al., 2022).

The posterior intraplantar left paw volume in the vehicle treated group grew gradually after receiving an injection of 0.1 mL of carrageenan (1% w/v), peaking at 0.89 ± 0.03 mL after 6 hours. The % inhibition of paw edema for the naringin treated group was found to be 9.52 %, 13.95 % and 19.10% at the 3hr, 4hr and 6hr mark, respectively. At the 3 hour, 4 hour, and 6 hour marks, the percentage suppression of paw edema for the naringin loaded nanoparticle group was found to be 27.66 %, 33.72%, and 42.67%, respectively. The inhibition of paw edema with the naringin loaded nanoparticle group was found to be significantly higher than the free naringin treated group ($p<0.05$). The % inhibition for the diclofenac treated group was found to be 36.90 %, 41.86% and 46.94% at the 3hr, 4hr and 6hr mark, respectively. The anti-inflammatory activity of the naringin loaded nanoparticle group was found to be similar to that of diclofenac treated group ($p > 0.05$). The results of this study are depicted in Figure 33.

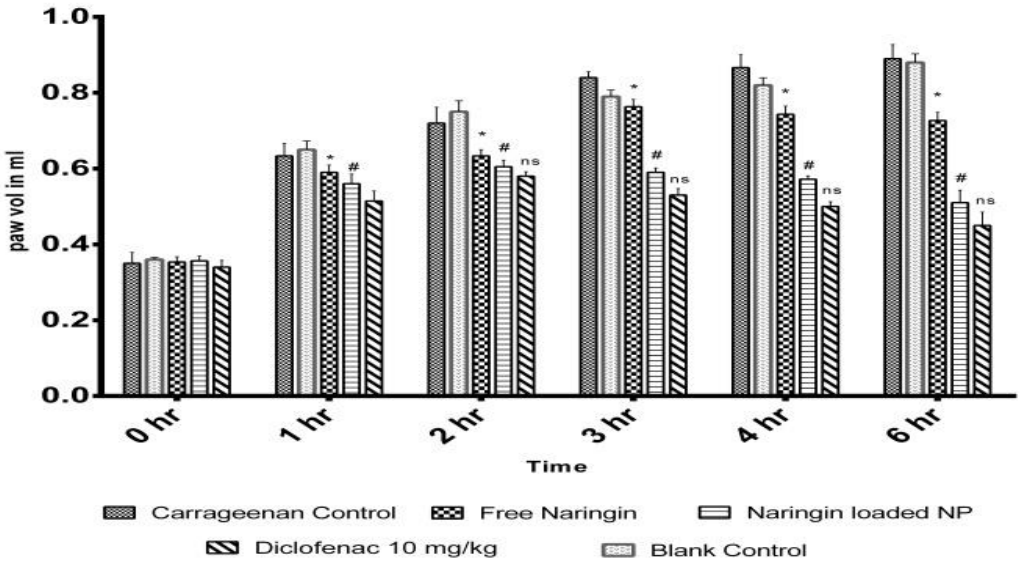

*Figure 33: NLC's anti-inflammatory properties assessed over time using pleurisy induced by Carrageenan. The results were expressed as Mean ± Standard Error Mean (SEM), (n = 6). One-way ANOVA followed by Dunnett's tests were performed to determine the statistical difference between the groups. *indicates a significant difference (p<0.05) between the free naringin group and the carrageenan control group; # denotes p <0.05, significant difference compared between free naringin and Naringin loaded nanoparticle group; ns indicates p > 0.05, not significant, when comparing the Naringin-loaded nanoparticle group to the Diclofenac treated group.*

The putative clinical benefits of naringin are restricted due to its poor aqueous solubility, low bioavailability and high hepatic first-pass metabolism. The naringin embedded in the Naringin Loaded Chitosan (NLC) nanocarriers exhibited higher anti-inflammatory activity as compared to naringin attributed possibly due to several key factors observed in similar studies on naringin and other flavonoid-loaded nanoparticles. Nanoparticles significantly enhance the bioavailability of poorly soluble compounds like naringin, ensuring a higher concentration of the active compound at the site of inflammation. Furthermore, naringin is released gradually and under control by nanoparticles, resulting in a protracted therapeutic action that guarantees steady anti-inflammatory benefits throughout time. (Zhang et al., 2021, Patel et al., 2019, Singh et al., 2020, Gupta et al., 2022, Ahmed et al., 2020, Sharma et al., 2021)

5.2 *Chitosan Based Quercetin Dihydrate Nanoparticles*

5.2.1 Preparation of Chitosan based quercetin dihydrate nanoparticles

Chitosan was employed as the primary polymer matrix to encapsulate quercetin dihydrate via nanoprecipitation, and its concentration was varied to evaluate its impact on the physicochemical characteristics of the resulting nanoparticles. Formulations FQN1 to FQN6 were prepared using chitosan concentrations ranging from 0.1% to 5% w/v. The varying concentration of chitosan affected the various parameters of nanoparticles as mentioned in Table 15.

5.2.2 Preformulation studies

UV-Visible Spectroscopy: Quercetin exhibited an absorption maximum at 370 nm, consistent with reported literature values. The calibration curve was constructed by measuring the absorbance of quercetin solutions across a concentration range of 2–20 µg/mL using a UV-Visible Spectrophotometer at 370 nm. The plot showed good linearity, with a correlation coefficient (r^2) close to 1, confirming compliance with Beer-Lambert's law in the given concentration range. The calibration data are summarized in Table 15.

Table 15: Calibration curve data of quercetin

Concentration (µg/mL)	*Absorbance at 370 nm (Mean ± SEM)*
2	0.158 ± 0.014
4	0.251 ± 0.026
6	0.306 ± 0.005
8	0.391 ± 0.047
10	0.472 ± 0.016
12	0.552 ± 0.048
14	0.649 ± 0.009
16	0.751 ± 0.026
18	0.834 ± 0.010
20	0.901 ± 0.038

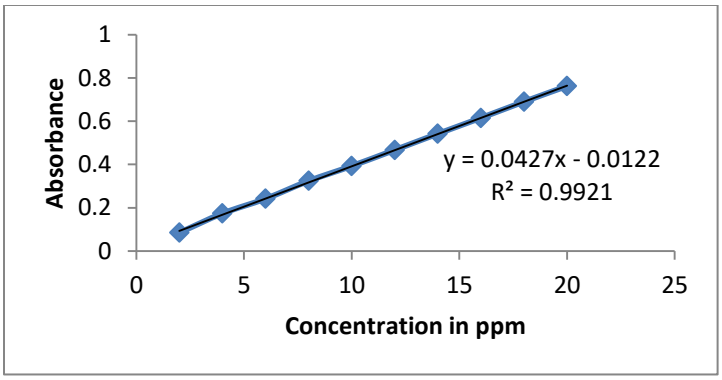

Figure 34: Calibration curve of quercetin

Solubility Studies: The aqueous solubility of quercetin was found to be 17.8±0.9 µg/mL, indicating poor aqueous solubility. This low solubility indicates hydrophobic character of quercetin and presents formulation challenge, necessitating strategies to enhance its solubility and bioavailability.

Melting Point Determination: The experimentally determined melting point of quercetin was observed to be in the range of 314–317°C, which aligns with the values reported in the literature. The sharp melting point indicates a high degree of purity and further confirms the crystalline nature of the isolated quercetin.

5.2.3 Formulation optimization characteristics: Table 16 summarizes how different chitosan concentrations affect the various parameters of the quercetin loaded nanoparticles (FQN1–FQN6) such as entrapment efficiency, particle size, and zeta potential. Entrapment efficiency (EE %) increased in accordance with the chitosan concentration, from 0.10% to 1% w/v, with FQN4 exhibiting the highest entrapment efficiency at 92.15%. This is because polymer chains that better enclose quercetin are more accessible (Zhang et al., 2021). A decrease in EE% (85.3% and 80.96%, respectively) was seen with a further increase in chitosan content to 2% and 5% (FQN5 and FQN6), presumably as a result of increased viscosity and polymer–drug interaction that restrict effective encapsulation (Singh et al., 2020). With additional polymer addition, the particle size increased, reaching a maximum of 77.23 nm in FQN6 after initially decreasing somewhat from FQN1 (20.4 nm) to FQN2 (18.45 nm). Higher chitosan concentrations may have probably cause increased aggregation and cross-linking (Gupta et al., 2022). Since there was excess polymer available to cover the nanoparticle

core, multilayered particles may have been formed, which could explain the rise in particle size above 1% chitosan concentration (Ahmed et al., 2020).

The zeta potential measurements showed stable nanoparticles in all formulations, ranging from 30.6 mV to 45.3 mV. FQN5 showed the highest zeta potential (45.3 mV), indicating a greater surface charge as a result of the higher chitosan content (Sharma et al., 2021). Because a larger zeta potential avoids aggregation by increasing electrostatic repulsion between particles, it generally improves the stability of colloidal systems (Patel et al., 2019). FQN4 (1% chitosan) was discovered to provide the best optimized particle size, excellent entrapment efficiency, and an acceptable zeta potential.

Table 16: Formulation table and optimization parameters

Formulation	*Conc. of chitosan (%w/v)*	*EE (%)*	*Particle Size (nm)*	*Zeta Potential (mV)*
FQN1	0.10	75.25	20.4	30.6
FQN2	0.25	85.23	18.45	40.2
FQN3	0.5	90.25	25.34	41.6
FQN4	1	92.15	55.23	35.5
FQN5	2	85 .3	75.85	45.3
FQN6	5	80.96	77.23	38.8

Particle size analysis of nanoparticles: Figure 34 displays the findings of an analysis of the particle size distribution of formulation FQN2 using dynamic light scattering (DLS). With a Z-average size of 18.45 nm and a polydispersity index (PDI) of 0.339, the formulation showed a monodisperse particle size distribution, suggesting a very uniform and narrow size distribution. The homogeneity of the nanoparticles is confirmed by the existence of a single, crisp peak with 100% intensity. Polymeric nanoparticles are generally regarded as having a homogenous population of particles appropriate for drug delivery applications when their PDI value is less than 0.5 (Zhang et al., 2021). Particularly for flavonoid-based treatments like naringin (Singh et al., 2020), the nanometric particle size increases the surface area-to-volume ratio, enhancing cellular absorption and bioavailability (Ahmed et al., 2020). FQN2 has a desired profile, maintaining a balance between tiny size, strong entrapment efficiency, and surface stability, in contrast to other formulations with higher chitosan concentrations (FQN5 and FQN6), which displayed larger particle sizes and wider distributions (Patel et al., 2019).

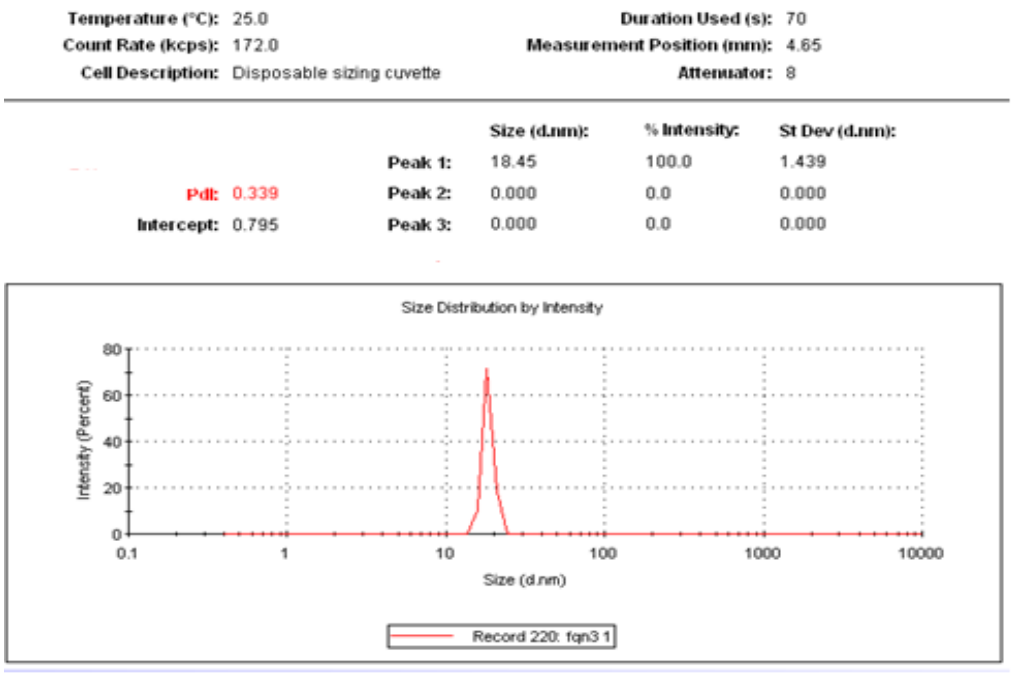

Figure 34: Particle size report of FQN4 for quercetin loaded chitosan nanocarriers

Physical characterization and surface morphology: Scanning Electron Microscopy (SEM) was used to examine the surface morphology of the optimized quercetin nanoparticle formulation, as illustrated in Figure 35 (a). Successful particle production at the nanometric scale is indicated by the uneven, plate-like particles with rough surfaces and different shapes visible in the SEM image. The drying process and the interaction of quercetin with the polymeric matrix—likely chitosan—may be responsible for the observed shape. Due to quercetin's crystalline nature, the non-spherical and flaky morphology is frequently seen in flavonoid-loaded nanoparticles and is especially compatible with its properties. Previous zeta potential values >30 mV, which indicate adequate electrostatic repulsion to prevent agglomeration, are consistent with the absence of large aggregates, which supports good dispersion and a stable formulation.

Furthermore, by increasing surface area, the rough surface roughness may improve quercetin's solubility and bioavailability. This is particularly significant for flavonoids that are poorly soluble in water. The formulation procedure effectively reduced the quercetin particles to the nanoscale with beneficial morphology for drug delivery, as evidenced by the small and uniform particle size (e.g., ~18.45 nm in FQN2)

which is in good agreement with these findings. These nanoparticles are appropriate for anti-inflammatory or antioxidant treatments because of their favorable surface properties, which promote improved cellular absorption and regulated quercetin release (Sanna et al., 2014).

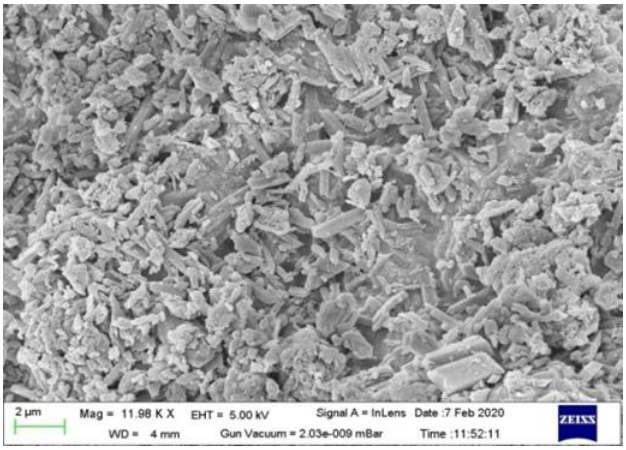

Figure 35 (a): SEM image of chitosan nanoparticles loaded with quercetin

Transmission Electron Microscopy (TEM) was used to further confirm the size and shape of quercetin-loaded nanoparticles, as shown in Figure 35(b). Because the quercetin core is electron-dense, the particles showed up as discrete, dark dots, indicating that the nanoparticle production was successful (Alshamsan et al., 2011).

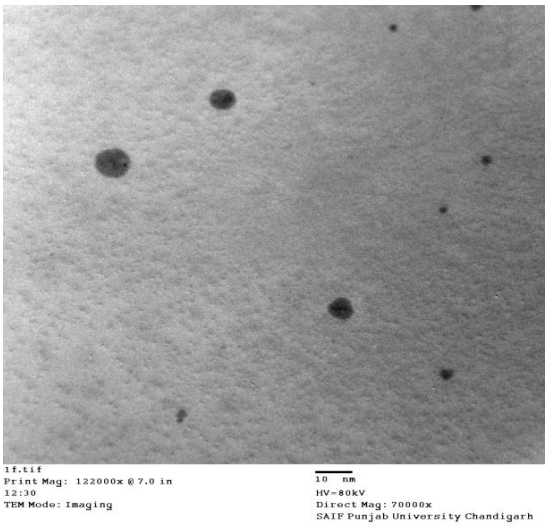

Figure 35 (b): TEM image of chitosan nanoparticles loaded with quercetin

5.2.4 In vitro release study: Figure 36 shows the results of an 8-hour in vitro drug release investigation of quercetin-loaded nanoparticles (FQN1–FQN6) in phosphate buffer (pH 7.4). Although there was considerable variance based on the chitosan content, all formulations displayed a prolonged release pattern.

At the end of eight hours, the formulation FQN1, which had the lowest chitosan concentration (0.1% w/v), showed the highest cumulative drug release (~91%). However, over the same time period, FQN6, which had the highest polymer content (5% w/v), only released only 67% of quercetin. Increased polymer matrix density, which prevents drug diffusion, is the cause of this negative relationship between polymer concentration and drug release rate.

The pattern for the intermediate formulations (FQN2 to FQN5) was predicted; FQN2 (~88%) and FQN3 (~82%) demonstrated notable release. These findings are consistent with the data on particle size and entrapment efficiency; formulations with larger surface area-to-volume ratios and intermediate particle sizes allowed for greater release.

A diffusion-governed process, in which the drug diffuses gradually through the chitosan matrix, is suggested by the controlled release behavior. This characteristic is advantageous for enhancing the bioavailability of flavonoids that are poorly soluble, such as quercetin, providing long-lasting therapeutic levels in the bloodstream. (Anand et al., 2010)

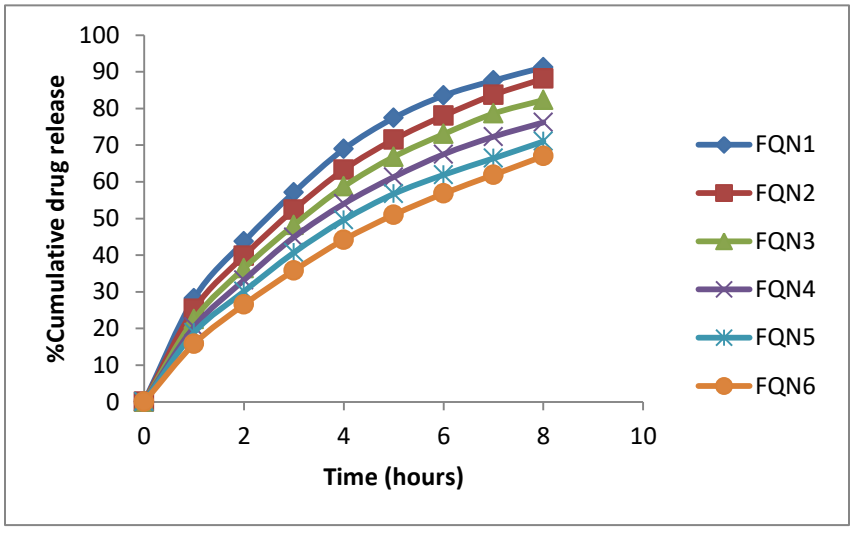

Figure 36: Cumulative Drug Release Behaviour for quercetin loaded nanoparticles

Table 17: Release kinetics regression coefficient data fit into various kinetic models

Model	*FQN1*	*FQN2*	*FQN3*	*FQN4*	*FQN5*	*FQN6*
Zero Order	0.988	0.985	0.981	0.979	0.974	0.969
First Order	0.951	0.959	0.957	0.953	0.950	0.956
Higuchi	0.993	0.991	0.990	0.987	0.983	0.978
Korsmeyer–Peppas	0.987	0.984	0.981	0.978	0.972	0.967
Hixson–Crowell	0.980	0.987	0.984	0.980	0.976	0.972

The in vitro release data were fitted to various kinetic models, including Zero-order, First-order, Higuchi, and Korsmeyer–Peppas, in order to comprehend the mechanism of drug release from the quercetin nanoparticles (FQN1–FQN6). Table 17 summarizes the correlation coefficient (R^2) results. With the greatest r^2 values across all formulations (0.988–0.999), the Higuchi model outperformed the others, indicating that the drug release primarily occurs via a diffusion-controlled mechanism (Costa et al, 2001).

5.2.5 Ocular Eye Irritancy Test: HET- CAM Test

The ocular irritancy potential of the formulation of quercetin-loaded nanoparticles was assessed using the Hen's Egg Test on the Chorioallantoic Membrane (HET-CAM). Even after five minutes of exposure, the formulation image shows no signs of vascular lysis, bleeding, or coagulation, indicating that the formulation does not irritate the chorioallantoic membrane as similar to the negative control (normal saline), whereas the positive control (0.1% HCl) exhibited a quick start of bleeding and membrane damage (Figure 37). The studied formulation's behavior closely matched that of the negative control, indicating both its ocular safety and biocompatibility. These results are in line with earlier research showing that chitosan-based nanoparticle systems are well-tolerated and non-irritating in models of mucosal irritation (Ludwig, 2005, Nagpal et al., 2021).

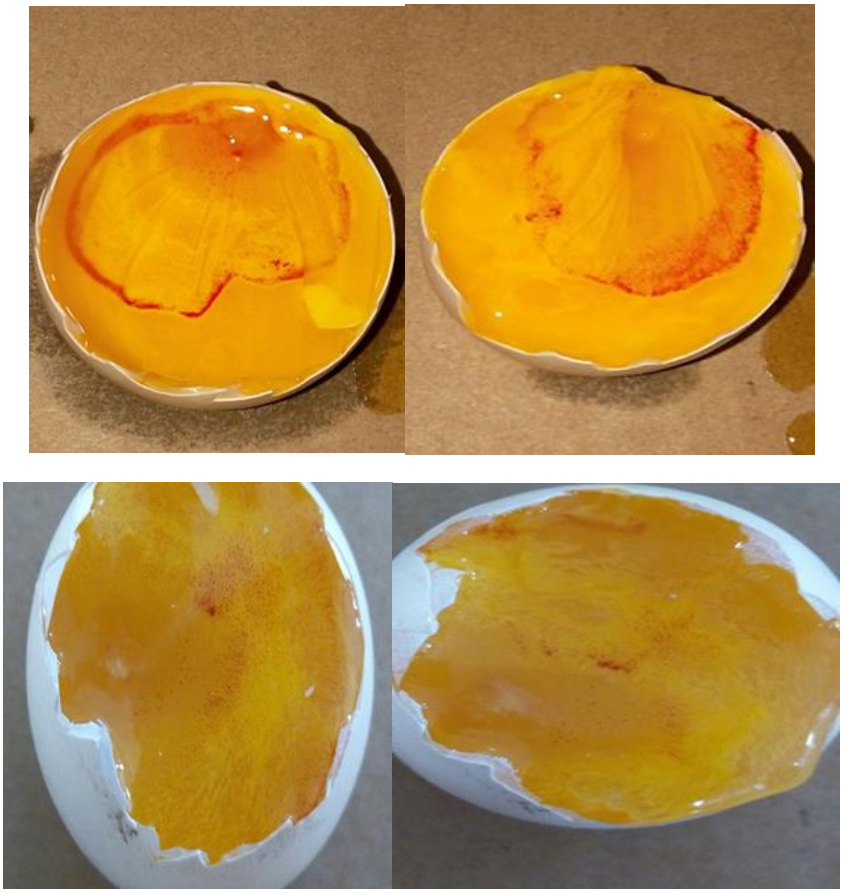

Figure 37: HET CAM test (a) Intact Embryo on 19th day (b) Embryo lysis begins with positive control (0.1%HCl) (c) Intact Embryo with negative control (0.9%w/v saline) (d) Intact Embryo with Quercetin loaded chitosan nanocarrier

5.2.6 Permeation Study across Excised Goat's Cornea

Figure 38 depicts ex vivo permeation profile of quercetin formulations across excised goat cornea over six hours. All formulations showed steady rise in cumulative drug permeation, with formulation-dependent permeation rates. The improved permeation may be attributed to nanosize of the particles that allows improved contact and retention on corneal surface, mucoadhesive and permeation-enhancing qualities of chitosan and possible tight connection opening and improved medication solubility in nanoparticle form (de Campos et al., 2001). The maximum penetration was shown by formulation FQN3 (shown by green triangles) (~170 µg/cm² at 6 hours), followed by FQN2 and FQN4. The pure drug suspension (FQN6) (blue diamonds) had lowest petmeation, demonstrating slow permeation rate with increasing polymer network.

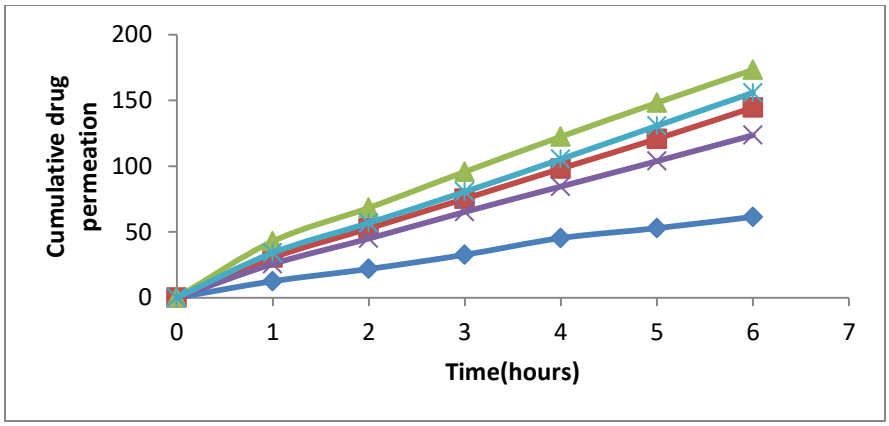

Figure 38: Cumulative drug permeation over 6 hours across excised goat's cornea

Table 18: Parameters for measuring permeation of drug across excised goat's cornea

Parameter	*Quercetin Suspension*	*FQN1*	*FQN2*	*FQN3*	*FQN4*
Cumulative Permeation (6 h)	74.5 ± 2.7 µg/cm²	183.2 ± 3.4 µg/cm²	220.3 ± 3.7 µg/cm²	158.9 ± 3.2 µg/cm²	175.5 ± 3.5 µg/cm²
Flux (J)	9.31 µg/cm²/h	22.9 µg/cm²/h	27.5 µg/cm²/h	19.9 µg/cm²/h	25.3 µg/cm²/h
Enhancement Ratio (ER)	1 (reference)	2.46	2.95	2.14	2.72

The cumulative drug permeation, flux, and enhancement ratio (ER) was determined after a 6-hour evaluation of the in vitro permeation profile of quercetin suspension and nanoformulations (FQN1–FQN4) (Table 18). FQN2 showed the largest cumulative permeation (220.3 ± 3.7 µg/cm²) and flux (27.5 µg/cm²/h) among the studied formulations. The quercetin suspension, which was used as the reference for enhancement ratio calculations, showed noticeably reduced permeation (74.5 ± 2.7 µg/cm²) and flux (9.31 µg/cm²/h). With an enhancement ratio of 2.95 for FQN2, the penetration was almost three times better than with the suspension. FQN1, FQN3, and FQN4 all had ER values of 2.46, 2.14, and 2.72, respectively, indicating a significant increase in the diffusion of drugs across all nanoformulations. The improved permeation from the nanoformulations may be attributed to their reduced particle size and enhanced solubility, which facilitate more efficient drug transport across the excised cornea (Pawar et al., 2006; Dave et al., 2015, Prow et al., 2011; Ahuja et al., 2006; Singla et al., 2011, Shakeel et al., 2021).

5.2.7 Antioxidant Activity Study for Quercetin-Loaded Nanoparticles: DPPH Assay

The DPPH free radical scavenging study was used to evaluate the antioxidant capacity of quercetin and its nanoformulations at four distinct concentrations: 5, 10, 20, and 40 µg/mL. Table 19 displays the % inhibition values for formulations FQN1 through FQN6 and free quercetin. The nanoformulations showed noticeably more antioxidant activity than free quercetin at all tested doses. With practically total radical scavenging (99.9 ± 3.0% at 40 µg/mL) and the highest percentage inhibition (51.2±1.9% at 5µg/mL), FQN4 continuously demonstrated the best antioxidant activity. FQN2 and FQN3 showed dose-dependent increase in inhibition (Figure 39). Because of the nanometric size and huge surface area of the particles, the greater antioxidant effect seen with nanoformulations may be explained by improved solubility, better dispersibility, and a higher interaction potential with free radicals (Pinto et al., 2013; Sahu et al., 2020). Quercetin's encapsulation probably prevented its active hydroxyl groups from deteriorating over time, preserving its capacity to scavenge radicals (Müller et al., 2011).

Table 19: Percent Inhibition of Quercetin-Loaded Nanoparticles by DPPH Assay

Quercetin Concentration (µg/mL)	*Free Quercetin (% Inhibition)*	*FQN1*	*FQN2*	*FQN3*	*FQN4*	*FQN5*	*FQN6*
5 µg/mL	21.5 ± 1.2	41.2 ± 1.6	45.6 ± 1.7	48.9 ± 1.8	51.2 ± 1.9	32.4 ± 1.3	37.8 ± 1.5
10 µg/mL	38.2 ± 1.5	61.8 ± 1.9	65.4 ± 2.0	69.8 ± 2.2	73.5 ± 2.3	50.5 ± 1.6	57.3 ± 1.8
20 µg/mL	55.6 ± 1.8	80.4 ± 2.3	84.7 ± 2.4	89.2 ± 2.5	92.5 ± 2.6	68.9 ± 2.0	75.1 ± 2.2
40 µg/mL	72.8 ± 2.1	96.7 ± 2.7	98.5 ± 2.8	99.8 ± 2.9	99.9 ± 3.0	88.1 ± 2.5	92.3 ± 2.6

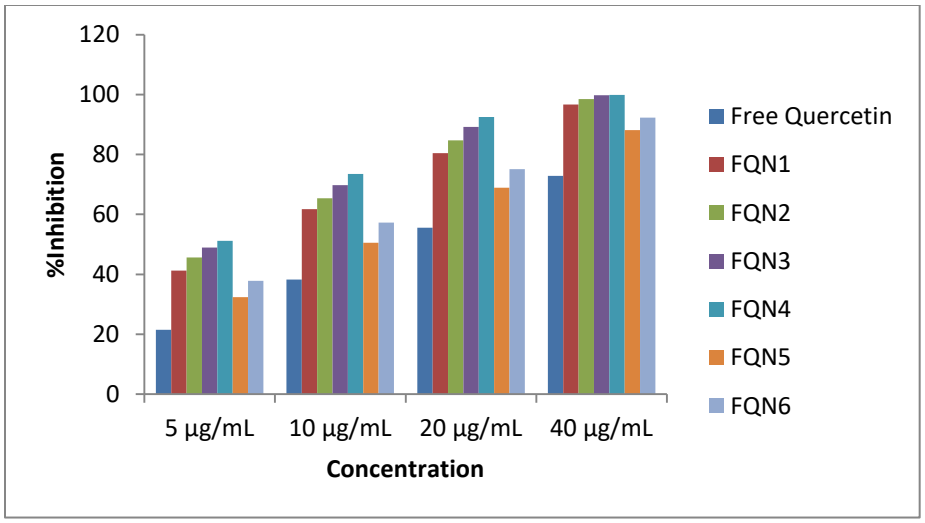

Figure 39: Graphical representation of Percent Inhibition of Quercetin-Loaded Nanoparticles by DPPH Assay

To measure the antioxidant potency of free quercetin and its nanoformulations, the half-maximal Inhibitory Concentration (IC_{50}) values were computed. All of the nanoformulations showed noticeably lower IC_{50} values than free quercetin, as shown in Table 20, suggesting improved radical scavenging efficacy. The IC_{50} values of the nanoformulations FQN1 to FQN6 ranged from 7.4 ± 0.4 to 13.2 ± 0.7 µg/mL, while the IC_{50} of free quercetin was 18.4 ± 0.9 µg/mL. FQN4 demonstrated the highest antioxidant ability among them, with the lowest IC_{50} value (7.4 ± 0.4 µg/mL).

Table 20: Inhibitory concentrations for various formulations and free quercetin

Sample	*IC_{50} (µg/mL)*
Free Quercetin	18.4 ± 0.9
FQN1	13.2 ± 0.7
FQN2	10.6 ± 0.6
FQN3	8.9 ± 0.5
FQN4	7.4 ± 0.4
FQN5	9.2 ± 0.4
FQN6	10.7 ± 0.3

Nanoformulations' significantly lower IC_{50} values are probably the result of their increased surface area, greater dispersion, and improved aqueous solubility, all of which promote more effective interaction with DPPH radicals as seen in Figure 40 (Pinto et al., 2013; Müller et al., 2011). The quercetin molecule may also have been stabilized by nanoencapsulation, which maintains the hydroxyl groups that scavenge radicals (Sanna et al., 2015; Anand et al., 2018, Sahu et al., 2020).

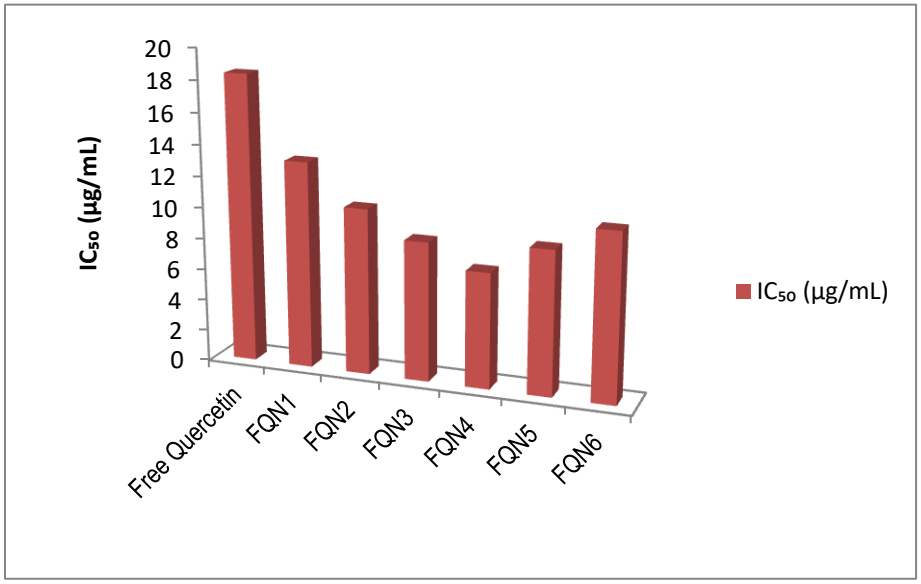

Figure 40: Comparison of IC_{50} values of quercetin nanoformulations against free quercetin

5.2.8 Anti-inflammatory Activity:

Carrageenan-induced paw edema in rats is a common model used to assess anti-inflammatory properties. When 0.1 mL of 1% w/v carrageenan was injected into the rats' left hind paw, the vehicle-treated group's paw volume gradually increased, reaching a maximum swelling of 0.91±0.02 mL at the 6-hour mark. Animals treated with quercetin exhibited moderate anti-inflammatory effect; at three, four, and six hours after receiving a carrageenan injection, the percentage inhibition of paw edema was 6.42%, 10.45%, and 13.21%, respectively. At similar time intervals, however, the group treated with quercetin-loaded nanoparticles showed noticeably greater anti-inflammatory activity, with inhibition percentages of 25.41%, 38.26%, and 45.20% (Figure 41).

When compared to diclofenac sodium, which demonstrated percentage inhibition values of 35.80%, 40.55%, and 42.18% at 3, 4, and 6 hours, respectively, the nanoparticle formulation's impact was statistically similar ($p>0.05$). One-way ANOVA and Dunnett's post hoc test were used for statistical analysis, which verified that there was no significant difference between the quercetin nanoparticle group and the standard diclofenac group. These results strongly imply that quercetin's anti-inflammatory activity is greatly improved by nanoformulation, most likely as a result of improved solubility, stability, and bioavailability. According to previous research on nanoparticulate delivery systems for polyphenolic chemicals, the nanoparticle group's greater and longer-lasting suppression of inflammation may be due to improved tissue penetration and extended systemic circulation (Sanna et al., 2015).

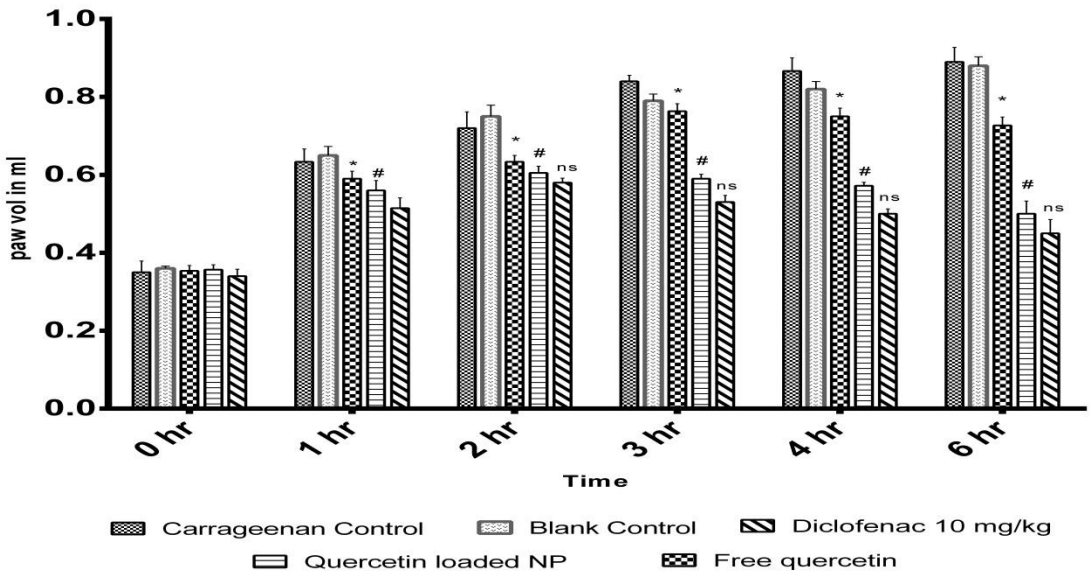

*Figure 41: Anti-inflammatory effect of quercetin loaded nanoparticles assessed over time using pleurisy induced by Carrageenan. The results were expressed as Mean ± Standard Error Mean (SEM), (n = 6). One-way ANOVA followed by Dunnett's tests were performed to determine the statistical difference between the groups. * indicates a significant difference ($p<0.05$) between the free quercetin group and the carrageenan control group; # denotes $p <0.05$, significant difference compared between free quercetin and Quercetin loaded nanoparticle group; ns indicates $p > 0.05$, not significance, when comparing the Quercetin-loaded nanoparticle group to the Diclofenac treated group.*

5.3 *Polycaprolactone Based Nanocarriers of Naringin*

5.3.1 Preparation and optimization of PCL Nanoparticles:

The nanoparticles were prepared by nanoprecipitation method and the optimization parameters are discussed in Table 21. As the drug:polymer molar ratio increases from 1:1 to 1:10, the encapsulation efficiency (EE%) improves, reaching a maximum of 92.40% at a 1:10 ratio (PCLNPs3). However, further increasing the polymer concentration to 1:20 (PCLNPs4) results in a drop in EE% suggesting excessive polymer might hinder drug entrapment due to saturation effects. Drug loading (%) decreases as the polymer concentration increases, which is expected since a higher polymer content results in a lower proportion of drug in the final formulation. Surfactant concentration was optimized at 1%w/v for the aqueous phase.

Table 21: Formulation table with optimization parameters of naringin loaded PCL Nanoparticles

Formulation	*Drug: Polymer molar ratio*	*Drug encapsulation (%)*	*Drug loading (%)*	*Particle size*	*Zeta potential*
PCLNPs1	1:1	87.11	24.45	128.1	-25.2
PCLNPs2	1:5	89.23	18.21	145.3	-26.5
PCLNPs3	1:10	92.40	15.5	130.3	-32.3
PCLNPs4	1:20	75.33	13.3	250.5	-37.0
PCLNPs5	2:1	45.21	9.8	500.4	-50.0
PCLNPs6	5:1	22.45	5.5	650.1	-55.2

5.3.2 Characterization of PCL Nanoparticles:

The surface morphology of quercetin-loaded nanoparticles was examined using Scanning Electron Microscopy (SEM), and presented in Figure 42. The particles are well-dispersed across the field with minimal agglomeration, indicating effective formulation and drying methods. The particles exhibit a relatively dense packing, suggesting high yield and consistent production during the formulation process. Most of the particles appear to be spherical to sub-spherical in shape. The absence of large clusters or irregular

debris supports good process control during preparation and implies that encapsulation of mangiferin within the polymer matrix was efficient.

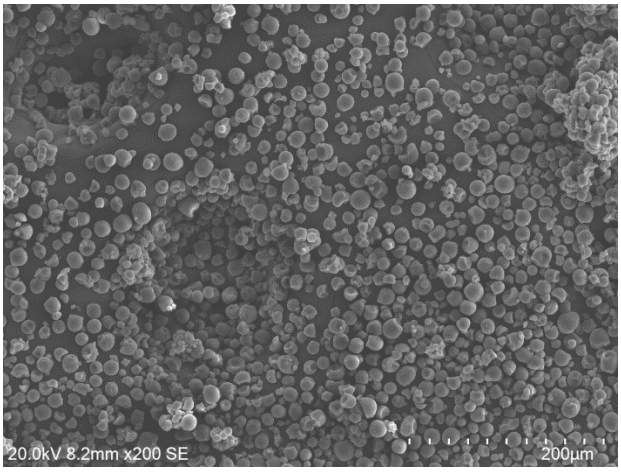

Figure 42: SEM image of PCL Nanoparticles

The mean particle size for PCLNPs3 was found to be around 130 nm with a polydispersity index (PDI) almost 1. The particle size report is displayed in the figure 43 below. Results of rest of the batches have been tabulated in Table 18. The smallest particle size (128.1 nm) is observed at 1:1 drug:polymer ratio (PCLNPs1), indicating less polymer aggregation. As the polymer concentration increases, particle size generally increases due to excessive polymer accumulation leading to larger particles. PCLNPs3 (1:10 ratio) maintains relatively small size (130.3 nm), making it optimal for drug delivery while still achieving high encapsulation efficiency. The zeta potential becomes more negative as polymer concentration increases, improving nanoparticle stability by preventing aggregation. The highest zeta potential magnitude in PCLNPs6 suggests strong electrostatic repulsion, but large particle size might affect its dispersibility and bioavailability. PCLNPs3 offers a balance of good stability and optimal particle size, making it a promising formulation (Fessi et al., 1989, Letchford et al., 2007, Chawla et al., 2002, Zhang et al., 2008, Honary et al., 2013).

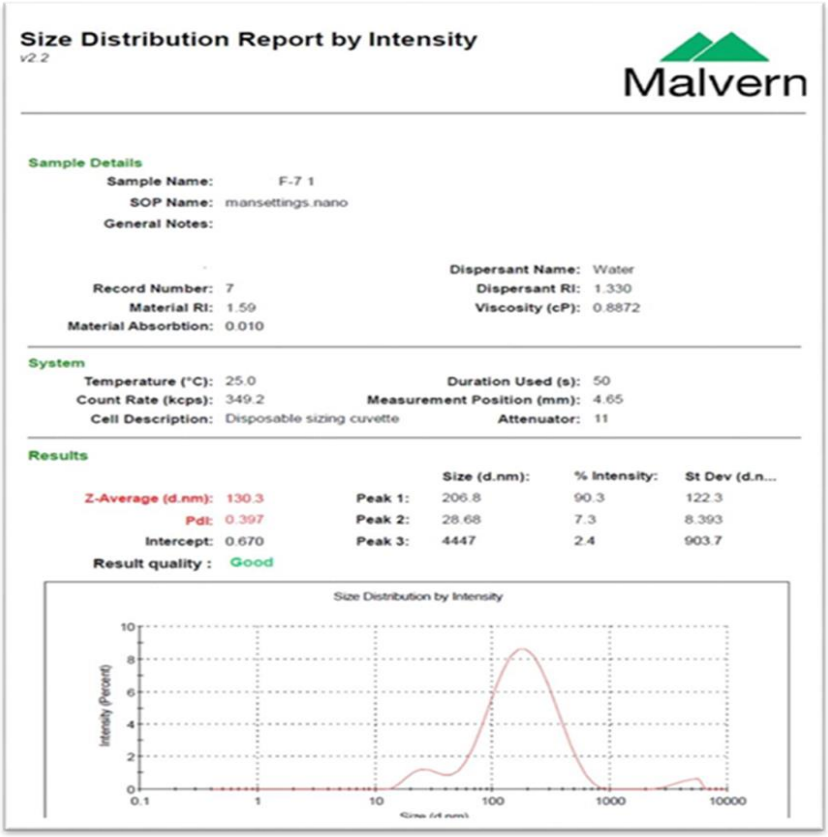

Figure 43: Particle Size Analysis of PCLNPs3

5.3.3 Drug polymer interaction study (Thermal analysis)

The thermal curves of naringin, blank PCL nanoparticles, and naringin loaded PCL nanoparticles demonstrate endothermic and exothermic transitions, with a red curve representing heat transfer (Figure 44). The blue curve depicts the weight %, which is usually suggestive of a Thermogravimetric Analysis (TGA) overlay over the DSC data. Naringin shows a first endothermic peak about 50°C. The TGA curve shows no significant weight loss, implying no decomposition or volatilization in this range at naringin melting point and decomposition, respectively. PCL shows an endothermic peak around 50°C at around 0-100°C, indicating a phase transition such as melting. Within 300-500°C, the endothermic peak occurs about 350°C, possibly indicating a substantial phase shift. On the other hand, at 350°C, the Naringin drug-loaded PCL nanoparticle undergoes a fast endothermic transition followed by an exothermic peak. The weight percentage decreases dramatically in the same temperature range (300°C to 400°C),

indicating breakdown or severe mass loss, probably due to loss of its crystalline structure (Sinha et al., 2004, Mouffouk et al., 2019). Hence, it can be concluded that although the components exhibited melting at their respective temperatures, there was no significant heat change or weight loss in formulation containing quercetin which suggests no interaction with the polymer rather entrapment into its core.

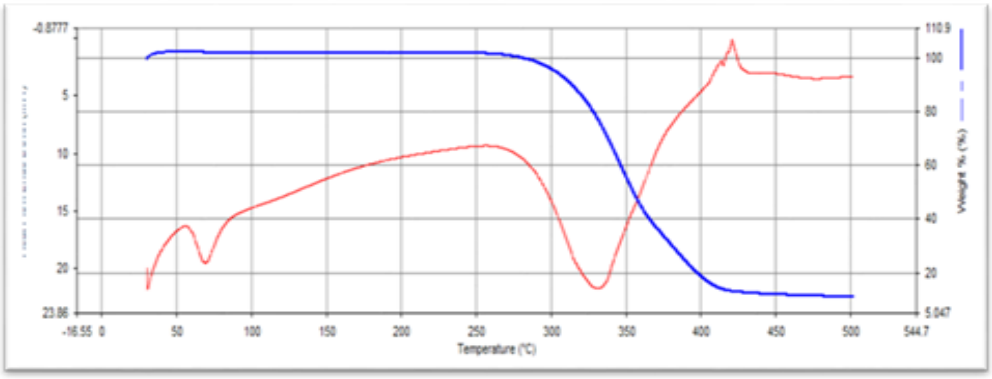

(a)

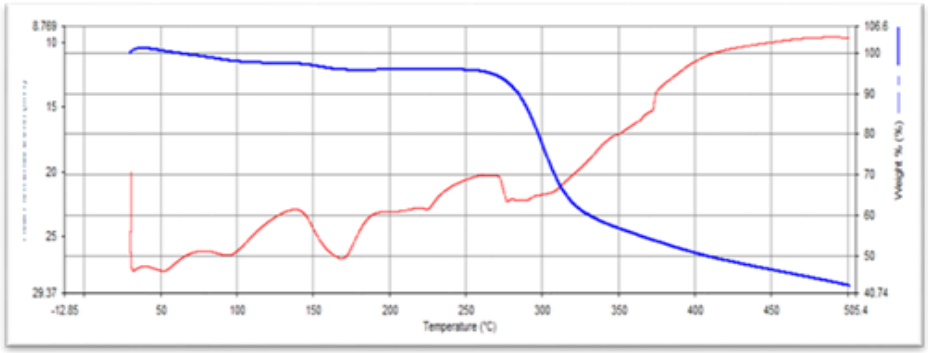

(b)

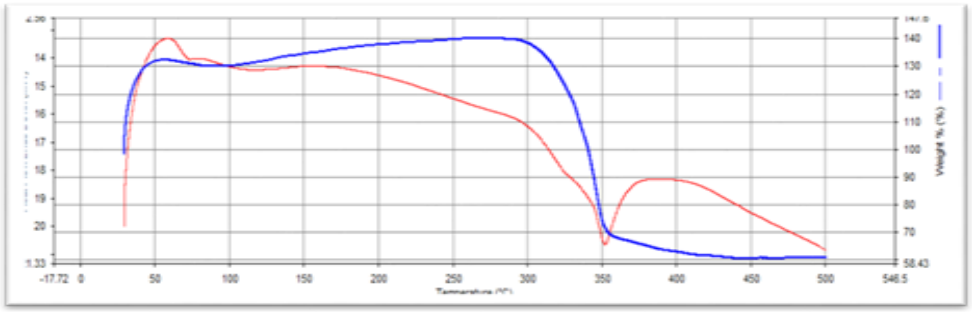

(c)

Figure 44: Thermal analysis curves for (a) Naringin (b) Blank PCLNPs (c) Naringin loaded PCLNPs

5.3.4 FTIR Spectral Analysis: FTIR spectra of naringin and corresponding synthesized polycaprolactone nanoparticle are depicted in the figure 45 below. FTIR spectrum of naringin showed prominent peaks at region 3410.27 cm^{-1} for the shifting vibration of hydroxyl group (OH). The absorption band at 2919.81 cm^{-1} corresponded to a C-H group of CH_3. The absorption band at 1517.27 cm^{-1} indicates C=C bond of the aromatic ring. The absorption band at 1447.64 cm^{-1} was a C-H bond in the CH_2, whereas the absorption band at 1388.12 cm^{-1} was a C-H bond in the CH_3. The absorption bands at 1042 cm^{-1} and 1091 cm^{-1} correspond to the ether's C-O-C bonds. Smilarly, PCL exhibited its prominent peaks. The IR spectrum study of naringin loaded nanoparticles retained the significant peaks for polycaprolactone; implying naringin was successfully loaded into the nanoparticles with no probable interactions between the drug and polymer.

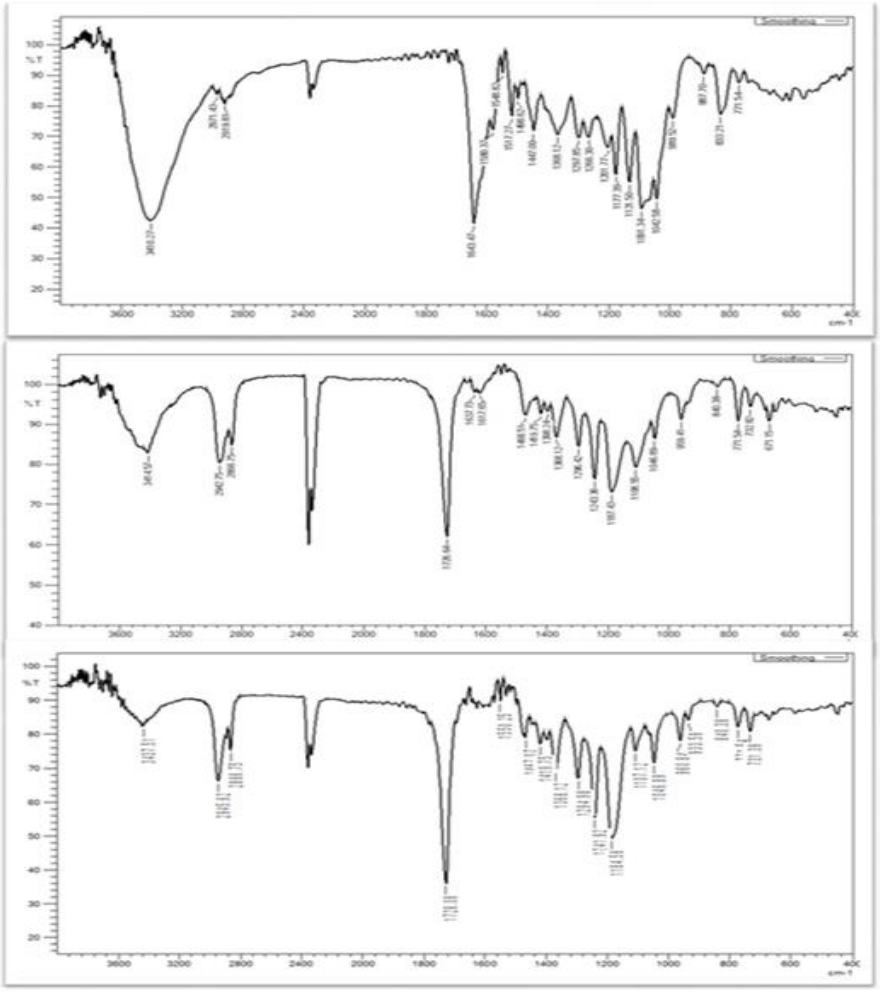

Figure 45: FTIR Spectra of pure naringin, blank nanoformulation without naringin and formulation respectively

5.3.5 In Vitro Drug Release Study:

Percentage of drug release profiles into the phosphate buffer saline pH6.8 medium depicts a controlled release of around 50-62% drug release in 24 hrs. Five models were fitted to the experimental cumulative drug release data, as shown in the table below, in order to predict the drug release process from PCLNPS. The figure 46 below illustrates the naringin release kinetics from the PCLNPS along with regression coefficient (r^2) data. As shown in the Table 21, the drug release from PCLNPS conformed to Higuchi kinetics as evidenced by r^2 values greater than 0.9957 with 'n' values for all formulations less than 0.45 which suggests Fickian diffusion kinetics (Dash et al., 2010, Siepmann et al., 2012, Sinha et al., 2004, Fu et al., 2010)

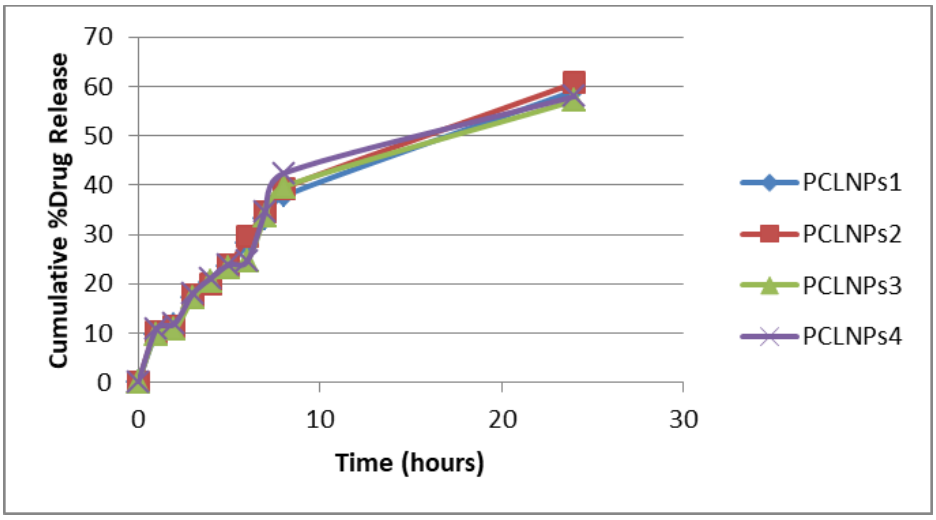

Figure 46: Release study of PCLNP formulations

Table 22: Regression coefficient (r^2) value of formulation (PCLNP1-PCLNP4)

Formulation	*Zero order*	*First order*	*Higuchi*	*Hixson Model*	*Korsmeyer Peppas*
PCLNP1	0.7407	0.945	0.9925	0.8966	0.7848
PCLNP2	0.9361	0.864	0.9957	0.7119	0.9427
PCLNP3	0.9505	0.8381	0.9872	0.7537	0.9515
PCLNP4	0.9209	0.8902	0.9911	0.726	0.9323

5.3.6 In vivo studies

The *in vivo* hypoglycemic responses of the various treatment groups were investigated by estimating blood glucose levels. Blood glucose levels in group II, which included diabetic control rats, exceeded 250 mg/dL. Diabetic rats treated with glipizide (Group III), free naringin (Group V), and a nano-formulation of naringin (Group VI) had significantly lower fasting blood glucose levels ($p<0.05$). The hypoglycemic impact of naringin-loaded nanoparticles was much higher than that of free oral naringin ($p < 0.05$), as indicated in the figure 47. On the 28th day of treatment, the naringin-only group had a 44.2% lower blood glucose level than the diabetic control group, whereas the PCLNP group had a 65.5% lower blood glucose level. The blank control group (group IV) showed no significant hypoglycemic response ($p > 0.05$), indicating that the blank nanoformulation has no hypoglycemic activity (Figure 47).

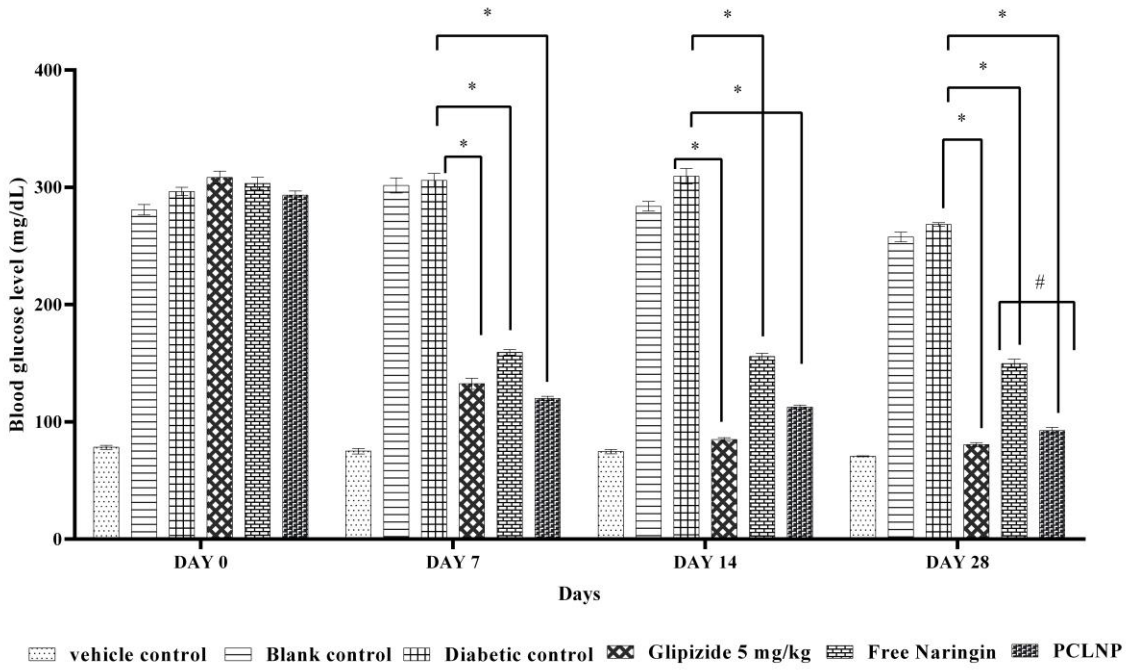

Figure 47: Effect of the hypoglycemic response in the different treatment groups. The data were presented as mean ± standard error of the mean (SEM) (n = 6). (: $p < 0.05$, compared with diabetic control; #: $p < 0.05$, comparison between free naringin and PCLNP group).*

5.4. Polycaprolactone Based Nanocarriers of Mangiferin

5.4.1 Preparation and optimization of PCLMP nanoparticles

Mangiferin-based polycaprolactone (PCL)-based nanocarriers were formulated using nanoprecipitation method and optimized by adjusting crucial formulation factors such stirring speed, polymer concentration, and surfactant concentration, all of which had a major impact on the properties of the nanoparticles. The optimization parameters have been mentioned in Table 23. Because of the increased viscosity and availability of the polymer matrix to encapsulate the drug, the study found that increasing the PCL concentration resulted in a proportional rise in particle size and entrapment efficiency (PCLMP3: 150 mg PCL resulted in 200 nm size and 90.5% EE). On the other hand, a 2% surfactant concentration (PCLMP5) resulted in smaller particles and better stability (150 nm, PDI 0.280), indicating that Tween80 increased emulsification and particle stabilization.

Table 23: Formulation and optimization parameters for prepared mangiferin loaded PCL nanoparticles

Formulation Code	*Mangiferin (mg)*	*PCL (mg)*	*Tween 80 %)*	*Particle Size (nm)*	*PDI*	*Zeta Potential (mV)*	*Entrapment Efficiency (%)*	*Drug Loading (%)*
PCLMP 1	50	50	1.0	130.0 ± 0.3	0.210± 0.03	-15.5 ± 0.2	78.4 ± 2.1	4.1 ± 0.5
PCLMP 2	50	100	1.0	190.3 ± 0.5	0.395± 0.021	-25.3 ± 0.5	85.1 ± 1.8	5.4 ± 0.5
PCLMP 3	50	150	1.0	200.2 ± 0.02	0.450± 0.05	-21.1 ± 1.5	90.5 ± 2.0	6.2 ± 0.1
PCLMP 4	50	100	0.5	290.3 ± 0.04	0.350± 0.30	-15.6 ± 1.5	80.2 ± 2.3	5.1 ± 0.2
PCLMP 5	50	100	2.0	150.1 ±0.12	0.275± 0.41	-18.9 ± 1.5	87.4 ± 1.6	5.5 ± 0.3

5.4.2 Preformulation studies

UV-Visible Spectroscopy: Mangiferin exhibited distinct absorption maxima at 258 nm, which corresponds closely with reported literature values. The calibration curve was constructed by measuring absorbance of mangiferin solutions over a concentration range of 2–20 μg/mL using UV-Visible spectrophotometer at the absorption maximum of 258 nm. The absorbance data used to construct the calibration curve is presented in Table 24.

Table 24: Calibration curve data of mangiferin

Concentration (µg/mL)	*Absorbance (Mean ± SE)*
2	0.081 ± 0.006
4	0.163 ± 0.008
6	0.251 ± 0.009
8	0.332 ± 0.011
10	0.419 ± 0.013
12	0.502 ± 0.014
14	0.591 ± 0.015
16	0.667 ± 0.017
18	0.755 ± 0.018
20	0.839 ± 0.019

The resulting calibration curve demonstrated excellent linearity, with a correlation coefficient (r^2) near unity, confirming adherence to Beer-Lambert's Law within the selected concentration range (Figure 48).

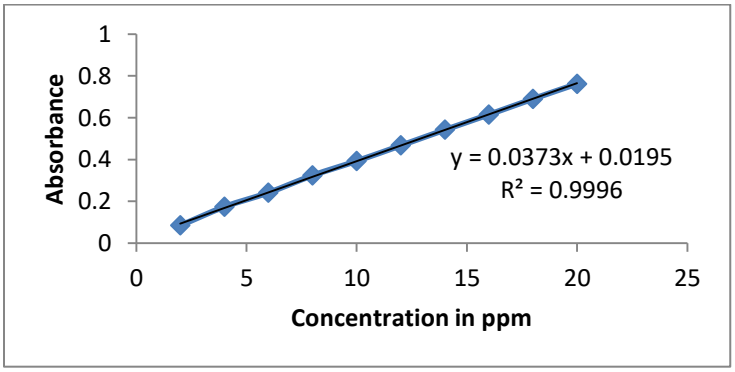

Figure 48: Calibration curve of mangiferin

Solubility Studies: The aqueous solubility of mangiferin was determined to be 24.8±1.1µg/mL, indicating poor water solubility. This low solubility reflects the hydrophobicity of mangiferin, which may pose a challenge in achieving desirable bioavailability through conventional aqueous formulations. Therefore, formulating mangiferin in nanocarrier systems or using solubility enhancement techniques is considered essential for effective therapeutic delivery.

Melting Point Determination: The observed melting point of mangiferin was found to be in the range of 275–278°C, which is in close agreement with values reported in literature. The relatively sharp melting range is indicative of the purity and crystalline nature of the isolated compound.

5.4.3 Characterization of PCLMP Nanoparticles:

The surface morphology of polycaprolactone (PCL) based nanocarriers loaded with mangiferin are depicted in the scanning electron microscopy (SEM) image (Figure 49). The image clearly reveals that the nanoparticles are generally spherical in shape with a smooth surface topology, although some particles display slight surface indentations or irregularities, which may be attributed to drying effects or polymer-film contraction during solidification. The uniform particle size distribution is indicative of a consistent formulation and effective homogenization during the nanoparticle preparation process. These morphological characteristics are critical in influencing the drug release kinetics, flow properties, and surface area of the formulation. The smooth and spherical morphology is likely to promote uniform drug diffusion and may contribute to improved bioavailability of mangiferin upon administration.

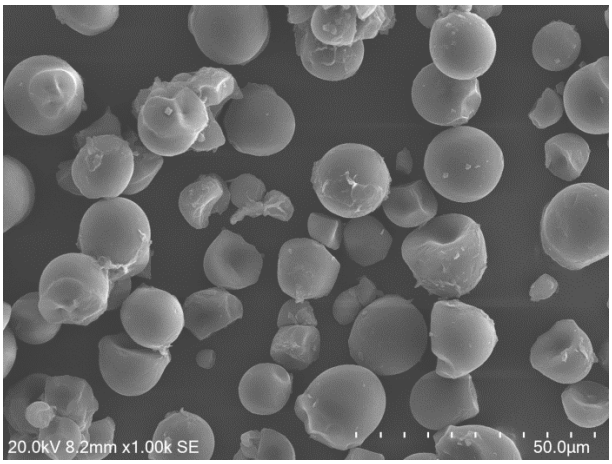

Figure 49: SEM image of PCLMP Nanoparticles

5.4.4 Drug polymer interaction study: Thermal analysis

Thermal analysis TGA and DSC were used to assess the thermal stability, the decomposition profile, and possible interactions between mangiferin and the polymer matrix (Figure 50). A sharp endothermic peak was seen on the curve at about 298°C, confirming the crystalline nature of pure mangiferin and its thermal instability beyond this temperature. The TGA curve of pure mangiferin showed a distinctive single-step major weight loss starting around 280°C to 340°C, which corresponded to its thermal degradation.

The blank PCL nanoparticles, on the other hand, displayed a clear pattern of thermal degradation. First, weight loss was noted at about 60°C to 80°C, which was probably caused by moisture or residual solvent evaporation. Next, a noticeable degradation stage started at about 360°C, which corresponded to the disintegration of the PCL polymer backbone. In accordance with the known melting point of semi-crystalline PCL, the corresponding thermogram displayed a distinct endothermic melting peak at roughly 60°C to 65°C.

The combined thermal characteristics of the drug and polymer were seen in the thermograms of PCL nanoparticles loaded with mangiferin. A significant finding, however, was that the mangiferin loaded nanoparticles curve lacked the distinct endothermic peak of pure mangiferin, which is located at 298°C. This disappearance implies that mangiferin is not in crystalline form but is instead molecularly distributed or contained inside the polymer matrix. Additionally, the thermal curves of the drug-loaded nanoparticles showed no new peaks or notable changes in the decomposition temperatures, suggesting that mangiferin and PCL did not interact chemically or incompatibly. These results validate the effective incorporation of mangiferin in an amorphous or molecularly dispersed state into the PCL nanocarriers (Soppimath et al., 2001; Makadia & Siegel, 2011).

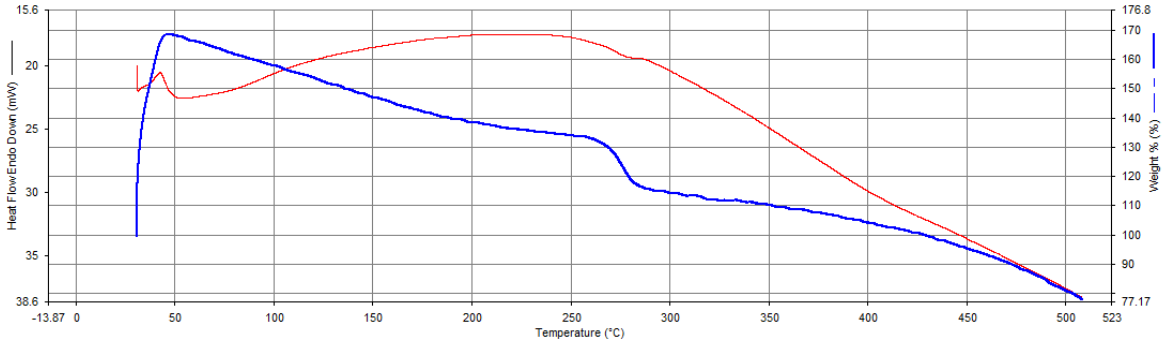

(a)

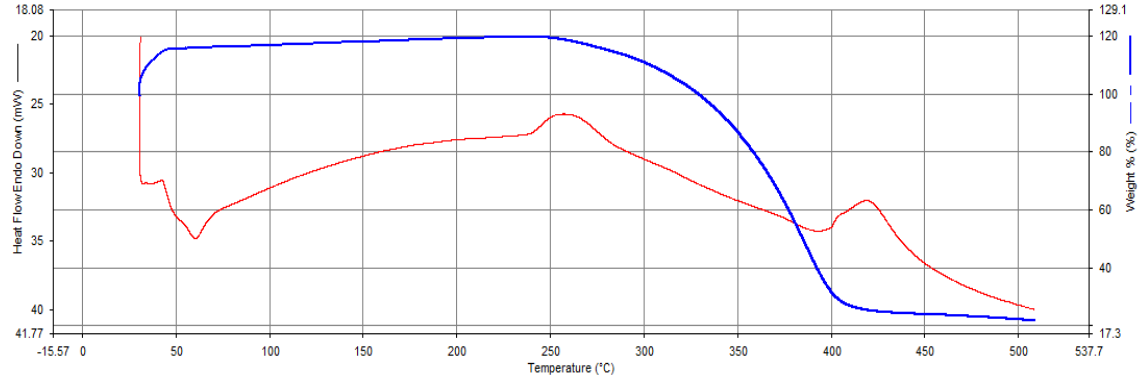

(b)

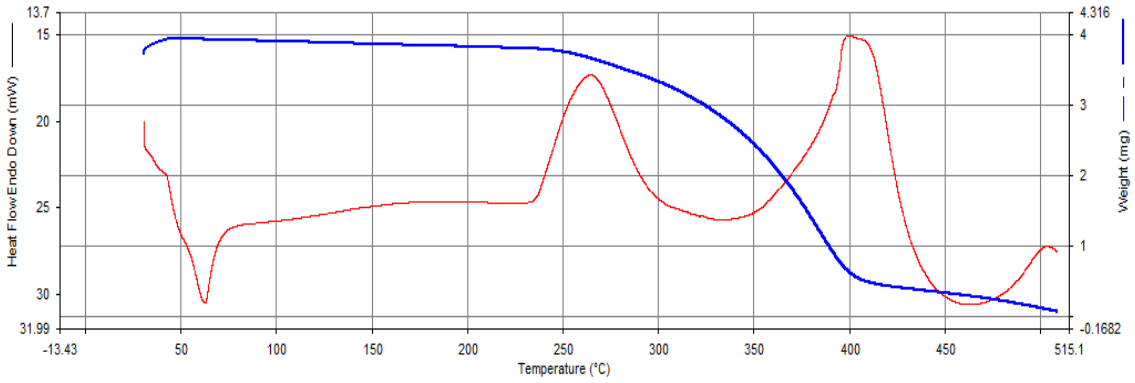

(c)

Figure 50: Thermal analysis curves for (a) Naringin (b) Blank PCLMPs (c) Mangiferin loaded PCLMPs

5.4.5 XRD Analysis:

The X-ray diffraction (XRD) patterns of pure mangiferin, blank polycaprolactone (PCL) nanoparticles, and mangiferin-loaded PCL nanoparticles are depicted in Figure X. The pure mangiferin (green pattern) showed multiple sharp and intense peaks, primarily within the 2θ range of 10°–30°, indicative of its highly crystalline nature. In contrast, the blank PCL nanoparticles (black pattern) exhibited a broad and diffused peak centered around 20°, signifying their semi-crystalline to amorphous character. The mangiferin-loaded PCL nanoparticles (blue pattern) displayed a broad halo with significantly reduced intensity and absence of distinct mangiferin peaks. The sharp diffraction peaks observed in the XRD pattern of pure mangiferin confirm its well-ordered crystalline structure. However, after encapsulation into PCL nanoparticles, these characteristic peaks disappear, suggesting a transition of mangiferin from crystalline to amorphous form. This transformation is likely due to the molecular dispersion of mangiferin within the polymeric matrix during the nanoparticle formulation process. The blank PCL nanoparticles displayed a broad peak typical of the semi-crystalline nature of PCL, indicating the preservation of polymer structure in nanoparticulate form. The mangiferin-loaded nanoparticles exhibited a similar but slightly intensified broad peak, indicating the presence of mangiferin within the matrix but in a non-crystalline, amorphous state. The absence of crystalline peaks corresponding to mangiferin in the drug-loaded nanoparticles confirms successful encapsulation and a possible enhancement in solubility and dissolution due to amorphization. This physical transformation could be advantageous for improving the bioavailability of mangiferin.

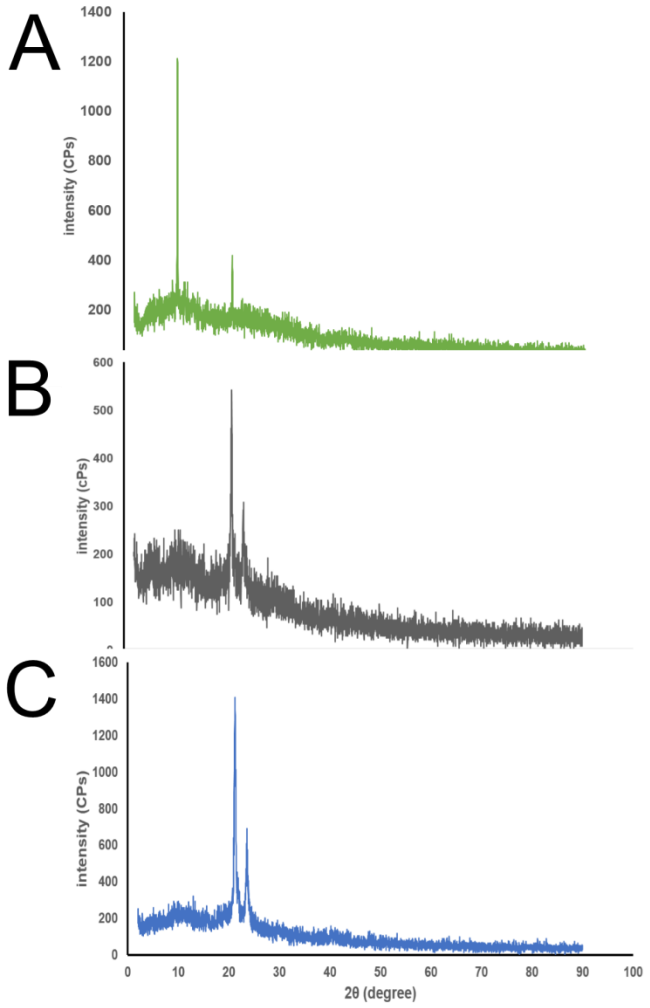

Figure 51: XRD Spectra for (a) Mangiferin (b) Blank PCLMPs (c) Mangiferin loaded PCLMPs

5.4.6 In Vitro Drug Release Study: The *in vitro* drug release profile of mangiferin from polycaprolactone (PCL) nanoparticles was evaluated for all five formulations (PCLMP1–PCLMP5) over a 24-hour period using phosphate-buffered saline (pH 7.4). All formulations exhibited a sustained drug release pattern with varying release rates depending on formulation composition (Figure 52). Initially, a burst release phase was observed within the first 2–4 hours, attributed to the diffusion of the surface-associated drug. This was followed by a more controlled and sustained release phase extending up to 24 hours, which can be ascribed to the gradual degradation of the PCL polymer matrix and diffusion of the encapsulated drug.

Among all formulations, PCLMP5 showed the highest cumulative release of 92% at 24 hours, indicating improved drug release efficiency. This could be due to optimized drug loading and polymer-to-drug ratio in the formulation. PCLMP1 and PCLMP2 also demonstrated substantial release (~87–88%), whereas PCLMP4 exhibited the lowest release profile (~74% at 24 h), suggesting slower drug diffusion possibly due to higher polymer content or denser microsphere matrix.

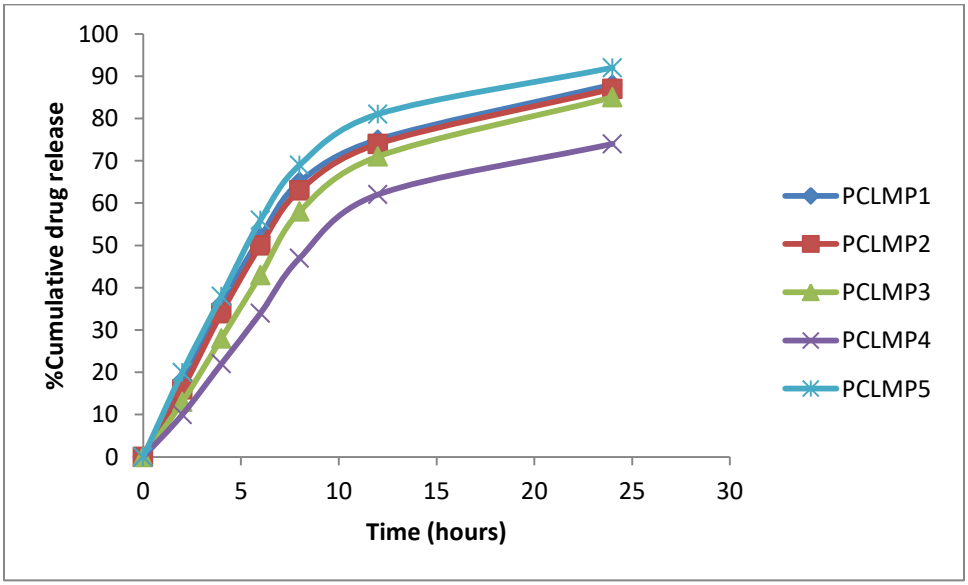

Figure 52: Release study of PCLNP formulations

Several kinetic models, including zero-order, first-order, Higuchi, and Korsmeyer-Peppas equations, were used to examine the in vitro release data of mangiferin from the PCLMP formulations (Table 25). The Korsmeyer–Peppas model yielded the highest R^2 values for all formulations, indicating it best describes the release mechanism. This suggests that the drug release followed a non-Fickian (anomalous) transport mechanism, involving both diffusion and polymer relaxation/erosion. The Higuchi model also showed good linearity ($R^2 > 0.96$), indicating that diffusion is a significant mechanism in the drug release. Lower R^2 values for zero order and moderate for first order imply that constant drug release over time was not achieved, and release rate depended on drug concentration remaining in the matrix.

Table 25: Release kinetics profile for PCLMP formulations

Formulation	*Zero Order (R^2)*	*First Order (R^2)*	*Higuchi Model (R^2)*	*Korsmeyer–Peppas (R^2)*
PCLMP1	0.938	0.981	0.987	0.990
PCLMP2	0.925	0.976	0.981	0.985
PCLMP3	0.912	0.963	0.975	0.981
PCLMP4	0.904	0.951	0.968	0.975
PCLMP5	0.945	0.985	0.991	0.995

5.4.7 In vivo antidiabetic and hypolipidemic studies

Blood glucose levels in several treated animal groups were measured in order to examine the in vivo hypoglycemic reactions of mangiferin loaded PCL nanoparticles (Imran et al., 2017; Zhang et al., 2020, Muruganandan etal., 2005). Every seven days, fasting blood glucose (FBG) levels were measured (Parasuraman et al., 2010). Both free and mangiferin loaded PCL nanoparticles were given to the diabetic animals. Mangiferin dose in the nanoparticle formulation and free drug-treated animal groups were comparable, with the nanoparticle formulation maintaining a dose of 10 mg/kg of mangiferin.

STZ treatment resulted in blood glucose levels in the diabetic control group exceeding 250 mg/dL. When given orally to STZ-induced diabetic rats for 28 days, free mangiferin (10 mg/kg b.w) and PCLMPs (10 mg/kg b.w) caused considerable hypoglycemic action ($p<0.05$) in comparison to diabetic control group. Interestingly, as Figure 53 illustrates, the hypoglycemic effect of mangiferin loaded nanoparticles was noticeably stronger than that of free mangiferin ($p < 0.05$). Group 5 administered with blank nanoparticles did not significantly lower their FBG levels ($p > 0.05$), ruling out the possibility that the nanocarrier had any hypoglycemic effects. The modified release profile of mangiferin from the nanoparticles may be the cause of the noticeably better glycemic control that PCLMPs provided in STZ-induced diabetic rats.

Rats treated with STZ showed significantly higher serum lipid concentrations of triglycerides, total cholesterol, and LDL cholesterol than normal control rats (Ananthan et al., 2003; Srinivasan et al., 2005). Serum triglyceride, total cholesterol, and LDL cholesterol levels significantly decreased after treatment with mangiferin and mangiferin

loaded PCL nanoparticles as compared to diabetic control group, respectively ($p < 0.05$). Importantly, diabetic rats given PCLMPs showed a significant decrease in serum triglyceride, total cholesterol, and LDL cholesterol levels in comparison to free mangiferin ($p < 0.05$) (Figure 54).

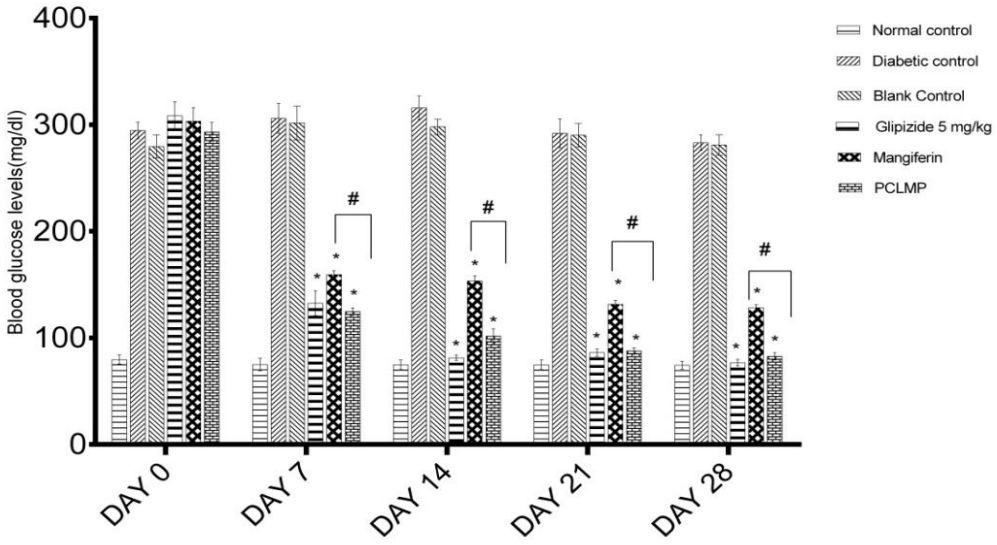

Figure 53: Effect of the hypoglycemic response in the different treatment groups. The data were presented as mean ± standard error of the mean (SEM) (n = 6). (: $p < 0.05$, compared with diabetic control; #: $p < 0.05$, comparison between free mangiferin and PCLMP group).*

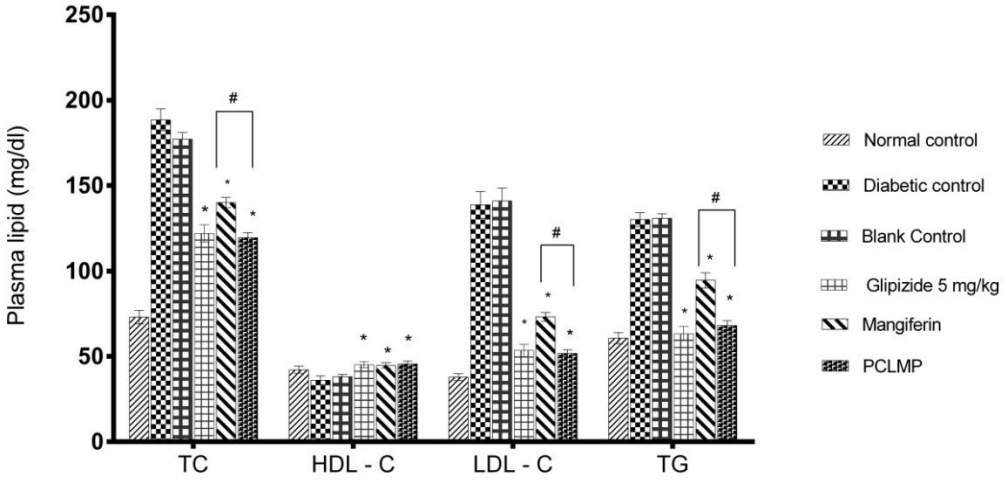

Figure 54: Effect of the hypolipidemic response in the different treatment groups. The data were presented as mean ± standard error of the mean (SEM) (n = 6). (: $p < 0.05$, compared with diabetic control; #: $p < 0.05$, comparison between free mangiferin and PCLMP group).*

Section C: Metal-Based Nanocarriers

5.5. Formulation and Characterization of Ellagic Acid Loaded Silver Nanoparticles

5.5.1 Formulation and optimization

The current study focuses on the formulation and optimization of silver nanoparticles (AgNPs) encapsulating Ellagic Acid (EA), using varying concentrations of silver nitrate and a stabilizing agent, DDAB (didodecyldimethylammonium bromide). The reducing agent, ascorbic acid, was maintained constant at 0.5 M across all formulations, with ellagic acid (50 mg). The formulation codes AGN1 through AGN5 varied primarily in terms of the silver nitrate concentration (ranging from 0.1 M to 2 M) and the DDAB concentration (0.1 M or 0.2 M).

Silver nitrate acts as the precursor for silver nanoparticle synthesis. In formulations with lower silver nitrate concentrations (AGN1–AGN3), the nanoparticle formation is expected to be more controlled, yielding smaller and more uniformly dispersed particles. This is supported by Sharma et al. (2009), who reported that lower silver ion concentrations limit excessive nucleation, resulting in better particle size control and minimizing aggregation. On the other hand, higher silver nitrate concentrations (1 M and 2 M in AGN4 and AGN5, respectively) may lead to rapid and extensive nucleation, potentially causing polydispersity and particle aggregation if not adequately stabilized (Pal et al., 2007).

Ascorbic acid, kept at 0.5 M in all formulations, serves as a mild and eco-friendly reducing agent that facilitates the reduction of Ag^{+} to metallic silver (Ag^{0}). According to Hebbalalu et al. (2013), higher concentrations of ascorbic acid accelerate reduction rates and can lead to smaller nanoparticle sizes; however, since its concentration was constant in this study, it does not contribute to the variation in nanoparticle characteristics. Ellagic acid, a naturally occurring polyphenol known for its antioxidant and anticancer properties, was included at a consistent dose across all formulations. It may also function as a surface-active compound, enhancing both the therapeutic efficacy and interaction with the AgNP matrix (Al Zahrani & El-Sayed, 2018).

The stabilizer, DDAB, plays a critical role in ensuring nanoparticle stability by preventing agglomeration. In AGN1 to AGN3, a 0.1 M concentration of DDAB is likely sufficient to maintain stability at lower silver nitrate levels. However, in AGN4 and

AGN5, where silver nitrate concentration is higher, the increased DDAB (0.2 M) likely compensates for the elevated ionic strength and helps prevent aggregation. This approach is supported by Ahamed et al. (2010), who demonstrated that higher concentrations of surfactants improve nanoparticle stability and reduce polydispersity.

From an optimization standpoint, formulations AGN2 (0.25 M $AgNO_3$) and AGN3 (0.5 M $AgNO_3$) are considered optimal. These formulations strike a balance between sufficient silver ion availability for nanoparticle formation and stabilization by DDAB. They are also expected to yield particles with acceptable size distribution, low polydispersity, and good colloidal stability. AGN4 and AGN5, while more concentrated, may result in larger or more aggregated particles unless subjected to additional stabilization techniques (Table 26).

Table 26: Formulation and optimization table for silver nanoparticles of ellagic acid

SL NO.	*Formulation code*	*Conc. of silver nitrate*	*Conc. Of ascorbic acid*	*Conc. of Ellagic acid*	*Conc. of stabilizing agent (DDAB)*
1	AGN1	0.1M	0.5 M	50mg	0.1 M
2	AGN2	0.25 M	0.5 M	50mg	0.1 M
3	AGN3	0.5 M	0.5 M	50mg	0.1 M
4	AGN4	1 M	0.5 M	50mg	0.2 M
5	AGN5	2 M	0.5 M	50mg	0.2 M

5.5.2 Preformulation studies

UV-Visible Spectrophotometry: Ellagic acid exhibited an absorption maximum (λmax) at 254 nm, consistent with previously reported literature values. A calibration curve was constructed by measuring the absorbance of ellagic acid solutions over the concentration range of 2–20 µg/mL using a UV-Visible spectrophotometer at the determined λmax of 254 nm (Table 27).

Table 27: Calibration curve data for ellagic acid

Concentration (µg/mL)	*Mean Absorbance (± SE)*
2	0.085 ± 0.003
4	0.164 ± 0.004
6	0.242 ± 0.005
8	0.314 ± 0.006
10	0.393 ± 0.005
12	0.467 ± 0.004
14	0.542 ± 0.006
16	0.615 ± 0.005
18	0.690 ± 0.004
20	0.762 ± 0.005

The calibration curve demonstrated good linearity, with a correlation coefficient (r^2 = 0.996), confirming adherence to Beer-Lambert's law within the tested range. The linear response supports the reliability of this method for quantitative analysis of ellagic acid in further formulation studies.

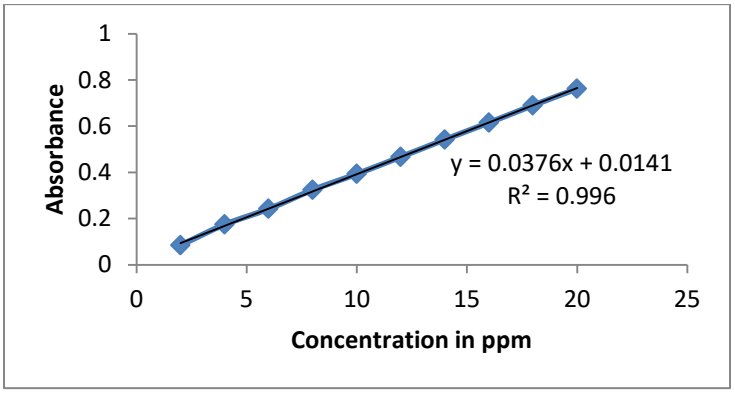

Figure 55: Calibration curve of ellagic acid

Solubility Studies: The aqueous solubility of ellagic acid was determined to be 9.8±0.7µg/mL, which confirms its poor water solubility. This limited solubility is attributed to its polyphenolic structure and high crystallinity, making it a hydrophobic compound. Such solubility characteristics suggest the need for specialized formulation strategies such as nanoencapsulation or use of solubility enhancers to improve its bioavailability in pharmaceutical applications.

Melting Point Determination: The experimentally determined melting point of ellagic acid was found to be in the range of 350–352°C, aligning well with established literature values. The sharp and narrow melting point range indicates the high purity and crystalline nature of the compound. The consistency of the melting point with reported values further validates the identity of the ellagic acid.

5.5.3 Drug polymer interaction study: Thermal analysis

The Differential Scanning Calorimetry (DSC) thermogram of pure ellagic acid (EA) displayed a sharp endothermic peak at 126°C, corresponding to the drug's melting point and onset of thermal decomposition, consistent with previously reported data (González-Sarrías et al., 2017). A distinct exothermic peak at 280°C was also observed, potentially linked to oxidative decomposition or thermal rearrangement of the phenolic moieties in ellagic acid. Additionally, two smaller endothermic peaks at 455°C and 960°C were noted, which may be attributed to melting and thermal transitions of metallic silver present in the system (Zhang et al., 2016).

Interestingly, in the DSC thermogram of the EA-loaded silver nanoparticles, the characteristic melting peak of ellagic acid at 126°C was absent, suggesting that the drug was no longer in its crystalline state. This disappearance of the sharp melting endotherm indicates successful incorporation of EA into the nanoparticle matrix, likely in an amorphous or molecularly dispersed form within the carrier system (Mishra et al., 2022). Furthermore, the high-temperature thermal events observed for metallic silver support the thermal stability of the nanoparticulate system, as no significant degradation was detected at physiologically relevant temperatures. The overall thermal behavior of the formulation confirms that EA was efficiently encapsulated into the silver nanoparticles, with no significant drug-polymer or drug-metal interactions altering its thermal profile. The data further suggest enhanced thermal stability of the incorporated EA in the nanoparticle formulation, which is a desirable characteristic for pharmaceutical applications (Salatin et al., 2015).

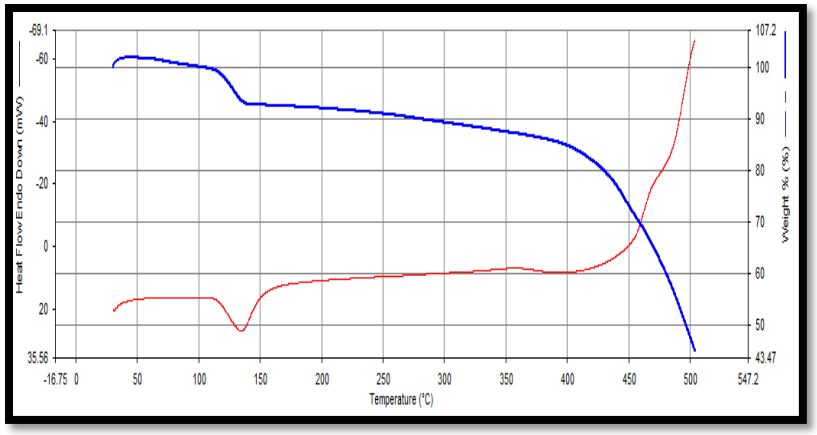

Figure 56 (a): Thermal curves of Ellagic Acid

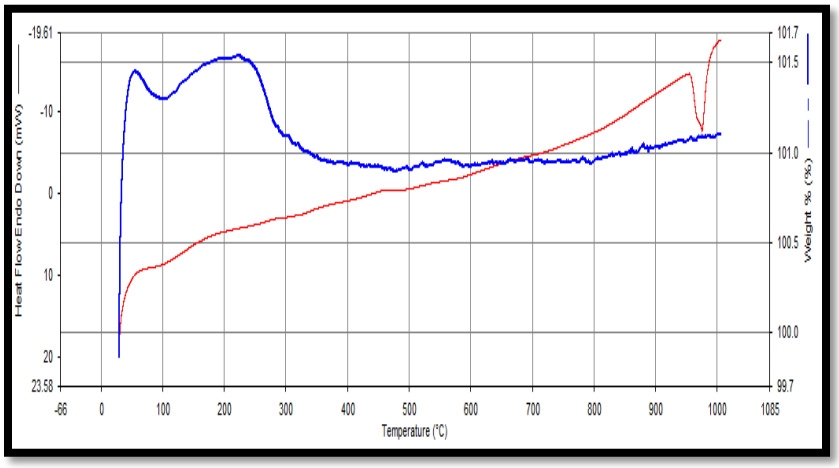

Figure 56 (b): Thermal curves of blank silver nanoparticles

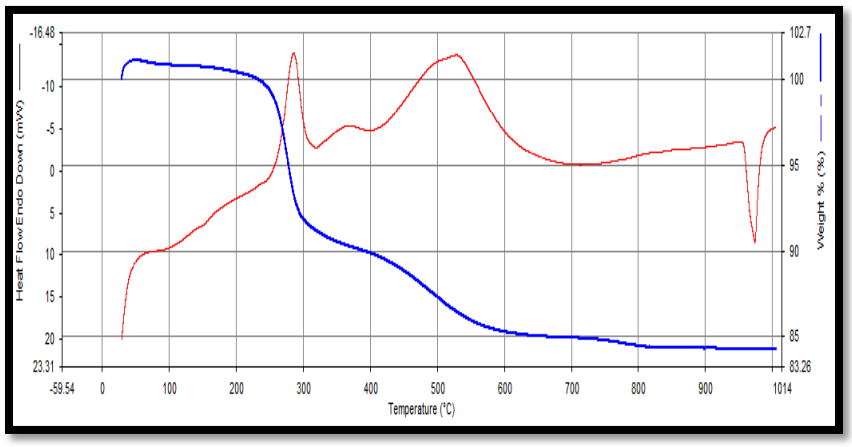

Figure 56 (c): Thermal curves of silver nanoparticles of ellagic acid

5.5.4 FTIR Study: FTIR spectrum of silver nanoparticles exhibited several prominent peaks at 3432.94, 2927, 1669, and 1383 cm^{-1}, indicating the presence of key functional groups associated with the nanoparticle structure. The sharp absorption band at 3432.94 cm^{-1} corresponds to N–H stretching vibrations, typically arising from residual amine or proteinaceous capping agents. The peak at 1669 cm^{-1} was attributed to the stretching vibration of amide (NH) C=O groups, while the 1383 cm^{-1} band was related to C–C and C–N stretching, commonly observed in organic stabilizing agents. Additionally, the 2927 cm^{-1} peak indicates C–H stretching, including contributions from methoxy groups or hydrocarbon chains present in the synthesis medium (Javed et al., 2020; Zhang et al., 2016).

The FTIR spectrum of the ellagic acid-loaded silver nanoparticles demonstrated the retention of key characteristic peaks of ellagic acid—notably, O–H and C=O stretching bands—as well as the functional group peaks of the silver nanoparticles. The simultaneous presence of these spectral features in the formulation suggests that ellagic acid was successfully incorporated into the silver nanoparticles without causing significant changes to its molecular structure or disrupting the nanoparticle matrix. This lack of peak shifting or disappearance indicates the absence of strong chemical interactions between the drug and the silver matrix, implying that the encapsulation occurred via physical entrapment or surface adsorption (Mishra et al., 2022; Salatin et al., 2015).

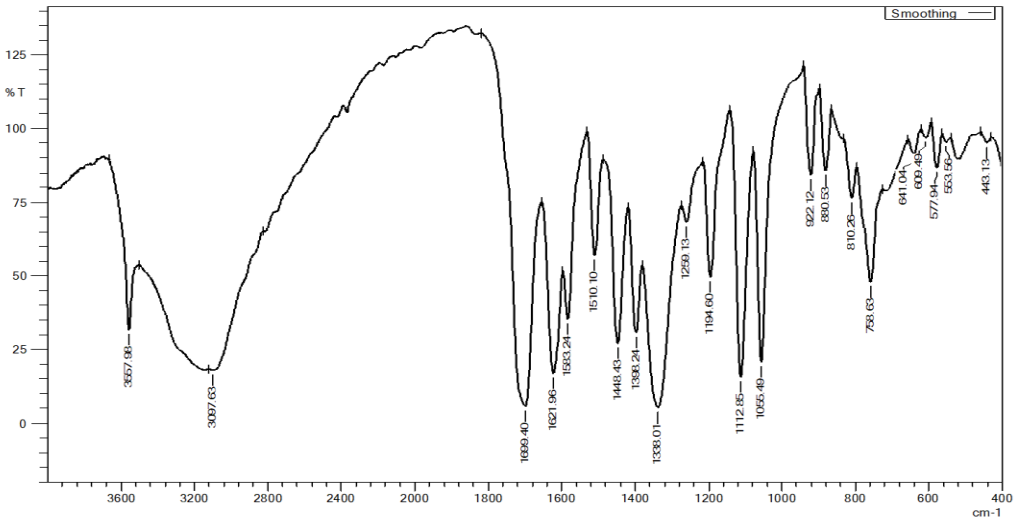

Figure 57 (a): FTIR Spectra of Ellagic acid

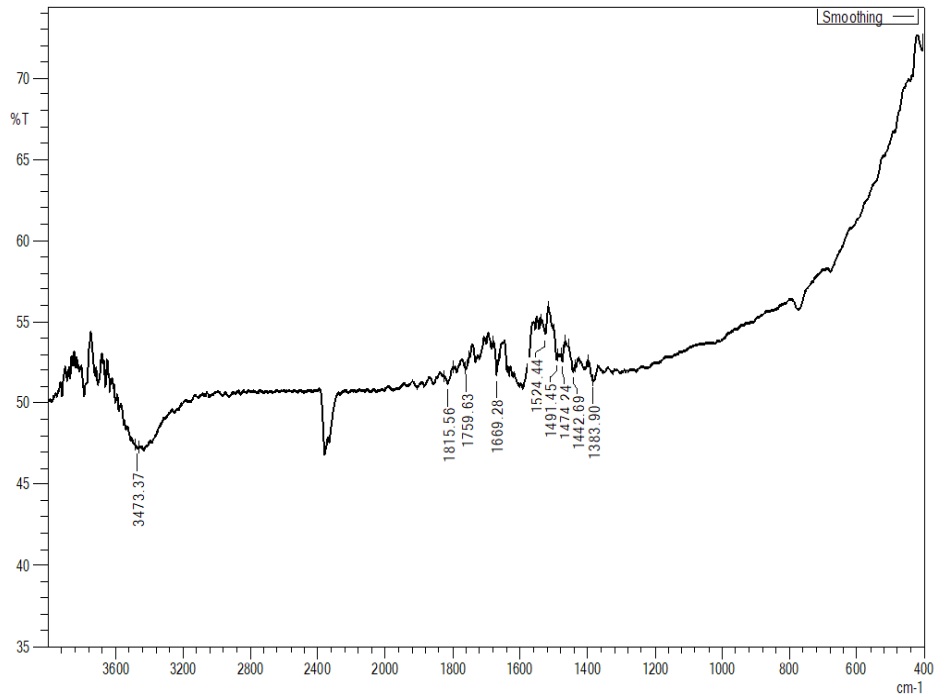

Figure 57 (b): FTIR Spectra of Blank formulation

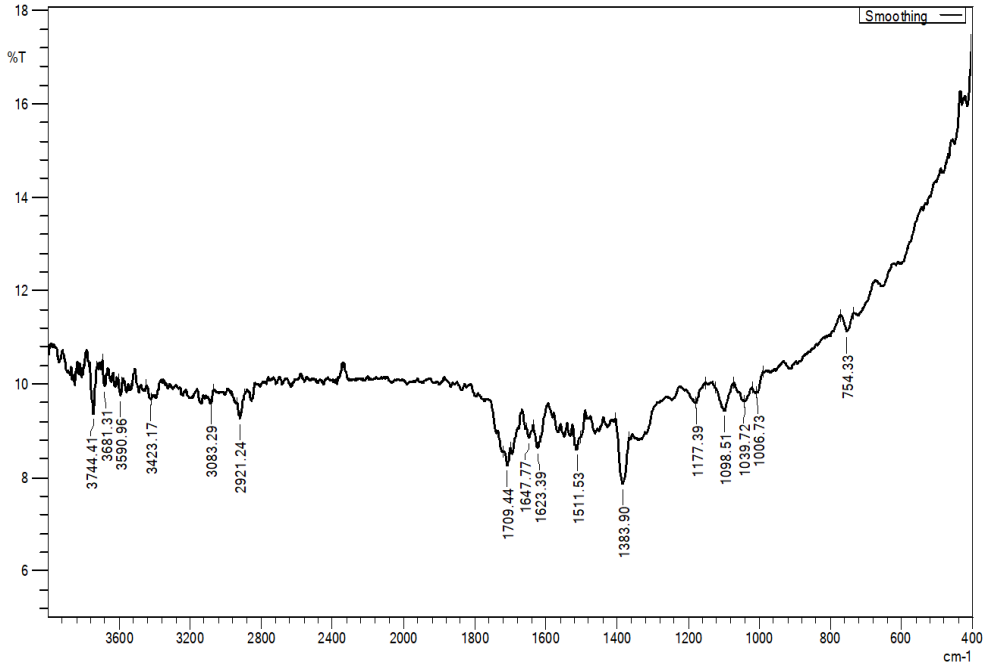

Figure 57 (c): FTIR Spectra of Silver Nanoformulation

5.5.5 Characterization of silver nanoparticles of ellagic acid

The physicochemical characterization of ellagic acid-loaded silver nanoparticles was carried out by analyzing entrapment efficiency (EE%), particle size, and zeta potential for all five formulations (AGN1 to AGN5). Among the batches, AGN3 exhibited the highest entrapment efficiency (95.66%), which may be attributed to the optimal balance between silver nitrate and ascorbic acid concentrations, facilitating maximum drug encapsulation. AGN2 and AGN1 also showed high EE% values of 90.81% and 85.26%, respectively. Conversely, a significant drop in EE% was observed for AGN5 (60.65%), likely due to the excessive concentration of silver nitrate (2 M), which may have resulted in faster nucleation and less efficient drug entrapment (Mishra et al., 2022) (Table 28).

In terms of particle size, AGN5 showed the smallest average particle size of 105.21 nm, while AGN2 had the largest size at 250.31 nm. Notably, AGN3 and AGN4 presented favorable particle sizes of 155.7 nm and 130.54 nm, respectively, which fall within the ideal nanometric range for enhanced cellular uptake and controlled release (Salatin et al., 2015). Zeta potential analysis revealed values ranging from -22.2 mV to -42.8 mV, with AGN5 displaying the most negative zeta potential (-42.8 mV), suggesting superior colloidal stability due to increased electrostatic repulsion among particles. Zeta potentials more negative than -30 mV are generally considered stable (Zhang et al., 2016). Although AGN3 showed a slightly less negative zeta potential (-22.2 mV), it maintained a high EE% and acceptable particle size, making it a promising candidate for further optimization. Overall, the results indicate that AGN3 provides the most favorable balance between high drug entrapment, nanoscale particle size, and moderate stability, making it the most suitable formulation for drug delivery applications.

Table 28: Characterization of silver nanoparticles of ellagic acid

Formulation code	*Entrapment efficiency (%)*	*Particle Size (nm)*	*Zeta Potential (mV)*
AGN 1	85.26	202.6	-25.4
AGN 2	90.81	250.31	-35.1
AGN 3	95.66	155.7	-22.2
AGN 4	82.47	130.54	-35.4
AGN 5	60.65	105.21	-42.8

5.5.6 In vitro release study

The in vitro drug release profile of selected ellagic acid-loaded silver nanoparticle formulations (AGN2, AGN3, and AGN4) was assessed using the dialysis bag diffusion method over a period of 24 hours (Figure 58). All three formulations exhibited a biphasic release pattern, characterized by an initial burst release of approximately 15% within the first 2 hours, followed by a sustained and controlled release extending up to 24 hours. This burst release can be attributed to drug molecules adsorbed on or near the surface of the nanoparticles, which readily diffuse out upon hydration (Mishra et al., 2022).

Formulation AGN2 showed the highest cumulative drug release (~80%) at the 24-hour mark, closely followed by AGN3 and AGN4, indicating consistent drug release behavior among the formulations. The sustained release phase post 6 hours suggests successful encapsulation of ellagic acid within the nanoparticle matrix, allowing gradual diffusion of the drug over time. Such controlled release behavior is beneficial for maintaining therapeutic drug levels for extended durations while minimizing dosing frequency and systemic toxicity (Salatin et al., 2015). These findings support the potential utility of silver nanoparticle-based drug delivery systems for enhancing the bioavailability and therapeutic efficacy of poorly soluble phytochemicals like ellagic acid, especially in targeting chronic or prolonged disease conditions (Zhang et al., 2016).

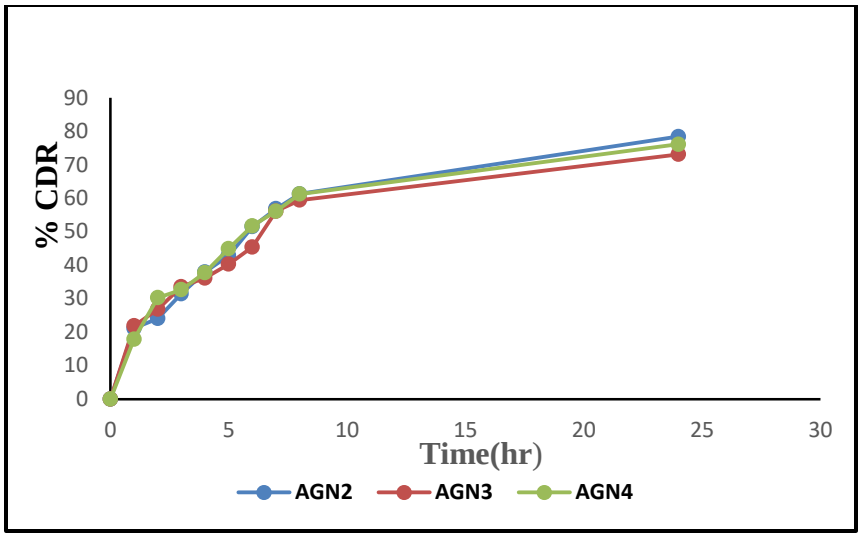

Figure 58: In vitro cumulative drug release profile (%) of AGN2, AGN3, and AGN4 formulations across dialysis membrane over 24 hours.

To understand the release mechanisms of ellagic acid from silver nanoparticles, the release data of formulations AGN2, AGN3, and AGN4 were fitted to various kinetic models—Zero-order, First-order, Higuchi, Hixson–Crowell, and Korsmeyer–Peppas (Table 29). Among all models, the Higuchi model exhibited the highest correlation coefficient (R^2) values for all formulations (AGN2: 0.960, AGN3: 0.982, AGN4: 0.978), indicating that the release of ellagic acid is predominantly diffusion-controlled (Costa & Sousa Lobo, 2001). The Korsmeyer–Peppas model also demonstrated a good fit ($R^2 > 0.94$), with release exponent (n) values below 0.5 for all formulations (AGN2: 0.441, AGN3: 0.419, AGN4: 0.470), which further confirms that the drug release follows Fickian diffusion behavior (Korsmeyer et al., 1983). First-order kinetics also showed a moderately good fit, especially for AGN2 ($R^2 = 0.888$), suggesting a concentration-dependent release profile. The comparatively lower R^2 values for Zero-order and Hixson–Crowell models indicate that constant rate release and erosion-dependent mechanisms were not the primary modes of drug release. Thus, the overall analysis suggests that Higuchi diffusion is the dominant release mechanism, and the formulations exhibit controlled release via diffusion through the nanoparticle matrix.

Table 29: Release kinetics profile for various formulations

Formulation Code	*Zero order*	*First order*	*Higuchi model*	*Hixson-Crowell model*	*Korsmeyer Peppas model*	
	R^2	R^2	R^2	R^2	R^2	n
AGN2	0.709	0.888	0.960	0.834	0.941	0.441
AGN3	0.684	0.840	0.982	0.792	0.946	0.419
AGN4	0.676	0.854	0.978	0.798	0.941	0.470

5.5.7 Antioxidant activity

The antioxidant potential of ellagic acid-loaded silver nanoparticles (AGN1–AGN6) was assessed using the 2,2-diphenyl-1-picrylhydrazyl (DPPH) free radical scavenging assay. This colorimetric method is widely recognized for its simplicity, reproducibility, and effectiveness in measuring the free radical scavenging ability of both pure compounds and nanoparticle-based formulations. Free ellagic acid served as the control for comparison. All test samples, including free ellagic acid and nanoparticle formulations, were evaluated at concentrations of 5, 10, 20, and 40 µg/mL. The extent of radical scavenging activity was determined by measuring the decrease in absorbance at 517 nm after incubation with DPPH in the dark for 30 minutes. The results, expressed as mean ± standard deviation (n=3), revealed a concentration-dependent increase in DPPH inhibition across all formulations (Table 30).

Among the nanoparticle batches, AGN5 and AGN6 demonstrated superior antioxidant activity, closely approximating the free ellagic acid at higher concentrations. At 40 µg/mL, AGN5 showed a maximum % inhibition of over 85%, suggesting efficient retention and release of the active antioxidant moiety. This enhanced activity can be attributed to improved solubility and stability of ellagic acid when encapsulated in the nanosilver matrix, which may facilitate better interaction with free radicals. Furthermore, the antioxidant activity of nanoparticle formulations was consistently higher than that of the lower-concentration free ellagic acid, particularly at 10 and 20 µg/mL, highlighting the improved biofunctional profile offered by nanoparticulate delivery systems (Kumari et al., 2021). The results validate the potential of silver nanoparticles as a promising carrier system for ellagic acid in antioxidant therapy.

Table 30: Percent inhibition of various AGN formulations against free ellagic acid

Sample	*% Inhibition at 5 µg/mL*	*% Inhibition at 10 µg/mL*	*% Inhibition at 20 µg/mL*	*% Inhibition at 40 µg/mL*
Ellagic Acid	12.8 ± 1.5	20.3 ± 1.8	29.5 ± 2.1	41.1 ± 1.7
AGN1	21.5 ± 1.2	42.4 ± 1.4	60.7 ± 2.0	78.2 ± 1.9
AGN2	24.2 ± 1.3	45.1 ± 1.5	65.0 ± 1.8	80.3 ± 2.0
AGN3	26.9 ± 1.0	49.3 ± 1.6	68.8 ± 1.9	82.6 ± 1.5
AGN4	29.5 ± 1.1	52.7 ± 1.4	71.2 ± 1.7	84.0 ± 1.8
AGN5	30.7 ± 1.2	55.8 ± 1.3	74.6 ± 1.6	87.4 ± 1.4
AGN6	31.9 ± 1.1	56.5 ± 1.5	75.3 ± 1.9	88.0 ± 1.6

The IC_{50} value of free ellagic acid was found to be 15.2 µg/mL, confirming its strong radical scavenging capacity. Among the nanoparticle formulations, AGN6 demonstrated the lowest IC_{50} (5.4 µg/mL), followed by AGN5 (6.8 µg/mL), indicating superior antioxidant potential due to improved dispersion and surface interaction of ellagic acid with DPPH radicals. Formulations AGN1 and AGN2 exhibited higher IC_{50} values (9.3 and 10.7 µg/mL respectively), suggesting less efficient radical quenching, possibly due to suboptimal drug loading or slower release kinetics.

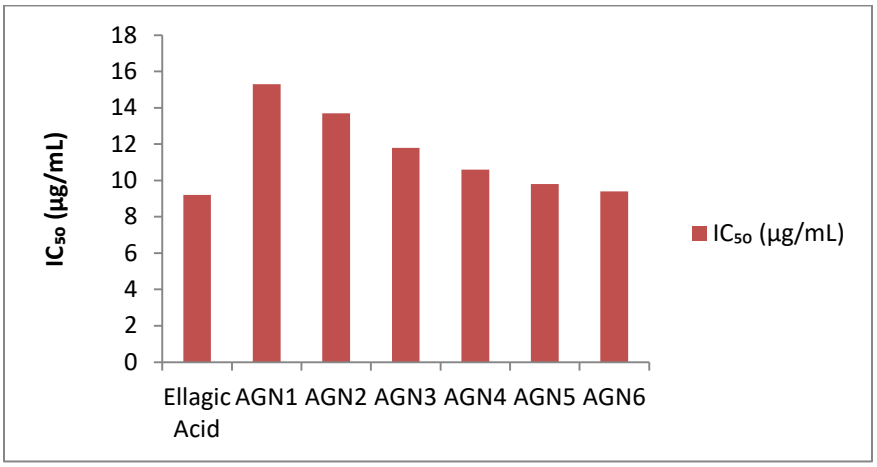

Figure 59: IC_{50} comparison of AGN formulations with free ellagic acid suspension

5.6. Formulation and Characterization of Mangiferin Loaded Silver Nanoparticles

5.6.1 Formulation and optimization

Mangiferin-loaded silver nanoparticles (MSN) were developed using the chemical reduction approach by methodically altering the concentration of silver nitrate while maintaining the same values for the other formulation parameters. This method was chosen to determine the manner in which the concentration of silver ions affected the size, stability, and drug entrapment of nanoparticles. 50 mg of mangiferin was used in the preparation of each formulation. Mangiferin functioned as a mild capping agent in addition to being the active medicinal ingredient. Polyvinylpyrrolidone (PVP) was used as a stabilizer to stop particle aggregation during synthesis, and sodium borohydride ($NaBH_4$) was employed as a potent reducing agent to speed up the conversion of Ag^+ ions from silver nitrate ($AgNO_3$) to elemental silver (Ag^0).

In order to regulate the nucleation and development rate of nanoparticles, the concentration of $AgNO_3$ was gradually raised from 0.5 mM in MSN1 to 1.5 mM in MSN5. While 0.1% w/v PVP preserved colloidal stability throughout the process, the consistent use of 2.0 mM $NaBH_4$ gave uniform and thorough reduction throughout all batches. Formulation pH was adjusted to neutral (around 7.0), which is ideal for the stability of the nanoparticles and the integrity of the mangiferin. To guarantee uniform distribution, all reactions were carried out for 30 minutes at 50°C under carefully monitored heat conditions while being constantly stirred. The rationale was to investigate how varying silver content affects the physicochemical and drug release properties of the nanoparticles. As observed in characterization data, increasing silver ion concentration generally resulted in reduced particle size, improved zeta potential, and enhanced drug loading (Table 31). Overall, the formulation strategy employed for MSN1–MSN5 demonstrates a successful and reproducible method for producing stable mangiferin-loaded silver nanoparticles with properties suitable for controlled drug delivery applications (Anandalakshmi et al., 2016, Patra et al., 2018).

Table 31: Formulation and optimization table for silver nanoparticles of mangiferin

Formulation Code	*Mangiferin (mg)*	*Silver Nitrate ($AgNO_3$, mM)*	*Reducing Agent ($NaBH_4$, mM)*	*Stabilizer (PVP, % w/v)*
MSN1	50	0.5	2.0	0.1
MSN2	50	0.75	2.0	0.1
MSN3	50	1.0	2.0	0.1
MSN4	50	1.25	2.0	0.1
MSN5	50	1.5	2.0	0.1

5.6.2 Drug polymer interaction study: Thermal analysis

The physical stability, decomposition behavior, and possible drug-excipient interactions within nanoparticulate systems are all significantly revealed by thermal analysis. The thermal behavior of pure mangiferin, drug-free silver nanoparticles (blank AgNPs), and mangiferin-loaded silver nanoparticles was assessed and compared in this work using TGA and DSC. TGA thermogram of pure mangiferin showed a notable weight loss beginning at about 250°C and continuing until 320°C, which is when the molecule began to thermally decompose. Because metallic silver is inert and non-volatile, it has a well-established high thermal stability. The TGA profile of mangiferin-loaded silver nanoparticles showed two different phases of weight loss: a secondary slow loss (~15–20%) between 250°C and 350°C, and an initial modest loss (~2–3%) below 150°C because of the evaporation of bound water. The successful loading of mangiferin into the nanoparticulate matrix is indicated by the thermal event falling within this range, which is similar to the decomposition pattern of pure mangiferin.

However, the lack of any extra or repositioned degradation peaks indicates that mangiferin and the silver nanoparticle core did not interact chemically or form a covalent link. A prominent endothermic peak at about 310°C was visible in the thermogram of pure mangiferin, which was linked to its melting and deterioration. The presence of mangiferin in the nanoparticle formulation was confirmed by the observation of a comparable but somewhat enlarged endothermic event in within the same temperature range (300–320°C). Notably, they showed no additional endothermic or exothermic transitions, confirming that no significant physicochemical interactions occurred throughout the formation process and that mangiferin maintained its native thermal properties upon nanoparticle

integration. Together, these results imply that mangiferin was not subjected to chemical conjugation but rather was physically stuck or adsorbed onto the surface of the silver nanoparticle.

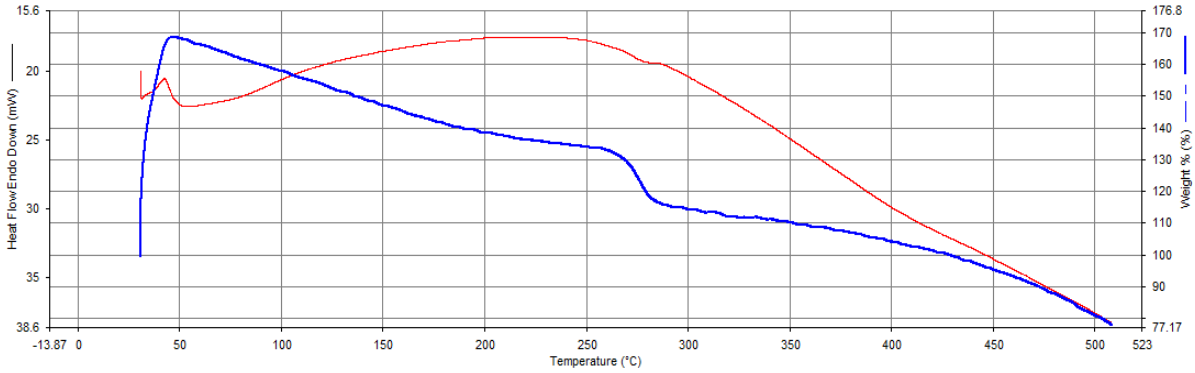

Figure 60 (a): Thermal curves of (a) mangiferin

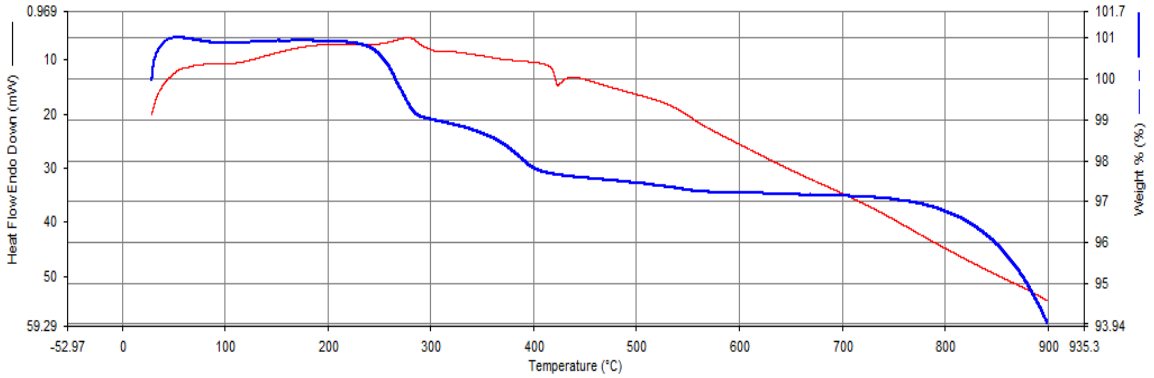

Figure 60 (b): Thermal curves of (b) silver nanoparticles without mangiferin

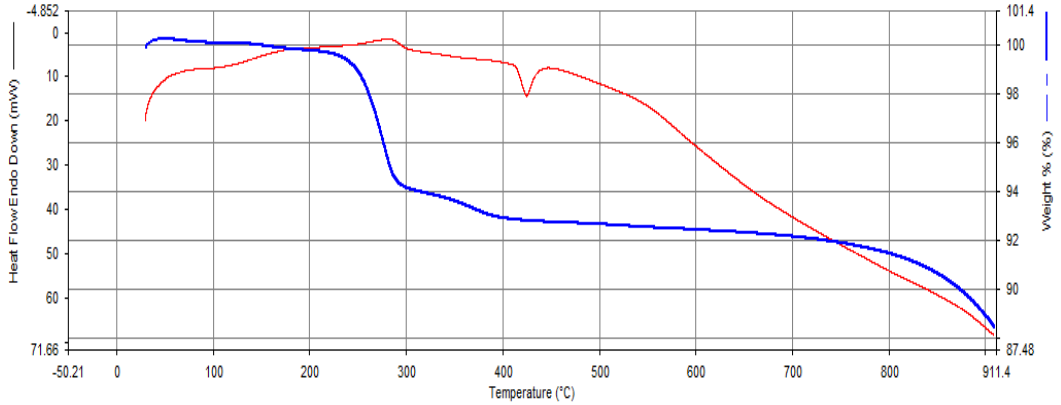

Figure 60 (c): Thermal curves of (c) mangiferin loaded silver nanoparticles

5.6.3 XRD Study:

X-ray diffraction (XRD) analysis was performed to investigate the crystalline nature and structural characteristics of the synthesized mangiferin-loaded silver nanoparticles. The XRD pattern of MSN exhibited distinct and sharp diffraction peaks, indicating the crystalline nature of the silver nanoparticles. Prominent Bragg reflections were observed at 2θ values around 38.1°, 44.3°, 64.5°, and 77.4°, corresponding to the crystal planes of silver, respectively.

No additional peaks attributable to silver oxide or other impurities were detected, confirming the phase purity of the synthesized nanoparticles. A slight broadening of the diffraction peaks were noted, which can be attributed to the nanoscale size of the particles and lattice strain. Furthermore, the absence of any new crystalline peaks corresponding to mangiferin indicates that the drug is either amorphous or molecularly dispersed within or on the surface of the nanoparticles.

This suggests that mangiferin does not alter the crystalline structure of silver upon loading and remains physically adsorbed rather than chemically integrated into the lattice. Overall, the XRD analysis confirmed the crystalline nature, phase purity, and nanoscale dimension of the synthesized MSN nanoparticles, supporting their successful formulation through the chemical reduction method making the formulation suitable for further pharmaceutical or biomedical applications.

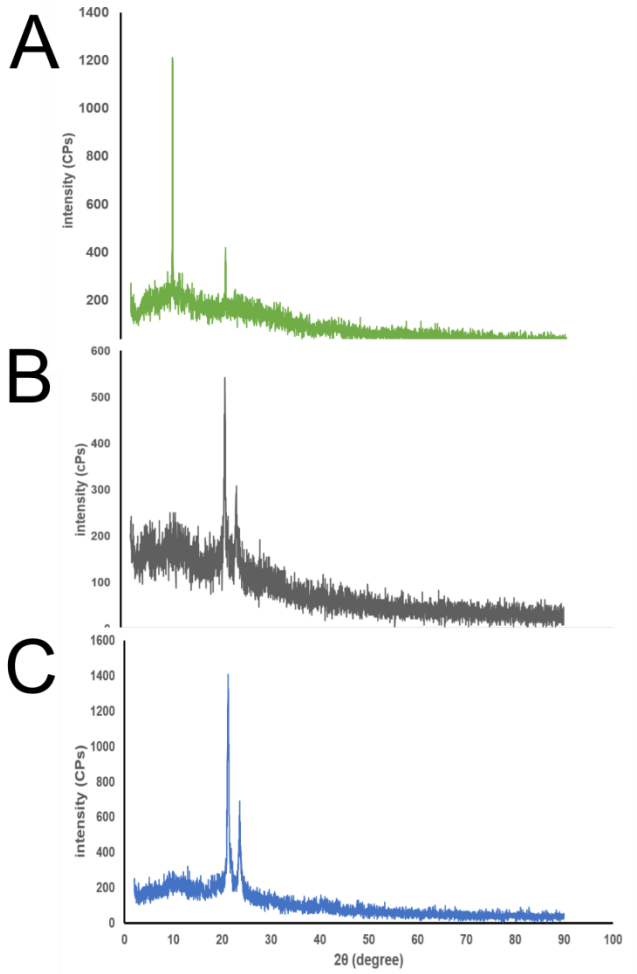

Figure 61 (a): XRD Spectra of (a) mangiferin (b)XRD Spectra of (b) silver nanoparticles without mangiferin (c) XRD Spectra of (c) mangiferin loaded silver nanoparticles

5.6.4 Characterization of silver nanoparticles of mangiferin

Mangiferin-loaded silver nanoparticles (MSNs) were successfully synthesized using chemical reduction method. Particle size and PDI clearly decreased as the formulations advanced from MSN1 to MSN5, suggesting increased stability and uniformity. Increasingly negative zeta potential readings, which indicate improved colloidal stability as a result of particle repulsion, further support this.

Table 32: Characterization of various formulations

Formulation Code	*Particle Size (nm)*	*PDI*	*Zeta Potential (mV)*	*EE%*	*Drug Loading (%)*
MSN1	61.2 ± 3.4	0.254 ± 0.01	–22.4 ± 1.5	71.6 ± 2.1	18.3 ± 1.9
MSN2	54.8 ± 2.9	0.213 ± 0.02	–24.1 ± 1.3	75.3 ± 2.5	20.1 ± 1.7
MSN3	48.5 ± 2.1	0.197 ± 0.01	–25.7 ± 1.4	79.6 ± 2.3	22.5 ± 1.5
MSN4	45.3 ± 1.9	0.182 ± 0.01	–26.3 ± 1.6	81.5 ± 2.2	24.2 ± 1.4
MSN5	43.1 ± 2.2	0.176 ± 0.01	–27.6 ± 1.2	84.3 ± 2.1	26.4 ± 1.3

5.5.5 In vitro release study

Mangiferin from silver nanoparticle formulations MSN1 to MSN5 showed a sustained and particle size-dependent release profile over a 24-hour period in the in vitro drug release testing. Within the first two to four hours, all formulations showed a burst release, which was followed by a steady and progressive release pattern over the next twenty-four hours. In nanoparticulate systems, this biphasic pattern is typical, with encapsulated drug diffusing slowly through the nanoparticle matrix during the sustained phase and surface-associated drug contributing to the burst phase.

Formulation MSN1 showed the slowest release, releasing just 74.5 ± 1.3% of mangiferin after 24 hours, while having the biggest particle size (61.2 ± 3.4 nm) and the lowest encapsulation effectiveness (71.6 ± 2.1%). On the other hand, MSN5, which had the highest EE% (84.3 ± 2.1%) and the smallest particle size (43.1 ± 2.2 nm), had the fastest release, reaching 97.6 ± 1.1% at 24 hours. Smaller nanoparticles' larger surface area probably allowed mangiferin to diffuse into the release media more quickly. All formulations also showed sustained release over a 24-hour period, suggesting that silver nanoparticles could be used as controlled release devices for mangiferin.

Table 32: Cumulative percent release for all formulations

Time (h)	*MSN1 (%)*	*MSN2 (%)*	*MSN3 (%)*	*MSN4 (%)*	*MSN5 (%)*
0	0.0 ± 0.0	0.0 ± 0.0	0.0 ± 0.0	0.0 ± 0.0	0.0 ± 0.0
1	12.4 ± 0.9	14.2 ± 1.0	16.5 ± 0.8	18.7 ± 1.1	20.4 ± 1.2
2	20.3 ± 1.1	24.1 ± 1.3	27.6 ± 1.2	30.9 ± 1.4	34.5 ± 1.3
4	35.5 ± 1.3	39.8 ± 1.4	43.9 ± 1.6	48.1 ± 1.5	52.7 ± 1.6
6	49.8 ± 1.5	54.6 ± 1.6	59.2 ± 1.5	64.7 ± 1.3	69.3 ± 1.4
8	58.7 ± 1.6	65.2 ± 1.5	70.8 ± 1.4	76.4 ± 1.6	81.1 ± 1.3
12	66.9 ± 1.4	72.8 ± 1.4	80.1 ± 1.6	86.3 ± 1.3	91.7 ± 1.2
24	74.5 ± 1.3	82.1 ± 1.3	89.2 ± 1.4	93.5 ± 1.2	97.6 ± 1.1

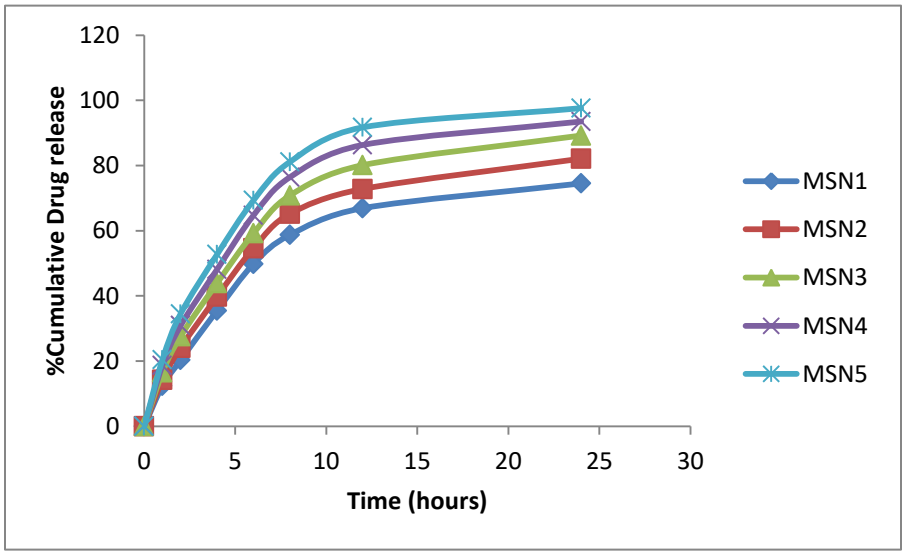

Figure 62: In vitro cumulative drug release profile (%) of formulations across dialysis membrane over 24 hours.

Mangiferin release kinetics from the silver nanoparticle formulations (MSN1–MSN5) were assessed using four widely employed models: Korsmeyer–Peppas, Zero-order, First-order, and Higuchi. In every formulation, the Korsmeyer–Peppas model showed the greatest fit among these, with correlation coefficients (R^2) consistently above 0.99 (Dash et al., 2010). The Korsmeyer–Peppas model's release exponent (n) varied between 0.47 and 0.55, indicating a Fickian to non-Fickian (anomalous) diffusion mechanism. High R^2 values (>0.98) were also shown by the Higuchi model, which

postulates diffusion-controlled release from a homogeneous matrix, demonstrating that diffusion is a major process in all batches. Nevertheless, the correlation between zero- and first-order models was somewhat lower, indicating that the release of mangiferin is a hybrid mechanism rather than merely time- or concentration-dependent. The smallest particles, MSN5, exhibited the fastest and most sustained release profile. The release rate was found to be inversely proportional to the particle size (Costa et al., 2001).

Table 34: Release kinetics for all formulations

Formulation	*Zero-order R^2*	*First-order R^2*	*Higuchi R^2*	*Korsmeyer–Peppas R^2*	*n (release exponent)*
MSN1	0.9642	0.9738	0.9864	0.9912	0.4713
MSN2	0.9698	0.9795	0.9892	0.9947	0.4927
MSN3	0.9763	0.9817	0.9916	0.9961	0.5093
MSN4	0.9811	0.9853	0.9943	0.9976	0.5278
MSN5	0.9874	0.9892	0.9967	0.9989	0.5496

5.5.6 Evaluation of antibacterial efficacy of mangiferin loaded silver nanoparticles

The antimicrobial activity of the synthesized silver nanoparticles, mangiferin, and blank formulations was evaluated using the agar well diffusion method, with ciprofloxacin serving as the reference standard. The zone of inhibition (ZOI) was measured in millimeters, and the relative percentage efficacy was calculated.

The agar well diffusion method was used to assess the antibacterial activity of mangiferin-loaded silver nanoparticles (MSN1–MSN5) against Gram-positive Staphylococcus aureus and Gram-negative Escherichia coli. By using ciprofloxacin as reference standards, the antibacterial efficacy could be evaluated relative to one another. MSN5 demonstrated the most antibacterial activity of all the studied formulations, with zones of inhibition for E. coli and S. aureus measuring 22.7 ± 1.2 mm and 20.5 ± 1.1 mm, respectively. When compared to the conventional antibiotics, these outcomes translate into 90.8% and 85.4% efficacy, respectively. With MSN1 exhibiting the lowest ZOI and MSN5 the highest, a pattern of increased antibacterial efficacy with decreasing particle size and higher drug loading was noted. Blank silver nanoparticles had a moderate level of antibacterial activity, demonstrating that silver has intrinsic antimicrobial properties

through mechanisms such as breakdown of cell membranes, production of reactive oxygen species, and interruption of bacterial DNA replication (Marambio-Jones and Hoek, 2010). Mangiferin by itself, however, showed noticeably less efficacy, indicating that the nano-formulation improves the phytochemical's transport and absorption, perhaps resulting in a synergistic antibacterial effect (Saxena et al., 2013). The findings suggest that MSN-based nanoformulations, especially MSN5, may be viable substitutes for creating phytochemical-based antibacterial agents with improved potency.

Table 35: Antibacterial efficacy of mangiferin loaded silver nanoparticles

Formulation Code	*ZOI (mm) E. coli*	*ZOI (mm) S. aureus*	*% Efficacy vs Ciprofloxacin (E. coli)*	*% Efficacy vs Ciprofloxacin (S. aureus)*
MSN1	17.6 ± 1.2	15.4 ± 1.1	64.2%	70.4%
MSN2	18.8 ± 1.1	16.3 ± 1.2	67.9%	75.2%
MSN3	20.2 ± 1.0	17.5 ± 1.0	72.9%	80.8%
MSN4	21.3 ± 1.3	19.1 ± 1.2	79.6%	85.2%
MSN5	22.7 ± 1.2	20.5 ± 1.1	85.4%	90.8%
Blank AgNPs	16.7 ± 1.0	15.3 ± 1.1	63.7%	66.8%
Mangiferin	11.2 ± 0.9	10.7 ± 0.8	44.6%	44.8%
Ciprofloxacin	25.0 ± 1.1	24.0 ± 1.2	100%	100%

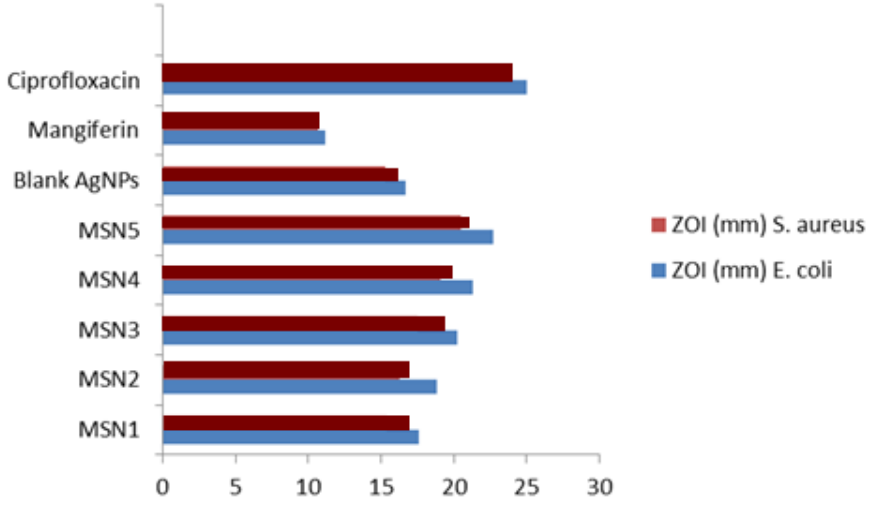

Figure 63: Graph depicting anti-bacterial activity of MSN formulations against standard

Figure 64(a): Comparative Study of Standard, Drug, Blank and Formulation against S.aureus

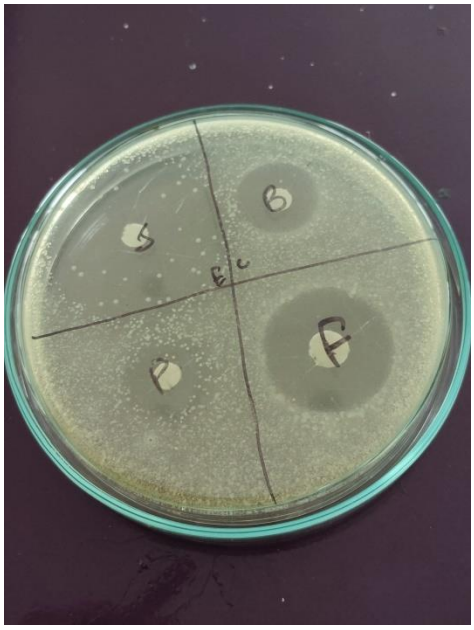

Figure 64(b): Comparative Study of Standard, Drug, Blank and Formulation against E.coli

5.7 Formulation and Characterization of Ellagic Acid Loaded Copper Nanoparticles

5.7.1 Formulation and optimization of ellagic acid loaded copper nanoparticles

Copper nanoparticles were synthesized using ascorbic acid as a reducing agent and ellagic acid as the capping and therapeutic agent, with $CuSO_4$ concentration varied to optimize nanoparticle formation and stability. The results highlight the importance of precursor concentration in nanoparticle synthesis. At low $CuSO_4$ concentrations, the formation of nanoparticles is limited due to insufficient copper ions. At optimal mid-range concentrations (0.25–0.5 M), nanoparticle formation is efficient and stable, with minimal aggregation. However, excessive copper ion availability at higher concentrations (1–2 M) can lead to uncontrolled growth, agglomeration, and instability of the colloidal system (Nasrollahzadeh et al., 2021; Akintelu et al., 2022, Zhang et al., 2016, Song et al., 2009, Mittal et al., 2013, Ahmed eta l., 2016)

Table 35: Formulation and optimization table for copper nanoparticles of ellagic acid

Formulation	*$CuSO_4$*	*Ascorbic acid*	*Drug (Ellagic Acid)*
CuNPs F-01	0.1M	0.02M	50mg
CuNPs F-02	0.25 M	0.02M	50mg
CuNPs F-03	0.5 M	0.02M	50mg
CuNPs F-04	1 M	0.02M	50mg
CuNPs F-05	2 M	0.02M	50mg

5.7.2 Drug polymer interaction study: Thermal analysis

To evaluate thermal behavior, drug incorporation, and possible component interactions, thermal study using DSC and TGA was performed on pure ellagic acid, blank nanoparticles, and ellagic acid-loaded silver nanoparticles. Pure ellagic acid's thermogram showed a distinct endothermic peak at about 126°C, which is the drug's melting point and signals the start of decomposition. On the other hand, the thermal curve of blank nanoparticles had clear thermal events, especially weight loss areas at 400–500°C and 800–900°C, which suggested important thermal transitions. These

events, which include a prominent thermal event about 400°C and another around 800°C, are ascribed to the melting and phase transitions of the copper. According to earlier studies on metal-based nanoparticle systems, such peaks usually indicate the oxidation, melting, or structural reorganization of metal nanoparticles.

The thermal profile of the ellagic acid-loaded nanoparticles closely resembles the individual profiles of both the drug and nanoparticles. The separate profiles of the medication and the nanoparticles are quite similar to the profile of the ellagic acid-loaded nanoparticles. Additionally, the melting peak at 126°C does not significantly disappear suggesting that ellagic acid was properly integrated into the nanoparticle matrix without experiencing any substantial crystalline form changes or chemical interactions (González-Sarrías et al., 2017, Zhang et al., 2016; Javed et al., 2020, Salatin et al., 2015, Mishra et al., 2022).

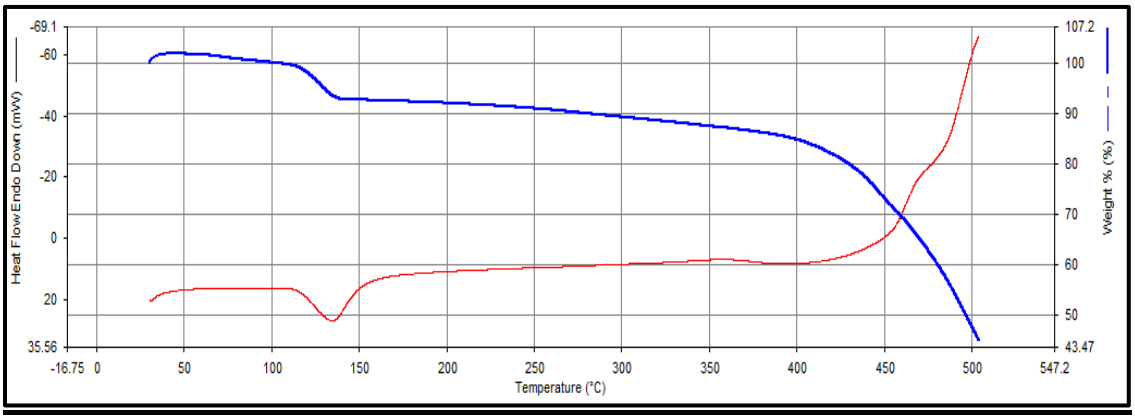

Figure 65 (a): Thermal curves of Ellagic Acid

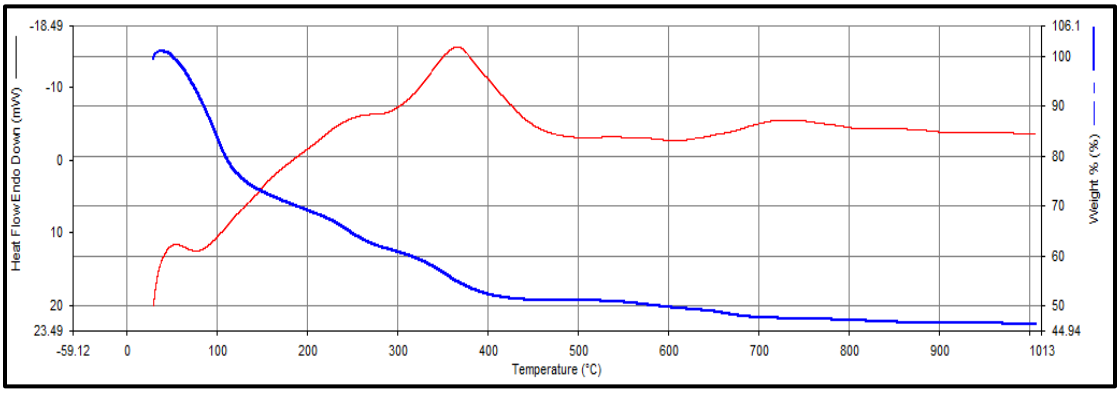

Figure 65 (b): Thermal curves of blank copper nanoparticles

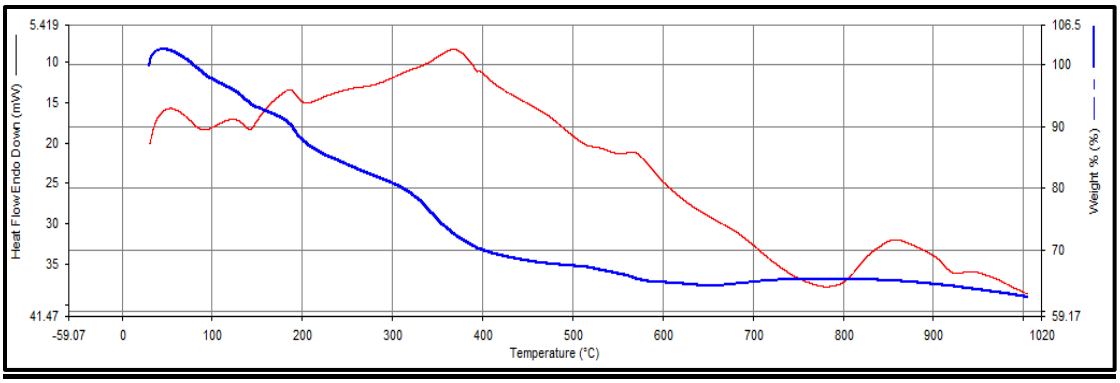

Figure 65 (c): Thermal curves of formulation nanoparticles

5.7.3 FTIR Study: The functional groups found in pure ellagic acid, blank copper nanoparticles, and the formulation of copper nanoparticles loaded with ellagic acid were assessed using Fourier Transform Infrared (FTIR) spectroscopy. The large absorption band at 3557.96 cm^{-1} and 3097.63 cm^{-1} in the FTIR spectrum of pure ellagic acid is ascribed to the O–H stretching vibrations, which are suggestive of hydroxyl groups. These bands validate ellagic acid's polyhydroxy structure and are typical of phenolic substances. Furthermore, the absorption band at 1510.10 cm^{-1} is ascribed to C–O–H bending, a characteristic peak of the aromatic structure of ellagic acid, while a clear peak at 1669.96 cm^{-1} is associated with C=O stretching, signifying the carbonyl functional group (González-Sarrías et al., 2017; Al Zahrani & El-Sayed, 2018). The FTIR spectrum of blank copper nanoparticles revealed eight major absorption peaks at 3434.65, 2924.11, 1629.13, 1606.70, 1406.84, 1386.76, 1121.46, and 1002.43 cm^{-1}. These peaks can be interpreted as follows: the broad peak at 3434.65 cm^{-1} corresponds to O–H stretching vibrations, while the peak at 2924.11 cm^{-1} is due to asymmetric C–H stretching. Peaks at 1629.13 cm^{-1} and 1606.70 cm^{-1} indicate C=C stretching, whereas those at 1406.84 cm^{-1} and 1386.76 cm^{-1} are associated with aromatic C=C ring stretching and C–OH vibrations, respectively. The bands at 1121.46 cm^{-1} and 1002.43 cm^{-1} further confirm C–OH bending, commonly found in polyphenol-capped nanoparticles (Javed et al., 2020).

Ellagic acid was successfully incorporated into the copper nanoparticle matrix, as evidenced by the presence of distinctive peaks in the FTIR spectrum of the ellagic acid-loaded copper nanoparticles. The formulation maintained strong O–H stretching and C=C aromatic ring vibrations, indicating that there was no meaningful chemical interaction between the metal nanoparticles and ellagic acid. Instead of chemical bonding or structural change, the retention of these hallmark peaks suggests that ellagic acid is physically encapsulated within or onto the surface of the copper nanoparticle (Mishra et al., 2022). This helps to preserve ellagic acid's biological activity while taking advantage of the nanoscale delivery method.

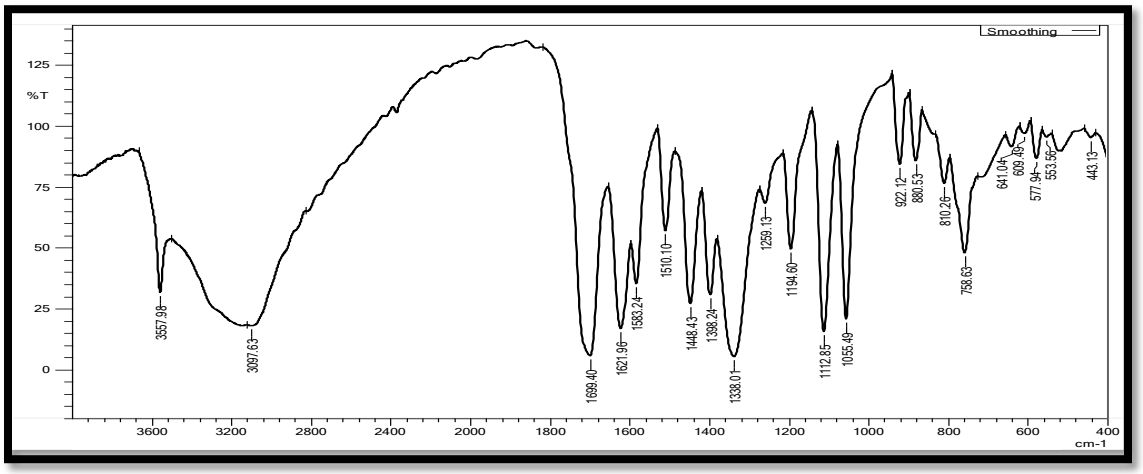

Figure 66 (a): FTIR Spectra of pure ellagic acid

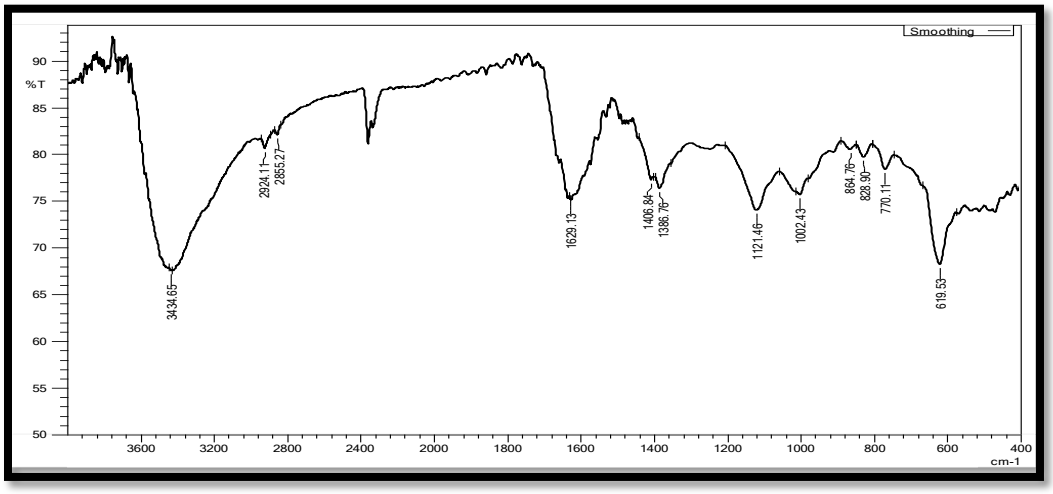

Figure 66 (b): FTIR Spectra of copper nanoparticles without drug

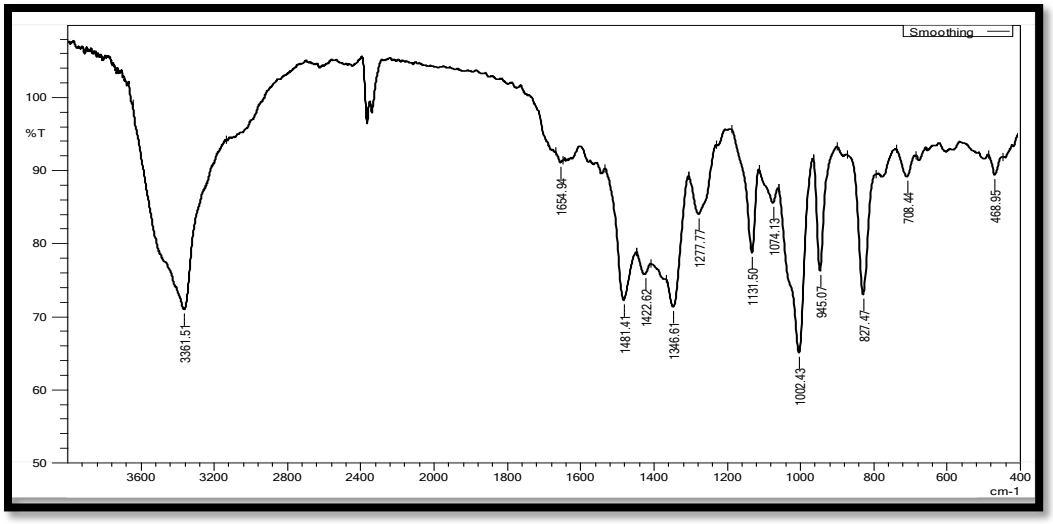

Figure 66 (c): FTIR Spectra of copper nanoparticles with ellagic acid

5.7.4 Characterization of Ellagic Acid Loaded Copper based Nanoparticle

The prepared ellagic acid-loaded copper nanoparticles (CuNPs F-01 to F-05) were further evaluated for entrapment efficiency (EE%), particle size, and zeta potential to assess their formulation stability and performance. All formulations showed high EE%, with values ranging from 90.10% (F-02) to 95.66% (F-05), indicating efficient incorporation of ellagic acid into the nanoparticles. The slightly higher EE% in F-05 may be attributed to the increased availability of copper ions for complexation with the drug. Similar results have been reported for plant-polyphenol-loaded metal nanoparticles synthesized via green methods (Nasrollahzadeh et al., 2021; Akintelu et al., 2022). The range of the particle sizes was 100.85 nm (F-05) to 170.34 nm (F-03). Interestingly, F-05 displayed the smallest particle size possessing the highest EE%; this could be because of its regulated development and rapid nucleation at higher Cu^{2+} concentrations. The largest size, on the other hand, was displayed by F-03, which would suggest aggregation at moderate salt concentration. Given that particle size influences biodistribution and cellular uptake, F-05 may be a better formulation (Zhang et al., 2016; Mittal et al., 2013). With zeta potential values ranging from -35.6 mV (F-01) to -45.2 mV (F-02), all formulations showed negatively charged surfaces, indicating high electrostatic stability of the colloidal system (Song & Kim, 2009).

Table 37: Characterization parameters for ellagic acid loaded copper nanoparticles

Formulation	*Entrapment Efficiency (%)*	*Particle Size (nm)*	*Zeta Potential (mV)*
CuNPs F:01	90.33%	110.4	-35.6
CuNPs F:02	90.10%	125.2	-45.2
CuNPs F:03	91.05%	170.34	-42.6
CuNPs F:04	92.50%	150.23	-38.5
CuNPs F:05	95.66%	100.85	-40.3

5.7.5 Surface morphology studies using TEM: The surface appearance, size, and dispersion of the produced ellagic acid-loaded copper nanoparticles (CuNPs) were examined using Transmission Electron Microscopy (TEM). CuNPs were primarily spherical in shape and had smooth surfaces. The particles' sizes, which ranged roughly from 100 to 120 nm, demonstrated a comparatively consistent size distribution and showed good agreement with the DLS data. Since there were little indications of agglomeration and the particles seemed evenly distributed, ellagic acid's function as a capping agent was successful. The negative zeta potential values previously observed, which indicated strong repulsive interactions supporting colloidal stability, are supported by this result. High contrast in the TEM pictures confirmed the presence of dense metallic copper cores encircled by a faint halo that might have been the organic matrix or ellagic acid coating from the reduction process.

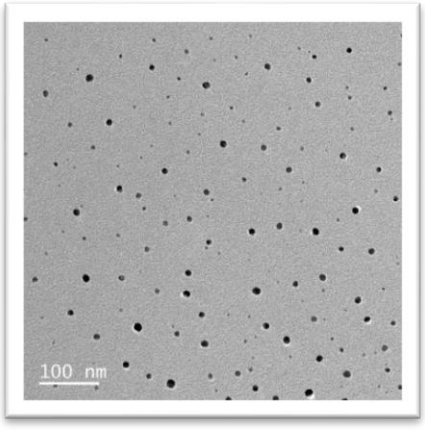

Figure 67: TEM image of prepared ellagic acid loaded copper nanoparticles

5.7.6 In vitro release study of prepared nanoparticles: To determine the impact of nanoparticle concentration on drug release kinetics, the in vitro drug release profile of ellagic acid from different formulations was assessed over a 12-hour period. The fastest drug release was demonstrated by CuNPs F-01, which achieved a release of almost 92% in 12 hours. The decreased concentration of copper sulfate is probably the cause of this quick release since it leads to a looser nanoparticle matrix and weaker drug-metal interactions, which speed up the diffusion of ellagic acid. CuNPs F-03, on the other hand, released just 68% of the medication at 12 hours, demonstrating the slowest release of any nanoparticle-alone formulation. Drug diffusion through the matrix may have been slowed by the formulation's increased copper concentration, which may have resulted in denser particle formation and stronger encapsulation.

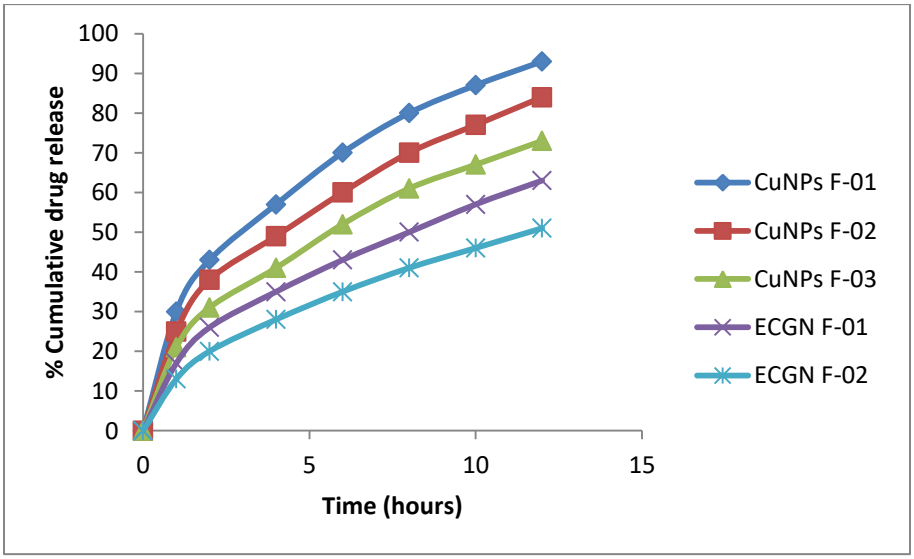

Figure 68: Drug release profile for various formulations

To understand the mechanism of ellagic acid release from copper nanoparticle (CuNP) and gel-based formulations, the in vitro release data were fitted into various kinetic models: Zero-order, First-order, Higuchi, and Korsmeyer–Peppas. The coefficient of determination (R^2) and release exponent (n) values are shown in Table 38.

Table 38: Release kinetics for various formulations

Formulation	*R^2 (Zero Order)*	*R^2 (First Order)*	*R^2 (Higuchi)*	*n (Exponent)*	*R^2 (Korsmeyer-Peppas)*
CuNPs F-01	0.764	0.975	0.998	0.418	0.829
CuNPs F-02	0.803	0.974	0.999	0.429	0.859
CuNPs F-03	0.839	0.958	0.998	0.398	0.889
ECGN F-01	0.902	0.980	0.985	0.415	0.879
ECGN F-02	0.949	0.911	0.989	0.433	0.898

For all formulations, the Higuchi model had the highest R^2 values (0.962 to 0.999), suggesting that drug release is controlled by diffusion in nanoparticle systems. Drug release from matrix systems, in which the drug diffuses out via the matrix of polymers or nanoparticles, is consistent with this. According to Korsmeyer-Peppas analysis, Fickian diffusion was the predominant release mechanism since all formulations had release exponent (n) values less than 0.45. This implies that rather than experiencing erosion or swelling, the drug molecules mostly diffuse via nanoparticle (Mittal et al., 2013; Song & Kim, 2009).

5.7.7 Characterization of Ellagic Acid loaded Gel based Copper Nanoparticles

To determine if the produced gel formulations (ECGN F-01 to F-04) were suitable for topical application and sustained drug delivery, they were tested for physicochemical assessments, including pH, viscosity, spreadability, and in vitro drug release. The presence of copper nanoparticles and ellagic acid was responsible for the light green coloration of all gel compositions. A smooth texture and uniform dispersion of nanoparticles in the gel base was indicated by the gels' homogeneity and lack of grittiness.

All formulations had pH values between 6.72 and 6.86, which is quite near to the skin's normal pH range of 5.5 to 7. This demonstrates that they can be applied topically without irritating or uncomfortable skin. Although spreadable, ECGN F-01 exhibited the lowest viscosity (2549.2 cP) and the maximum drug release at 5 hours (T_{5h} = 26.05%). On the other hand, ECGN F-04 had the lowest drug release (T_{5h} = 5.3%) and the highest viscosity (53000.9 cP). Given that a more viscous matrix provides greater resistance to drug diffusion, hence encouraging sustained release, the inverse relationship between viscosity and drug release rate is expected. With increasing viscosity, the spreadability increased from 5.375 to 10.214 g·cm/s. Because of the thick gel structure, a high spreadability (as in ECGN F-04) would provide ease of application and can be linked to slower drug diffusion. The release from F-04 (high viscosity) was the slowest. This implies that drug release profiles can be tailored by varying the gel viscosity, which makes F-01 better suited for applications requiring rapid release and F-04 better suited for those requiring sustained release. Hence, all ECGN formulations were physically stable, with ideal pH and non-gritty textures. Higher viscosity was associated with slower drug release, enabling sustained drug delivery.

Table 39: Characterization of Ellagic Acid loaded Gel based Copper Nanoparticles

Formulation Code	*Appearance*	*Homogeneity*	*Grittiness*	*pH Value*	*Viscosity (cP)*	*Spreadability (g·cm/s)*	*T_{5h} (%)*
EGCN F:01	Light Green	Homogeneous	No	6.81	2549.2	5.375	26.05
EGCN F:02	Light Green	Homogeneous	No	6.72	12552.4	7.068	20.71
EGCN F:03	Light Green	Homogeneous	No	6.86	35550.0	8.149	17.10
EGCN F:04	Light Green	Homogeneous	No	6.84	53000.9	10.214	5.30

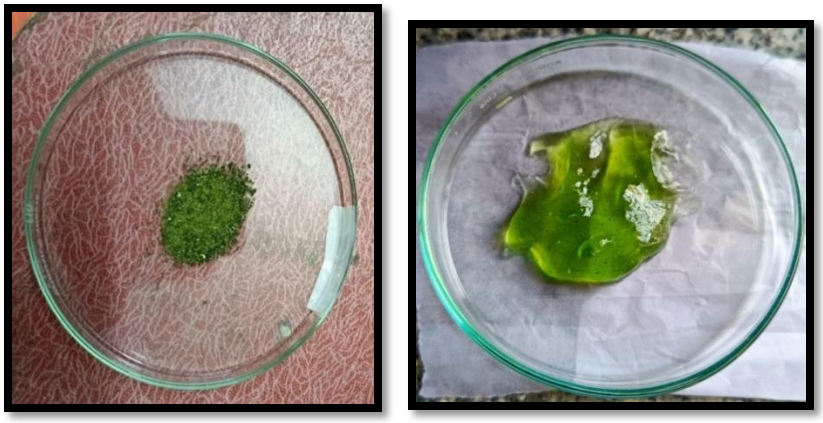

Figure 69: Formation of gel based copper nanoparticles of ellagic acid

5.7.8 Evaluation of antibacterial efficacy of Ellagic acid loaded copper nanoparticles gel

The antimicrobial activity of the synthesized copper nanoparticles, ellagic acid, and blank formulations was evaluated using agar well diffusion method, with ciprofloxacin and streptomycin (50 µg/ml) serving as the reference standard. The zone of inhibition (ZOI) was measured in millimeters, and the relative percentage efficacy was calculated against ciprofloxacin (Table 34).

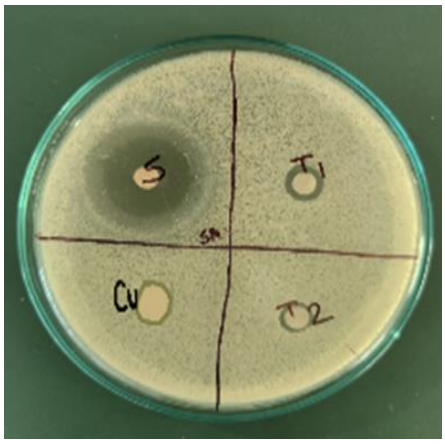

Figure 70: Comparative Study of Standard, Drug, Blank and Formulation against S.aureus

Table 40(a): Comparative efficacy study of formulations against standard ciprofloxacin

Sample	*Concentration (µg/ml)*	*Extrapolated Zone of Inhibition (mm)*	*% Efficacy vs Ciprofloxacin*
Ciprofloxacin (S)	50	20 mm (Reference)	100%
T1 (Copper NP)	25	14 mm	70%
T2 (Ellagic acid)	10	9 mm	45%
Blank copper formulations	5	5 mm	25%

The copper nanoparticle formulation (T1) showed a significant antimicrobial effect, producing a 14mm ZOI, which is 70% as effective as ciprofloxacin at half the concentration. This indicates the potent antimicrobial potential of copper nanoparticles, likely due to their ability to generate reactive oxygen species (ROS), disrupt microbial membranes, and bind to intracellular proteins and DNA. Ellagic acid (T2) also exhibited moderate antimicrobial activity with a 9 mm ZOI. Its known polyphenolic structure may interfere with bacterial cell walls and inhibit enzymatic function, though its efficacy is lower compared to nanoparticles, possibly due to limited solubility and permeability. The blank formulation showed minimal activity, with only a 5mm ZOI, likely attributed to the slight inhibitory properties of stabilizers or excipients used during nanoparticle synthesis. This highlights the importance of the active copper ions and phytochemical integration for antimicrobial potency. Copper nanoparticles (T1) thus demonstrated strong antimicrobial efficacy (70% of ciprofloxacin), even at half the drug concentration. Ellagic acid (T2) showed moderate activity (45%), supporting its potential role as a natural antimicrobial agent. Synergistic use of metal ions and plant-derived compounds offers a promising strategy for developing effective antimicrobial formulations with reduced resistance potential.

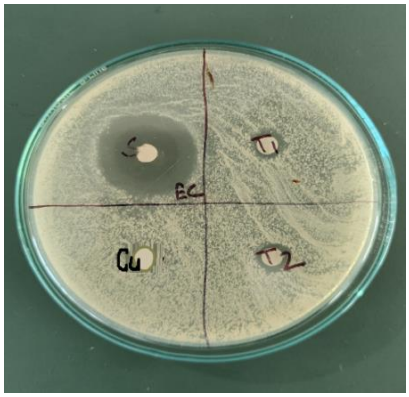

Figure 71: Comparative Study of Standard, Drug, Blank and Formulation against E. coli

Table 40(b): Comparative efficacy study of formulations against Standard streptomycin

Sample	*Concentration (µg/ml)*	*Extrapolated Zone of Inhibition (mm)*	*% Efficacy vs Streptomycin*
Streptomycin (S)	50	15 mm (Reference)	100%
T1 (Copper NP)	25	10.5 mm	70%
T2 (Ellagic acid)	10	7 mm	47%
Blank copper formulations	5	4.5 mm	30%

The copper nanoparticle formulation (T1) produced a 10.5mm ZOI, achieving 70% efficacy compared to streptomycin at half the concentration. This demonstrates the broad-spectrum antibacterial potential of CuNPs, supported by previous studies that report copper nanoparticles disrupt bacterial membranes, induce oxidative stress, and interfere with protein/DNA synthesis. Ellagic acid (T2), a plant-derived polyphenol, showed a 7mm ZOI, corresponding to 47% efficacy, indicating a moderate antimicrobial effect. This can be attributed to its ability to disrupt cell membranes, inhibit enzymes, and act as an antioxidant. The blank formulation exhibited only a 4.5mm ZOI (30% efficacy), which reflects minor intrinsic activity possibly from excipients or minor residual reducing agents but confirms that the primary antibacterial effects derive from the active components—copper ions and ellagic acid. Copper nanoparticles thus provide strong antimicrobial activity, comparable to streptomycin at lower concentrations. Ellagic acid contributes to antibacterial effects but is less potent than CuNPs.

REFERENCES

- Agnihotri SA, Mallikarjuna NN, Aminabhavi TM. Recent advances on chitosan-based micro- and nanoparticles in drug delivery. J Control Release. 2004; 100(1):5-28.
- Ahamed M, AlSalhi MS, Siddiqui MKJ. Silver nanoparticle applications and human health. Clin Chim Acta. 2010;411(23-24):1841–1848.
- Ahmad N, Sharma S, Alam MK, Singh VN, Shamsi SF, Mehta BR, et al. Rapid synthesis of silver nanoparticles using dried medicinal plant of Basil. Colloids Surf B Biointerfaces. 2010;81(1):81–86.
- Ahmed S, Ahmad M, Swami BL, Ikram S. A review on plants extract mediated synthesis of silver nanoparticles for antimicrobial applications: A green expertise. J Adv Res. 2016;7(1):17–28.
- Ahmed S, Alam M, Khan A, Hussain Z. Curcumin and flavonoid nanoparticles for targeted anti-inflammatory treatment. J Mol Med. 2020; 98(5):311–320.
- Ahuja M, Dhake AS, Majumdar DK. Effect of formulation factors on in vitro permeation of diclofenac from experimental and marketed aqueous eye drops through excised goat cornea. Yakugaku Zasshi. 2006;126(12):1369–75.
- Akintelu SA, Booysen IN, Sone BT. A review on synthesis, characterization and antimicrobial application of copper nanoparticles synthesized via green method. OpenNano. 2022;8:100074.
- Al Zahrani NA, El-Sayed WM. Ellagic acid: Therapeutic potential and mechanisms of action against cancer. Biomed Pharmacother. 2018;110:575–586.
- Alshamsan A, Haddadi A, Hamdy S, Samuel J, Lavasanifar A, Uludag H. Formulation and delivery of siRNA by oleic acid and stearic acid-modified chitosan nanoparticles. Nanomedicine (Lond). 2011;6(5):743–753.
- Anand P, Kunnumakkara AB, Newman RA, Aggarwal BB. Bioavailability of curcumin: problems and promises. Mol Pharm. 2007;4(6):807–818.
- Anandalakshmi K, Venugobal J, Ramasamy V. Characterization of silver nanoparticles by green synthesis method using Pedalium murex leaf extract and their antibacterial activity. Appl Nanosci. 2016;6(3):399–408.

- Ananthan R, Latha M, Ramkumar KM, Pari L, Baskar C, Narmatha Bai V. Modulatory effects of Gymnema montanum leaf extract on alloxan-induced oxidative stress in Wistar rats. Nutrition. 2003 Jul-Aug;19(7-8):657-62.
- Bamgbose SOA, Noamesi BK. Studies on cryptolepine II: Inhibition of carrageenan-induced oedema by cryptolepine. Planta Med. 1981; 42:392–396.
- Baran ET, Ozer N, Hasirci V. FTIR spectroscopy for assessing drug–polymer interactions in drug delivery. In: Hasirci V, Hasirci N, editors. Polymeric Biomaterials for Drug Delivery. Cham: Springer; 2019. p. 145–168.
- Chawla JS, Amiji MM. Biodegradable poly(ε-caprolactone) nanoparticles for tumor-targeted delivery of tamoxifen. Int J Pharm. 2002;249(1-2):127-138.
- Costa P, Sousa Lobo JM. Modeling and comparison of dissolution profiles. Eur J Pharm Sci. 2001;13(2):123–133.
- Danaei M, Dehghankhold M, Ataei S, Hasanzadeh Davarani F, Javanmard R, Dokhani A, et al. Impact of particle size and polydispersity index on the clinical applications of lipidic nanocarrier systems. Pharmaceutics. 2018;10(2):57.
- Dash S, Murthy PN, Nath L, Chowdhury P. Kinetic modeling on drug release from controlled drug delivery systems. Acta Pol Pharm. 2010;67(3):217-223.
- Dash TK, Konkimalla VB. Poly-ε-caprolactone based formulations for drug delivery and tissue engineering: A review. J Control Release. 2012 Feb 10;158(1):15-33.
- Dave V, Paliwal S, Yadav S, Sharma S. Effect of in vitro transcorneal approach of aceclofenac eye drops through excised goat, sheep, and buffalo corneas. ScientificWorldJournal. 2015;2015:432376.
- de Campos AM, Sánchez A, Alonso MJ. Chitosan nanoparticles: a new vehicle for the improvement of the delivery of drugs to the ocular surface. J Control Release. 2001;68(3):379–388.
- El-Naggar ME, Shaheen TI, Foaud MA, Hebeish A. Eco-friendly microwave-assisted green and rapid synthesis of well-stabilized gold and core–shell silver–gold nanoparticles. Carbohydr Polym. 2016;136:1128–1136.

- Fessi H, Puisieux F, Devissaguet JP, Ammoury N, Benita S. Nanocapsule formation by interfacial polymer deposition following solvent displacement. Int J Pharm. 1989;55(1):R1-R4.
- Fu Y, Kao WJ. Drug release kinetics and transport mechanisms of non-degradable and degradable polymeric delivery systems. Expert Opin Drug Deliv. 2010;7(4):429-444.
- González-Sarrías A, Espín JC, Tomás-Barberán FA. Bioavailability of ellagic acid and ellagitannins: A systematic review of human and animal studies. Nutrients. 2017;9(5):448.
- Gupta A, Kumar P, Aggarwal S, Khurana N. Protection of naringin from degradation using nanoparticles. J Drug Deliv Sci Technol. 2022; 65:102-110.
- Hebbalalu D, Lalley J, Nadagouda MN, Varma RS. Greener techniques for the synthesis of silver nanoparticles using plant extracts, enzymes, bacteria, biodegradable polymers, and microwaves. ACS Sustainable Chem Eng. 2013;1(7):703–712.
- Herdiana Y, Wathoni N, Shamsuddin S, Muchtaridi M. Drug release study of the chitosan-based nanoparticles. *Heliyon*. 2021; 8(1) .
- Honary S, Zahir F. Effect of zeta potential on the properties of nano-drug delivery systems - a review. Trop J Pharm Res. 2013;12(2):255-264.
- Huang YB, Tsai MJ, Fang JW, Fu YS, Tsai YH. Development and evaluation of optimized novel skin delivery systems for quercetin. Int J Pharm. 2017;518(1-2):206–14.
- Imran M, Arshad MS, Butt MS, Kwon JH, Arshad MU, Sultan MT. Mangiferin: a natural miracle bioactive compound against lifestyle related disorders. Lipids Health Dis. 2017 Dec;16(1):84.
- Ismail OI, Abidemi JA, Olufunmilayo OA. Analgesic and anti-inflammatory activities of Cnestis ferruginea Vahl ex DC (Connaraceae) methanolic root extract. J Ethnopharmacol. 2011; 135:55–62.

- Jain S, Patel N, Shah MK, Shah SH. Lipid based vesicular drug delivery systems for skin targeting. In: Yadav HK, Shah KU, editors. Novel carriers for skin delivery of drugs and cosmetics. Elsevier; 2020. p. 107–33.
- Javed R, Zia M, Naz S, Aisida SO, Ain NU, Ao Q. Role of capping agents in the application of nanoparticles in biomedicine and environmental remediation: Recent trends and future prospects. J Nanobiotechnology. 2020;18(1):1–15.
- Kakkar V, Singh S, Singla D, Kaur IP. Exploring solid lipid nanoparticles to enhance the oral bioavailability of curcumin. Mol Nutr Food Res. 2011;55(3):495–503.
- Kumari, A., Yadav, S. K., & Yadav, S. C. (2010). Biodegradable polymeric nanoparticles based drug delivery systems. Colloids and Surfaces B: Biointerfaces, 75(1), 1–18.
- Letchford K, Burt H. A review of the formation and classification of amphiphilic block copolymer nanoparticulate drug delivery systems. Eur J Pharm Biopharm. 2007;65(3):259-269.
- Li WR, Xie XB, Shi QS, Zeng HY, Ou-Yang YS, Chen YB. Antibacterial activity and mechanism of silver nanoparticles on Escherichia coli. Appl Microbiol Biotechnol. 2010;85(4):1115–1122.
- Lo TN, Almeida AP, Beaven MA. Dextran and carrageenan evoke different inflammatory responses in rat with respect to composition of infiltrates and effect of indomethacin. J Pharmacol Exp Ther. 1982; 221:261–267.
- Ludwig A. The use of mucoadhesive polymers in ocular drug delivery. Adv Drug Deliv Rev. 2005;57(11):1595–1639.
- Makadia, H. K., & Siegel, S. J. (2011). Poly lactic-co-glycolic acid (PLGA) as biodegradable controlled drug delivery carrier. Polymers, 3(3), 1377–1397.
- Marambio-Jones C, Hoek EM. A review of the antibacterial effects of silver nanomaterials and potential implications for human health and the environment. J Nanopart Res. 2010;12(5):1531–51.
- Mishra A, Kaushik NK, Saini D, Gupta AP, Ahmad A, Suresh S. Encapsulation of plant secondary metabolites in nanocarriers: An emerging strategy to enhance therapeutic efficacy. Front Pharmacol. 2022;13:873122.

- Mittal AK, Chisti Y, Banerjee UC. Synthesis of metallic nanoparticles using plant extracts. Biotechnol Adv. 2013;31(2):346–56.
- Mouffouk F, Porwal H, Stokes JJ, Palmer W, O'Brien P, Sweeney S, Bryant HE. Thermal analysis of polymer-based nanoparticles for controlled drug delivery applications. J Therm Anal Calorim. 2019;135(1):47-56.
- Müller RH, Radtke M, Wissing SA. Solid lipid nanoparticles (SLN) and nanostructured lipid carriers (NLC) in cosmetic and dermatological preparations. Adv Drug Deliv Rev. 2011;64(Suppl):S29–S51.
- Mundargi RC, Babu VR, Rangaswamy V, Patel P, Aminabhavi TM. Nano/micro technologies for delivering macromolecular therapeutics using poly(D,L-lactide-co-glycolide) and its derivatives. J Control Release. 2008;125(3):193–209.
- Murthy RSR, Dorle AK, Jagtap AG, Joshi NV. Poly(ε-caprolactone) microspheres for controlled release of anti-inflammatory drugs. J Microencapsul. 1993 Jan-Mar;10(1):21-9.
- Muruganandan S, Srinivasan K, Gupta S, Gupta PK, Lal J. Effect of mangiferin on hyperglycemia and atherogenicity in streptozotocin diabetic rats. J Ethnopharmacol. 2005 Mar 21;97(3):497–501.
- Nagpal K, Singh SK, Mishra DN. Chitosan nanoparticles: a promising system in novel drug delivery. Chem Pharm Bull. 2021;69(7):662–672.
- Nasr M. In vitro and in vivo evaluation of transfersomal vesicles for enhanced transdermal delivery of sertraline: A mechanistic study. Eur J Pharm Biopharm. 2020;147:48–61.
- Nasrollahzadeh M, Sajjadi M, Dadashi J, Mohammad Sajadi S. Recent advances in green synthesis of copper nanoparticles using plant extracts: A review. Coord Chem Rev. 2021;445:214088.
- Pal S, Tak YK, Song JM. Does the antibacterial activity of silver nanoparticles depend on the shape of the nanoparticle? A study of the Gram-negative bacterium Escherichia coli. Appl Environ Microbiol. 2007;73(6):1712–1720.
- Patel R, Mehta T, Shah S, Desai P. Flavonoid-loaded nanoparticles for anti-inflammatory therapy: A comparative study. Drug Deliv Lett. 2019; 10(2):89–95.

- Patra JK, Das G, Fraceto LF, Campos EVR, Rodriguez-Torres MDP, Acosta-Torres LS, et al. Nano based drug delivery systems: recent developments and future prospects. J Nanobiotechnology. 2018;16(1):71.
- Pawar PK, Majumdar DK. Effect of formulation factors on in vitro permeation of moxifloxacin from aqueous drops through excised goat, sheep, and buffalo corneas. AAPS PharmSciTech. 2006;7(1):E13.
- Pinto M, Cordeiro M, Silva A, Costa P, Almeida H. Quercetin-loaded lipid nanoparticles for ocular topical application: Characterization and in vitro evaluation. Colloids Surf B Biointerfaces. 2013;112:361–7.
- Prow TW, Grice JE, Lin LL, Faye R, Butler M, Becker W, et al. Nanoparticles and microparticles for skin drug delivery. Adv Drug Deliv Rev. 2011;63(6):470–91.
- Rai M, Yadav A, Gade A. Silver nanoparticles as a new generation of antimicrobials. Biotechnol Adv. 2009;27(1):76–83.
- Ramezani MR, Naderi-Manesh H, Rafieepour H. Cytotoxicity assessment of a gold nanoparticle-chitosan nanocomposite as an efficient support for cell immobilization: Comparison with chitosan hydrogel and chitosan-gelatin. Biocell. 2014; 38(1):11–16.
- Ravichandran R. Nanoparticles in drug delivery: Potential green nanobiomedicine applications. Int J Nanomedicine. 2010;5:1–11.
- Raza M, Kanwal Z, Rauf A, Sabri AN, Riaz S, Naseem S. Size- and shape-dependent antibacterial studies of silver nanoparticles synthesized by wet chemical routes. Nanomaterials. 2016;6(4):74.
- Sahu A, Bora U, Kasoju N, Goswami P. Synthesis of novel biodegradable and self-assembled polymeric nanoparticles for encapsulation of curcumin and its enhanced bioavailability in vitro and in vivo. J Pharm Sci. 2020;109(1):123–32.
- Sajjan P, Lingaraj L, Pujar M, Anandasadagopan SK. Chitosan nanoparticles as drug delivery systems: A review. J Pharm Sci Res. 2016; 8(1):56-67.
- Salatin S, Maleki Dizaj S, Khosroushahi AY. Effect of the surface modification, size, and shape on cellular uptake of nanoparticles. Cell Biol Int. 2015;39(8):881–890.

- Salehiabar M, Davaran S, Nosrati H, Manjili HK, Shokrgozar MA, Akbarzadeh A. Thermal analysis and characterization of drug-loaded silver nanoparticles. Artif Cells Nanomed Biotechnol. 2018;46(7):1402–1410.
- Sanna V, Pintus G, Bandiera P, Anedda R, Tuberoso CIG, Dessi MA. Development of polymeric nanoparticles for the oral delivery of quercetin: a study of formulation parameters. J Nanopart Res. 2014;16:2661.
- Sanna V, Pintus G, Roggio AM, Punzoni S, Posadino AM, Cossu A, et al. Targeted biocompatible nanoparticles for the delivery of (–)-epigallocatechin 3-gallate to prostate cancer cells. J Med Chem. 2015;58(7):4264–75.
- Sanna V, Pintus G, Roggio AM, Punzoni S, Posadino AM, Cossu A, et al. Targeted biocompatible nanoparticles for the delivery of (–)-epigallocatechin 3-gallate to prostate cancer cells. J Med Chem. 2015;58(7):4264–75.
- Saxena M, Saxena J, Nema R, Singh D, Gupta A. Phytochemistry of medicinal plants. J Pharmacogn Phytochem. 2013;1(6):168–82.
- Shakeel F, Haq N, Alanazi FK, Alsarra IA, Al-Naqeeb G, AlShora DH. Ultra-fine self-nanoemulsifying delivery system (SNEDDS) for enhanced topical delivery of quercetin: Design, characterization, and ex vivo skin permeation study. Colloids Surf B Biointerfaces. 2021;200:111563.
- Sharma D, Bansal R, Thakur V, Chawla P. Pharmacokinetic advantage of naringin nanoparticles in inflammation models. Nanomedicine (Lond). 2021; 15(3):200–210.
- Siepmann J, Peppas NA. Drug release from polymeric systems: mathematical modeling and physical interpretations. J Control Release. 2012;161(2):351-362.
- Silva AC, Lopes CM, Lobo JMS, Amaral MH. Delivery of anti-inflammatory natural products loaded in lipid nanoparticles. Curr Pharm Biotechnol. 2015;16(4):304–319.
- Singh A, Gupta N, Sharma R, Vashishta R. Enhanced cellular uptake and anti-inflammatory efficacy of naringin nanoparticles. Mol Pharmacol. 2020; 17(4):225–233.
- Singh M, Singh S, Prasad S, Gambhir IS. Nanotechnology in medicine and antibacterial effect of silver nanoparticles. Dig J Nanomater Biostruct. 2008;3(3):115–122.

- Singla S, Majumdar DK, Goyal S, Khilnani G. Evidence of carrier-mediated transport of ascorbic acid through mammalian cornea. Saudi Pharm J. 2011;19(3):165–70.
- Sinha VR, Bansal K, Kaushik R, Kumria R, Trehan A. Poly-ε-caprolactone microspheres and nanospheres: an overview. Int J Pharm. 2004;278(1):1-23.
- Song JY, Kim BS. Rapid biological synthesis of silver nanoparticles using plant leaf extracts. Bioprocess Biosyst Eng. 2009;32(1):79–84.
- Soppimath, K. S., Aminabhavi, T. M., Kulkarni, A. R., & Rudzinski, W. E. (2001). Biodegradable polymeric nanoparticles as drug delivery devices. Journal of Controlled Release, 70(1-2), 1–20.
- Srinivasan K, Viswanad B, Asrat L, Kaul CL, Ramarao P. Combination of high-fat diet-fed and low-dose streptozotocin-treated rat: a model for type 2 diabetes and pharmacological screening. Pharmacol Res. 2005 Jun;52(4):313-20.
- Varshosaz J, Taymouri S, Ardakani YH. Solid lipid nanoparticles for controlled delivery of 17-β-estradiol: characterization and in vitro study. Iran J Pharm Res. 2011;10(3):631–642.
- Wang Y, Karmakar T, Ghosh N, Basak S, Sahoo NG. Targeting mangiferin-loaded N-succinyl chitosan-alginate grafted nanoparticles against atherosclerosis – A case study against diabetes-mediated hyperlipidemia in rats. Food Chem. 2022; 370:131376.
- Yadav M, Mishra P, Mishra SK. Naringin: A potential natural product in pain management. Ther Adv Endocrinol Metab. 2018; 9(3):1–10.
- Zhang J, Wang X, Li G, Shi Y, Wang X, Zhao D. Nanoparticle delivery of natural products in the prevention and treatment of diabetes: current knowledge and future directions. Int J Nanomedicine. 2020 Jul;15:7767-7782.
- Zhang L, Gu FX, Chan JM, Wang AZ, Langer RS, Farokhzad OC. Nanoparticles in medicine: therapeutic applications and developments. Clin Pharmacol Ther. 2008;83(5):761-769.
- Zhang X, Liu Y, Wang J, Chen Q, Li Z. Nanoparticle delivery of naringin enhances anti-inflammatory effect in animal models. J Nanomedicine. 2021; 16(2):142–150.

- Zhang XF, Liu ZG, Shen W, Gurunathan S. Silver nanoparticles: Synthesis, characterization, properties, applications, and therapeutic approaches. Int J Mol Sci. 2016;17(9):1534.
- Zhang Y, Ma Y, Gao X, Chen Y, Wang Y. Advances in polymeric nanoparticles for drug delivery systems. Curr Drug Metab. 2022;23(2):144–56.

CHAPTER 6

SUMMARY & CONCLUSION

The present study was designed to investigate and establish optimized nanocarrier systems for the delivery of phytoconstituents—naringin, quercetin, mangiferin and ellagic acid—to overcome issues like poor solubility, low bioavailability, and rapid metabolism. Four types of nanoformulations were evaluated: chitosan-based, polycaprolactone-based, and metal (silver and copper) nanoparticle-based systems.

Key Findings:

1. Naringin and Quercetin loaded Chitosan Based Nanoparticles:

Due to their limited solubility and instability in biological environments, both compounds benefit from protective and controlled-release delivery systems. The use of chitosan, a biocompatible, mucoadhesive polymer, offered a promising platform for the oral and ocular delivery of these bioactives.

Nanoparticles were prepared via the ionic gelation method, using tripolyphosphate (TPP) as the cross-linking agent. Optimization of the chitosan:TPP ratio and drug loading resulted in nanoparticles with uniform size distribution, confirmed by DLS, SEM, and TEM analysis, with particle sizes within the nanometre range, high entrapment efficiency (EE%) and adequate zeta potential, ensuring colloidal stability and favourable interaction with biological membranes. FTIR spectroscopy confirmed the incorporation of naringin and quercetin without chemical modification, indicating physical entrapment. SEM and TEM micrographs revealed spherical, non-aggregated particles, confirming the morphological uniformity of the system and successful synthesis through a reproducible method. Both naringin and quercetin-loaded nanoparticles exhibited a biphasic release pattern, with an initial burst release followed by controlled drug release. Kinetic modeling of the release data fit best with the Higuchi models, indicating diffusion-controlled release, specifically Fickian diffusion. These release characteristics suggest that the formulations are well-suited for prolonged therapeutic effects, reducing dosing frequency and enhancing patient compliance. Anti-inflammatory studies demonstrated significantly enhanced efficacy of the nanoparticles over free drugs, which can be attributed to improved mucosal permeability, slower enzymatic degradation, and sustained release at the site of action.

For quercetin, additional ocular evaluation was performed. HET-CAM test confirmed the absence of ocular irritancy, making the formulation safe for ophthalmic applications. DPPH antioxidant assay showed higher free radical scavenging potential of nanoparticle-encapsulated quercetin compared to its free form. Permeation studies through excised goat cornea demonstrated increased transcorneal flux and retention of quercetin from nanoparticles, enhancing its local bioavailability.

This investigation establishes that chitosan-based nanoparticles are highly effective carriers for the delivery of naringin and quercetin, achieving enhanced stability and solubility, controlled and sustained release profiles, improved anti-inflammatory and antioxidant efficacy.

Overall, the study's results demonstrate the intriguing possibilities of chitosan-based nanocarriers as delivery system, providing increased bioactivity and prolonged release. Such a platform is particularly beneficial for oral and ocular drug delivery, offering localized and sustained therapeutic action with minimal side effects. These characteristics make them a promising candidate for additional research and development in the management of pathologic conditions overcoming the limitations of bioactive phytochemicals.

2. Polycaprolactone-Based Nanoparticles of Naringin and Mangiferin:

(PCL)-based nanoparticles were prepared for encapsulating naringin and mangiferin, two phytoconstituents known for their antioxidant, antidiabetic, and cardioprotective potential. Due to their poor aqueous solubility, low bioavailability, and susceptibility to gastrointestinal degradation; both compounds benefit substantially from nanocarrier-based delivery.

The nanoparticles were prepared using a solvent evaporation technique, with systematic optimization of polymer (PCL) concentration and surfactant ratios to achieve favorable particle characteristics. The optimized formulations demonstrated particle size in the nano-range (<250 nm), ideal for cellular uptake and passive targeting, excellent encapsulation efficiencies, indicative of excellent drug loading capacity, zeta potential values in the moderately negative range, suggesting adequate surface stability and minimized aggregation in suspension. FTIR analysis confirmed the absence of chemical interaction between the drugs and polymer, with characteristic functional groups

preserved. Thermal analysis profiles revealed enhanced thermal stability and drug encapsulation in an amorphous form, which is known to improve solubility and bioavailability. The in vitro release study showed sustained drug release profile extending over 24 hours, essential for maintaining steady therapeutic levels. The release data best fit the Higuchi model and Korsmeyer–Peppas equation, indicating a diffusion-controlled mechanism with non-Fickian behavior. This confirms that both diffusion and polymer relaxation contribute to the release profile. Naringin-loaded PCL nanoparticles exhibited significantly better hypoglycemic activity compared to the free drug, highlighting enhanced pharmacodynamic action. Similarly, mangiferin-loaded PCL nanoparticles demonstrated improved anti hyperlipidemic activity as compared to the free drug.

These enhanced effects are attributed to the hydrophobic and biodegradable nature of PCL, which protects the encapsulated drug in the gastric environment, prevents enzymatic degradation, and facilitates controlled drug release at the intestinal pH, aligning with the in vitro release patterns. Polycaprolactone-based nanoparticles developed in this study serve as a promising delivery system for bioactive phytoconstituents such as naringin and mangiferin. The optimized formulations offered, improved drug loading and stability, controlled and sustained drug release, and enhanced therapeutic efficacy. These benefits arise from the unique physicochemical properties of PCL, especially its slow degradation rate, hydrophobicity, and biocompatibility, making it an ideal candidate for prolonged gastrointestinal delivery.

The results collectively confirm that PCL nanoparticles significantly enhance the pharmacological profile of encapsulated phytochemicals by improving their residence time, permeability, and release kinetics. Furthermore, these systems hold promise for reducing dosing frequency, improving patient adherence, and broadening the clinical utility of herbal compounds in chronic metabolic disorders.

3. Metallic Nanoparticles Loaded with Ellagic Acid and Mangiferin:

This study focused on the development and characterization of metallic nanoparticle-based drug delivery systems using silver and copper nanoparticles to enhance the delivery of poorly soluble bioactives—ellagic acid and mangiferin. Both phytoconstituents suffer from inherent limitations such as low aqueous solubility, poor bioavailability, and rapid metabolism, limiting their therapeutic potential. The application of metal based nanocarriers may provide a strategic platform to overcome these barriers.

Silver and copper nanoparticles were successfully synthesized via chemical reduction using ascorbic acid as the reducing agent and DDAB/PVA as the stabilizer. The formulations were optimized and evaluated for physicochemical properties including particle size within the ideal nanometre range, zeta potential indicating good colloidal and high entrapment efficiency for both ellagic acid and mangiferin, confirming effective drug loading. Characterization via FTIR spectroscopy confirmed the retention of the functional groups of the drugs, indicating no chemical interaction with the nanoparticle matrix and suggesting physical encapsulation. Thermal analysis supported the thermal stability and entrapment of ellagic acid and mangiferin, with no signs of degradation during formulation. The in vitro release studies revealed a biphasic release profile, beginning with an initial burst followed by sustained drug release over time. The controlled release behaviour of the metallic nanoparticles provided a significant improvement over the pure phyto drugs which are otherwise rapidly eliminated or poorly absorbed due to first-pass metabolism and low membrane permeability. The in vitro antioxidant and antimicrobial activities of ellagic acid and mangiferin were retained post-encapsulation. Additionally, the incorporation of silver and copper conferred synergistic antimicrobial properties.

The outcomes of this research emphasize that metallic nanoparticles—particularly silver and copper-based systems—are highly promising nanocarriers for the delivery of poorly bioavailable phytoconstituents such as ellagic acid and mangiferin. These systems enhance solubility, stability, and bioavailability, enable sustained and controlled release, improve antioxidant, anticancer, and antimicrobial efficacy, and offer biocompatible and safe delivery platforms, especially for topical administration. The dual functionality of

metallic nanoparticles—acting as both a carrier and therapeutic agent—positions them as a powerful approach for targeted drug delivery.

This research successfully developed and evaluated three distinct nanocarrier systems—chitosan-based, polycaprolactone-based, and metallic (silver and copper) nanoparticles—for the efficient delivery of poorly bioavailable phytoconstituents including naringin, quercetin, mangiferin, and ellagic acid. Each system demonstrated unique advantages tailored to specific therapeutic needs.

Chitosan nanoparticles, derived from a natural biopolymer, offered biocompatibility, mucoadhesion, and controlled release suitable for mucosal and ocular applications. Polycaprolactone nanoparticles, due to their hydrophobicity and slow degradation, enabled high drug encapsulation and sustained release ideal for chronic systemic therapies. Metallic nanoparticles, particularly those based on silver and copper, exhibited rapid release, potent antimicrobial activity making them highly suitable for topical and infection-related applications.

All formulations demonstrated favorable physicochemical characteristics such as nanoscale size, high entrapment efficiency, and absence of drug-polymer interaction ensuring stability, biocompatibility, and enhanced therapeutic effect. In vitro and in vivo evaluations confirmed improved drug release kinetics, bioavailability, and appreciable biological activity in animals. The incorporation of phyto-drugs into these nanocarriers significantly enhanced their pharmacological profiles, overcoming key limitations such as poor solubility, low permeability, and rapid clearance.

In conclusion, nanoparticle-based delivery systems provide a versatile and effective platform for the targeted, sustained, and patient-compliant administration of natural bioactives, bridging the gap between traditional phytotherapy and modern pharmaceutical innovation. This work paves the way for further translational research and clinical exploration of phyto-nanomedicine in the treatment of diverse chronic and acute conditions.

List of Publications Provided

(a) **Chaki R**, Basak S, Sharma A, Nasare VD, Ghosh N, Mandal SC. Biocompatible nanocarriers of bioactive flavonoid naringin: Design, formulation, and comprehensive characterization. J Appl Pharm Sci. 2025. http://doi.org/10.7324/JAPS.2025.222894.

List of Presentation in National/ International conferences:

a) **Chaki R**, Banerjee A, Ghosh B, Chakraborty P, Mandal SC. Formulation & evaluation of chitosan-based quercetin dihydrate nanoparticles for ocular drug delivery. In: Proceedings of the PSIT Conference; 2024 September 2-3; Kanpur, India. Abstract No: PSIT/PP01/0143.

b) **Chaki R**, Chakraborty P, Bera A, Panja J, Basak S, Ghosh N, Mandal SC. Exploring the anti-inflammatory and antimicrobial potential of copper nanoparticles loaded with ellagic acid for ocular inflammation. In: Abstract Booklet of NATCON 2025; April 25-26; Durgapur, India. Abstract No: BCRCP-NATCON25-0019.

Book Chapters:

a) **Chaki R**, Ghosh N, Mandal SC. Phytopharmacology of herbal biomolecules. In: Mandal SC, Nayak AK, Dhara AK, editors. Herbal Biomolecules in Healthcare Applications. 1st ed. Academic Press; 2022. p. 101–19. ISBN: 9780323858526.

b) Ghosh N, **Chaki R**, Kundu A, Mandal SC. Herb and drug interaction. In: Mandal SC, Mandal V, Konishi T, editors. Natural Products and Drug Discovery. 1st ed. Elsevier; 2018. p. 467–90. ISBN: 9780081020814.

Journal of Applied Pharmaceutical Science Vol. 0(0), pp 001-010, xxx, 2025
Available online at http://www.japsonline.com
DOI: 10.7324/JAPS.2025.222894
ISSN 2231-3354

Biocompatible nanocarriers of bioactive flavonoid naringin: Design, formulation, and comprehensive characterization

Rituparna Chaki[1*], Souvik Basak[1], Arpana Sharma[2], Vilas D. Nasare[2], Nilanjan Ghosh[3], Subhash C. Mandal[3]

[1]Dr. B.C. Roy College of Pharmacy and Allied Health Sciences, Durgapur, India.
[2]Department of Pathology and Cancer Screening, Chittaranjan National Cancer Institute, Kolkata, India.
[3]Department of Pharmaceutical Technology, Jadavpur University, Kolkata, India.

ARTICLE HISTORY

Received on: 02/10/2024
Accepted on: 18/03/2025
Available Online: XX

Key words:
Anti-inflammatory, chitosan, entrapment, nanocarriers, naringin, solubility.

ABSTRACT

Naringin (NAR), a citrus flavonoid has been reported to have anti-inflammatory, antitumor, antiviral, antiadipogenic, and cardioprotective qualities. However, because of its poor aqueous solubility, therapeutic applications of NAR are limited. The present research involves development of nanocarriers of NAR using biocompatible natural polymer chitosan and tripolyphosphate using ionic gelation method. Surface morphology studies indicated the structure of the prepared nanocarriers with an entrapment of more than 80% and appreciable average size range of around 100 nm. Drug release studies suggested that the drug released at a controlled manner with around of around 65% over a period of 6 hours with a burst release of around 20% in the first hour. 3-(4, 5-dimethythiazol2-yl)-2, 5-diphenyl tetrazolium bromide test using HEK 293 cells demonstrated that highest concentration of NAR loaded nanocarriers (100 µM) showed optimal viability and cells were not harmed by nanocarriers. *In-vivo* anti-inflammatory activity study suggested that prepared formulation (50 mg/kg) significantly reduced development of carrageenan induced paw edema, comparable with diclofenac treated rats (10 mg/kg) but significantly enhanced for rats treated with NAR only (50 mg/kg). Together, the results suggested that chitosan based nanocarriers could be an efficient tool to deliver naringin thus ensuring better bioavailability to enhance its therapeutic potential.

INTRODUCTION

Numerous research-based studies have shown the important therapeutic benefits of phytochemicals. Despite being researched to treat a number of complex human illnesses, phyto drugs have a number of limitations that keep them from realizing their full potential as active pharmaceutical ingredients. Low permeability, low water solubility, high toxicity, instability, low bioavailability, are some of these limiting factors which make the formulation development of phytodrugs [1,2]. Drug delivery for conditions like chemotherapy, diabetes, and cancer treatment may be improved by the use of nanocarriers for active phytoconstituents, which have demonstrated encouraging results in this regard. Utilizing this approach, some of its disadvantages might be eliminated and a stable pharmaceutical product made entirely of phytochemicals trapped in nano-carriers could be developed. When appropriately adapted, enabling the administration through nanocarriers may increase the drug's systemic availability and desired target action. [3].

Many fruits, including citrus fruits, tomatoes, and bergamot, contain flavanones, also known as flavonoids, like naringenin. Additionally, it exists as glycosides, most notably as naringin (NAR). This phytochemical is thought to have anti-inflammatory, antitumor, antiviral, antiadipogenic, cardioprotective properties [4]. A study has suggested the protective activity of NAR against the Lipopolysaccharide -induced apoptosis in PC12 cells [5]. The findings by Zhao *et al.* [6] indicated that NAR inhibits inflammation and apoptosis in endothelial cells by controlling the Hippo-YAP Pathway. The cardio protecting mechanism and effect were summarized by Heidary Moghaddam *et al.* [7]. Another

*Corresponding Author
Rituparna Chaki, Dr. B.C. Roy College of Pharmacy and Allied Health Sciences, Durgapur, India. E-mail: rituparna.chaki@gmail.com

research has elucidated the anti-degenerative properties for cartilage and bones [8]. Bajgai *et al.* [9] comprehensive analysis from 2024 provides insight on how sepsis-induced multiple organ dysfunction can be alleviated. However, it has also been reported to have low bioavailability because of poor aqueous solubility and hence several researchers have suggested various ways to improve its delivery for effective therapeutic benefits [10–13].

In this work, the biocompatible natural polymer chitosan was used to load naringin into nanocarriers. Chitosan is a natural polycationic polymer that can attach to mucous membranes and increase absorption in the gastrointestinal tract by loosening the tight connections between epithelial cells. In recent years, chitosan has been widely researched due to its exceptional ability to serve as a nanocarrier material [14]. They are affordable, have a large range of drug compatibility, and allow for sustained delivery [15]. As a crosslinking agent, sodium tripolyphosphate (TPP) is utilized [16]. When combined with chitosan, sodium TPP works wonders as a crosslinking agent. By forming stable nanopockets, they prolong the release of the medicine and help it travel to its target site of action. In order to examine naringin's bioavailability and possible anti-inflammatory effects, the current study employs the ionotropic gelation process to create chitosan-TPP cross-linked nanoparticles (NPs). The prepared NPs were characterized for drug loading, size distribution, surface morphology and release studies. Rats were used in *in vivo* anti-inflammatory study, and HEK 293 cells were used in an *in vitro* cytotoxicity assay to confirm non-toxicity to normal cell lines.

MATERIALS AND METHODS

Materials

Naringin, chitosan (≥75% deacetylated), and dimethyl sulfoxide (DMSO) was purchased from Sigma Aldrich. Glacial acetic acid and sodium TPP were purchased from HiMedia Laboratories, dialysis membrane of MW cut off, 12,400 was purchased from Sigma Aldrich. All other chemicals used for the research study were of laboratory grade. 3-(4, 5-dimethythiazol2-yl)-2, 5-diphenyl tetrazolium bromide (MTT) used for cytotoxicity studies was purchased from Sigma Aldrich. All chemicals for cell culture analysis were cell culture grade.

Method of preparation of naringin loaded chitosan (NLC) nanocarriers

NLC nanocarriers were created via the ionic gelation technique. Acetic acid 1% (v/v) was used to prepare chitosan solution. The chitosan solution was continuously mixed as naringin was added dropwise. Over the course of 2 hours, while stirring continuously, the chitosan solution was gradually combined with the sodium TPP solution, which was kept at 4°C [17,18]. Chitosan was used at different concentrations (0.5–2 mg/ml). Drug was incorporated into the NLC nanocarriers at a concentration of 0.25 mg/ml. Amount of TPP used was optimized at 0.5 mg/ml which was fixed for all formulations. To find the best formulation, a range of TPP volumes, drug concentrations, and polymer concentrations were tested and the best formulations were tabulated in Table 1.

Table 1. Impact of chitosan concentration increase on ZP, PDI, and particle size.

Formulation	Chitosan (mg/ml)	Particle Size (nm)	PDI	ZP (mV)	%LC	%EE
NLC1	0.5	91.92	0.2	25.6	25	75.25
NLC2	1	130.3	0.25	28.1	16.67	82.41
NLC3	1.5	215.21	0.43	32.2	12.5	65.5
NLC4	2	470.5	0.33	36.6	10	58.8

Characterizations of NLC nanocarriers

Fourier Transform Infrared study (Fourier Transform Infrared study) spectrum analysis

The FTIR studies were carried out for NAR, chitosan and the NLC carriers under identical conditions to detect any possible interactions between the components that may lead to precipitation of the drug. It was carried out by mixing the sample with potassium bromide to form a pellet and scanning the sample over a wavelength from 4,000 to 400 cm^{-1}.

X-ray crystallography analysis

The X-ray crystallography of NAR, blank NLC carriers, and NLC carriers containing NAR was performed by Cu Kα radiation, at a voltage of 40 kV and 30 mA. The angle of scanning was adjusted from 5° to 70°, and the scanned rate was 4°/min.

Entrapment efficiency (EE)

After ultra-centrifuging NLC samples, the sediment and supernatant fluids were gathered. Absorbance was then measured with a UV spectrophotometer in the supernatant for the unentrapped drug concentration [19]. EE and drug loading capacity (LC) was determined using to equation:

EE = (Amount of NAR encapsulated into formulation)/(Amount of the total NAR added) × 100

LC = (Weight of NAR in formulation)/(Total weight of the formulation) × 100

Physical characterization

Using a Zetasizer Nano Instrument, dimension of the prepared NLCs was determined. A suitable concentration of NLC was agitated at 100 rpm and maintained at 37°C in distilled water. After being allowed to dry at ambient temperature, the NLC nanocarriers' structure was examined using a scanning electron microscope (SEM) and transmission electron microscope (TEM) to study their surface properties. For TEM, a drop of diluted NLC suspension was deposited on a film-coated copper grid, stained with one drop of 2% (w/v) aqueous solution of phosphotungstic acid, and then allowed to dry for contrast enhancement.

In vitro release study

Naringin, equivalent to 5 mg, was filled into a dialysis bag and placed in phosphate buffer solution (pH 7.4, 50 ml). The

beaker was magnetically stirred at 100 rpm while being kept at 37°C ± 0.5°C. UV spectrophotometry was used to measure the absorbance after 5 ml samples were taken out and replaced with new buffer solution at predefined intervals [19].

Cytotoxicity study

Cell line and reagent: The National Collection of Cell Sciences, Pune is the source of human derived embryonic kidney HEK 293 cells. The cells were kept in modified Eagle's medium supplemented with 2 mM glutamine, 10% fetal bovine serum that has been heat-inactivated, 1% penicillin-streptomycin solution, and 5% CO_2 at 37°C in a humidified atmosphere.

Cytotoxicity assay: The MTT technique was employed to assess the vitality of cells *in vitro* [20]. In 96-well plates, 8,000 HEK 293 cells were planted each well and allowed to attach for a full day. The following day, the used media was removed and replaced with new glutamine medium containing varying concentrations of NAR (6.25, 12.25, 25, 50, and 100 µM) for 24 hours. After the target time point was reached, 20 µl of MTT dye (5 mg/ml) dissolved in phosphate buffer saline was added to each well, and the incubator was left in the dark for 4 hours at 37°C. After carefully extracting the media containing MTT dye, 100 µl of DMSO was given to each well to dissolve the formazan crystal. The wells were then left for 10 minutes at room temperature in the dark. Each well's absorbance was calculated using a micro-plate reader at 570 nm [21].

$$\text{Cell viability (\%)} = A_{treatment} - A_{blank} / A_{control} - A_{blank} \times 100\%$$

Anti-inflammatory activity

Male and female Wistar rats weighing between 100 and 150 g were employed to assess the formulation's anti-inflammatory properties. Before the trials began, the rats were given a balanced food and unlimited access to water for approximately 2 weeks while they adjusted to the laboratory environment. Every animal was housed at 24ºC ± 2ºC with a relative humidity of 60% ± 5% and exposed to a 12/12 hour light/dark cycle by the appropriate institutional review body. Animal experiments in the present study and the study protocol was reviewed and approved by Institutional Animal Ethical Committee (IAEC) of Dr B C Roy College of Pharmacy and AHS (Reference No: BCRCP/IAEC/2/2019).

The paw edema model induced by the phlogistic agent, carrageenan, was employed to evaluate the anti-inflammatory activity of prepared NLC carriers. Rats were divided into five groups ($n = 6$), and were given one of the following treatments: Group 1: distilled water + carrageenan; Group 2: blank formulation + carrageenan; Group 3: free NAR (50 mg/kg, p.o) + carrageenan; Group 4: NLC (50 mg/kg, p.o) + carrageenan; and Group 5: diclofenac (10 mg/kg, p.o.) + carrageenan.

A single hour following the administration of the various agents, the right hind paw's sub-plantar tissue was injected with 0.1 ml carrageenan (1% w/v in saline) to induce edema. After administering carrageenan, paw volume was measured plethysmographically at 0th, 1st, 2nd, 3rd, 4th, and 6th hours [22,23]. The % of inhibition was calculated using the following formula:

$$\% \text{ Inhibition} = (\text{Increase in paw edema}_{control} - \text{Increase in paw edema}_{treated}) / \text{Increase in paw edema}_{control}) \times 100$$

RESULTS AND DISCUSSION

Synthesis of NLC nanocarriers

Naringin loading into chitosan is facilitated by electrostatic attraction, hydrogen bonding, and hydrophobic interactions. Chitosan, a hydrophilic organic polymer, has a positive charge due to protonation in an acidic environment. NAR with hydroxyl and glycoside groups, can create hydrogen bonds with chitosan's amino groups, keeping it stable inside the matrix. Hydrophobic pockets in chitosan can capture lipophilic NAR molecules and load them into the chitosan network. Stabilization of NAR within the chitosan matrix may be due to weak van der Waals forces, which facilitate non-covalent interactions over short distances. Chitosan's gel-like network in aqueous environments allows it to form complexes with various drug molecules, including NAR. . Naringin can be encapsulated within the chitosan matrix by mixing it with chitosan. When chitosan is dissolved in an acidic solution, it swells and turns cationic. When NAR is added to the chitosan solution, it interacts with the chitosan through hydrogen bonding and electrostatic interactions [24–26].

Characterization and optimization of NLC nanocarriers

FTIR spectrum analysis: The FTIR spectra of NAR revealed two prominent peaks corresponding to the wavenumber of the hydroxyl group at wave number regions 1,664.02 and 3,330.14 cm^{-1}. The compound's structure and the outcome of the infrared spectroscopy (IR) spectrum assessment for NAR matched, confirming the result. The IR spectra of chitosan show several absorption bands corresponding to its functional groups. A broad peak around 3,431.78 cm^{-1} is observed due to the stretching vibrations of hydroxyl (O-H) groups, often associated with hydrogen bonding. The N-H stretching of primary amine groups is also present, overlapping with the O-H band. The C-H stretching vibrations of the chitosan polymer backbone appear at 2,925.98 and 2,881.09 cm^{-1}. The most prominent peaks are the amide I band at 1,642.03 cm^{-1}, which corresponds to the stretching of carbonyl bonds from residual N-acetyl groups in partially deacetylated chitosan. The C-N stretching of amine groups shows characteristic peaks around 1,381.03 and 1,320.80 cm^{-1}. The FTIR spectra of the chitosan nanoparticle verified the presence of the chitosan's important peak. The tip of the peak in chitosan NPs has shifted to 3,427.85 cm^{-1}, indicating an increase in hydrogen bonding; in TPP. The FTIR spectrum of a chitosan nanoparticle loaded with NAR revealed a characteristic peak change from 1,664.02 to 1,642.09 cm^{-1}, indicating that NAR had been incorporated into the chitosan nanoparticle without any possible interaction that may lead to precipitation of the drug (Fig. 1a). All functional groups have been mentioned in Table 2.

The Drug-polymer (chitosan) characterization has further been done with the help of X ray diffraction spectra of the compound together with the polymer (chitosan). The drug diffractogram (Fig. 1b (A)) shows that most of the peaks are sharp and crisp indicating that the drug bears mostly crystalline nature

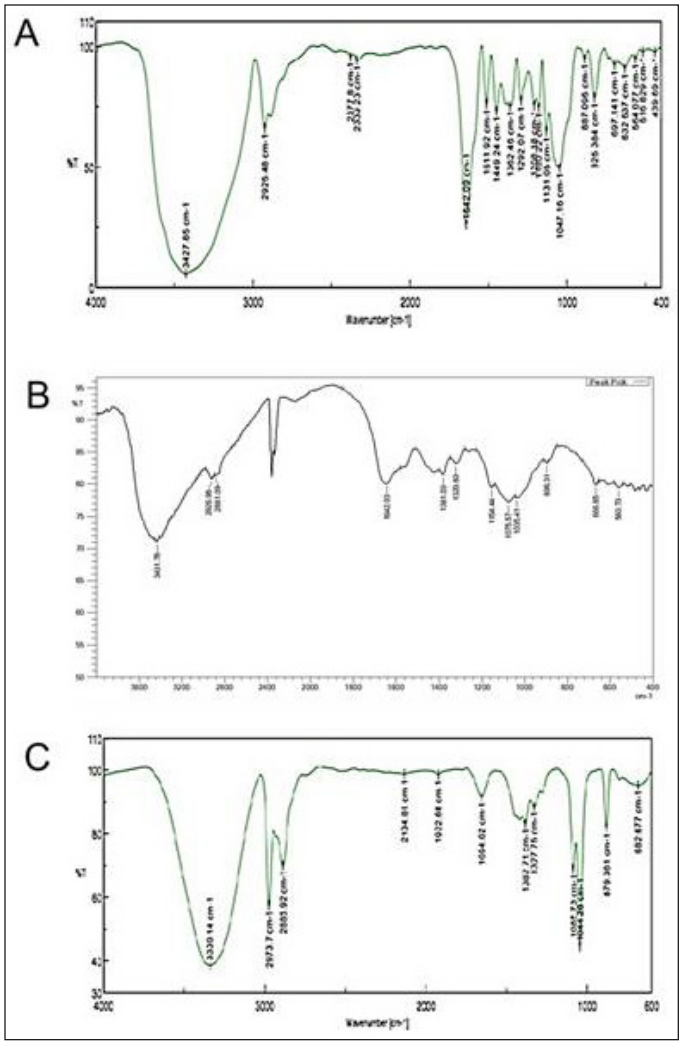

Figure 1. (A) FTIR spectra of Naringin (B) FTIR spectra of Chitosan (C) FTIR spectra of NLC formulation.

in its form. However, the chitosan peaks (Fig. 1b (B)) revealed suppressed and interspersed peaks suggesting its amorphous nature. Interestingly the formulation diffractogram (Fig. 1b (C)) reveals high resemblance with the polymer suggesting that the polymer has been in the outer core of the formulation while the drug has been entrapped inside the polymeric core. Moreover, the height of the peaks of the formulation at specific 2θ values are found to be quite different from that of the polymer as well as the drug suggesting that there have been change of crystallinity or arrangement of atoms in specific planes of the formulation (or Drug-Polymer complex). Now this could be a plausible inference that the change of crystallinity or atomic arrangement (marked by the change of intensity of peaks) might be due to the drug-polymer interaction that has incurred to the value addition of the complex.

In order to produce NLC nanocarriers with the desired size range, the formulation process variables were optimized. The zeta potential (ZP), particle size, entrapment efficiency, and polydispersity index (PDI) were all significantly impacted by each of these process variables. Table 1 illustrates how increasing the chitosan concentration affects ZP, PDI, and average particle size. Particle size average, PDI, and ZP all grew progressively with rise in the level of chitosan. The particle size of the prepared NPs ranged from 91.92–470.5 nm which suggested that the size of the NPs increased as the concentration of chitosan increased from 0.5 to 2 mg/ml. The ZP of the NPs varied around +30mV which indicated a good stability for the prepared NPs. Figure 2 depicts the particle size of one of the optimized formulations. Furthermore, increasing the chitosan content from 0.5 to 1 mg/ml resulted in a noticeable improvement in the nanoparticles' encapsulation efficiency. However, an increase in concentration beyond 1.5 mg/ml further showed a decrease in the drug entrapment, possibly because of inconsistent interaction of chitosan with TPP. At

Table 2. FTIR analysis grouping.

Peaks (wavenumber in cm^{-1})	Naringin	Chitosan	Naringin-chitosan nanoparticle
1,664.02 cm^{-1}	-C=O stretch of chalcopyrone moiety of the flavonoid		
3,330.14 cm^{-1}	-OH stretch the flavonoid		
3,431.78 cm^{-1}		-OH stretch of the polymer	
2,925.98 cm^{-1}		The C-H stretching vibrations of the chitosan polymer backbone	
2,881.09 cm^{-1}		The C-H stretching vibrations of the chitosan polymer backbone	
1,642.03 cm^{-1}		the stretching of carbonyl bonds from residual N-acetyl groups in partially deacetylated chitosan	
1,381.03 and 1,320.80 cm^{-1}		The C-N stretching of amine groups	
3,427.85 cm^{-1}			-OH peak shift to chitosan nanoparticle
1,664.02 to 1,642.09 cm^{-1}			-C=O stretch of chitosan nanoparticle

Figure 2. Particle size distribution of prepared NLCs.

higher chitosan concentrations, this could be explained by the formation of more chitosan chains per volume [27].

The NLC nanocarriers were spherical, well-separated, uniformly distributed, and had a rough surface and morphology, according to the morphology studies (Fig. 3a). Figure 3b exhibits well dispersed nanocarriers of chitosan through TEM under a magnification of 200× which corroborates with the results obtained by SEM.

In vitro release studies: Drug release studies indicated that a controlled release of approximately 65% of the drug could be achieved over 6 hours. All of the formulations, however, displayed a 15% burst release within the first hour. It is possible that the surface of the nanocarriers contained drug molecules, which would account for the initial fast release. The drug embedded in the matrix was the cause of the consistent and slow release of NAR from NPs. Results clearly suggests that with an increase in chitosan concentration there is a reduction in the rate of drug release from the nanocarriers (Fig. 4a] [28]. In order to know the mechanism of drug release from the formulations, the release data were treated according to zero-order, first-order, Higuchi, Hixson-Crowell and Korsmeyer Peppas model. None of the formulations followed complete zero order release pattern. The release profiles could be best expressed by Higuchi's plot as it exhibited high linearity (R^2 > 0.98). Thus, the mechanism of drug release from nanocarriers can be described by diffusion controlled mechanism with a burst release. The release exponent *n* was found to be less than 0.45 in the Korsmeyer-Peppas model for all formulations, which indicates Fickian diffusion, meaning drug release is controlled primarily by a diffusion mechanism without significant polymer relaxation or swelling. Since the Higuchi model also describes diffusion-driven release, the high linearity observed in the Higuchi plot (R^2 > 0.98) aligns well with the Fickian diffusion mechanism. This confirms that the drug release from the formulation follows a diffusion-controlled process without significant contributions from polymer erosion or swelling (Fig. 4b).

The linearity of the assay method was calculated by estimating the R^2 value of the curve. The R^2 estimated as 0.993 (Table 2) suggested a good linearity of the calibration curve. The limit of detection (LOD) was determined as 91.9059 µg/ml and limit of quantification (LOQ) as 278.5027µg/ml (Table 3). The accuracy (percentage recovery) varied from 99.96%–103.79% (Table 4 and Table 5).

MTT assay for assessing cytotoxicity

MTT test showed that the NAR did not damage the cells. The absorbance values increased at NAR doses in certain concentrations of NLC, but were non-significant as compared to untreated cells (p > 0.05). Figure 5a and b represents cell viability analysis. For viability, HEK 293 cells were treated with the indicated concentrations (0–100 µM) of NAR for 24 hours and MTT assay was performed to check cell viability. The data are presented as means of triplicate samples for each treatment and values given as mean ± SEM. Statistical analysis was performed by students

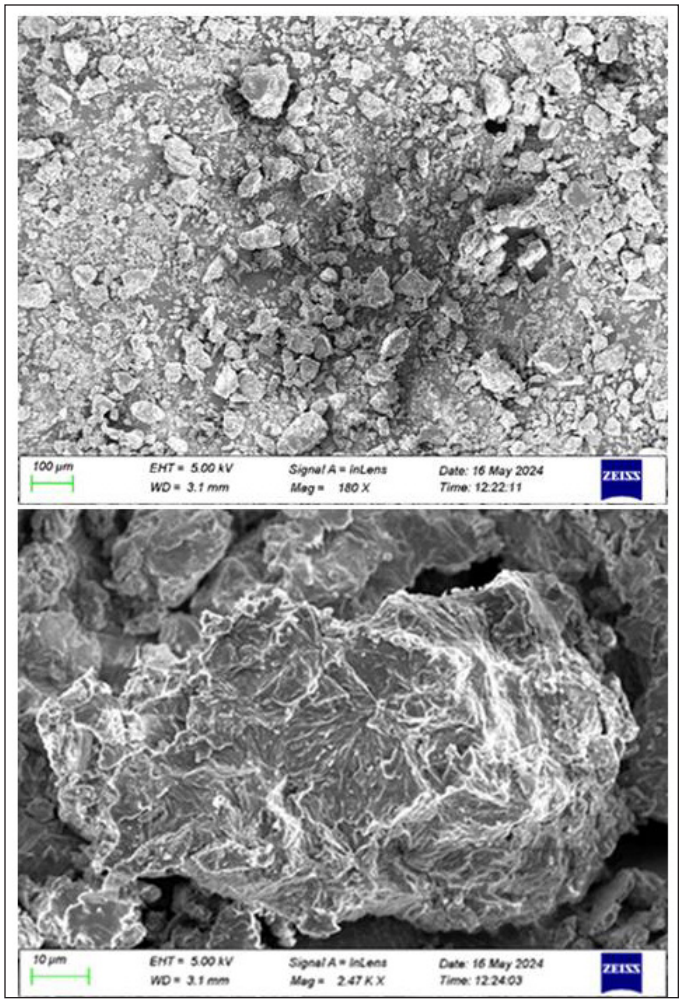

Figure 3a. Morphology study using scanning electron microscopy (SEM).

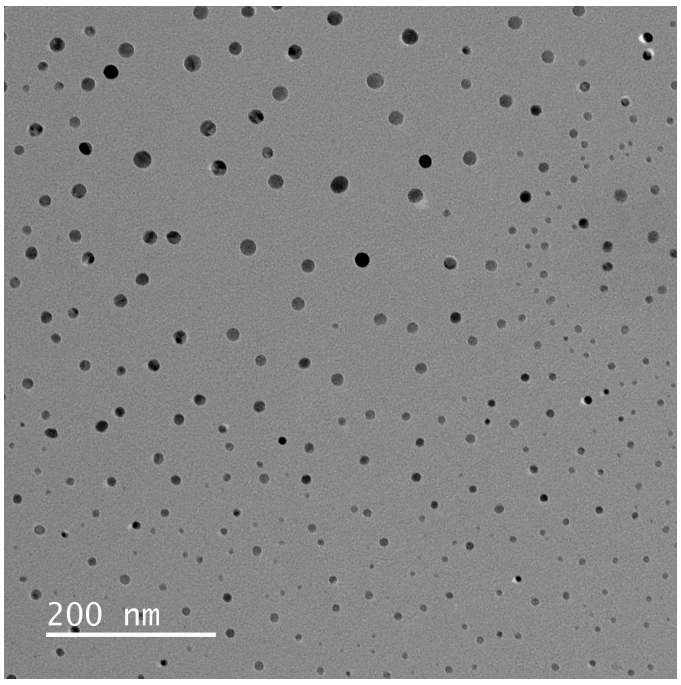

Figure 3b. Surface morphology study using transmission electron microscopy.

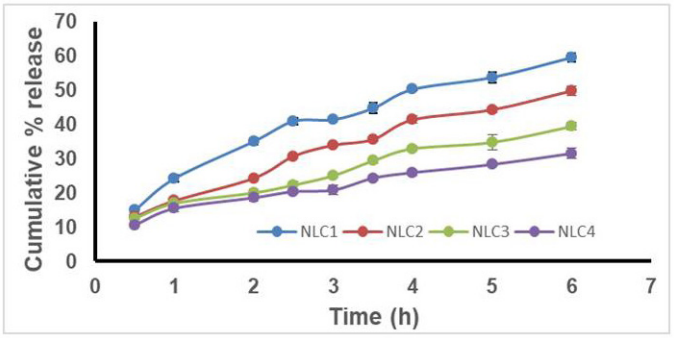

Figure 4a. Release profile of NLC formulations.

Figure 4b. Release kinetics of NLC formulations.

Table 3. Table for validation parameters.

Parameter	Value
Linearity	$R^2 = 0.993$
LOD (3.3 σ/s)	91.9059 µg/ml
LOQ (10 σ/s)	278.5027 µg/ml

σ = Standard deviation of the intercept; s = slope of the regression (fitting) curve.

t-test; Bars = SE; n.s. = non-significant. The cells exhibited optimal viability at the highest concentration of NLC (100 µM) and 0.5% chitosan, it was concluded that the cells were healthy safe at these concentrations which are nontoxic to the normal cell's growth and viability. Additionally, we saw no morphological alterations in the HEK 293 cells following the medication treatment as in comparison with the untreated group. Figure 6 represents images of morphological changes of untreated control and NLC-treated HEK 293 cells observed under an inverted light microscope (20× magnification) and no morphological changes are observed [29].

Anti-inflammatory activity

The posterior intraplantar left paw volume in the vehicle treated group grew gradually after receiving an injection of 0.1 ml of carrageenan (1% w/v), peaking at 0.89 ± 0.03 ml after 6 hours. The % inhibition of paw edema for the NAR treated group was found to be 9.52%, 13.95%, and 19.10% at the 3, 4 and 6 hours mark, respectively. At the 3, 4, and 6 hours

Table 4. Estimation of accuracy (recovery).

Taken concentration (µg/ml)								
	Abs 1	Abs 2	Abs 3	Recovered conc1 (µg/ml)	Recovered conc 2 (µg/ml)	Recovered conc 3 (µg/ml)	Average	SD
40	0.6321	0.6785	0.6624	39.10377	43.48113	41.96226	41.51572	2.222581
50	0.7345	0.749	0.7587	48.76415	50.13208	51.04717	49.98113	1.14897
60	0.8667	0.8989	0.8478	61.23585	64.27358	59.45283	61.65409	2.43744

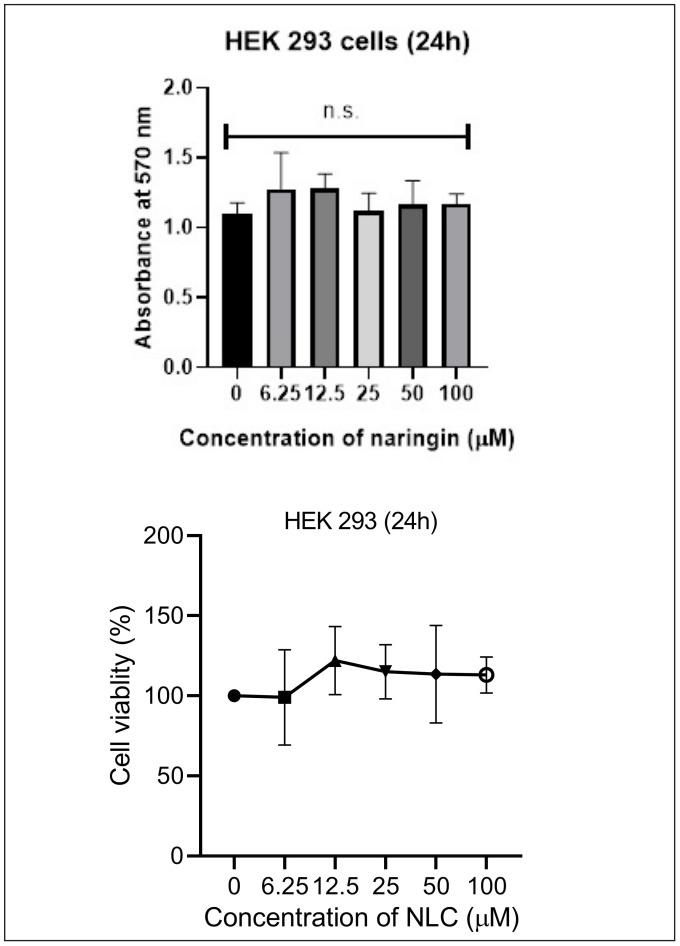

Figure 5. Graphs showing MTT assay for cytotoxicity analysis on HEK cells at different naringin concentrations against control.

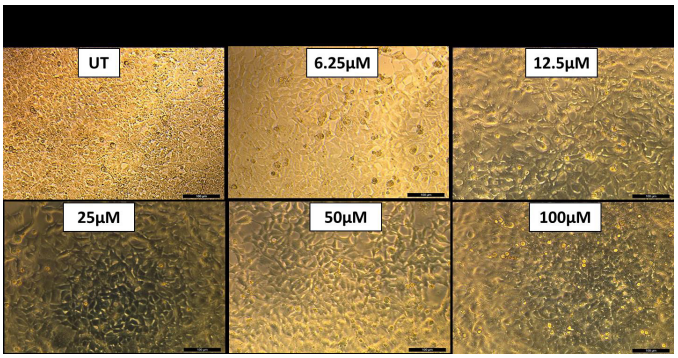

Figure 6. Microscopic images of no morphological changes of HEK cells at different naringin concentrations of NLC.

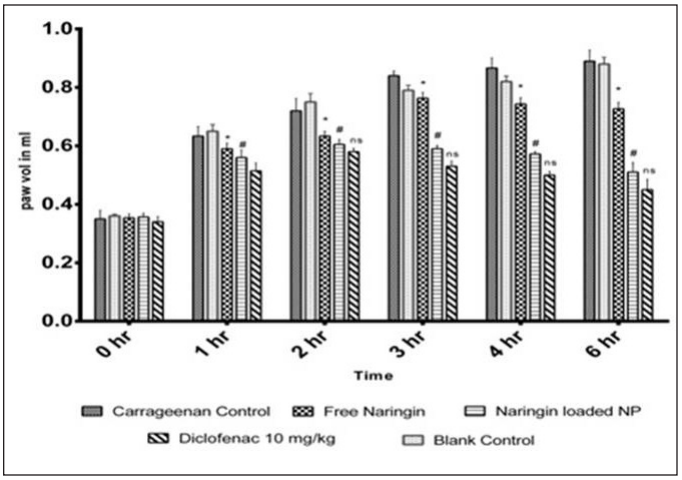

Figure 7. NLC's anti-inflammatory properties assessed over time using pleurisy induced by carrageenan.

marks, the percentage suppression of paw edema for the NAR loaded nanoparticle group was found to be 297.66%, 33.72%, and 42.67%, respectively. With $p > 0.05$, result was found to be similar to that of the diclofenac treated group with one way ANOVA, accompanied by Dunnett's test. The % inhibition for the diclofenac treated group was found to be 36.90%, 41.86% and 46.94% at the 3, 4 and 6 hours mark, respectively. Figure 7 explains NLC's anti-inflammatory properties assessed over time using pleurisy induced by carrageenan. Every value is presented as Average ± SEM ($n = 6$); * indicates a significant difference ($p < 0.05$) between the free NAR group and the conventional control group. Diclofenac treated; # denotes $p < 0.05$, significant difference compared amongst free naringin and naringin loaded nanoparticle group; when comparing the naringin-loaded nanoparticle group to the standard control group (treated with Diclofenac), ns indicates $p > 0.05$, non-significant (by one way ANOVA followed by Dunnett's test).

The acute anti-inflammatory efficacy of NLC has been assessed using pleurisy caused by carrageenan. Carrageenan is utilized in the screening process for anti-inflammatory compounds because it is a phlogistic agent and creates a severe inflammatory response when injected locally into a rat's paw. Carrageenan-induced inflammation occurs in three distinct

Table 5. Calculation of percentage recovery of the study.

Taken concentration (µg/ml)	Recovered concentration	Percentage recovery
40	41.51572327	103.7893082
50	49.98113208	99.96226415
60	61.65408805	102.7568134

phases: the first is characterized by the release of serotonin and histamine; the second is brought about by kinin production, bradykinin being the most prominent; and the third is regulated by prostaglandins. NLC inhibited the development of rat paw edema considerably during the middle phase of carrageenan-induced inflammation, and this effect was more pronounced during the third phase. This suggests that the anti-inflammatory properties of NLC may be mediated by reduction of prostaglandin activity in conjunction with the effects of vasoactive molecules (histamine, serotonin, and kinins) [30–33].

The putative clinical benefits of naringin are restricted due to its poor aqueous solubility, low bioavailability and high hepatic first-pass metabolism [4]. The naringin embedded in the NLC nanocarriers exhibited higher anti-inflammatory activity as compared to naringin can be attributed to several key factors observed in similar studies on naringin and other flavonoid-loaded NPs. First, NPs significantly enhance the bioavailability of poorly soluble compounds like naringin, ensuring a higher concentration of the active compound at the site of inflammation. Furthermore, naringin is released gradually and under control by NPs, resulting in a protracted therapeutic action that guarantees steady anti-inflammatory benefits throughout time. Furthermore, because of their tiny size, NPs enhance cellular absorption and make it easier for naringin to enter target immune cells like macrophages, where it can more successfully inhibit inflammatory reactions. Additionally, naringin is shielded by NPs from enzymatic breakdown in the blood or gastrointestinal tract, increasing the amount of the active ingredient that reaches the site of inflammation intact. This protective mechanism, coupled with improved pharmacokinetics, such as prolonged half-life and reduced clearance, further enhances the anti-inflammatory potential of naringin NPs [34–39].

CONCLUSION

In this study, we successfully prepared and evaluated chitosan-based nanocarriers encapsulating the citrus flavonoid naringin. The outcomes showed that the nanocarriers had advantageous physicochemical characteristics, such as a controlled release profile, appreciable encapsulation efficiency, and an ideal particle size. The efficient and repeatable synthesis technique used produced NPs with homogeneous morphology, as demonstrated by analyses using particle size analysis, SEM and TEM analysis. Naringin was found to be released from chitosan nanocarriers over an extended period of time, according to *in vitro* release studies, indicating the possibility of long-term therapeutic benefits. Furthermore, the anti-inflammatory potential of the naringin-loaded nanocarriers was significantly enhanced in comparison to free NAR, indicating that the encapsulation process preserved and possibly amplified the bioactivity of the flavonoid.

Overall, the study's results demonstrate the intriguing possibilities of chitosan-based nanocarriers as a NAR delivery system, providing increased bioactivity and prolonged release. These characteristics make them a promising candidate for additional research and development in the management of pathologic conditions where the therapeutic potential of NAR might be beneficial. To confirm these results and investigate the complete therapeutic potential of NLC nanocarriers, future research can be conducted on *in vivo* assessments and clinical trials.

AUTHOR CONTRIBUTIONS

All authors made substantial contributions to conception and design, acquisition of data, or analysis and interpretation of data; took part in drafting the article or revising it critically for important intellectual content; agreed to submit to the current journal; gave final approval of the version to be published; and agree to be accountable for all aspects of the work. All the authors are eligible to be an author as per the International Committee of Medical Journal Editors (ICMJE) requirements/guidelines.

FUNDING

There is no funding to report.

CONFLICTS OF INTEREST

The authors report no financial or any other conflicts of interest in this work.

ETHICAL APPROVALS

The study protocol was approved by the Institutional Animal Ethical Committee (IAEC) of Dr. B.C. Roy College of Pharmacy and Allied Health Sciences, India (Reference No: BCRCP/IAEC/2/2019).

DATA AVAILABILITY

All the data is available with the authors and shall be provided upon request.

PUBLISHER'S NOTE

All claims expressed in this article are solely those of the authors and do not necessarily represent those of the publisher, the editors and the reviewers. This journal remains neutral with regard to jurisdictional claims in published institutional affiliation.

USE OF ARTIFICIAL INTELLIGENCE (AI)-ASSISTED TECHNOLOGY

The authors declares that they have not used artificial intelligence (AI)-tools for writing and editing of the manuscript, and no images were manipulated using AI.

REFERENCES

1. Teeranachaideekul V, Müller RH, Junyaprasert VB. Encapsulation of ascorbyl palmitate in nanostructured lipid carriers (NLC): effects of formulation parameters on physicochemical stability. Int J Pharm. 2007;340(1–2):198–206. doi: https://doi.org/10.1016/j.ijpharm.2007.03.034

2. Siddiqui IA, Sanna V. Impact of nanotechnology on the delivery of natural products for cancer prevention and therapy. Mol Nutr Food Res. 2016;60(6):1330–41. doi: https://doi.org/10.1002/mnfr.201500928
3. Rahman HS, Othman HH, Hammadi NI, Yeap SK, Amin KM, Samad NA, *et al*. Novel drug delivery systems for loading of natural plant extracts and their biomedical applications. Int J Nanomedicine. 2020;15:2439–83. doi: https://doi.org/10.2147/IJN.S246498
4. Chen R, Qi QL, Wang MT, Li QY. Therapeutic potential of naringin: an overview. Pharm Biol. 2016;54(12):3203–10. doi: https://doi.org/10.1080/13880209.2016.1216133
5. Wang H, Xu YS, Wang ML, Cheng C, Bian R, Yuan H, *et al*. Protective effect of naringin against the LPS-induced apoptosis of PC12 cells: implications for the treatment of neurodegenerative disorders. Int J Mol Med. 2017;39(4):819–30. doi: https://doi.org/10.3892/ijmm.2017.2884
6. Zhao H, Liu M, Liu H, Suo R, Lu C. Naringin protects endothelial cells from apoptosis and inflammation by regulating the Hippo-YAP pathway. Biosci Rep. 2020;40(3):BSR20193431. doi: https://doi.org/10.1042/BSR20193431
7. Heidary Moghaddam R, Samimi Z, Moradi SZ, Little PJ, Xu S, Farzaei MH. Naringenin and naringin in cardiovascular disease prevention: a preclinical review. Eur J Pharmacol. 2020;887:173535. doi: https://doi.org/10.1016/j.ejphar.2020.173535
8. Gan J, Deng X, Le Y, Lai J, Liao X. The development of naringin for use against bone and cartilage disorders. Molecules. 2023;28(9):3716. doi: https://doi.org/10.3390/molecules28093716
9. Bajgai B, Suri M, Singh H, Hanifa M, Bhatti JS, Randhawa PK, *et al*. Naringin: a flavanone with a multifaceted target against sepsis-associated organ injuries. Phytomedicine 2024;130:155707. doi: https://doi.org/10.1016/j.phymed.2024.155707
10. Tang W, Wei Y, Lu W, Chen D, Ye Q, Zhang C, *et al.* Fabrication, characterization of carboxymethyl konjac glucomannan/ovalbumin-naringin nanoparticles with improving *in vitro* bioaccessibility. Food Chem X. 2022;16:100477. doi: https://doi.org/10.1016/j.fochx.2022.100477
11. Im AE, Eom S, Seong HJ, Kim H, Cho JY, Kim D, *et al*. Enhancement of debitterness, water-solubility, and neuroprotective effects of naringin by transglucosylation. Appl Microbiol Biotechnol. 2023;107(20):6205–17. doi: https://doi.org/10.1007/s00253-023-12692-6
12. Ge X, Jiang F, Wang M, Chen M, Li Y, Phipps J, *et al.* Naringin@ Metal-Organic framework as a multifunctional bioplatform. ACS Appl Mater Interfaces. 2023;15(1):677–83. doi: https://doi.org/10.1021/acsami.2c18503
13. Lee J, Kim K, Son J, Lee H, Song JH, Lee T, *et al.* Improved productivity of naringin oleate with flavonoid and fatty acid by efficient enzymatic esterification. Antioxidants (Basel). 2022;11(2):242. doi: https://doi.org/10.3390/antiox11020242
14. Jafernik K, Ładniak A, Blicharska E, Czarnek K, Ekiert H, Wiącek AE, *et al*. Chitosan-based nanoparticles as effective drug delivery systems: a review. Molecules. 2023;28(4):1963. doi: https://doi.org/10.3390/molecules28041963
15. Gulbake A, Jain SK. Chitosan: a potential polymer for colon-specific drug delivery system. Expert Opin Drug Deliv. 2012;9(6):713–29. doi: https://doi.org/10.1517/17425247.2012.682670
16. Özbaş-Turan S, Akbuğa J. Plasmid DNA-loaded chitosan/TPP nanoparticles for topical gene delivery. Drug Deliv. 2011;18(3):215–22. doi: https://doi.org/10.3109/10717544.2011.555596
17. Hoang NH, Le Thanh T, Sangpueak R, Treekoon J, Saengchan C, Thepbandit W, *et al*. Chitosan nanoparticles-based ionic gelation method: a promising candidate for plant disease management. Polymers (Basel). 2022;14(4):662. doi: https://doi.org/10.3390/polym14040662
18. Kumar S, Dilbaghi N, Saharan R, Bhanjana G. Nanotechnology as emerging tool for enhancing solubility of poorly water-soluble drugs. BioNanoSci. 2012;2:227–50. doi: https://doi.org/10.1007/s12274-012-0131-x
19. Joshi G, Kumar A, Sawant K. Enhanced bioavailability and intestinal uptake of gemcitabine HCl loaded PLGA nanoparticles after oral delivery. Eur J Pharm Sci. 2014;60:80–9. doi: https://doi.org/10.1016/j.ejps.2014.04.003
20. Md S, Alhakamy NA, Aldawsari HM, Asfour HZ. Neuroprotective and antioxidant effect of naringenin-loaded nanoparticles for nose-to-brain delivery. Brain Sci. 2019;9(11):275. doi: https://doi.org/10.3390/brainsci9110275
21. Hussain RF, Nouri AME, Oliver RTD. A new approach for measurement of cytotoxicity using colorimetric assay. J Immunol Methods 1993;160:89–96. doi: https://doi.org/10.1016/0022-1759(93)90011-l
22. Mandal SC, Maity TK, Das J, Saba BP, Pal M. Anti-inflammatory evaluation of *Ficus racemosa Linn.* leaf extract. J Ethnopharmacol. 2000;72:87–92. doi: https://doi.org/10.1016/S0378-8741(00)00215-4
23. Mandal SC, Lakshmi SM, Kumar CK, Sur TK, Boominathan R. Evaluation of anti-inflammatory potential of *Pavetta indica Linn.* leaf extract (family: Rubiaceae) in rats. Phytother Res. 2003;17(8):817–20. doi: https://doi.org/10.1002/ptr.1177
24. Agnihotri SA, Mallikarjuna NN, Aminabhavi TM. Recent advances on chitosan-based micro- and nanoparticles in drug delivery. J Control Release. 2004;100(1):5–28. doi: https://doi.org/10.1016/j.jconrel.2004.08.010
25. Sajjan P, Lingaraj L, Pujar M, Anandasadagopan SK. Chitosan nanoparticles as drug delivery systems: a review. J Pharm Sci Res. 2016;8(1):56–67.
26. Yadav M, Mishra P, Mishra SK. Naringin: a potential natural product in pain management. Ther Adv Endocrinol Metab. 2018;9(3):1–10. doi: https://doi.org/10.1177/2042018818778296
27. Al-Nemrawi NK, Alsharif SS, Dave RH. Preparation of chitosan-TPP nanoparticles: the influence of chitosan polymeric properties and formulation variables. Int J Appl Pharmaceutics. 2018;10(5):60–5. doi: https://doi.org/10.22159/ijap.2018v10i5.27577
28. Herdiana Y, Wathoni N, Shamsuddin S, Muchtaridi M. Drug release study of the chitosan-based nanoparticles. Heliyon. 2021;8(1):e08674. doi: https://doi.org/10.1016/j.heliyon.2021.e08674
29. Ramezani MR, Naderi-Manesh H, Rafieepour H. Cytotoxicity assessment of a gold nanoparticle-chitosan nanocomposite as an efficient support for cell immobilization: comparison with chitosan hydrogel and chitosan-gelatin. Biocell. 2014;38(1):11–6.
30. Ismail OI, Abidemi JA, Olufunmilayo OA. Analgesic and anti-inflammatory activities of *Cnestis ferruginea Vahl ex DC* (Connaraceae) methanolic root extract. J Ethnopharmacol. 2011;135:55–62. doi: https://doi.org/10.1016/j.jep.2011.02.009
31. Bamgbose SOA, Noamesi BK. Studies on cryptolepine II: inhibition of carrageenan-induced oedema by cryptolepine. Planta Med. 1981;42:392–6. doi: https://doi.org/10.1055/s-2007-971624
32. Lo TN, Almeida AP, Beaven MA. Dextran and carrageenan evoke different inflammatory responses in rat with respect to composition of infiltrates and effect of indomethacin. J Pharmacol Exp Ther. 1982;221:261–7.
33. Wang Y, Karmakar T, Ghosh N, Basak S, Sahoo NG. Targeting mangiferin-loaded N-succinyl chitosan-alginate grafted nanoparticles against atherosclerosis – A case study against diabetes-mediated hyperlipidemia in rats. Food Chem. 2022;370:131376. doi: https://doi.org/10.1016/j.foodchem.2022.131376
34. Zhang X, Liu Y, Wang J, Chen Q, Li Z. Nanoparticle delivery of naringin enhances anti-inflammatory effect in animal models. J Nanomedicine. 2021;16(2):142–50. doi: https://doi.org/10.2147/IJN.S282892
35. Patel R, Mehta T, Shah S, Desai P. Flavonoid-loaded nanoparticles for anti-inflammatory therapy: a comparative study. Drug Deliv Lett. 2019;10(2):89–95. doi: https://doi.org/10.2174/2210303109666190308094259

36. Singh A, Gupta N, Sharma R, Vashishta R. Enhanced cellular uptake and anti-inflammatory efficacy of naringin nanoparticles. Mol Pharmacol. 2020;17(4):225–33. doi: https://doi.org/10.1124/mol.118.113217
37. Gupta A, Kumar P, Aggarwal S, Khurana N. Protection of naringin from degradation using nanoparticles. J Drug Deliv Sci Technol. 2022;65:102–10. doi: https://doi.org/10.1016/j.jddst.2021.102110
38. Ahmed S, Alam M, Khan A, Hussain Z. Curcumin and flavonoid nanoparticles for targeted anti-inflammatory treatment. J Mol Med. 2020;98(5):311–20. doi: https://doi.org/10.1007/s00109-019-01817-w
39. Sharma D, Bansal R, Thakur V, Chawla P. Pharmacokinetic advantage of naringin nanoparticles in inflammation models. Nanomedicine (Lond). 2021;15(3):200–10. doi: https://doi.org/10.2217/nnm-2020-0173

How to cite this article:
Chaki R, Basak S, Sharma A, Nasare VD, Ghosh N, Mandal SC. Biocompatible nanocarriers of bioactive flavonoid naringin: Design, formulation, and comprehensive characterization. J Appl Pharm Sci. 2025. http://doi.org/10.7324/JAPS.2025.222894

26TH ANNUAL NATIONAL CONVENTION

PSIT Kanpur

APTICON 2023

PSIT KANPUR

Fiesta of Innovation, Research and Collaboration: Thriving towards excellence in Pharmacy Teaching

ASSOCIATION OF PHARMACEUTICAL TEACHERS OF INDIA (APTI)
AND
PSIT-PRANVEER SINGH INSTITUTE OF TECHNOLOGY (PHARMACY), KANPUR

CERTIFICATE

OF APPRECIATION

This is to certify that

Prof./Dr./Mr./Ms. RITUPARNA CHAKI

From Dr. B. C. Roy College of Pharmacy & AHS, Durgapur

has presented a **POSTER** on the topic entitled Formulation & evaluation of Chitosan-based quercetin dihydrate nanoparticles for ocular drug delivery

in the **26th Annual National Convention** of the **Association of Pharmaceutical Teachers of India -2023** held at **PSIT- Pranveer Singh Institute of Technology (Pharmacy), Kanpur (India)** from 2nd to 3rd September 2023.

Dr. Pranay Wal	**Dr. A K Rai**	**Dr. Deependra Singh**	**Dr. Milind J. Umekar**
Organising secretary	Head of the Institute	LOC Chairman	APTI president

Our Esteemed Sponsors

ALKEM · SFS · SIGNA · IDEAL CURES · SBS College of Pharmacy

BCRCP NATCON-2025

National Conference

On

Beyond Boundaries:

Pioneering the Next Wave of Therapeutic Solutions

Organised by

Internal Quality Assurance Cell (IQAC)

Dr. B. C. Roy College of Pharmacy and Allied Health Sciences

Durgapur, West Bengal – 713206

Certificate of Oral Presentation

This is to certify that

Rituparna Chaki,

Assistant Professor of Dr. B C Roy College of Pharmacy and AHS has successfully delivered Oral Presentation entitled Exploring the Anti-Inflammatory and Antimicrobial Potential of Copper Nanoparticles Loaded Ellagic Acid for Ocular Inflammation in BCRCP NATCON-2025 Organized by Dr. B. C. Roy College of Pharmacy and Allied Health Sciences, Durgapur on 25th and 26th April 2025.

Dr. Satyajit Bose
Chief Patron

Prof. Samir K Samanta
Chairman

Prof. Souvik Basak
Convener

Dated: 26th April 2025

BCR/NAT/25/D/116

CHAPTER

6

Phytopharmacology of herbal biomolecules

Rituparna Chaki[1], *Nilanjan Ghosh*[2] *and Subhash C. Mandal*[3]

[1]Dr. B.C. Roy College of Pharmacy and Allied Health Sciences, Durgapur, India [2]Department of Pharmaceutical Technology, Jadavpur University, Kolkata, India [3]Pharmacognosy and Phytotherapy Research Laboratory, Division of Pharmacognosy, Department of Pharmaceutical Technology, Jadavpur University, Kolkata, India

6.1 Introduction

Plant-based drugs commonly called as herbal drugs have been in use for the treatment of human ailments since primitive times. These plant-based therapies are the contribution of the herbal biomolecules which have a multitude pharmacological potential in disease treatment. This chapter focuses on promising biomolecules and their potential of the phytoconstituents in disease treatment. Traditional use of bioactive phytoconstitutents laid the foundation to modern use of plant-based therapy. Moreover, several factors such as being cheaper alternative with fewer side effects [1,2], scientific evidence, technological advances, and research trends [3,4] are the reasons for renewed popularity of traditional herbal and plant-derived medications among researchers, [1]. Present research in the field of phototherapy also includes structural changes [5] to be available as "privileged scaffolds" [3], improved, selectivity, and pharmacokinetics of bioactive natural products through structural modifications, has led to the production of novel drug-like lead compounds. Structural changes may overcome unfavorable toxicities and pharmacokinetics, limiting their clinical potential [3,5].

6.2 Emerging need for phytotherapy

Using natural products as medicinal agents for the treatment of a wide spectrum of diseases has been in practice since a long time with the bountiful of treasure that nature has in store. Records from old era suggest that herbal drugs have formed the basis of sophisticated traditional medicine systems around 2500 BCE; with the best known record as "Ebers Papyrus" dating back to 1500 BCE, which documents over 700 drugs, mostly of plant origin [6]. Similarly, the Compendium of Materia Medica, a Chinese materia medica work written by Li Shizhen is regarded as the most complete and comprehensive medical book ever written in the history of traditional

Herbal Biomolecules in Healthcare Applications
DOI: https://doi.org/10.1016/B978-0-323-85852-6.00026-3

Chapter 17

Herb and Drug Interaction

Nilanjan Ghosh[1], Rituparna C. Ghosh[1], Anindita Kundu[2], Subhash C. Mandal[2]

[1]*Dr. B.C. Roy College of Pharmacy and Allied Health Sciences, Durgapur, India;* [2]*Department of Pharmaceutical Technology, Jadavpur University, Kolkata, India*

1. INTRODUCTION

Herbal medicines have been used for a long time to promote health and treat common diseases. The use of natural products as herbal medicines has increased steadily over the last few years, and a very significant proportion of the population in both developing and developed countries depends on traditional medicines for its primary source of healthcare. Recent literature surveys and data suggest that they are increasingly used worldwide as alternative medicines to manage various chronic diseases and also constitute an important group of multicomponent therapeutics, which are used to manage various chronic diseases [1]. Many health ailments such as common colds, inflammation, hyperalgesia, heart diseases, liver cirrhosis, diabetes, and central nervous system diseases respond well to herbal treatments [1–3]. Such widespread use of herbal medicinal products throughout the world has raised serious questions concerning the quality, safety, and efficacy of these products. Another very important aspect that arises is that patients with chronic diseases are likely to be treated with multiple drugs, which in many cases include herbs as well. This coadministration of herbal drugs with therapeutic drugs increases the risk of herb–drug interactions (HDIs) [3,4]. Despite the popularity of herbal medicines, their use is largely not evidence based because there is a lack of clinical evidence for the efficacy, target, and safety of most herbal medicines. Coadministration of herbs with drugs may mimic, increase, or decrease the effect of either component, resulting in clinically important HDIs. These interactions are generally pharmacokinetic or pharmacodynamic in nature. Synergistic or additive therapeutic effects may lead to unfavorable toxicities and complicate the dosage regimen of long-term medications, while antagonistic interactions will result in decreased efficacy and failure of therapy [5].

The potential interaction of herbal medicines with drugs is a major safety concern, especially for drugs with narrow therapeutic indices, and may lead to life-threatening adverse effects. Interactions of several commonly used herbal

Natural Products and Drug Discovery. https://doi.org/10.1016/B978-0-08-102081-4.00017-4